REAL-TIME ULTRASONIC DIAGNOSTIC TECHNOLOGY FOR POLYMER INJECTION MOLDING PROCESSES

Chin-Chi Cheng
(B.Eng., Cheng Kung University – Taiwan, R.O.C., 1992)
(M. Eng., Sun, Yat-Sen University – Taiwan, R.O.C., 1994)

Department of Electrical and Computer Engineering
McGill University
Montreal, Quebec, Canada
June 2007

A thesis submitted to McGill University in partial fulfillment of the requirements of the degree of Doctor of Philosophy.

Your file Votre référence
ISBN: 978-0-494-38571-5
Our file Notre référence
ISBN: 978-0-494-38571-5

Abstract

Integrated high-temperature (HT) ultrasonic sensors have been developed successfully by using piezoelectric bismuth titanate and lead zirconate titanate films HT ultrasonic transducers for real-time, non-destructive, and non-intrusive diagnosis of polymer injection molding (IM) processes. The HT ultrasonic sensors can be integrated onto the barrel and/or mold of IM machine, according to the customer's requirements. These sensors can be operated up to 400°C without cooling system and ultrasonic couplant, and can be miniaturized with sufficient signal strength and signal-to-noise ratio.

The chosen IM processes are grouped to large- and small-scale IM processes. The large-scale ones include conventional IM, co-injection molding (COIM), and fluid (gas/water) assisted injection molding (GAIM/WAIM). A filling incompleteness of 1 volume-% for IM of polycarbonate (PC) part, the core (PC) material movement and layers dimensions for COIM, the fluid motion, thickness and deformation of the hollowed high-density polyethylene (HDPE) part for GAIM/WAIM were diagnosed during processing by ultrasonic sensors and techniques developed.

The small-scale ones include IM for microfluidic device (IMMF) and micromolding (MM). The optimization of holding pressure for producing a flat polymethyl methacrylate (PMMA) part (surface roughness < 5 μm) having micro structures for IMMF, estimation of temperature of polyacetal copolymer (POM) melt in the barrel and filler concentration of nylon 66 (PA66) mixed with polyhedral oligomeric silsesquioxanes (POSS) part in the mold for MM, and evaluation of thickness variation of molded alumina ceramic powder part for MM were demonstrated. The melting stages and quality of low-density polyethylene (LDPE) in the barrel has been successfully monitored using ultrasound. The important phenomena during melting processes, such as partially melting pellets, air bubbles, melting completeness, and effects of melting temperature and rotation speed have been diagnosed by ultrasonic signatures. .

These diagnostic results verify that the developed integrated HT ultrasonic

sensors and techniques are capable of monitoring various IM processes to fabricate parts and products having complex formation, tiny size and micro structures, and evaluating the part quality in order to provide timely information for process optimization.

Résumé

Des capteurs ultrasonores haute température intégrés ont été développés avec succès en utilisant des transducteurs ultrasonores haute température sous forme de films piézoélectriques de titanate de bismuth et de titanate zirconate de plomb. Ces capteurs ont permis de diagnostiquer en temps réel, de façon non destructrice et sans intrusion, le procédé de moulage de polymères par injection. Les capteurs ultrasonores haute température peuvent être intégrés au fourreau et/ou au moule, suivant les besoins du client. Ces capteurs peuvent fonctionner jusqu'à 500°C sans refroidissement ni couplant. Ils peuvent être miniaturisés tout en conservant une amplitude de signal efficace et un bon rapport signal sur bruit. Le procédé choisi de moulage par injection peut être divisé en deux groupes suivant l'échelle de taille des pièces fabriquées : macro et micro moulages par injection. Le premier groupe comprend le moulage par injection conventionnel, la co-injection (co-IM) et l'injection assistée par fluide (gaz/eau). Un remplissage incomplet de 1% en volume pour l'injection conventionnelle de poly(carbonate) (PC), le déplacement du matériau de cœur (PC) et les dimensions des couches pour la co-injection, le mouvement du fluide, l'épaisseur et la déformation de la partie creuse dans le cas de l'injection assistée de poly(éthylène) haute densité (HDPE) ont été diagnostiqués grâce aux capteurs développés. Le second groupe de moulage par injection s'intéresse aux objets de petites dimensions et comprend l'injection de systèmes pour la micro-fluidique (IMMF) et le micro-moulage (MM). L'optimisation de la pression de maintien pour produire une pièce plane en poly(méthacrylate de méthyle) (PMMA) (rugosité de surface inférieure à 5 μm) figurant une microstructure pour la micro-fluidique, l'estimation de la température du polymère fondu dans le fourreau et la concentration des charges dans une pièce en Nylon 66 (PA66) renforcée par des oligomères de silsesquioxane polyhédral (POSS) pour le micro-moulage ainsi que l'évaluation de la variation d'épaisseur d'une pièce en alumine moulée ont été mis en évidence. Les phases de fusion et la qualité du poly(éthylène) basse densité

(LDPE) dans le fourreau ont été suivis avec succès en utilisant les ultrasons. Les phénomènes importants se produisant pendant la fusion tels que la fusion partielle des granules, l'apparition de bulles, la fusion totale, les effets de la température de fusion et la vitesse de rotation de la vis ont été caractérisés par des signatures ultrasonores. Les résultats de ces diagnostics montrent que les capteurs ultrasonores haute température intégrés associés aux techniques développées sont capables d'effectuer le suivi des différents procédés de moulage par injection pour la fabrication de pièces et de produits possédant une structure complexe, des petites dimensions et des microstructures, permettant ainsi d'évaluer la qualité des pièces et de récolter l'information nécessaire à l'optimisation du procédé.

Acknowledgements

I would like to thank my wife, Grace, my parents, brother and sisters for their love, encouragement and support during my studying period.

I also wish to express all my gratitude to my supervisor Dr. C.-K. Jen for his guidance, support and encouragement throughout this study. I appreciate him for what I have learned through him not only concerning research, but also concerning dedication and perseverance.

Special thanks go to Prof. Y. Ono (Carleton University, Ottawa, Ontario) for his kindness, support, suggestions and collaboration in most stages of this work. I appreciate him for presenting a diligent attitude on the research. I also thank Dr. M. Kobayashi for instruction of film sensor fabrication and consultation. My appreciation is given to IMI, NRCC, where the thesis research was performed. There, I had the privilege of making good friends. I also thank Prof. I.-S. Shih for his kind guidance and encouragement during all the processes.

My gratitude goes to the members of Characterization and Ultrasonic Sensor Group, Modeling and Diagnostics Section at IMI for their help and friendship. Many thanks go to Dr. L. Mulvaney-Johnson (Bradford University, UK) for his collaboration regarding the GAIM and WAIM experiments in Chapter 4; Prof. P.D. Coates, Dr. B.D. Whiteside, Dr. E.C. Brown, (Bradford University, UK) for their collaboration on the MM experiments in Chapter 5; Dr. H. Banakar, Dr. Z. Sun for their collaboration to the internal mixer experiment in Chapter 6; Prof. Ooi for his consultation in Chapter 6; Dr. J. Tatibouet for his consultation in operating ultrasonic PVT measurement machine and characteristics of polymers in Chapter 5; and Dr. H. Banakar for English corrections.

I am also indebted to Mr. H. Hébert for implementing most of the data acquisition and signal processing programs used in this research, and helpful discussions with respect to instrumentation. Many thanks are also devoted Mr. J.-

F. Moison, Dr. A. Derdouri, Mr. B. Gauthier, Mr. N. Nardini , Mr. Y. Simard, Dr. Y. Thomas and Miss S. Mercier for their contributions which make my work complete.

Finally, the financial support from Hsiuping Institute of Technology, Taiwan, and GSSSP, NRCC is gratefully acknowledged.

Table of Contents

List of Figures

List of Tables

List of Symbols

α	ultrasonic amplitude attenuation in polymer
α_M	ultrasonic attenuation in mold
α_P	ultrasonic attenuation in polymer
α_{PL}	ultrasonic longitudinal attenuation in polymer
α_{PS}	ultrasonic shear attenuation in polymer
ABS	Acrylonitrile Butadiene Styrene
A/D	analog to digital conversion
A_0	initial ultrasonic amplitude value
A_n	ultrasonic amplitude value in the n-th interface (n=1,2,..)
AI	artificial intelligent
BIT	bismuth titanate
CBR	clad buffer rod
ccm	cubic center meter
CFD	computational fluid dynamics
COIM	co-injection molding
Δt_H	ultrasonic echo round-trip propagating duration in mold
Δt_h	ultrasonic echo round-trip propagating duration in polymer
Δt_{H+h}	ultrasonic echo propagating duration through mode and polymer in transmission mold
Δt_{fc}	time difference of L_2' echoes appearing at UT2 and UT1 locations during COIM
Δt_{fg}	time difference of L_G echo appearing at UT-A and UT-B locations during GAIM
Δt_G	ultrasonic echo round-trip propagating duration in polymer during GAIM
Δt_l	ultrasonic echo round-trip propagating duration in polymer layer

Δt_m	duration of polymer melt flowing through two sensor locations
Δt_W	ultrasonic echo round-trip propagating duration in polymer during WAIM
D	distance between two sensor locations
DMA	dynamic mechanical analysis
$D_{max\,/\,min}$	external maximum and minimum diameters in each UT location of GAIM and WAIM parts
DSC	differential scanning calorimetry
EDD	external diameter distribution
EMAT	electromagnetic acoustic transducer
f	ultrasonic frequency (Hz)
∅	diameter
FEA	finite element analysis
G	shear modulus
G'	storage component of dynamic shear modulus
G''	loss component of dynamic shear modulus
GAIM	gas assisted injection molding
H	thickness of mold
h	thickness of polymer (mold cavity)
h_l	layer thickness of polymer
h_r	gap distance between internal surface of barrel and screw root
HARM	high aspect ratio microstructure
HDPE	high-density polyethylene
HT	high temperature
HTUT	high temperature ultrasonic transducers
im( )	imaginary components of complex variable
IM	Injection molding
IMMF	injection molding for fabrication of micro-fluidic devices
K	bulk modulus

L	longitudinal modulus
L'	storage component of dynamic longitudinal modulus
L''	loss component of dynamic longitudinal modulus
L^n	n-th round-trip ultrasonic echo reflected at mold / air or polymer interface in pulse-echo mold (n=1,2,..)
L^{nb}	n-th round trip ultrasonic longitudinal-wave echoes reflected at barrel/polymer melt interface in pulse-echo mold (n=1,2,..)
L_{2n}	n-th round-trip ultrasonic echo reflected at polymer / mold interface in pulse-echo mold (n=1,2,..)
L_{2nf} or L_{2nr}	n-th round-trip ultrasonic echo reflected from flight or root of screw through melt in pulse-echo mold (n=1,2,..)
L_{2n-1}	n-th ultrasonic echo transmitted through polymer/mold and reach to receiving UT in transmission mold (n=1,2,..)
$\|L_n\|$	amplitude of ultrasonic echo L_n (n=1,2,..)
$L_2' \sim L_2''''$	ultrasonic echo reflected from layer interface in polymer
L_S	ultrasonic echoes reflected at solid/liquid interface
L_G	ultrasonic echoes reflected at liquid/gas interface
L_W	ultrasonic echoes reflected at liquid/water interface
LDPE	low-density polyethylene
LIGA	X-ray lithography, galvanoformung (electroplating) and abformung
LiNb	lithium niobate
LVDT	linear voltage differential transformer
MB	mega byte
MEMS	micro electro mechanical system
MFR	melt flow rate
MM	micromolding
mod()	modulus of complex variable
MSD	moving standard deviation
N	Newton

P	pressure
PA66	nylon 66
PC	polycarbonate
PCA	principle component analysis
PID	proportional-integral- derivative
PIM	powder injection molding
PMMA	polymethyl methacrylate
POM	polyacetal copolymer
POSS	polyhedral oligomeric silsesquioxanes
PVT	pressure, volume, temperature
PZT	lead zirconate titanate
ρ_M	density of material M
re( )	real components of complex variable
R	reflection coefficient
R_M	reflection coefficients in mold
R_P	reflection coefficients in polymer
RPM	rotation per minute
RWT	residual wall thickness
$S^{(n)}$	(n-th round trip) shear wave echo reflected at mold/air or polymer interface
SD	standard deviation
SNR	signal-to-noise ratio
t	time
t_{2n}	ultrasonic echo L_{2n} propagating time delay in polymer
T	temperature
T_C	crystallization temperature
T_G	glass transition temperature
T_S	solidus temperature
T	transmission coefficient
T_M	transmission coefficient from polymer to mold
T_P	transmission coefficient from mold to polymer

TA	thermo-analytical
TGA	thermo-gravimetric analysis
TMA	thermo-mechanical analysis
UT	ultrasonic transducers
V	voltage
V	ultrasonic velocity
V_C	crystallization ultrasonic velocity
V_c	average core flow speed
V_S	solidus ultrasonic velocity
V_g	average gas flow speed
V_M	ultrasonic velocity in mold
V_m	average polymer melt speed during molding
V_P	ultrasonic velocity in polymer
V_{PL}	longitudinal ultrasonic velocity in polymer
V_{SL}	shear ultrasonic velocity in polymer
ω	angler frequency
WAIM	water assisted injection molding
wt	weight
Y	Young's modulus
Z_M	acoustic impedance of mold
Z_P	acoustic impedance of polymer

Chapter 1

Introduction

1.1 Background

1.1.1 Polymer process

Polymers are materials composed of molecules with high molecular weight used in producing plastics. Today, various parts and components, which have been traditionally made of woods, metals, ceramics or glasses, are redesigned with polymers as advanced polymeric materials with improved properties have become available. As a result, polymers that offer properties such as low density, corrosion resistance, low thermal and electrical conductivities, and ability to be shaped and molded at relatively low temperatures (compared to metals, ceramics or glasses [1]), are now common place. Indeed, productions of parts now becoming polymer are non labor-intensive and economical approach [2].

Polymer processing is referred to the sequence of operations carried out on polymers to transform them into useful products. The main steps in any polymer processes are to melt, then shape and finally cool the material in a new form. The heat required for melting may be supplied by radiation or conduction, or by mechanical work. Mixing of the melt is sometimes desirable to improve the properties of products. However, due to relatively complex behavior of the materials, polymer processes may appear to be difficult to understand and analyze quantitatively.

In the polymer/plastic industry, the general polymer processing techniques are extrusion, injection molding, foaming, blow molding, compression, lamination, etc. The details of various polymer processes employed in this thesis are described in chapter 2. Among these, the injection molding (IM) process preoccupies a major part of the polymer industry and has the lion-share of its global business. It consumes approximately 32 wt% of all polymers, and is in second place to extrusion (36 wt%) [3-5]. IM is the process of forcing a melted polymer into a mold cavity for designed parts, while extrusion process forces it through a die. In the United States alone, there are about 80,000 IM machines and about 18,000 extruders for production of all types of plastics [6]. In the past decade, increases in the number of IM machines and extruders in China and India have been dramatically fast and are expected to continue in the near feature.

The recent manufacturing trends in products such as consumer electronics, telecommunications components, and medical disposable tools and parts, are toward light, thin, short and small. Among these products, the growth in micro parts, ex. Micro-Electro-Mechanical System (MEMS) parts, and micro-fluidic devices has placed increasing demands on industry for product miniaturization. Polymers are well-suited for producing disposable micro parts at low cost and in mass production.

In order to meet the miniaturization requirements of micro-fabrication, most of the conventional manufacturing machines and processes have been either modified dramatically or replaced by other new techniques. Therefore, to fabricate high quality products under the combination of complex material

characteristics and miniaturization of products, the polymer industry has placed high priority on development of applicable techniques and instruments, including process diagnostic technologies.

1.1.2 Process diagnosis

Even though there are many ways to produce polymer products, in a competitive environment process efficiency, part quality, and low cost are always the keys to success for the manufacturing company . To achieve the optimal fabrication process state and good part quality needs process diagnosis and control [7-9]. Furthermore, in order to understand and analyze complex behavior of the materials, polymer processes need to be properly monitored.

Process control is an important tool to reduce raw material waste, production cost, and also improve product quality and process efficiency. The system needed to control a process can be as simple as a regulator implementing the proportional-integral-derivative (PID) controlling strategy, a well-known method for guiding the system to its desired stable states. Or, it can be a sophisticated computerized system executing an artificial intelligent (AI) based controlling strategy, designed to steer non-linear systems towards their optimal operating points [7]. Regardless of the control system type and control strategy, it is essential to have information on the evolution of the system dynamics during the process. Consequently, the ability to perform diagnosis of process parameters and complex control strategies is important for polymer fabrication processes [10, 11]. Especially, the precise feedback of

process parameters to the control system provides an opportunity to directly supervise the manufacturing process and assure products quality.

The properties of polymers depend on processing temperature, pressure, time, raw materials properties, and processing procedures. The complex interplay of these variables requires the use of real-time process diagnosis and quality control procedures. Currently, the widely used process diagnostic tools deploy pressure and temperature sensors for online measurements. These sensors, however, need to have direct contact with the molten material in order to provide information on its pressure and temperature profiles [12, 13]. There are also several off-line measuring methods, such as thermo-analytical (TA) methods, thermo-gravimetric analysis (TGA), differential scanning calorimetry (DSC), thermo-mechanical analysis (TMA) and dynamic mechanical analysis (DMA), for measuring the thermo-dynamical properties, weight, heat flow, dimensional changes, as well as viscoelastic properties of the tested polymers or products [6].

Some advanced techniques, such as optical, electrical and ultrasonic, have been considered for the polymer process diagnosis. However, these techniques are still under development or just recently proposed. In-line optical techniques for diagnosing fabrication processes are transmitting light to the polymer resin through a sapphire window, which is flush with the wall of the mold cavity [14]. Electrical pulse technique is one of the methods measuring the dynamic variation of mechanical force of rotating machinery (i.e. the torque applied to the machine rotor) by adding additional material during static processing state [15, 16]. The amount of mechanical (driving)

force needed to operate the extruder machine is related to the viscosity and elasticity of polymer. Ultrasonic techniques diagnose the process by sending the sound energy into the target material, and receiving it in transmission or reflection mode [17].

Each measurement method has its own advantages and drawbacks. Among the established methods, there are no specific methods which can measure all the parameters, such as processing temperature and pressure, melting or mixing quality, melt flow movement, products thermal and mechanical performances and quality. The detailed description of these measuring techniques will be presented in chapter 2. The measurements collected by process diagnosing sensors provide the information that is feedback to the process control system, depending on the choice of control strategy. These control actions affect process efficiency, cost and part quality. Furthermore, for micro-fabrication processes, the conventional process diagnosing sensors may not meet certain requirements of new products and machine setups, such as tiny mold cavity and small space of mold for installation. Therefore, development of high performance and cost effective diagnosing sensors that meet the process requirements could advance the process diagnostic technique and benefit the manufacturing industry.

1.2 Ultrasonic diagnostic technique

Ultrasonic technique is one of the excellent candidates for real-time diagnosis of polymer processes. It can measure physical and rheological properties of materials nondestructively and non-intrusively even these

materials are inside metallic die and molds at high temperature. The basic signatures of ultrasonic signals, such as velocity, attenuation, reflection and transmission coefficients, scatter signals from materials, have unique relationships with process dynamics, material characteristics, and product quality. The improvements in ultrasonic sensors' capabilities and the progresses in computerized data acquisition systems have made real-time on-line diagnosis of fast changing material and process properties convenient and practical for industry applications [18]. The applications of this technique to polymer processes are grouped into two: off-line and real-time on-line diagnoses.

It is well known that attenuation and velocity of the ultrasonic signal in materials are influenced by the material temperature and pressure and the frequency of the ultrasonic wave employed. For off-line diagnosis, Rokhlin, et al. [19] at Ohio State University, OH, investigated the frequency dependence of the ultrasonic wave velocity and attenuation during the curing reaction of epoxy resins. Their results indicated that the attenuation coefficient increases linearly with frequency at all stages of the curing reaction from liquid to solid state. Lee, et al. [20] at Inha University, Korea, found that the ultrasonic wave velocity is independent of the frequency over the range of 0.5-5.0MHz, but it varies with moderate temperature changes in the range of 25-75°C for polycarbonate. In general, the attenuation is found to be highly influenced by temperature changes and to increase as the frequency increases. Tanaka, et al. [21] at Kyoto University, Japan, demonstrated that ultrasonic velocity is also sensitive to morphology, crystallinity, and density of the test sample. Tatibouet, et al. [22] at Industrial Material Institute, National Research Council

(IMI/NRC), Canada, investigated how the ultrasonic velocity and attenuation vary with pressure. They have shown that melting, crystallization, and glass temperatures and their dependence on pressure can be determined from measured variations in ultrasonic characteristics (velocity and attenuation).

Huang, et al. [23] at Ohio State University, OH, investigated the relationship between the ratios of reflection to transmission coefficient with the thickness of a thin polymer layer in ultrasonic transmission method at the frequency of 2.25 and 5MHz. When the layer thickness is in the order of a wave length, the ratio is proportional to frequency and provides important information about the layer properties. Prasslanakis, et al. [24] at Technical University of Athens, Greece, presented experimental results showing differences in the ultrasonic signatures (velocity and attenuation) in the three characteristic states of the epoxy polymers (i.e. the liquid, the semi-solid, and solid states), during the polymerization, as well as the corresponding mechanical properties. Piche, et al. [25] at IMI/NRC, Canada, developed an ultrasonic technique for investigating flow behavior of polymer melts with different grades of fillers under extrusion conditions. The results showed that the larger the filler diameter, the higher the attenuation and the ultrasonic velocity. They further reported, [26], that the specific volume, ultrasonic velocity and attenuation in polystyrene are linearly dependent on temperature range from -150 to 225°C and pressure range from 13 to 71.5MPa.

Ultrasonic technique has been also applied to real-time, on-line, nondestructive diagnosis of IM processes due to its capabilities to probe the properties of polymers within the mold. Nishiwaki, et al. [27] at Tokyo

University of Agriculture and Technology, Tokyo, one of the pioneering teams in this area, in 1985 introduced the application of in-line ultrasonic monitoring for polymer processes. They reported that the flight time of ultrasonic waves through plastics decreases as the plastics cools down and eventually solidifies. The amplitude variation of the ultrasonic waves reflecting back from the mold and plastics interface can detect the air gap in the interface. They [28] also reported that ultrasonic velocity can measure the crystallinity of the part. The crystallinity of the part is related to thermal, geometric, mechanical properties and strength, as well as Young's modulus of elasticity. Konno, et al. [29] at Tokyo University of Agriculture and Technology, Tokyo, reported that the ultrasonic velocity is correlated to the melt temperature and pressure inside the mold. Their results show that the ultrasonic velocity can be used to estimate the mean value of the part temperature along its cross section, which cannot be obtained from contact temperature measured by a thermocouple.

Thomas, [30] at University of Utah, Utah, demonstrated the potential of ultrasonic velocity in monitoring the polymer state in the mold cavity during the IM process. He reported that the changes in velocity can be an indicator of the changes in polymer density during packing and cooling stages, and the variation of the reflection waves at the polymer and mold interface can be used to predict mold filling, flash and shrinkage. Thomas, et al. [31] also developed theoretical relationships between the static, isothermal, pressure-volume-temperature (PVT) behavior of polystyrene and its adiabatic bulk modulus. The relationships provide the ultrasonic velocity in the polymer as a function of temperature and pressure. The ultrasonic velocity estimated using these relationships is in good agreement with experimental results.

Brown, et al. [32] at University of Bradford, UK, developed an ultrasonic transit time measuring instrument for off-line and in-line polymer process diagnosis. They reported a strong interaction between transit time, melt pressure and temperature, and verified that ultrasound provides sensitive indications of melt process and material properties.

Researches conducted at IMI/NRC in this area started in 1990, with a comprehensive study for developing ultrasonic real-time polymer process monitoring sensors. Gendron, et al. [33] investigated an in-line ultrasonic technique for detecting filler concentration during extrusion. They found that increasing the filler concentration caused the attenuation to increase and ultrasonic velocity to decrease. Wang, et al. [34] performed an on-line ultrasonic monitoring of IM process and reported results on flow front of molten polymers and the development of air gap due to the shrinkage of the part in the mold. The velocity and the amplitude variations of ultrasonic waves also contributed to the interpretation of the solidification process. Wen, et al. [35] further investigated the fabrication procedure of the IM process and, using ultrasonic techniques, they detected the local flow front arrival, end of filling, solidification of the polymer melt, detachment of the part from the mold wall, and the retraction of the plunger during the injection cycle. They also developed a method for estimating part thickness and compared measurements generated by ultrasonic and pressure transducers for the same process.

Most of the previous researches have carried out their investigations using conventional room temperature ultrasonic transducers (UTs). However,

in many applications, UTs need to be applied at high temperature (HT) [36]. Also UTs often need to be attached to curved surfaces. For instance, in polymer extrusion, the processing temperature is between 150 and 250°C, and the shape of the barrel is cylindrical.

For real-time ultrasonic monitoring, UT of broadband frequency is much preferred, due to the contribution of high resolution in time domain. The broad bandwidth of most piezoelectric UTs is achieved by adopting an epoxy backing on top electrode [37], which is not suitable for thermal cycling. Since, during repeated thermal cycling, disbonding happens between the electrode and the epoxy, UTs may fail to function properly.

One of the solutions for obtaining HT measurements is adding a cooling system to the surrounding area of the UTs. However, the cooling system is often bulky and may not fit different machine setups. Another hurdle for UTs to operate at HT is the couplant between the UTs and the contact surface. The liquid couplant is necessary to enable efficient ultrasonic energy transmission. However, at elevated temperatures, the liquid couplant evaporates and quickly dries up. Thus it is not practical to use it for continuous, long-term, process monitoring at elevated temperatures. The flat probing surface of the UTs is not appropriate to be mounted over curved surfaces. For monitoring on the curved surface with UT having a flat probing head, a probe with curved shape is usually adopted. However, as the curved shape of the probe is fixed, it may not exactly fit the surface of the chosen spot. This may cause poor ultrasonic signal transmission to the target, and affect the diagnostic results. Therefore, there is a need for developing a transducer which can be fit to curved surfaces

and can operate at temperature higher than 150°C.

Several UTs have been developed for operating at elevated temperature, such as electromagnetic acoustic transducer (EMAT) [38-40], laser ultrasound [41] and piezoelectric UT. David, et al. [39] at University of Dayton, OH, developed a HT EMAT, which has been tested for defect detection, material characterization and measuring mechanical properties at elevated temperatures. Two drawbacks of using EMAT are that the target material should be electrically conductive, and the resulting signal-to-noise (SNR) ratio is often poor due to the insufficient ultrasonic energy radiation. Laser ultrasound can perform fast scanning and monitor parts with complex shapes; but, it is generally costly, has low pulse repetition rate (< 200Hz) and requires the use of moderate-power lasers for safety reasons [42]. Piezoelectric materials are commonly used for UTs because of low cost and exhibiting high efficiency of generating and receiving ultrasound with high pulse repetition rate (> 1KHz). Therefore, piezoelectric materials have become the dominant material for fabricating UTs.

Several efforts have been invested on the development of HT piezoelectric UTs [43-44] and the commercial HTUTs are supplied by many companies, such as Etalon (Lizton, IN), GE Panametrics-NDT (Waltham, MA), GE/Krautkramer GmbH (Cologne, Germany), RTD (Rotterdam, Netherlands), Ultran (Boalsburg, PA), Ishikawajima Inspection and Instrumentation Co. Ltd. (Tokyo, Japan), Sigma Transducer Inc. (Kennewick, WA). These commercial HTUTs can operate at temperatures approaching 500°C, but their SNRs are less than 20dB [45], which is not sufficient for

diagnosis of polymer processes. In addition to being expensive and having flat probing surfaces, they are also lack of proper HT couplant.

For HT ultrasonic measurements, buffer rod or delay line is one of the options favored due to its ability to insulate UT from elevated temperature easily and effectively. Most commercial HTUTs use buffer rods or delay lines [46, 47]. In 1985, Jen, et al. at IMI/NRC, Canada [47, 48], developed the clad buffer rods (CBRs) made by thermal spray techniques for HT applications. The ultrasonic delay line probe, which is the combination of CBR with broadband UT and cooling system, makes process monitoring at elevated temperature possible, providing not only high signal strength but also high SNR and broadband. Its use has been reported in [49] at 960°C in liquid aluminum. The ultrasonic delay line CBR probe has the advantage that it can be constructed to resemble in shape to commercial pressure and temperature sensors, such as Dynisco 467XL TPT, and fitted into the existing holes originally designed for the conventional sensors. Most conventional extruder machines have the holes for installing the sensors in the shape of Dynisco one. Therefore, the adoption of ultrasonic delay line probe for process monitoring is often quite convenient. However, for newly developed micro-fabrication machine, e.g. micromolding machine, these holes may not be available.

The ultrasonic delay line CBR probe has been already applied to on-line monitoring of die-casting [50], extrusion [46], and semi-solid metal processes [51]. In this thesis, this technique will be deployed to monitor the melting process in the internal mixer, which is the simulator of extruder [52]. Through this monitoring, the polymer melting quality in the extruder can be assured,

and the part quality in subsequent steps, such as molding, may be improved. However, the system with delay line probe is bulky due to the need for a cooling system. The HT couplant between UTs and buffer rods is still a concern. The attachment of buffer rods to target spots, either by drilling holes or a mechanical fix, is another hurdle for the micro-fabrication machine to clear.

In order to provide a solution for the cooling system problem, HT couplant, and attachment of UTs to the desired spots in HT ultrasonic measurement, in 2002 Kobayashi, et al. at IMI/NRC developed the piezoelectric film HTUTs made by a sol-gel spray technique [53, 54]. The piezoelectric film is made of piezoelectric materials, such as lead-zirconate-titanate (PZT), bismuth titanate (BIT) or lithium titanate. Due to the high Curie temperature (675°C) of BIT film [55]. the BIT piezoelectric film is allowed to operate up to 500°C It was also reported that the PZT piezoelectric film can operate up to 250°C [56] because of its 350°C Curie temperature. In addition, these films can operate at these elevated temperatures without a cooling system or ultrasonic couplant, and can be directly coated onto surfaces of any shape, flat or curved, with a miniature size. Both BIT and PZT also provide sufficient signal strength and high SNR. Their relevant fabrication procedures will be briefly described in chapter 3.

Advantages that are offered by piezoelectric film HTUTs make monitoring of polymer extrusion and IM processes straightforward, effective and practical at elevated temperatures. They may also meet the miniaturization requirements of micro-fabrication process diagnosis, such as small space for

sensor setup and small product size. In order to make the film HTUTs attractive to the manufacturing industry, practical customization of the film HTUTs for various polymer processes, according to their requirements, is necessary. Through the customization of film HTUTs, not only one can understand the polymer process more, but also can demonstrate the capabilities of film HTUTs in improving manufacturing process and product quality. However, due to intricate procedures and different machine setups needed for different polymer processes, adapting the HTUTs to the desired sensing locations and tuning the diagnosis for optimal performance remains a challenge.

1.3 Thesis content

1.3.1 Objective

There have been several investigations in the area of ultrasonic diagnostic techniques showing the potentials of the ultrasonic techniques in conducting real-time, nondestructive and non-intrusive polymer process diagnosis. However, these techniques are not yet to be considered practical for deployment in an actual production line in the polymer-related industries. Therefore, the objectives of this research are to develop integrated ultrasonic sensors using piezoelectric film HTUTs and process diagnostic techniques, customized for each IM machine and process and to demonstrate their capabilities for real-time and nondestructive diagnosis of IM processes. Once the suitability of integrated HT ultrasonic sensors for industry utilization has been established, the sensors and techniques developed here would be ready for practical use in actual industrial manufacturing processes.

1.3.2 Content

In order to apply the integrated HT ultrasonic sensors practically on various IM processes, several typical and advanced polymer processes are chosen. In chapter 2, the history, merits and challenge of various IM processes, such as IM, co-injection molding (COIM), gas assisted injection molding (GAIM), water assisted injection molding (WAIM), injection molding for fabrication of micro-fluidic devices (IMMF), micro-molding (MM) for polymer, nano-composite and ceramic materials will be described. To compare ultrasonic diagnostic technique with the conventional ones, the fundamentals of several general process diagnostic techniques, such as temperature, pressure, torque, optical and fluorescent measurements, are introduced. Their advantages, drawbacks and development history are discussed.

In chapter 3, ultrasonic measuring principles and systems, fabrication and characterization of piezoelectric films made by the sol-gel spray technique will be presented [54]. The procedures for analyzing ultrasonic signatures will be also presented. Details of a PC-based measurement acquisition system for real-time diagnosis application will be illustrated. The ultrasonic PVT measurement system, used for collecting information on the characteristics of polymers, will be introduced. The development of HT ultrasonic sensors by using piezoelectric films for application to various polymer IM processes and the evaluation of these ultrasonic HT sensors will be provided.

In chapter 4, process diagnosis of large-scale IM processes, such as IM, COIM, GAIM and WAIM, by HT ultrasonic sensor will be illustrated. Details

on four HT ultrasonic sensors, installed to a 150-ton Engle machine for IM and COIM, will be provided. In IM process, the phenomenon of polymer melt flow and filling incompleteness inside the mold and their monitoring techniques will be discussed. In COIM process, core movement and its dimension will be diagnosed during the molding process. Three HT ultrasonic sensors installed to a Battenfeld gas or water assisted IM machine for GAIM and WAIM will be demonstrated. In GAIM or WAIM process, gas or water movement, formation and thickness of hollow structure will be investigated.

In chapter 5, IM for the small-scale fabrication, such as, microfluidic devices and MM of polymer, nano-composite and ceramic powder materials, will be studied. Two miniature HT ultrasonic sensors will be installed into a 30-ton Boy machine for process diagnosis. The relationships among ultrasonic contact duration, velocity, holding pressure and part surface profile will be discussed. The optimal approach to process control and part quality will be reviewed. HT ultrasonic sensors integrated on the barrel and mold surface of a Battenfeld MM machine will be introduced. The melting process in the barrel and polymer solidification phenomena inside the mold will be monitored by ultrasonic signatures. Concentration of nano-composite in the mold will also be examined. For MM of powder materials, the fabrication and post-processing step of debinding-and-sintering will be presented. Part thickness can be evaluated by ultrasonic signatures and process parameter. The relationship between injection speed, pressure and part thickness will be explained.

In chapter 6, the ultrasonic delay line CBR probe, installed into the

chamber of an internal mixer, are introduced for the diagnosis of polymer melting process. Observed results, ultrasonic signatures and torque measurements will be compared during the melting process. The indications of air bubbles, temperature and rotation speed effects by ultrasonic signatures will be presented. It will be shown that the ultrasonic signatures can indicate different melting stages as well as viscosity information in the polymer.

In chapter 7, results of previous chapters will be summarized and original contributions to the subject of this study and future works will be presented.

Chapter 2

Polymer processes and process diagnosis

2.1 Introduction

Polymer processes, including injection molding (IM), extrusion, die casting, foaming, are employed in the manufacturing of most polymer / plastic products. In this thesis, the main focus is on design and applications of integrated HT ultrasonic sensor and ultrasonic probes in various IM processes for real-time diagnostic purposes. These processes include conventional IM, co-injection molding (COIM), fluid (gas or water) assisted injection molding (GAIM or WAIM), injection molding for the fabrication of microfluidic devices (IMMF), micromolding (MM) for polymer, nano-composite, ceramic materials, and melting of polymer in internal mixers.

In this chapter, different stages of polymer fabrication processes and their final products will be introduced. The process parameters (e.g. temperature, pressure, torque, optical and fluorescent emission) and their widely used measurement techniques are also discussed. The performance and suitability of these measuring techniques, under complicated fabrication requirements including micro-fabrication, are discussed.

2.2 Polymer processes

2.2.1 Injection molding processes

The IM process is a widely used manufacturing process for both prototyping and mass production of three-dimensional products, with general or complex geometries, made up of layered or hollow structures. Based on the market needs, the products can be large or small and their weights and volume can vary extensively. If required, the products can be molded with strict tolerances, having thicknesses in micrometers and weights down to fractions of a gram. The products are typically produced in-mass with a huge variety of end uses including automotive components, housings for consumer electronics, telecommunications components, child products, and low-cost disposable medical implements [57].

The IM machine contains three basic components: the injection unit, the mold and the clamping system. The injection unit, also called the plasticator, includes the hopper, barrel and screw for feeding and melting the polymer and transferring the polymer melt into the mold. The clamping system opens and closes the mold.

IM is the process of forcing melted polymer into a mold cavity for producing "a part" with a unique shape. Fig. 2-1 shows a typical cycle of the injection molding: (i) the polymer melt is injected into the cavity of a mold through a gate; (ii) the cavity is completely filled with the material and additional melt is forced into the cavity under high pressure until the gate is frozen in order to compensate for the shrinkage due to the continuous cooling. Then, the part is further cooled until it is sufficiently solidified; (iii) the mold is

opened and the part is detached from the fixed mold; and (iv) the part is ejected from the cavity of the mobile mold by the ejection pin. Then the mold is closed and the entire cycle is repeated.

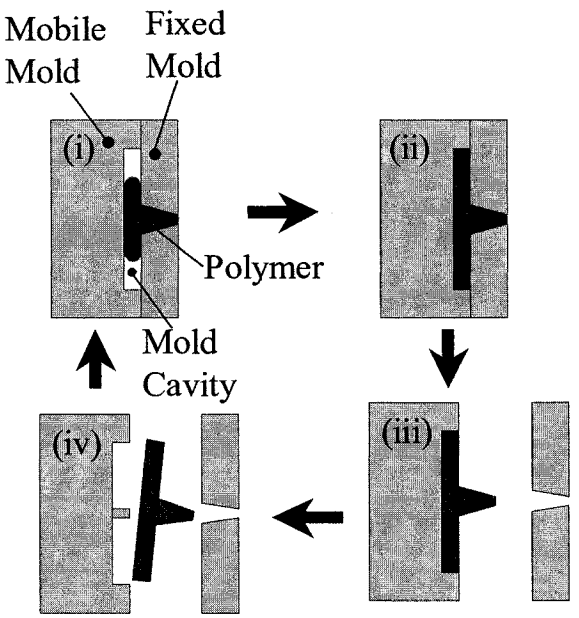

Fig. 2-1 Cycle of the IM process: (i) filling; (ii) packing, holding and cooling; (iii) mold opening; and (iv) part ejection.

During IM, a number of production-related problems can arise. They includes: short shots (incomplete filling of a mold), voids and sinks (holes in molded parts or insufficient material), weld lines and flow marks (e.g., seams and welding of cooler material around projections), sticking problems (mold or material adhesion), warping (bending or distortion of parts), burning, and shrinkage (reduction in size of molded parts) [58].

Since 1872 when the first U.S. IM patent was issued, a variety of special IM processes and machines have been developed. The development of special

IM processes is largely driven by the market requirements. They follow the basic IM principle of melting polymer and forcing the melt into the designed cavity to mold the products. But, they could involve special fabrication processes, mold designs or materials. They often utilize advanced techniques to meet fabrication requirements such as low cost, high quality, and high performance for the parts, and high efficiency (i.e. low waste, and low energy consumption) for the process [59-61]. In this thesis, a few specialized IM processes will be discussed, including COIM, GAIM, WAIM, IMMF, and MM for polymer, nano-composite and ceramic powder materials.

COIM

COIM, also known as sandwich molding, is a process in which two or more polymers are laminated together in a mold cavity. It has the ability to use recycled plastics to improve part performance and lower part production cost. The molded parts can attain special characteristics by combining different materials in their fabrication. For example, the skin material can be different from the core material to achieve required surface properties (e.g. appearance, hardness, thermal or chemical resistance, soft touch, etc.), while the core material only needs to have sufficient mechanical properties and recycled materials may be used. In [62] Selden discusses the material selections and combinations associated with mechanical properties of the COIM parts.

The COIM process was developed in 1970. Since then, there have been extensive research and development on the COIM process. Pioneering works were reported in [63-67]. Donovan, et al. [63] applied the COIM process to

thermoplastics recycling in molds of different geometries. White, et al. [64, 65] Young, et al. [66] and Akay [67] established the requirements to form the most uniform skin/core structure under isothermal and non-isothermal flow conditions during sequential injection of two melts, respectively. Furthermore, White, et al. [64] and Chen, et al. [68] investigated polymer melt flow behavior inside the mold cavity by visualization under the sequential COIM process.

Kadota, et al. [69], investigated the structure gradients as a function of the process history and injection sequence during the COIM. They found that a slower injection speed for core would cause core spreading uniformly in the flow direction. Selden [70] found that three molding parameters, namely injection velocity, core temperature and core content, were the most significant process variables affecting skin/core distribution, layer thickness and mechanical properties. In addition, Li, et al. [71] discovered that the proper selection of material rheological properties and processing parameters would affect the material distribution, penetration behavior, and breakthrough phenomena. However, COIM needs a two-barrel injection machine, requiring more complicated machine control than a single-barrel, conventional, IM. Therefore, it requires advanced technical skills to monitor and control the formation of the internal sandwich structure and the melt flow behavior.

GAIM and WAIM

Fluid (gas or water) assisted injection molding is a popular variant of the IM technology which incorporates gas or water injection in the mold filling

cycle to form hollow components and reduce undesirable side effects of material shrinkage during cooling [60, 72, 73]. Shah [74] reported that this technique offers a number of advantages, such as higher strength to weight ratio, reduced cycle time and material consumption, low injection pressure and clamp tonnage, reduced stresses, smoother surface finish (compared with structural foam), and tool design freedom. The hollow structure can be utilized to manufacture items such as automotive components, suitcase handles, grab handles and core out rib junctions [75, 76]. During the process, first polymer melt is injected into the mold cavity then the fluid (gas or water) is injected to displace the melt and leave a continuous bubble of fluid within the product. The fluid is maintained inside the molded part throughout the cooling cycle. After that, the fluid pressure is released, the mold is opened, and the molded part is ejected.

Due to incorporating the fluid (gas or water) system, the GAIM or WAIM processes are more complex than the conventional IM process, and need advanced techniques to control the formation of the hollow structure as well as the cavity wall performance. Zhao, et al. [77] used the relatively low viscosity of gas to assist in the GAIM process to attain structural rigidity without sacrificing surface quality. They found that the gas injection delay time is important in controlling gas bubble formation. Yang, et al. [78] investigated the fundamental phenomena during filling stage in GAIM process through an operation window. They observed distinctly different process dynamics for conventional filling, gas-assisted filling and gas-assisted packing. In addition, they noted that the distribution of the bubble and in particular the thickness of melt deposited against the cavity wall (residual wall thickness: RWT) is

important to the product mechanical performance, cooling rate and aesthetics.

IMMF

A microfluidic device, consisting of one or more micro channels with at least one dimension less than 1mm, has attractive features such as small sample requirement and low power consumption, realizing a lab-on-a chip device [79-81]. This device can be manufactured from glass, silicon wafer, metal or polymer. However, Choi, et al. [82] state that plastic substrates of the microfluidic devices offer a wide variety of surface properties, both physical and chemical, for the applications of biofluidic chips, which make production of multifunctional, low-cost, disposable microfluidic modules possible. For example, comparing to silicon wafer fabrication technology, IM requires much less investment in capital equipments. Choi, et al. [83] and also Madou, et al. [84] conclude that disposable microfluidic devices manufactured by mass production can give rise to many interesting applications in biomedical technology, such as clinical diagnosis, DNA analysis and cell manipulation.

Microfluidic devices can be fabricated by IM machines. Dimensions of the features within the devices are in micrometer scale. The accuracy and repeatability of the dimension and location of the micro channels will affect the structures and functions of the devices. Minor channel or surface differences can impact the fluid movement, the reliability and sensitivity of analyzers. Sinton, et al. [85] investigated the loading and dispensing of sub-nanolitre samples using a microfluidic cross chip, both experimentally and by numerical simulations. The results indicate that the shape, cross-stream

uniformity, and axial extent of the samples were sensitive to changes in the electric fields applied in the focusing channels. Therefore, due to narrow fabrication window and high part quality requirement, developing a reliable microfludic manipulation technique is a challenge.

MM

Micromolding (MM) technology has realized the mass production of MEMS components at a fraction of the cost of lithographic and silicon etching techniques [86-89]. This technology is also utilized to fabricate micro parts such as gears, latches and catchwheels for watches, micro lens for optical devices, drug delivery systems or implants for biomedical applications. Similar to conventional IM, MM can be used to produce low-cost, mass-produced plastic components and products [90]. However, the dimensions of the parts molded using conventional IM is generally in the order of centimetres to meters, while those of MM is in micrometers to millimetres. The MM process has the ability to mold micro-scale components and surface features with a precision that is impossible to achieve using conventional IM technology. It is also much more sensitive to process fluctuations and material consistency, where a small change in the environment or a slight material impurity can produce a sub-standard product.

Yang, et al. [91] investigated the filling characteristics during MM process. In their experimental settings, they found that the melt fronts advanced quickly and filled the cavity in less than 0.1 sec. Mcfarland, et al. [92] investigated the influence of different processing parameters upon the

final shape of micro-optic parts by computational fluid dynamics (CFD) and finite element analysis (FEA). The plastic micro-optic components often have the overall dimension smaller than 1mm, with lenses on the order of 50 microns. The maximum difference between the predicted and corresponding measured radius of curvature is roughly 3.4%. Zhao, et al. [93] developed a new micro molding machine, which comprised of a screw extruder and an electrically driven plunger injection unit. They investigated the effects of the process parameters on the MM process and part quality. They found that metering size and holding pressure time have the most significant effects on part quality. Schift, et al. [94] presented a quantitative approach to analyze the most important molding properties of polymers for achieving high replication fidelity. They found that, for molding of nanostructures, there is a strong dependence of the melt viscosity on the mold temperature. Despa, et al. [95] developed the three-step LIGA process to inexpensively manufacture high aspect ratio microstructures (HARMs). They found that replication of the HARMs can be achieved by increasing the injection speed, elevating the tool temperature, and venting the mold cavity. Thus, in MM processes, the micro-scale mold cavity features and extreme processing conditions, which are inherent in the process, can result in larger process variations than conventional IM, with a corresponding increase in the probability of producing unsatisfactory products [96].

MM for nano-composite material

There are many methods to improve plastic products characteristics, including adding additives, fillers, reinforcements, or mixing with wax,

ceramic and alloy. In this thesis, addition of polymer nanocomposite and mixing with ceramic powder for MM process is discussed. Alexandre, et al. [97] reported the very recent development in syntheses properties and applications of polymer-layered silicate nanocomposites. They found that polymer nanocomposites, which are a class of reinforced polymers with low quantities (<5%) of nanometric-sized clay particles, can have attractive and enhanced physical and chemical properties compared with parent polymers. The incorporation of polyhedral oligomeric silsesquioxanes (POSS) into polymeric materials is one such example. This incorporation often results in dramatic improvements in mechanical as well as thermal properties, such as increase in use temperature, oxidative resistance and surface hardening for the parent polymers [98], which are highly valued. The enhanced physical properties of polymers incorporating POSS segments stem from the ability of POSS to control the movement of the chains while maintaining the mechanical properties of the base resin. This is a direct result of POSS nanoscopic size and its relationship to polymer dimensions. Therefore, the POSS concentration in the parent polymers can influence the performance of the composition.

MM for powder material

Powder injection molding (PIM) is a manufacturing procedure, well-suited for the mass production of metallic or ceramic parts because of its ability to manufacture complex net-shape components using a variety of high-performance powder materials [99-101]. The process has all the benefits of conventional polymer IM but allows fabrication of products with superior physical properties such as high hardness, strength, and resistance to wear [99,

102]. MM for the powder material is similar to PIM. It is a promising manufacturing process for metal or ceramic micro-parts, because it allows a near net shape fabrication of micro-structured parts and almost without post-processing steps. Piotter, et al. [103] and Gietzelt, et al. [104] mentioned that the manufactured micro parts can be applied to many fields, e.g. biomedical, telecommunications, sensor and actuator. The process requires a molten feedstock, the mixture of fine powder and a sacrificial (usually wax/polymer) binder, to be injected into a mold to form the desired part. After molding, the as-molded part is subjected to debinding and sintering processes to remove the binder material and achieve the required density and dimensions [105]. However, because of the susceptibility of the molded parts to incomplete filling and shrinkage during processes, as suggested by Hongerholt, et al. [106, 107], control of precise dimensions of final products for micro components is a major technical challenge.

2.2.2 Extrusion

As mentioned in the beginning [108, 109], polymer extrusion is one of the most used industrial processes for mass-production of plastic products and has the highest polymer consumption ratio (36%) [3-5]. The extrusion process is used in manufacturing plastic rods, tubes, films, sheets, filaments and pipe for industrial, agriculture, building and house application [6]. In the process, polymer pellets are fed into the extruder's feed hopper, transported, melted, mixed and blended by screws in the heated barrel section under elevated temperatures (normally 150°C ~ 250°C), and then the melt is conveyed into the extruder exit die that shapes the product. The typical steps are feeding,

compression, melting and metering. During the process, the pellets are melted gradually as they are pushed through the barrel; thus, lowering the risk of overheating, which may cause polymer degradation. Extra heat is contributed by the intense pressure and friction taking place inside the barrel. During the extrusion process, temperature, pressure, rotation speed of screw as well as material feeding rate, selection and chemical reaction will affect the melting and mixing quality in the output, which decides the product quality [110-112].

The internal mixer is one of the essential instruments, widely used in most laboratories working on polymers or powder material processing, to simulate the behavior of polymers in extruders. Before the actual processing of polymers, their melting and mixing behaviors, chemical reactions, cross-linking and degradation are verified in an internal mixer [113]. This step, which involves small amounts of materials, offers an economic and efficient method of testing rare and expensive materials and can provide insights into quality of parts to be fabricated. Internal mixers are usually equipped with a torque meter and a thermal couple. Through the torque and temperature data, the melting and mixing qualities of tested materials are readily estimated.

Many researches have used internal mixer data to find the physical and chemical phenomena related to melting, mixing and reaction processes. Through numerical simulation, Jongen [114] and Ghoreishy, et al. [115] have demonstrated that different geometry or shape of chamber and blades affect the efficiency of the process. Zalc, et al. [116] suggest that the lower flow rates produced more effective mixing at a smaller energy cost in static mixers. Goodrich and Porter [117], Serpe et al. [118] and Bousmina [119] have

developed models and experimental procedures for indirect or direct estimation of shear rate and viscosity using internal mixer rotor speed and torque data. However, little effort has been directed at developing techniques and methodologies for determining the melting and mixing quality online in order to optimize the process and reduce the cost.

2.3 Process diagnosis

In order to feedback process dynamic information and material property to control process efficiency and product quality, diagnosis of process parameters is needed. As mentioned in chapter 1, the methods of process diagnosis can be summarized as direct and indirect diagnosis. In this section, we introduce common process parameters and diagnostic techniques used by the industry, to be later compared with those of ultrasonic technique. General descriptions of these diagnostic techniques are provided below; however, their installation and application details will be given in chapters 4 to 6.

2.3.1 Pressure and temperature measurements

Melt pressure and temperature, measured by pressure and temperature sensors, are the most common process parameters used in polymer IM processes [10, 12-13, 120-121]. The piezo-resistive pressure sensors are usually used for hydraulic pressure measurements, while piezo-electric ones are for the mold or melt flow path measurements [6]. Thermocouples are also widely used to monitor different temperature levels in the IM process. These two kinds of instruments are widely used because they are technically mature,

reliable, easy to install and economical. Infrared (IR) technologies for measuring temperature are becoming popular because they are essentially non-contact measurements. In addition, IR probes have a much faster response time than those of standard thermocouples. Therefore, several researches have adopted the IR technologies in measuring polymer process temperatures.

The applications of pressure and temperature measurements during different stages of IM process are described here. In the plastication stage, barrel temperature is measured for the indication of the polymer melting state [122]. The melt quality in the barrel affects the product quality directly. Kamal, et al. [122] studied the dynamics of the pressure at the different points in the IM machine, such as the nozzle and cavity, by installing different pressure sensors. They [123] and Agassant, et al. [124] found that the nozzle pressure is a significant parameter for monitoring the IM process, while the cavity pressure is a direct indicator of the part final quality. Pressure sensing [125] and ultrasonic techniques [126, 127] can be employed for monitoring the flow advancement. In the filling stage, investigating the injection speed by monitoring the flow advancement can avoid damaging mold and flash of part. In the holding stage, when molded parts start to solidify, switch-over time and cavity pressure have impacts on the completeness of the part, weight and flash formation. The solidification and detachment of the molded part is related to its cooling efficiency, while the quality is affected by the melt temperature (i.e. its profile across molded part, and between the cavity walls).

Researches indicate that it may be feasible to assess the process dynamics through measurements of pressure and temperature under certain

circumstances. However, in most cases, that may not be practical since sensors have to be mounted inside the mold cavity. This may cause a detrimental effect on parts, which require high tolerances and good surface finish. Additionally, in the case of melt temperature, the insulating properties of the polymer and the need for the thermocouple to be immersed in the melt stream to have accurate measurements make it difficult for thermocouples to work effectively. Utilization of the IR technique is often discouraged, as one needs special hardware to have direct access to the polymer. Difficulties also arise from errors in collecting, interpreting, and analysis of the IR signals. The data collection errors are largely attributable to low conductivity, radiation, and optical properties of polymers [30].

The pressure and temperature sensors used in the NRC lab to support the research in this thesis are of three types. First, for temperature measurement, the K-type thermocouple is used. The second one is the Kistler 6190A sensor (Kistler Instrument AG, Winterthur, Switzerland), shown in Fig. 2-2. This sensor, having a front diameter of 4mm, is used to measure mold cavity pressure and temperature. The pressure acts over the entire front of the sensor and is transmitted to a quartz-measuring element, which produces a proportional electric charge. This charge is converted into a voltage from 0 to10 V and is made available as an amplifier output. The measured pressure range is from 0 to 200MPa. The contact temperature of the melt is measured on the front of the sensor by a pair of type K thermocouples. The measured temperature at front of the sensor is limited to 450°C. The front of sensor cannot be machined [128]. This sensor will be used in IM and COIM in chapter 4.

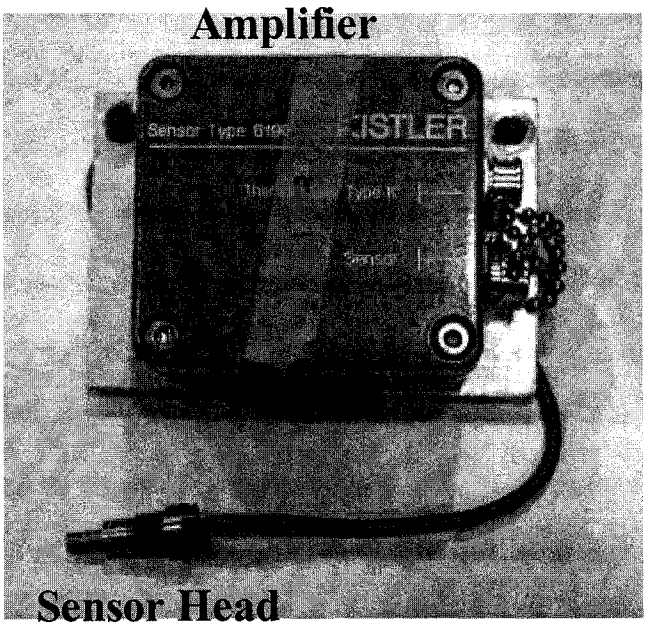

Fig. 2-2 Photograph of a pressure and temperature sensor with amplifier box from Kistler (6190A).

The third sensor type is the PCI-4011 and 4006 (Dynisco PCI-4011 and PCI-4006), shown in Fig. 2-3. These two are piezo-load transducers for cavity and injection pressure measurement. The PCI-4011 and PCI-4006 one is 11 and 6mm in diameter, respectively, and can work respectively in a force range of 0~10N and 0~2.5N, in temperatures ranging from –40 to 200°C [129]. These sensors will be discussed in Chapter 5, in conjunction with MM processes for polymer, nano-composite and powder materials.

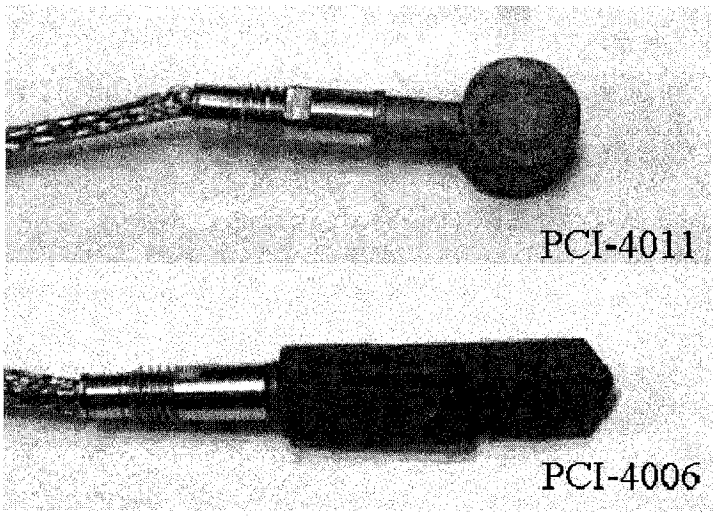

Fig. 2-3 Photographs of pressure sensors from Dynisco (PCI-4011 and 4006).

2.3.2 Torque measurement

Torque is a mechanical parameter associated with the functional performance of the rotating machinery, such as engines, motors, turbines, pumps, and threaded fasteners. Measuring this quantity accurately is essential for determining a machine's efficiency and for establishing operating regimes that are both safe and conducive to long and reliable services. In-line measurement of this quantity in polymer processing machines (i.e. extruder and internal mixer) enables real-time control, helps to ensure consistency in product quality, and can provide early indications of impending problems[130]. Therefore, the need for accurate torque measurement is increasing [131].

Torque is measured by either sensing the actual shaft deflection in response to a twisting force, or by detecting the effects of this deflection. Early torque sensors consisted of mechanical structures fitted with strain gages. Their high cost and low reliability kept them from gaining broad industrial

acceptance. Use of modern technologies, such as rotating strain gages, stationary proximity, magneto-strictive, and magneto-elastic sensors, has lowered the cost and increased the accuracy and reliability of torque meters. Torque measurement can determine the amount of power, which the driving source generates or the driven load consumes. Kristensen, et al. [132] reported that the torque measurements can be used to control the production of pellets. In [133] they demonstrated that keeping variations of the torque in a narrow band can produce pellets of the same size on a direct pelletization process.

In the case of polymer processing machines, such as extruders and internal mixers, torque measurements represent the overall friction or viscoelastic forces acting on the machine shaft during the melting and mixing processes. The extruder shaft consists of feeding, compression, melting and metering segments. The rheological states of the polymer during the melting and mixing processes can be identified according to these segments. Shih, et al. [15] defined the rheological states of polymers during the melting process in the internal mixer as elastic solid pellets, deformable solid pellets, transition materials, and viscoelastic fluid. Wetzel, et al. [134] defines them during the extrusion process by adding additional material into the static processing state. The processes include complex elastic and viscous phenomena of polymers. The torque value varies with the forces required to melt and mix polymer and the rheological state of polymer. Therefore, it can be used to represent the viscosity of the polymer during the process.

The torque meter (C.W. Brabender) employed in the lab for this thesis is shown in Fig. 2-4. The strain gage is mounted on the shaft of the driving motor,

and converts the driving force to the measured torque value. This meter will be used for melting quality diagnosis in chapter 6.

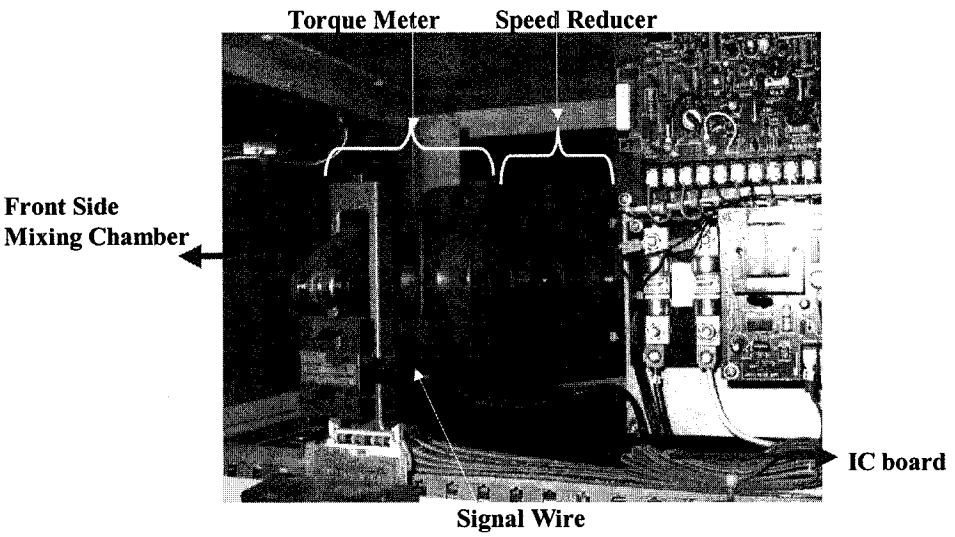

Fig. 2-4 Photograph of a driving motor with a torque meter inside the internal mixer (C. W. Brabender).

2.3.3 Optical and fluorescent detection measurements

In-line optical sensing technique is also popular in the polymer process diagnosis. This technique is based on transmitting light to the melt / resin through a sapphire window positioned flush with the wall of the mold cavity or barrel surface. Variations in the light intensity during the process are used to measure different process parameters. The fluorescent detection technique is based on adding a fluorescent dye to the investigated material. It uses fluorescence radiation to monitor the process and material parameters. The variation of the light intensity and wave length of the fluorescence signal are used for monitoring the process.

During the extrusion, the average particle size of polymer blend

materials is obtained by using light scattering [135]. During the IM process, the mold filling, start of solidification, crystallization, part detachment, and part shrinkage are monitored by optical techniques [136]. Fluorescent dyes are mixed into the polymer resin and the strong temperature-dependent emission spectrum of the fluorescent dyes is utilized to measure local temperature, including temperature profiles in the polymer between cavity walls [30, 137]. The fluorescence spectroscopy is employed to monitor the mixing of polymer melts with filler material. It is found that constant fluorescence intensity, as a function of time, is an indication of a uniform mixing [138].

Optical techniques are only applicable to transparent polymers; that is, they are of little help when dealing with opaque polymers. Furthermore, the mold wall must be modified to accommodate a transparent sapphire window for the transmission of the light into the transparent polymer. Moreover, adding fluorescent dyes (additional material) into the polymer melt, even in small concentrations, is not an attractive solution for producing high quality products.

2.4 The needs for and limitations of process diagnostic technologies

As mentioned above, for COIM, GAIM, and WAIM, fabrication processes and formation of internal sandwiches or hollow structures of molded parts are complicated. In order to improve the product quality, real-time process monitoring and control, as practiced by technically advanced industries, are needed. To study system dynamics, IM processes typically possess basic process monitoring instrumentations, such as temperature,

pressure and optical sensors. However, these sensors are usually not well-suited for the afore-mentioned complex fabrication processes. They provide insufficient information on the internal boundary of the layered or hollow components as well as dimension and thickness of core layers and hollow structure or wall of the molded parts, which can be critical to part performance and process cost. Previous research on COIM, GAIM and WAIM processes were reviewed above. Evidently, little effort has been spent on evaluating the part quality in real-time. Current methods to evaluate the parameters of interest are currently limited to visual or off-line techniques. In these methods, the parts need to have transparent skin or, following ejection, a part is periodically selected and cut to measure the layer/wall thicknesses at desired locations. Such monitoring methods, which involve either special transparent windows or destruction of parts, are basically manual and are not sufficiently fast to make timely adjustments to the process parameters, once deterioration in product quality is detected.

For micro-fabrication processes, the small product size necessitates reduced mold size and brief manufacturing process time. The materials, therefore, need to be selected and modified in advance in order to meet microstructures process requirements within their brief process time. Because of this complexity, it is desirable to have real-time process monitoring and control, aimed at improving the quality of the molded part and optimizing the process. At the same time, the limited space of the mold as well as the stringent quality requirement of the final products, with their highly detailed microstructures, will increase the difficulty of designing and implementing the required process control system.

At present, only a few temperature and pressure sensors for monitoring and control of molding process, whose sizes may be suited to the mold cavity of MM, are commercially available. For instance, a 6183AE pressure sensor (Kistler Instrument AG, Winterthur, Switzerland), having a probing head diameter of 1mm, may be applicable to MM, depending on mold configuration and cavity dimensions. However, pressure sensors installed at the cavity surface are known to underestimate the true melt pressure, due to the influence of the layer of frozen material at the cavity wall. In addition, temperature sensors can only measure the surface (or contact) temperature of a molded part. Because of their drawbacks, these techniques have not been used in monitoring the condition of an entire part (including its internal properties) or for providing full information on the process state.

For IM process, the polymer melts through the extrusion process. In order to improve the quality of final products in the mold, it is important to monitor the polymer in the barrel during the melting process. The melting process in extruder can be simulated in the internal mixer. In the internal mixer, the melting stages, as determined by torque and temperature sensors, are longer than those in the actual situation. Thus, using the internal mixer results as a reference for actual fabrication may cause material degradation and/or increase the product's cost. Furthermore, the torque measurement represents the integrated information from all segments of the extruder; that is the total material under processing. It may not be able to sense local phenomena, such as air bubble or presence of partially-melt pellets.

Therefore, in addition to the temperature, pressure, optical and torque sensors, the integrated HT ultrasonic sensors and ultrasonic delay line probe proposed in this thesis are our candidates to diagnose the properties of materials during the IM processes. The goal of this thesis is to demonstrate that integrated HT ultrasonic sensors and ultrasonic delay line probe are suitable for real-time, nondestructive diagnosis of IM processes, and can be used to enhance process efficiency and part quality.

2.5 Summary

The IM processes, such as IM, COIM, GAIM, WAIM, IMMF, MM for polymer, nano-composite, and ceramic materials, for fabrication plastic products are described. The procedures of IM process include forcing the melt polymer into a mold cavity with a special design shape, cooling the molded part and ejecting it out. During the process, there is a possibility to generate part defects including short shots, voids and sinks, and shrinkage, etc.

COIM, GAIM and WAIM are the techniques to manufacture the multi-layer or hollow structure plastic products by using recycled, low-cost materials or injecting air or water during filling process to improve part performance, reduce cycle time and lower part production cost. However, due to the complex control and forming procedures involved in these technologies, advanced process diagnosis and control are necessary to perform process optimization and obtain high product quality.

IMMF and MM processes have the capability to produce micro parts

with precise dimensions, strict tolerances, high aspect ratios for biomedical, optical and telecommunication applications. The narrow process window and high product quality requirement in these applications re-emphasize the importance of process diagnosis and control. However, machining limitations and mold space restrictions further complicates their adoption as diagnosis sensors.

Pressure, temperature, torque, optical and fluorescent detecting techniques can indicate certain dynamic changes in process parameters, including viscosity, heat flow, and mechanical force. However, their implementations are limited by the need to drill a hole, have direct contact with or add a foreign material into the processed material, measure local variations, or have a transparent window. Furthermore, when the target system lacks enough space for installing the sensors, at the expense of performance and product quality, the sensors' designs need to be modified in order for the sensors to be fitted into available space. Therefore, there is an urgent need for high performance, low cost, miniature sensors that are able to meet the criteria of various polymer IM processes.

Chapter 3

Ultrasonic measurement technique: Principles, sensors and systems

3.1 Introduction

Ultrasonic signatures reflect physical and rheological properties of materials, process dynamics, material dynamics, process parameters and product qualities. Therefore, they are utilized for process diagnosis in the thesis.

As mentioned in chapter 1, a conventional UT can operate properly at temperatures below 50°C without using a cooling system. This is true only when the UT is mounted on a flat surface. When mounted on a curved surface, even with addition of a cooling system, the UT may still exhibit poor performance, as ultrasonic energy does not transmit effectively through curved surfaces, given its plane and non-flexible probing ends. In addition, commercially available and widely-used HT ultrasonic couplants generate noises which deteriorate SNR of the ultrasonic signals. Furthermore, the ultrasonic couplants have to be regularly replaced as the HT causes their sealing lubricants to evaporate, which renders them ineffective. Thus, developments of new ultrasonic sensors that can overcome current difficulties are highly desired. Piezoelectric ceramic film HTUTs developed at IMI/NRC [53, 54] are suitable for operating at HT (>200°C), and can be mounted on curved surfaces and in constricted areas. Therefore they could be used for IM process diagnosis, including actual industrial processes at HT.

In this chapter, first, ultrasonic measurement principles and systems for obtaining ultrasonic signatures are described. High speed data acquisition system for real-time ultrasonic measurements is also presented. In addition, details of an off-line ultrasonic PVT measurement system [26], used to obtain ultrasonic

signatures of polymers for predicting and interpreting the polymer state during the molding process is provided. Then, a fabrication method for production of piezoelectric ceramic film HTUTs is described [54]. Finally integrated HT ultrasonic sensors that use the film HTUTs, and are specially designed and developed for the research reported in this thesis are presented. The performance of the ultrasonic sensors, developed and customized for each IM machine and process, is also evaluated and presented.

3.2 Ultrasonic measurement principles and systems

3.2.1 Measurement principles

An ultrasonic echo propagating through a material can be utilized to measure material properties and property alterations throughout the testing process [17]. The ultrasonic echo transmitted is seen as a plane wave. This propagating model can be in pulse-echo (reflection) or transmission mode. The pulse-echo mode adopts one UT to radiate and receive ultrasonic signal for testing target, while transmission mode uses two UTs. The pulse-echo mode is utilized for all of the real-time IM processes diagnosis, and will be discussed first.

Pulse-echo mode

Fig. 3-1 (a) and (b) show the schematic drawings of ultrasonic propagation through the mold and testing material in pulse-echo mode, and the amplitude of ultrasonic echoes with respect to their related propagating time delays, respectively. The thicknesses of mold and testing polymer are H and h, respectively. The initial ultrasonic amplitude value is A_0. Along the propagating direction, there are losses or absorption of ultrasonic energy from the mold and testing polymer. When the ultrasonic echo reaches the interface between mold 1 and testing polymer, the ultrasonic echo A_1 at the interface is [26, 139-140]:

$$A_1 = A_0 e^{-\alpha_M H} e^{j\omega(t-H/V_M)} \qquad \text{(Eq. 3-1)}$$

where

α_M is the ultrasonic attenuation in the mold

$\omega = 2\pi f$, f is the ultrasonic frequency

V_M is the ultrasonic velocity in the mold

t is the time.

Equation 3-1 is valid for both longitudinal and/or shear wave, provided α_M and V_M are chosen accordingly. However, the longitudinal wave is chosen for process diagnosis in most of the experiments in the thesis.

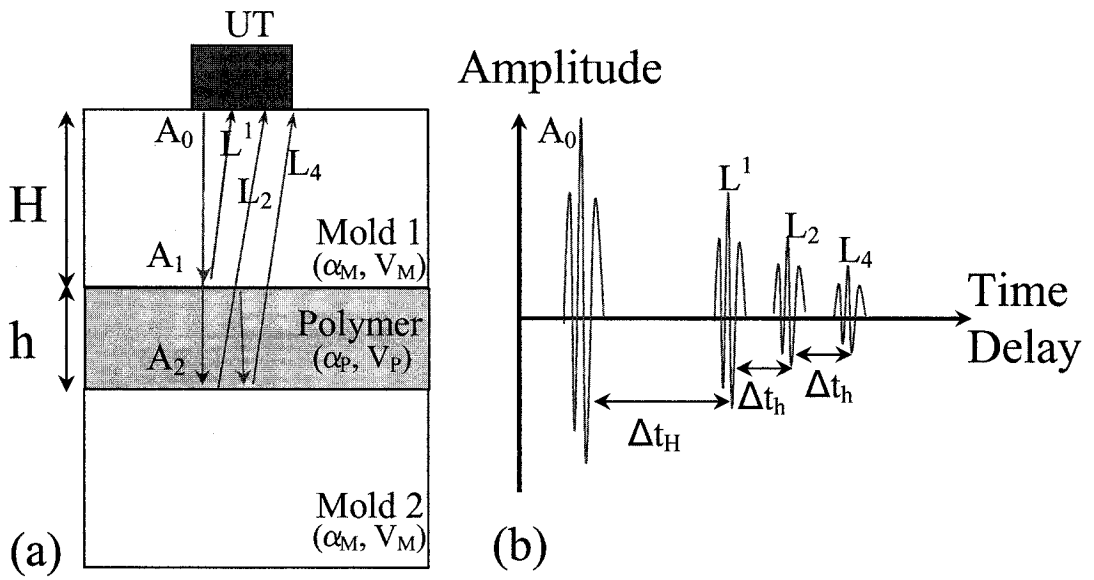

Fig. 3-1 (a) Schematic drawing of ultrasonic propagation in pulse-echo mode, and (b) the amplitude of ultrasonic echoes with respect to the related propagating time delays.

At the mold 1 / testing polymer interface, part of the ultrasonic energy is reflected back to the mold 1, referred as the reflected echo, and part is transmitted into testing polymer, referred as the transmitted echo. They can be noted as reflection (R) and transmission (T) coefficients, respectively, by:

$$R_M = (Z_M - Z_P)/(Z_M + Z_P) \qquad \text{(Eq. 3-2)}$$

$$R_P = (Z_P - Z_M)/(Z_P + Z_M) \qquad \text{(Eq. 3-3)}$$

$$T_P = 2Z_P/(Z_M + Z_P) \quad \text{(Eq. 3-4)}$$

$$T_M = 2Z_M/(Z_M + Z_P) \quad \text{(Eq. 3-5)}$$

where

R_M and R_P are the reflection coefficients which the ultrasonic echo reflects back to mold (1 and 2) and testing polymer, respectively. Here molds 1 and 2 are of the same material and depth.

T_P and T_M are the transmission coefficients which the ultrasonic echo transmits from mold (1 and 2) to testing polymer and from testing polymer to mold (1 and 2), respectively.

Z_M and Z_P are the acoustic impedance of mold (1 and 2) and testing polymer, respectively.

The acoustic impedances from Eq. 3-2 to 3-5 can be expressed as:

$$Z_M = \rho_M V_M(1 + j\alpha_M V_M/\omega) \quad \text{(Eq. 3-6)}$$

where ρ_M is the density of material M.

Eq. 3-6 is a complex quantity. Therefore, it is apparent that Eq. 3-2 to 3-5 are complex quantities. When the reflected echo arrives to the ultrasonic transducer, the reflected echo can be expressed as:

$$L^1 = R_M A_0 e^{-2\alpha_M H} e^{-j\omega 2H/V_M} e^{j\omega t} \quad \text{(Eq. 3-7)}$$

The amplitude and phase angle of L^1 can be expressed by:

$$\left|L^1\right| = \mathrm{mod}(R_M) A_0 e^{-2\alpha_M H} \quad \text{(Eq. 3-8)}$$

$$\phi = \tan^{-1}\left[im(R_M)/re(R_M)\right] - 2\omega H/V_M \quad \text{(Eq. 3-9)}$$

where

$\mathrm{mod}(R_M)$ represents the modulus of the complex variable R_M

$im(R_M)$ and $re(R_M)$ are the imaginary and real components of R_M.

The ultrasonic echo A_2, which is transmitted into the testing polymer and reaches to the testing polymer / mold 2 interface, can be expressed as:

$$A_2 = T_P A_0 e^{-\alpha_M H} e^{-j\omega H/V_M} e^{-\alpha_P h} e^{-j\omega h/V_P} e^{j\omega t} \quad \text{(Eq. 3-10)}$$

where

α_P is the ultrasonic attenuation in the testing polymer

V_P is the ultrasonic velocity in the testing polymer

h is the thickness of the testing polymer

The ultrasonic echo L_2, which is reflected at the testing polymer / mold 2 interface and reaches to the transducer, can be expressed as:

$$L_2 = T_M R_P T_P A_0 e^{-2\alpha_M H} e^{-j\omega 2H/V_M} e^{-2\alpha_P h} e^{-j\omega 2h/V_P} e^{j\omega t} \quad \text{(Eq. 3-11)}$$

The ultrasonic echo L_4, which is round-trip reflected at the testing polymer / mold 2 interface and reaches the transducer, can be expressed as:

$$L_4 = T_M R_P^3 T_P A_0 e^{-2\alpha_M H} e^{-j\omega 2H/V_M} e^{-4\alpha_P h} e^{-j\omega 4h/V_P} e^{j\omega t} \quad \text{(Eq. 3-12)}$$

The amplitude of initial and reflected ultrasonic echoes can be presented in Fig. 3-1 (b) with respect to their related propagating time delay. The time delays between A_0, L^1, L_2 and L_4 echoes are Δt_H, Δt_h, and Δt_h, respectively. The ultrasonic velocities in the mold and testing polymer can be calculated by:

$$V_M = 2H/\Delta t_H \quad \text{(Eq. 3-13)}$$

$$V_P = 2h/\Delta t_h \quad \text{(Eq. 3-14)}$$

The ultrasonic velocity in the material is a function of material characteristics, temperature and pressure.

The ultrasonic attenuation of testing polymer can be calculated by the amplitude ratio of L_2 and L_4 echoes, by:

$$\alpha_P = \left[\ln(\mathrm{mod}(R_P^2) \times (|L_2|/|L_4|)\right] / 2h \quad \text{(Eq. 3-15)}$$

where $|L_2|$ and $|L_4|$ are the amplitude of L_2 and L_4.

However, during the practical molding process, it is difficult to estimate the acoustic properties such as acoustic impedance of the mold and the testing polymer due to their temperature change, which is necessary to calculate the ultrasonic attenuation in the testing polymer. Hence the attenuation, α, of the amplitudes of the L_2 and L_4 echoes, which is associated with the ultrasonic attenuation in the testing polymer, is calculated by [140, 141]:

$$\alpha = \frac{10}{h}\log_{10}\left(\frac{|L_2|}{|L_4|}\right) \qquad \text{(Eq. 3-16)}$$

Because of the sensitivity of ultrasound to characteristics of testing material and process variation, ultrasonic echo is used to detect any layer interface, defect or void inside the testing sample non-intrusively and non-destructively. Fig. 3-2 (a) and (b) show the schematic drawing of ultrasonic propagation in pulse-echo mode through the testing polymer containing a layer interface, and the amplitude of ultrasonic echoes with respect to their related propagating time delays, respectively. The interface may not be observed from the surface. Therefore, the optical methods may not be able to detect this interface when the sample isn't transparent. When the interface is located on the ultrasonic propagation path, the ultrasonic echo will be reflected or scattered partially by the interface, and the reflected echo L_2' will show on the propagating time delay after L^1. The depth of the interface can be calculated by:

$$h_l = (V_P \times \Delta t_l)/2 \qquad \text{(Eq. 3-17)}$$

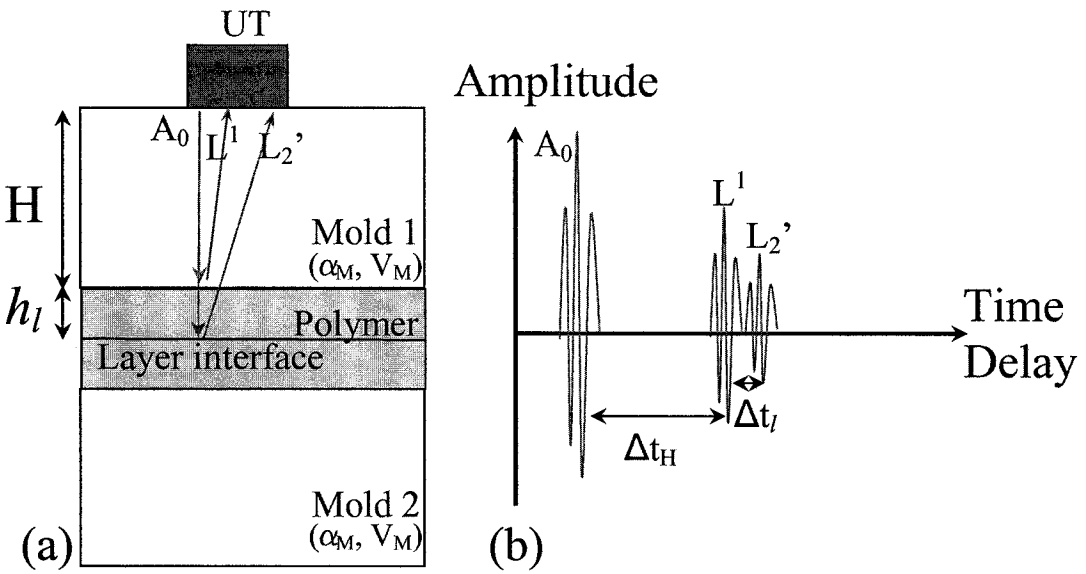

Fig. 3-2 (a) Schematic drawing of ultrasonic propagation in pulse-echo mode. Testing polymer contains a layer interface. (b) Amplitude of ultrasonic echoes with respect to their related propagating time delays.

Transmission mode

In the transmission mode, the ultrasonic echo, which has traversed the full path of the mold and testing polymer from the transmitting transducer to the receiving transducer, is measured. Due to the limited space in most IM machines, this mode may not be suitable for process diagnosis application. In this thesis, this mode is utilized for ultrasonic PVT measurement system. Fig. 3-3 (a) and (b) show the schematic drawings of ultrasonic propagation in transmission mode, and the amplitude of ultrasonic echoes with respect to their related propagating time delays, respectively. Here, UT1 and UT2 are the transmitting and receiving transducers, respectively.

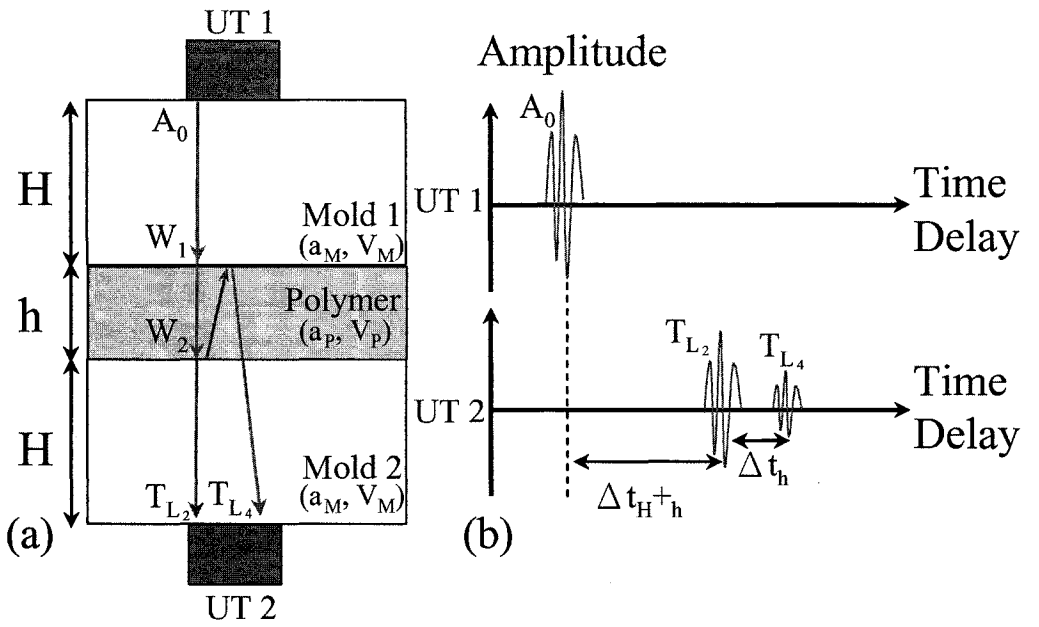

Fig. 3-3 (a) Schematic drawing of ultrasonic propagation paths in transmission mode, and (b) amplitude of ultrasonic echoes at UT1 and UT2 with respect to related propagating time delays.

The setup of mold and testing polymer is the same as that in pulse-echo mode. The ultrasonic echoes A_1 and A_2, which propagate through mode 1 and testing polymer, are expressed in Eq. 3-1 and 3-10, respectively. The ultrasonic echo L_1, which transmits through the polymer / mold 2 interface and reaches UT2, can be expressed as:

$$L_1 = T_M T_P A_0 e^{-2\alpha_M H} e^{-j\omega 2H/V_M} e^{-\alpha_P h} e^{-j\omega h/V_P} e^{j\omega t} \qquad \text{(Eq. 3-18)}$$

The ultrasonic echo L_3, which is round-trip reflected at the testing polymer / mold 1 interface and reaches to UT2, can be expressed as:

$$L_3 = T_M R_P^2 T_P A_0 e^{-2\alpha_M H} e^{-j\omega 2H/V_M} e^{-3\alpha_P h} e^{-j\omega 3h/V_P} e^{j\omega t} \qquad \text{(Eq. 3-19)}$$

The amplitude of initial and transmitted ultrasonic echoes can be presented in Fig. 3-3 (b) with respect to their related propagating time delays. The time

delays between A_0, L_1 and L_3 echoes are Δt_{H+h}, and Δt_h, respectively. The ultrasonic velocities in the testing polymer and mold can be calculated by:

$$V_P = 2 \times h / \Delta t_h \quad \text{(Eq. 3-20)}$$

$$V_M = 2 \times H / (\Delta t_{H+h} - \Delta t_h / 2) \quad \text{(Eq. 3-21)}$$

The ultrasonic attenuation of testing polymer can be calculated by amplitude ratio of L_1 and L_3 echoes, by:

$$\alpha_P = \left[\ln(\mathrm{mod}(R_P^2) \times (|L_1| / |L_3|)\right] / 2h \quad \text{(Eq. 3-22)}$$

where $|L_1|$ and $|L_3|$ are the amplitude of L_1 and L_3.

Again, during the practical process, the attenuation, α, of the amplitudes of the L_1 and L_3 echoes, which is associated with the ultrasonic attenuation in the testing polymer, is calculated by [140, 141]:

$$\alpha = \frac{10}{h} \log_{10}\left(\frac{|L_1|}{|L_3|}\right) \quad \text{(Eq. 3-23)}$$

3.2.2 Data acquisition system

The application of ultrasonic technique on monitoring subsurface has been developed for several decades. However, it is successfully combined with process control strategy for process optimization after the significant improvement of the digital technology and the computers. After this progress, even complex signals may be acquired, recorded and processed in short time duration to achieve on-line process monitoring and control. In some cases, a high acquisition repetition rate (e.g. 1000Hz) is used to monitor short duration process. For example, during filling stage of MM process, the molten polymer may be filled into the cavity in duration of 50ms and the acquired data interval should cover 1ms in which enough process information may be obtained. The development of a PC-based plug-in ultrasonic acquisition system is mentioned in [142]. Here, the updated

acquisition system adopted in this thesis for on-line real-time polymer process diagnosis will be introduced.

Fig. 3-4 shows a schematic view of an IM mold fitted with the ultrasonic sensors and data acquisition system using an ultrasonic pulse-echo technique. The ultrasonic data acquisition system is composed of two pulser-receivers (Panametrics Inc., 5072PR, Waltham, MA), a 12-bit dual-channel digitizing board (Gage Applied Science Inc., Montreal, QC, Canada), a frequency generator (Standard Research Systems, DG535, Sunnyvale, CA), an optional oscilloscope (Tektronix 2246, Markham, ON, Canada) and a Pentem-III personal computer with a data acquisition and analysis program by LabVIEW. The normal acquisition rate is 100Hz. However, it can be adjusted according to the requirement of process diagnosis.

The pulser-receiver is a broadband, negative spike pulser, and broadband receiver. It can be applied in reflection or transmission mode. The digitizing board has the maximum sampling rate of 100MHz for single channel and 50MHz for dual channels. It has 8MB on-board memory and 12 bits A/D resolution. The frequency generator is used to generate a synchronizing signal with the desired frequency to synchronize all the devices, including the oscilloscope, two pulser-receivers and digitizing board. Through this, one can control the acquisition rate. The two pulser-receivers and the digitizing board are operated in the external trigger mode and to achieve the synchronization. The range of acquisition rate is from 0.001 to 1MHz for this frequency generator (DG535). The oscilloscope is used to monitor the signals in real time.

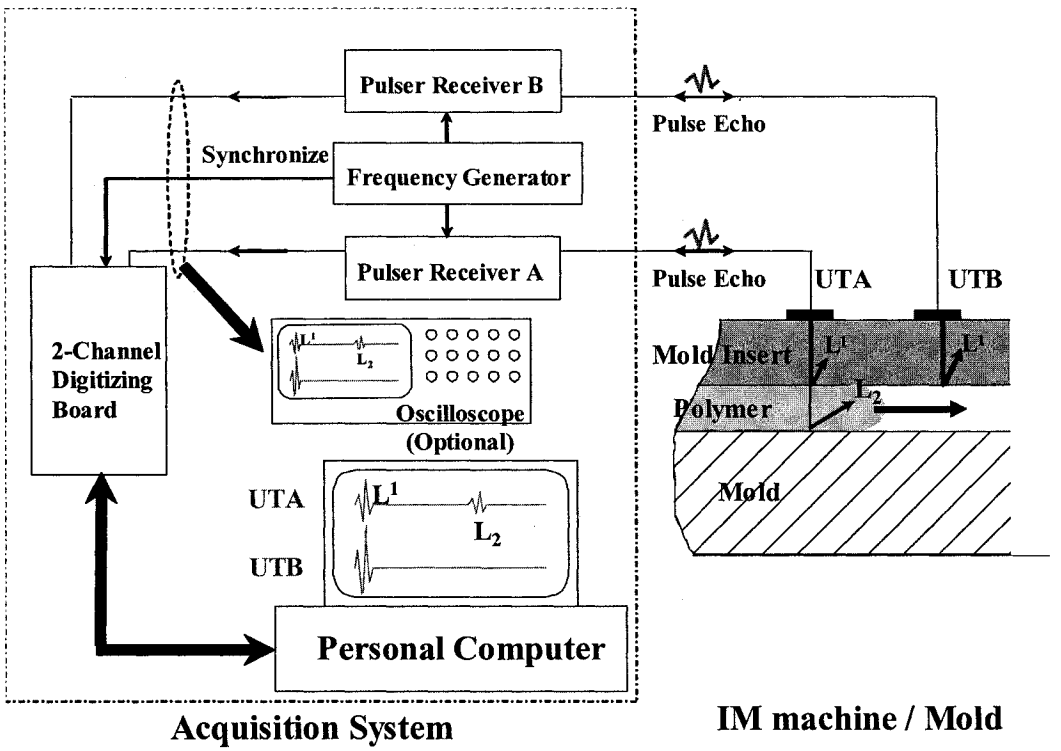

Figure 3-4 Schematic view of mold in IM machine with UTs and data acquisition system for ultrasonic diagnosis of IM process using ultrasonic pulse-echo technique.

The virtual instrument on Windows environment using Labview software is used to design the entire acquisition system. By using Labview, the users can easily build instrument systems with standard computers and cost-effective hardware. These software-centered systems combine the computation, display and connective capabilities of computers to provide the robust and flexible instrumentation functions. Fig. 3-5 and 3-6 show the panel diagrams of the virtual scope of the two-channel acquisition and analytic programs employed for the experiments, respectively. Acquisition configurations, such as operation mode, triggering and data recording requests can be easily set up as a conventional instrument with user friendly interfaces. Integrating with the high-speed digitizer board, the system works well as a wide bandwidth oscilloscope. The functions of the system can be modified easily to meet different situations with the graphical programming method.

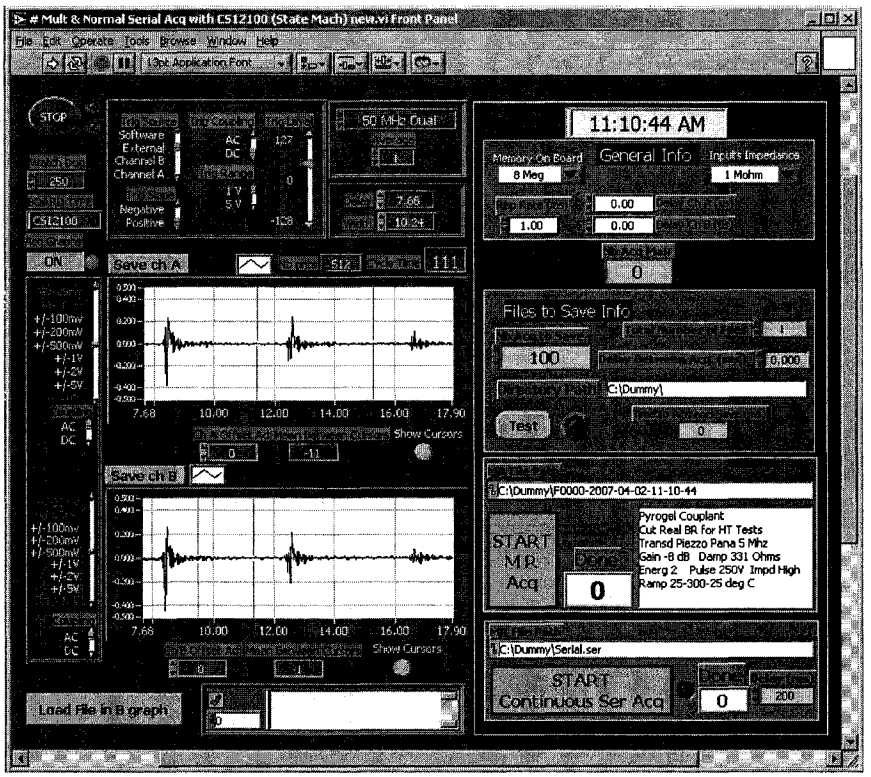

Fig. 3-5 Panel diagram of the virtual scope of the two-channel acquisition system employed for the real-time polymer process diagnosis.

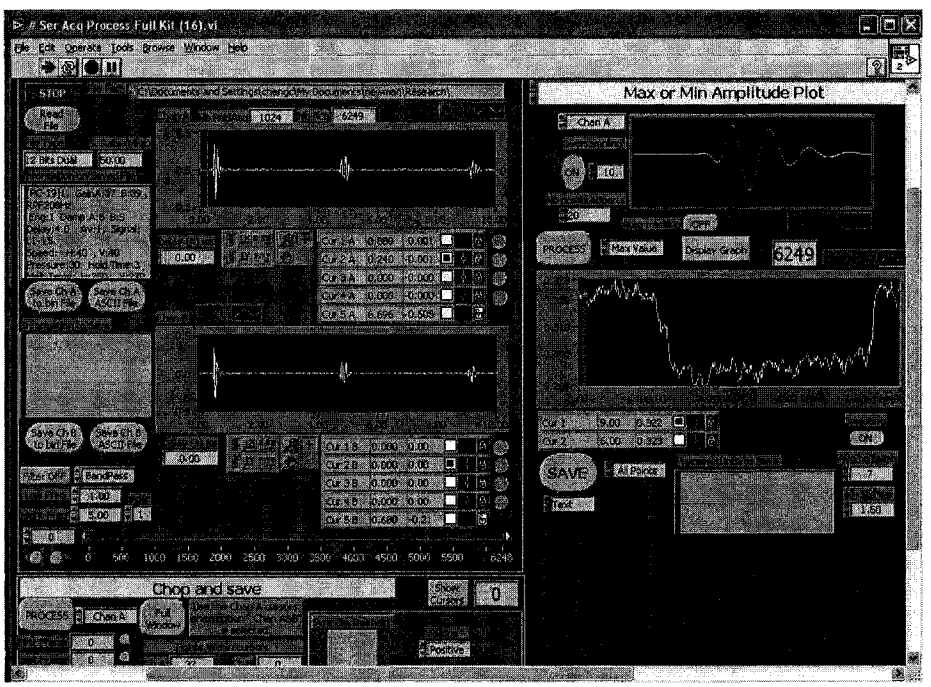

Fig. 3-6 Panel diagram of the two-channel analytic program employed for the analysis of process diagnosis results.

3.2.3 PVT measurement system

In order to predict and interpret the state of the polymer inside the mold using the ultrasonic signatures obtained during process, we have conducted off-line measurements of ultrasonic properties of the polymers using an ultrasonic pressure-volume-temperature (PVT) measurement system [26]. This system can measure the specific volume, ultrasonic velocity and ultrasonic attenuation of the polymeric materials simultaneously with a function of temperature and pressure. Fig. 3-7 shows a photograph of the ultrasonic PVT measurement system with the testing module and data acquisition system. The data acquisition system can acquire the profiles of the ultrasonic signatures, pressure, temperature, and volume of tested specimen.

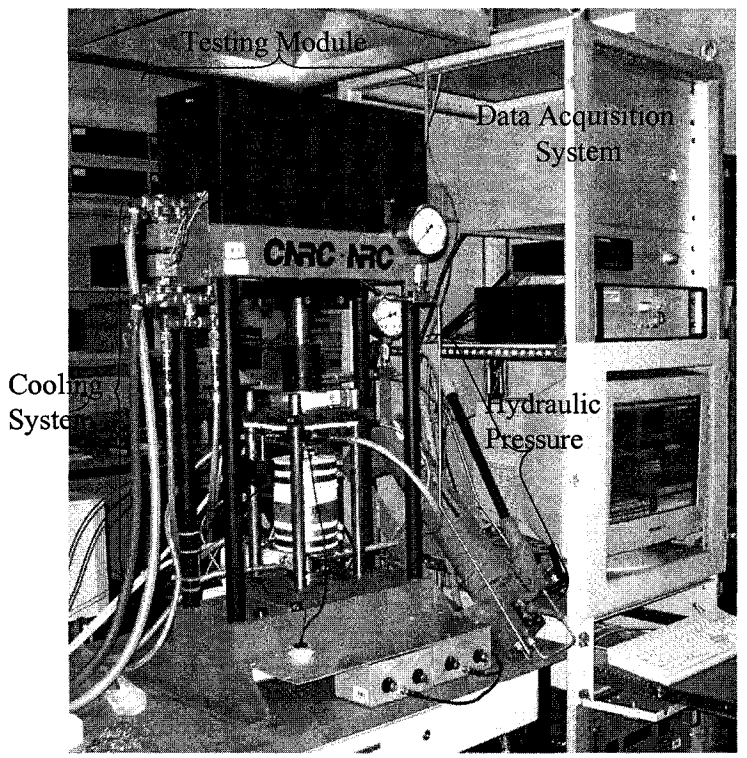

Fig. 3-7 Photograph of the ultrasonic PVT measurement system with the testing module and data acquisition system.

Fig. 3-8 presents a cross-sectional schematic drawing of the testing module of the ultrasonic PVT measurement system, including ultrasonic transducers, buffer rod, a Linear-Voltage-Differential-Transformer (LVDT) for position measurement, thermostat and thermometer. The ultrasonic transducers are made of lithium niobate ($LiNbO_3$) crystals. Their central frequency is 2.5 MHz in the transmission mode. The dimensions of steel buffer rod are 25.4mm in diameter and 153mm in length. For measuring the thickness of the polymer sample during testing, a LVDT is attached to a guiding column and includes a probe element movable with the plate for sensing the position. The range and changing slope of temperature and pressure measurement are described in Table 3-1. The weight of each testing sample is around 4 to 5g.

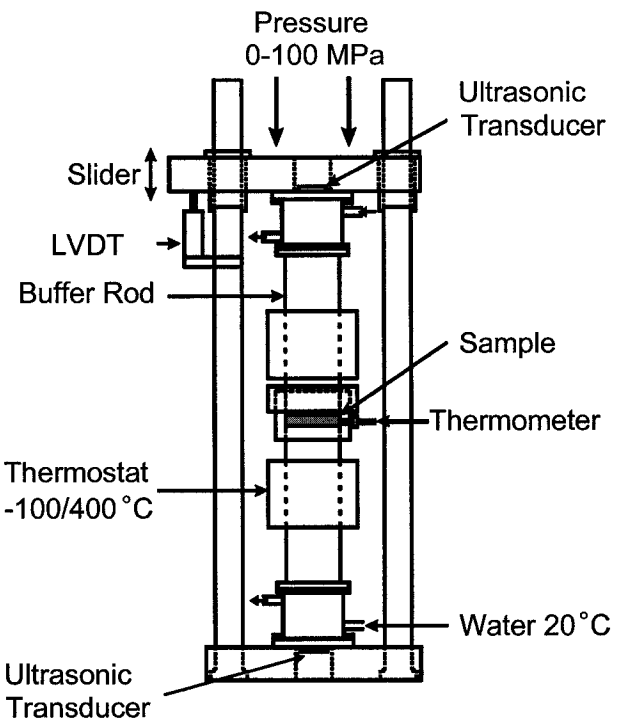

Fig. 3-8 Schematic drawing of the testing module of the ultrasonic PVT measurement system.

Table 3-1 Specifications of temperature and pressure measurement.

Items	Range	Changing slope	Accuracy
Temperature	-150 ~ 400°C	0.015 ~ 50 °C/min	±1°C
Pressure	0 ~ 200 MPa	0.1 ~ 1 MPa/min	±1.5MPa

The information concerning the thermal and pressure history of the experimental conditions is entered in the computer. The system needs to calculate the initial states of the measured quantities, such as pressure (P), temperature (T), thickness, ultrasonic referenced velocity and attenuation. Then, the computer initiates, runs and controls the experiment in the prescribed manner. Simultaneously, the computer also acquires and stores the pertinent data mentioned above. The recorded data, such as specific volume, ultrasonic velocity and attenuation can be plotted versus either temperature (T) or pressure (P) and presented on the computer's screen. The equations established for calculating the ultrasonic velocity (V) and attenuation (α) in transmission mode are presented in section 3.2.1.

3.3 Piezoelectric ceramic film HTUTs

As mentioned in chapter 1, several fabrication methods for film HTUT have been developed recently. These films HTUTs are mainly composed by the piezoelectric ceramic materials. These ceramic materials have the characteristics of high Curie temperature and piezoelectricity. They are suitable for desired HT ultrasonic sensors. This kind of piezoelectric ceramic films (thickness >40 μm) can be made by the technologies of jet printing [143], screen printing [144], dipping [145], tape casting [146], etc. However, they may not meet all the requirements mentioned in Chapter 1. Here, an attractive sol-gel spray technique is used, which was firstly developed at Queen's University [147]. In this technique, the piezoelectric particles are dispersed in the sol-gel solution for producing thick piezoelectric film [148-150]. The ceramic piezoelectric film can

be composed by piezoelectric materials, such as PZT ceramics, BIT powder or lithium titanate crystals [148-150]. Here, the fabrication procedure related to the BIT powder is illustrated. The difference between BIT and PZT films is their Curie temperature as well as their piezoelectric strength. Convenient electric poling and top electrode deposition methods will be employed.

A flow chart of the fabrication procedure of film HTUT by a sol-gel spray technique is shown in Fig. 3-9. The piezoelectric BIT powder is purchased with an average diameter of 50μm and dispersed into self made PZT solution by ball milling method to achieve the gel (step S1). The final diameter of the BIT powder is estimated to be less than 1μm. An air gun is then used to spray the sol-gel BIT/PZT composite directly onto metallic substrates [149-152] having a flat or curved surface as shown in Fig. 3-10(a) (step S2). In this thesis, BIT film is used to represent BIT/PZT composite. With this technique, the BIT films can easily be produced at desired locations through a shadow mask made of even paperboard. After spray coating, thermal treatments such as drying, firing and annealing are carried out at temperatures of 90, 430 and 650°C, respectively, with the optimal time duration (step S3). Multiple layers are made in order to reach the desired thickness for proper operating ultrasonic frequency by repeating the steps S2 and S3 (step S4).

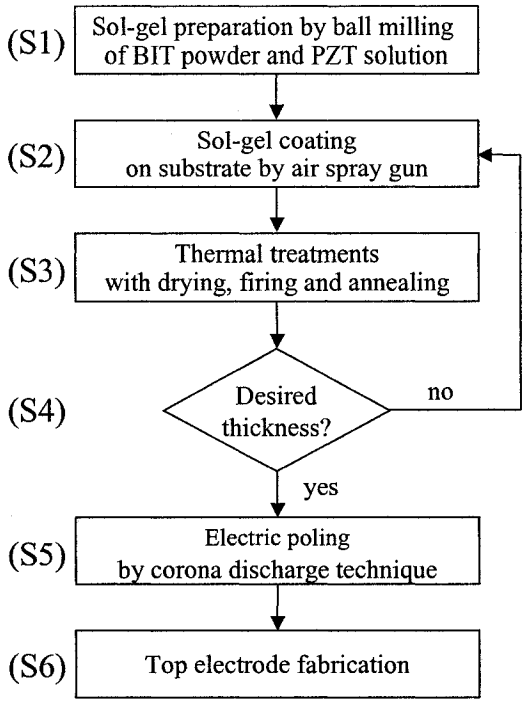

Fig. 3-9 Flow chart showing the fabrication steps of high temperature ceramic film ultrasonic transducers by a sol-gel spray technique.

The films are then electrically poled using a corona discharging technique [151, 152] as shown in Fig. 3-10 (b) (step S5). The corona poling method is chosen because it can pole the thick piezoelectric ceramic film of a large area and on curved surfaces. A high positive voltage (e.g. 25KV) supplied from a high voltage power supply is applied to a needle, which is located several centimeters above the film coated on the metal substrate serving as the ground electrode. The poling time is several minutes. The distance and voltage are optimized for different film thickness and geometries. The temperature of the substrate is between 200°C and 400°C during poling.

Finally a top electrode is fabricated on the BIT film as shown in Fig.3-10 (c) (step S6). We use a silver paste to form the top electrode at room temperature instead of vacuum sputtering reported in [147, 148]. This convenient approach makes the selection of electrode size, which is the sensor size, simple. The silver paste is tested and its operating temperature could be above 400°C. The optimum

diameter of the top electrode for the BIT film ultrasonic sensor in order to obtain the highest signal strength is around 11mm and that for PZT film ultrasonic sensor 6mm [53]. In addition to the signal strength the choice for the size of top electrode for different film also depends on the desired resolution and substrate dimension.

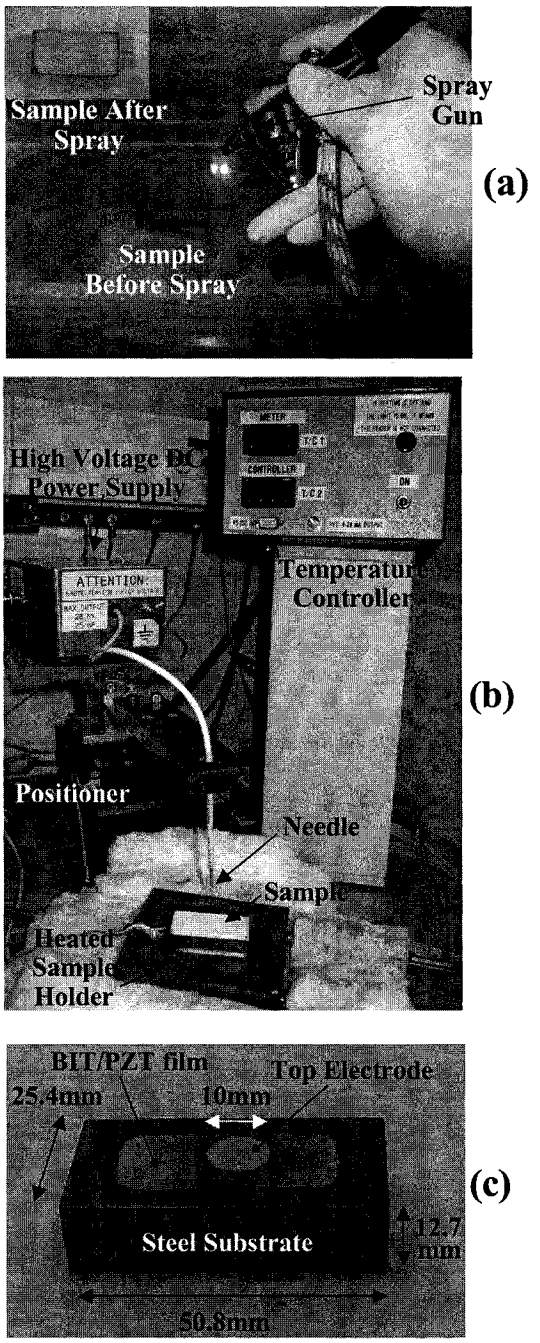

Fig. 3-10 Setup for fabrication of ceramic film UT by a sol-gel spray technique: (a) setup for sol-gel spray; (b) setup for corona poling and (c) 90μm-thick BIT film transducer deposited on steel substrate.

To provide the desired center frequency in the range of 3-30MHz, 40-200μm thick films are produced onto various shapes of substrates such as planar and curved surfaces. This frequency range is commonly preferred for non-destructive evaluation of polymers because of its sufficient ranging resolution and acceptable ultrasonic attenuation in such materials. Here, we only present one HT ultrasonic sensor's performance fabricated onto a 50.8mm-long, 25.4mm-wide and 12.7mm-thick steel substrate shown in Fig.3-10 (c). The thickness of the BIT film is 90μm and the top electrode diameter is 10mm. The BIT film HT ultrasonic sensor in Fig.3-10 (c) is placed on an electric hot plate and heated. The temperature is measured on the top surface of the substrate, 20mm apart from the top electrode, by a thermocouple.

Fig. 3-11 (a) presents an ultrasonic longitudinal wave signals reflected at the substrate-air interface measured in pulse-echo technique at a temperature of 500°C. L^n denotes n-th round trip echo propagating in the substrate. The SNR for the first round trip echo, L^1, is 34dB. The SNR defined in this thesis is the ratio of the strength of the first echo signal traveling one round trip through the thickness direction over that of the spurious noise. Fig. 3-11 (b) shows frequency spectrum of the L^1 echo. The center frequency is 8.5MHz and the 6dB bandwidth is 4MHz. Such performance is sufficient for monitoring of polymer IM processes, for which the melt temperatures are usually less than 400°C [26]. Therefore the achieved characteristics of desired BIT film HT ultrasonic sensor for real-time monitoring of the IM processes are that these ultrasonic sensors (1) are applicable at temperatures higher than 400°C, (2) are miniature, (3) can be coated on curved surfaces, such as steel barrel for polymer IM and extrusion, and flat steel mold inserts, (4) do not need ultrasonic couplant, (5) can be operated in low and medium MHz frequency range with sufficient frequency band width and (6) have sufficient piezoelectric strength and SNR [54].

If piezoelectric PZT powders are used, the fabrication procedures of PZT film (or PZT/PZT composite) ultrasonic sensor is identical to the flow chart

shown in Fig. 3-9. However, the PZT film HT ultrasonic sensors are applicable at temperature only up to 250°C. When the polymers with temperatures less than 200°C, PZT film HTUT is preferred for monitoring because it has higher piezoelectric strength than BIT film one in the low temperature range (< 200°C). The measured relative dielectric constant of the BIT and PZT film was about 80 and 320, respectively. The d33 measured by an optical interferometer is 11 (10-12 m/V) for BIT and 30 (10-12 m/V) for PZT film. The electromechanical coupling constant measured was 0.2 for PZT film and that for BIT/PZT was weaker. [153].

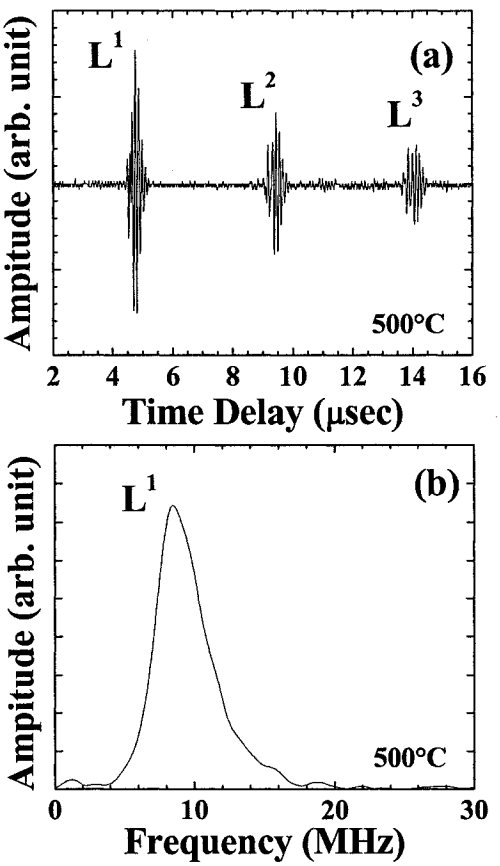

Fig. 3-11 (a) Longitudinal wave ultrasonic signals reflected at the substrate-air interface and (b) frequency spectrum of the L^1 echo, measured at 500°C. L^n (n=1, 2, 3...) denotes n-th round trip echo in the steel substrate.

3.4 Development and evaluation of HT ultrasonic sensors

The film HTUTs have many merits suitable for real-time, non-destructive processes diagnosis of various polymer IM processes described in chapter 2. These polymer processes have different specifications and requirements, such as machine size, mold design, used material, processing procedure, and fabricated products. Their variation could be large, form huge to small, and from simple to complex. In order to meet the criteria of each IM machine and process, the proper design of HT ultrasonic sensors and the desired locations will be quite important. The chosen polymer processes are IM, COIM, GAIM, WAIM, IMMF and MM. The MM processes are mainly conjugated with polymer, nano-composite and ceramic powder materials. The development and evaluation of HT ultrasonic sensors for each machine and process will be introduced; however, their setup descriptions, experimental conditions, and results will be discussed in the following chapters.

3.4.1 IM and COIM

For IM and COIM processes, a rectangular sensor insert is developed by using films HTUTs for process diagnosis. Fig. 3-12 presents the integrated HT ultrasonic sensor inserts without (left) and with (right) electrical connection by using the coaxial cable, which can connect to the pulser-receiver. The coaxial cable is attached to sensor and fixed on the sensor insert by a piece of polyimide (VESPEL, from Du Pond) plate and two screws. The polyimide plate can sustain high temperature up to 300°C, and be an electrical insulator. The core of cable is attached to the top electrode by the polyimide plate. The ground of cable is connected to insert substrate by a screw. The insert substrate is used as the bottom electrode of the ultrasonic sensor.

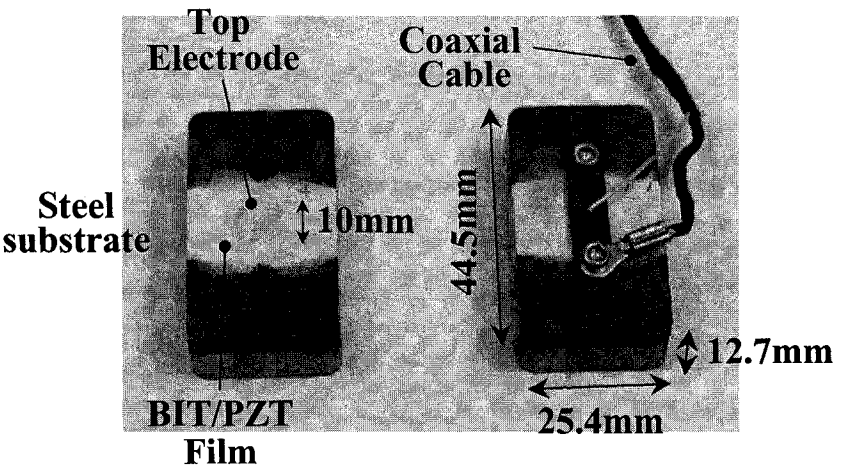

Fig. 3-12 BIT film HT ultrasonic sensor inserts with (right) and without (left) an electrical connection used for monitoring of injection molding process.

Four designed sensor inserts are installed into a mold insert for fabricating a flat IM plate part. Fig. 3-13 (a) and (b) present the mobile mold with four HT sensor inserts embedded in the mold insert in the polymer side and UT side, respectively. In this mold, mold insert and four sensor inserts compose one side of the mold cavity. Mold inserts are commonly used by injection molders, in particular, for multi-cavity molding processes. By replacing the mold insert, the shape and dimensions of the molded part can be easily modified to meet the customer's demands. Our approach of using the sensor inserts in combination with the mold insert is practical for molds of all sizes. This design also demonstrates that sensor array configuration is feasible. The sensor inserts are made of the same type of the steel as the mold and mold insert.

The mold cavity dimension is 76mm-wide, 165mm-long and 1mm-deep for conventional IM process, while 3mm-deep for COIM process. A hole at the center of the mold insert is for the part ejection pin. The bottom surfaces of the sensor inserts are flush with the mold insert surface (cavity surface), as seen in Fig. 3-13 (a). The polymer melt is expected to flow through these four sensor inserts during molding process. Therefore, in order to monitor the behavior of the polymer

inside the mold cavity during the IM process, HT ultrasonic sensors fabricated on the backside of mold insert or sensor inserts are possible places.

Fig. 3-13 (b) presents the backside of the mobile mold with the mold insert, in which four sensor inserts are embedded with electrical connection. The ultrasonic performance of BIT film HT ultrasonic sensor is shown in Fig. 3-11. All the HT ultrasonic sensors have almost the same ultrasonic performance, which indicates that fabrication of the sensors is consistent. A distance between the center of the UT1 (UT3) and UT2 (UT4) is 34.9mm and that of the UT2 and UT3 is 44.5mm as shown in Fig. 3-13 (b). This HT ultrasonic sensor for IM and COIM processes is the prototype developed by using film HTUT for potential industrial applications.

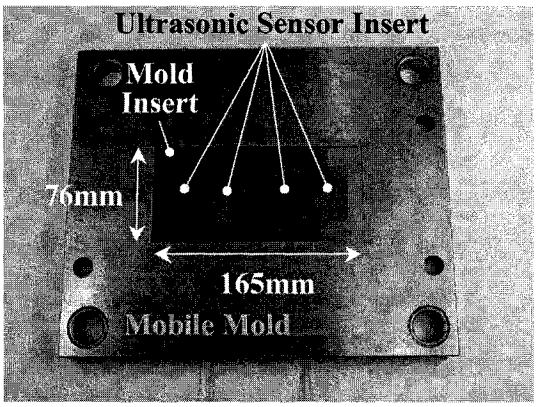

(a) Front View (Polymer Side)

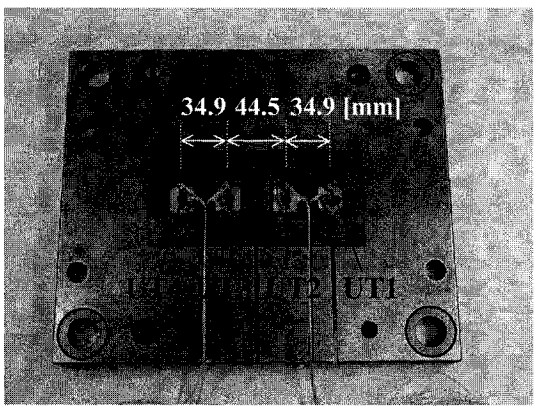

(b) Back View (UT Side)

Fig. 3-13 Mobile mold with four BIT film HT ultrasonic sensor inserts embedded in the mold insert in the (a) polymer side and (b) UT side.

The mobile mold with developed sensor inserts embedded in the mold insert in Fig. 3-13 is installed into the mobile plate of the IM machine, as shown in Fig. 3-14. A 150tons IM machine (from Engel GmbH, Schwertberg, Austria), as shown in Fig. 3-15, is employed for carrying out all the IM and COIM experiments. This IM machine is equipped with horizontal and vertical barrel/screw plasticating units for injecting two materials in the same injection cycle. The horizontal and vertical barrels are ∅40mm and ∅30mm internal diameter with maximum melt delivery rate of 105 and 82ccm/s, respectively. For IM, only the horizontal barrel is employed. But, for COIM, the horizontal and vertical plasticating units are for the injection of skin and core materials, respectively. This designed mold and integrated HT ultrasonic sensors are ready for IM and COIM processes diagnosis applications. The experiments and results will be discussed in chapter 4.

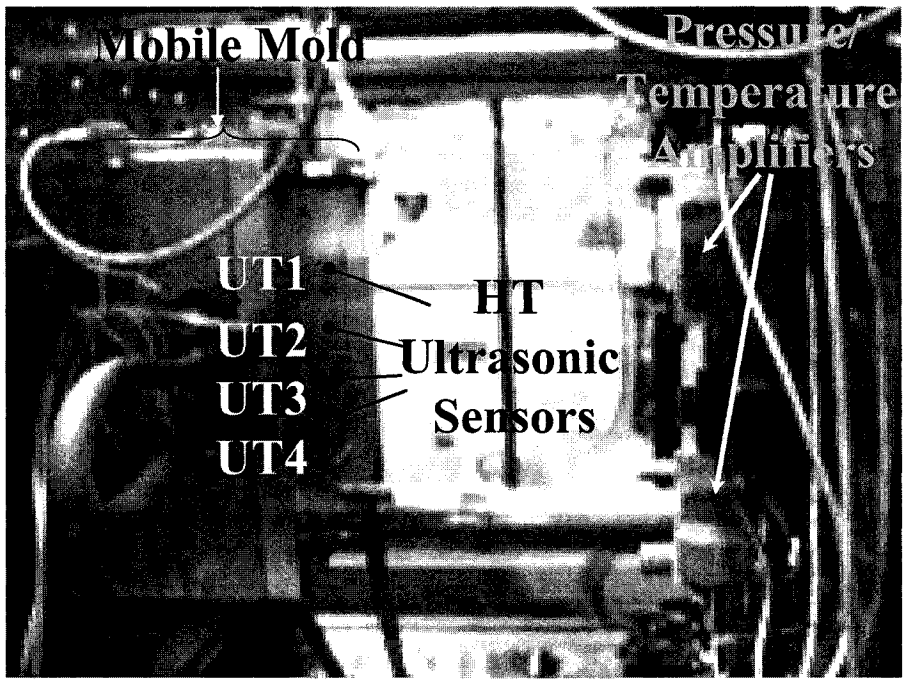

Fig. 3-14 Photograph of the mobile plate with mold and four HT ultrasonic sensors.

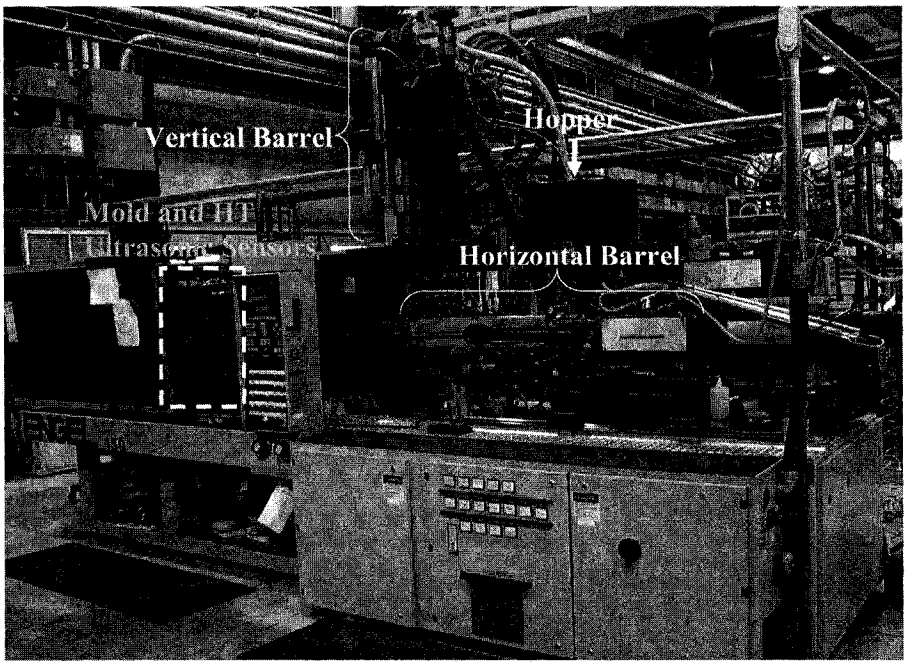

Fig. 3-15 Photograph of an IM machine from Engle Inc. (150 tons), equipped with horizontal and vertical barrel/screw plasticating units.

3.4.2 GAIM and WAIM

For GAIM and WAIM processes, a special designed mold and mold insert are developed. Fig. 3-16 (a) shows the polymer side of the mold insert having a half cylindrical cavity with Ø20mm. Fig. 3-16 (b) shows three integrated PZT film HT ultrasonic sensors (UT-A, B, C) fabricated at the UT side of the mold with an interval of 35mm. In order to fabricate these HT ultrasonic sensors, a rectangular shape cavity is machined on the mold of the UT side. The dimension of the sensors cavity is 20mm-wide, 90mm-long and 10mm-deep. This modification won't affect the process procedure and product quality, but increase the convenience and flexibility of process diagnosis. These HT ultrasonic sensors have a centre frequency of 9 MHz and 6dB bandwidth of 6 MHz. Fig. 3-17 (a) and (b) present the performances of UT-A in time domain and frequency spectrum, respectively, at 25°C. SNR of the first round trip longitudinal wave echo, reflected at the substrate/air interface measured in pulse-echo technique, is above 30dB at 25°C. In addition, it is confirmed that these sensors could be

operated up to 250°C. Such performance is sufficient for monitoring of polymer GAIM and WAIM processes. Each of these integrated HT ultrasonic sensors is attached with a coaxial cable for electrical connection. In order to prevent damage of the HT ultrasonic sensors caused by leaking water during WAIM process, the cavity in Fig. 3-16 (b), including three HT ultrasonic sensors and their electrical connections, is sealed by a Fortafix sealant. This sealant can sustain HT up to 300°C and has heat insulation property.

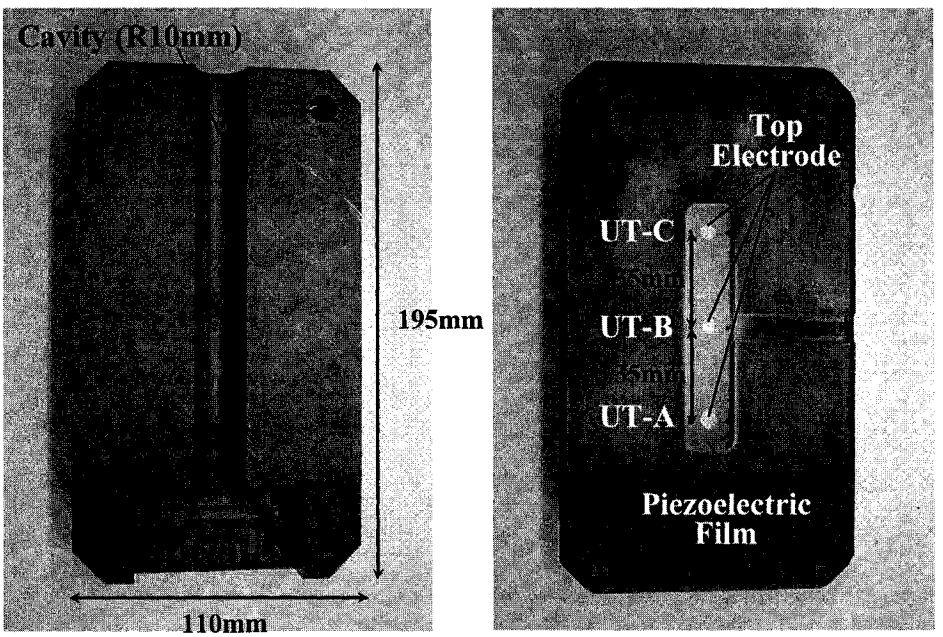

(a) Cavity (Polymer) Side **(b) Ultrasonic Sensor Side**

Fig. 3-16 Photographs of (a) polymer side of mold insert having a half cylindrical cavity with Ø20mm, and (b) three PZT film HT ultrasonic sensors (UT-A, B, C) fabricated on opposite side of the cavity.

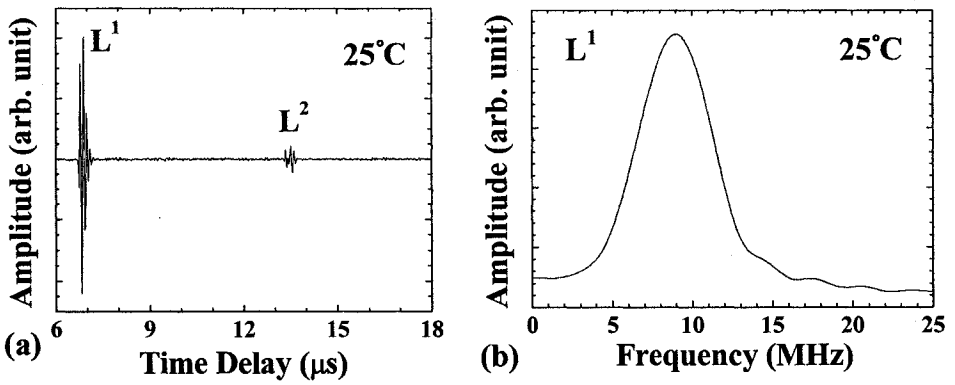

Fig. 3-17 Performance of the ultrasonic sensor UT-A (a) in time and (b) in frequency domain at 25°C.

The mold insert with three developed integrated HT ultrasonic sensors are installed into the mobile mold of the GAIM/WAIM machine, as shown in Fig. 3-18 (a). This specially designed mold is utilized for fabrication of the hollow structured part during GAIM and WAIM processes. The mold is comprised of a main mold insert that form the mold cavity. Exchange of the mold inserts allows for fabricating different parts and studying polymer / fluid flow phenomena. The polymer melt is injected into the cavity at the middle of fixed mold and follows a runner to the bottom of the mold, where the fluid injection needle is located. The needle is located at the bottom of the mold, which is a requirement for a successful extraction of the water using gravity at the end of the molding cycle. The mold insert, shown in Fig. 3-18, contained the instrumented straight ∅20mm tubular region of the sample. The polymer and fluid will fill and stay in this region to form the final product during the process. This region is equipped with pressure and temperature transducers in the fixed mold. This setup may give an opportunity to provide the comparing temperature and pressure data for ultrasonic sensor in the same location. The HT ultrasonic sensors with the mold insert are ready for process diagnosis of GAIM and WAIM processes.

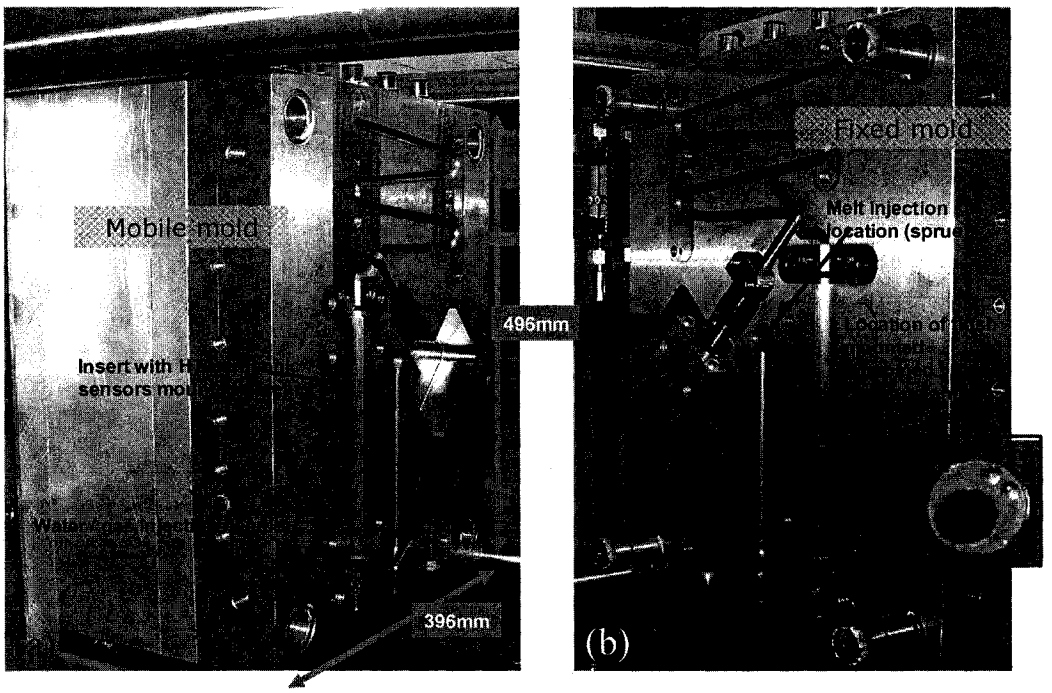

Fig. 3-18 Photograph of the (a) mobile and (b) fixed mold for the GAIM and WAIM, showing a cavity made up from interchangeable inserts. The ∅20 mm straight tube insert fitted with HT ultrasonic sensors (mobile side) along with combined piezoelectric pressure and thermocouple temperature transducer (fixed side) is shown.

The mold in Fig. 3-18 is installed into a GAIM/WAIM machine (TM1300 / 350 + 210 BM from Battenfeld) for practiced GAIM/WAIM experiments, as shown in Fig. 3-19. This machine is fitted with a gas compressor/water reservoir and a pressure controller. The barrel is internal ∅40mm with a maximum specific melt pressure of 160MPa and maximum melt delivery rate of 132ccm/s. The experiments and results will be discussed in chapter 4.

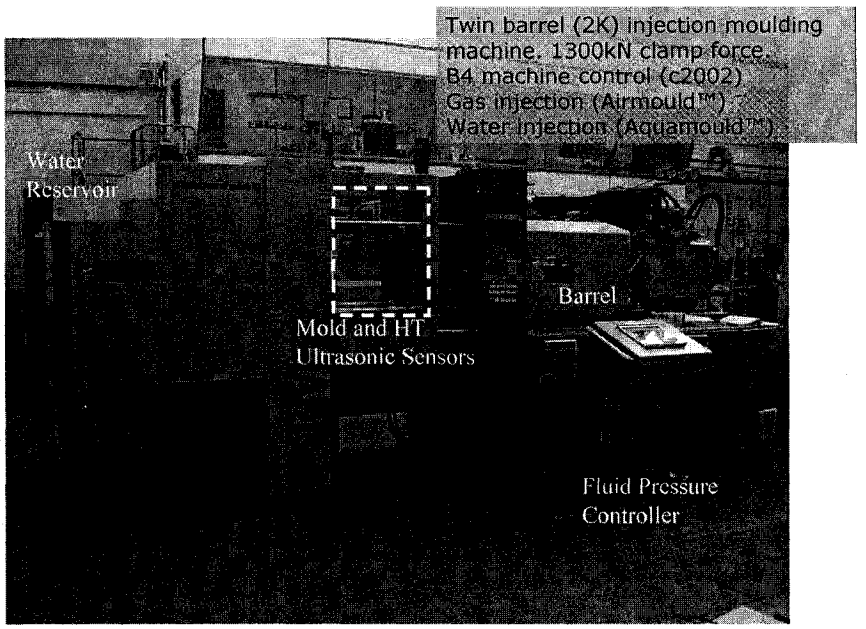

Fig. 3-19 Photograph of a gas/water assisted injection molding machine from Bettenfeld (TM1300 / 350 + 210 BM) with separate gas / water injection controller shown in the foreground. The water injection reservoir is shown behind the machine.

3.4.3 IMMF

The challenge of the sensor for diagnosing micro-fabrication molding process is the small mold space for installation and tiny cavity space. Two advantages of the film HTUT, which are miniature and integrated, may provide solutions for these difficulties. Fig. 3-20 (a) and (b) show the prototype type of the designed HT ultrasonic probe with the dimensions of 4mm-diameter and 12mm-long. This ultrasonic probe has the same dimensions with the pressure and temperature sensor (e.g. Kistler 6190A), which means that the pressure and temperature sensor and ultrasonic probe are interchangeable. A PZT film HTUT is fabricated onto UT end of the steel probe using a sol-gel spray technique. The top electrode size is 2mm in diameter. The probe itself serves as a bottom electrode. In Fig. 3-20 (a), the probe periphery is flat surface, and the ultrasonic signal reflected at the probing end is presented in Fig. 3-21 (a). The trailing echoes are observed between L^1 and L^2 echoes. The trailing echoes are generated

due to mode conversion, wave reverberation and diffraction within the probe of finite diameter and specific shape [127, 155]. These trailing echoes may interfere with the desired echoes and deteriorate the SNR of the desired signals during the monitoring.

In order to improve the SNR of ultrasonic echo and clear the time delay area between L^1 and L^2 echoes, two spiral like V-grooves with a depth of 0.5mm and with a periodicity of 0.8mm are machined on the probe periphery, as shown in Fig. 3-20 (b) [154, 155]. These V-grooves increase the surface roughness on the probe periphery, and the waves, generated due to mode conversion, are scattered at the boundary and are not added in phase at the receiver [154, 155]. Fig. 3-21 (b) presents the ultrasonic signals reflected at the probing end, obtained by the sensor with the V-grooves on the rod periphery. The trailing echoes are reduced to noise level and the SNR of the L^1 echo is significantly improved to 33dB. By doing this, the desired L_{2n} echoes won't be affected by the trailing echoes between L^1 and L^2 echoes. Fig. 3-21 presents the performance of the integrated HT ultrasonic sensor with V-grooves on the rod periphery in frequency domain at 25°C. The central frequency and 6dB bandwidth of the L^1 echo at 25°C are 17 and 14MHz, respectively, as shown in Fig. 3-22.

For the purpose of further miniaturization of the sensor, the electrode diameter of 1mm is tested. It is found that the signal amplitude (strength) and the SNR of the sensor having the electrode diameter of 1mm decrease 21dB and 12dB, respectively, comparing with the one having the electrode diameter of 2mm. Fig. 3-20 (c) presents the promoted miniaturized HT ultrasonic probe with the steel holder and electrical connection. The steel holder can attach and fix the cable to the sensor.

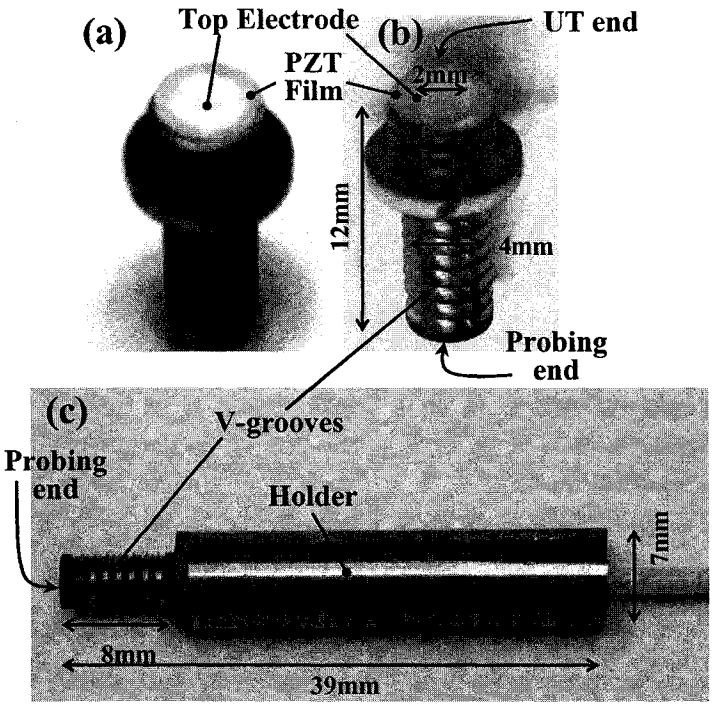

Fig. 3-20 Photographs of miniature HT ultrasonic probe: steel buffer rod with PZT film HTUT (a) without V-grooves and (b) with V-grooves on the probe periphery. (c) Miniature HT ultrasonic probe with steel holder and electrical connection.

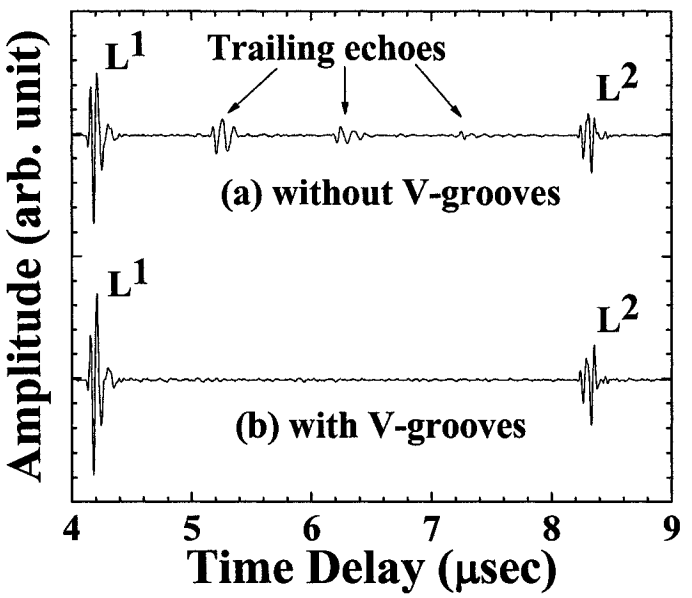

Fig. 3-21 Ultrasonic signals reflected at the probing end, measured by the probe (a) without and (b) with V-grooves on the rod periphery at 25°C. L^1 and L^2 are the first and second round trip longitudinal-wave echoes, respectively.

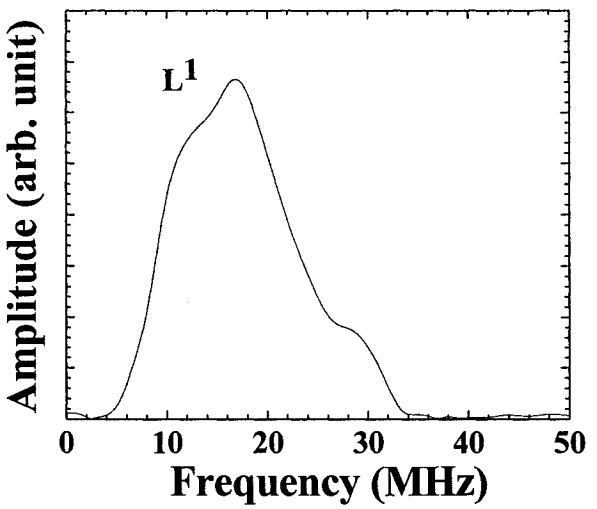

Fig. 3-22 Performance of the integrated HT ultrasonic sensor with V-grooves on the rod periphery in frequency domain at 25°C.

Fig. 3-23 (a) and (b) present a mold of the IM machine used in the experiments of IMMF. The mold used in the experiments is composed of a mobile mold, including six ejection pins and two existed holes with ∅4mm, and a fixed mold, on which a replaceable mold insert having testing microstructures is attached. These two existed holes are for installing the sensors. There are several sensors, such as, Kistler 6190A pressure and temperature sensor, fitting the dimension of the holes. The developed PZT film HT ultrasonic sensors in Fig. 3-20 (c) are installed into the holes for the fabrication process diagnosis of microfluidic devices. The sensors' probing ends are flush with the cavity surface of the mobile mold as shown in Fig. 3-23 (a). For the fabrication of microfluidic devices, a replaceable mold insert with testing microstructures is utilized. This mold insert is inter-changeable in order to fabricate various micro-structures.

The dimension of the mold cavity is 96mm-long, 16mm-wide and 1.1mm-deep. The microstructures, which are printed on the surface of the molded parts, are fabricated on one side of the steel mold insert facing to the mold cavity, as shown in Fig. 3-23 (b). The mold insert used in the experiments has test patterns of 22 line grooves (width: 1mm; length: 6 or 12mm; depth: 0.01, ···, 0.3 or 0.5mm) and 57 holes (diameter: 0.77mm; depth: 0.01, ···, 0.3 or 0.5mm). The

sensor 1 location is above the hole with depth of 0.5mm, and sensor 2 is above the two lines with depths of 0.3mm and 0.5mm. If required, integrated HT ultrasonic sensors can be fabricated either on the back sides of mold insert or mobile mold.

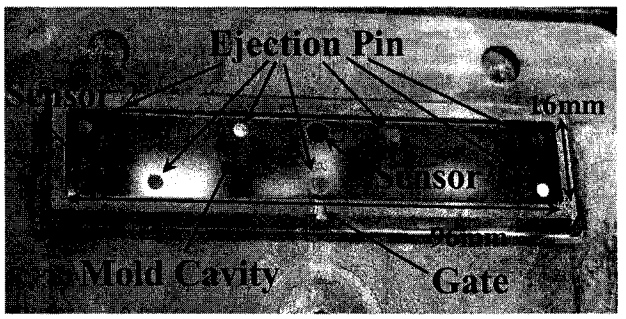

(a) Mobile Mold

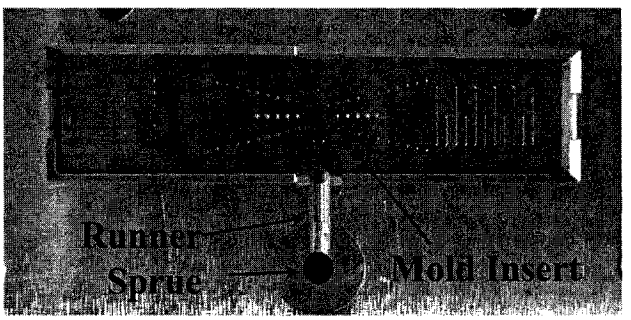

(b) Fixed Mold

Fig. 3-23 Photographs of a mold of an injection molding machine used in the experiments for IMMF. (a) Mobile mold with six ejection pins and two existed holes having installed sensors; and (b) fixed mold with a steel mold insert having test patterns.

The mobile and fixed molds in Fig. 3-23 are installed into the mobile and fixed plate of an IM machine, as shown in Fig. 3-24 (a) and (b), respectively. A 30 tons IM machine (BOY30, BOY Machines Inc., Exton, PA), as shown in Fig. 3-25, is employed for carrying out the experiments of IMMF. This machine has a horizontal plasticating unit, and the diameters of the barrel and screw are 40 and 24mm, respectively. The maximum melt injection rate of polystyrene is 51.3 g/s. The experiments and results will be discussed in chapter 5.

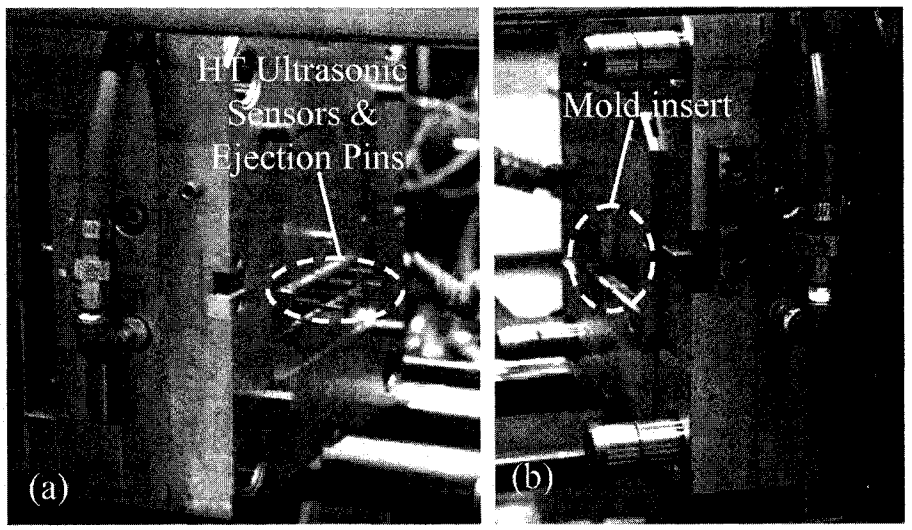

Fig. 3-24 Photograph of the (a) mobile and (b) fixed plates of IM machine.

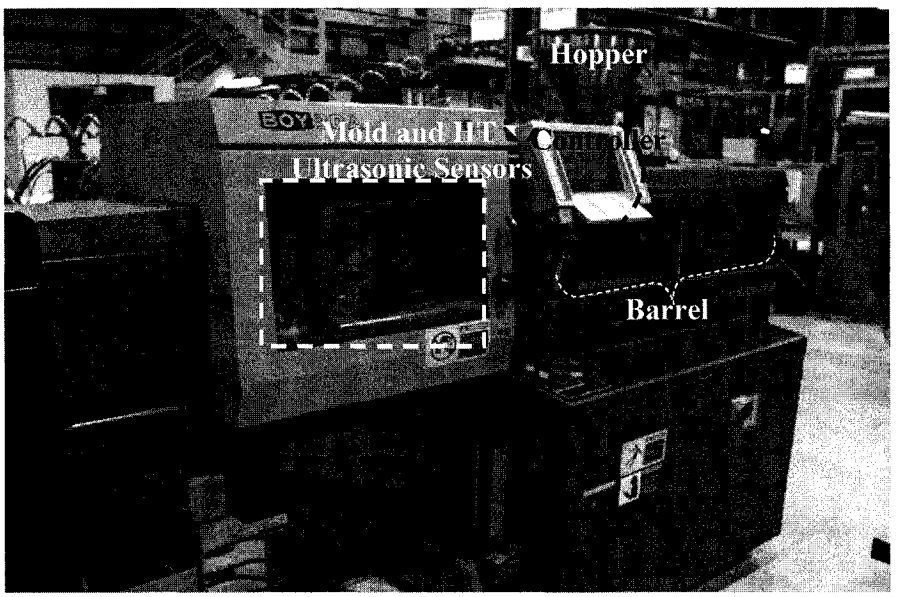

Fig. 3-25 Photograph of the machine for IMMF process from Boy Inc. (30 tons)

3.4.4 MM for polymer and nano-composite materials

In MM process, because of the more narrow process window of material than IM, it is my interesting to diagnose the process from the beginning to the end, which is from barrel to the mold. During the process, polymeric materials are melted at the barrel of the MM machine by two means: an electric heater attached outside of the barrel; and frictional heat caused by rotation of the extrusion screw

inside the barrel. Temperature of the materials needs to be precisely controlled within a recommended temperature range of the materials employed in order to achieve molten polymers desired for subsequent injection stage. Material degradation due to over heating is undesirable. Therefore, monitoring of temperature and state of the polymer at the barrel is crucial to produce high quality products.

For most MM process, the temperature settings of barrel and mold are 200~300°C and 40~80°C, respectively. The operating temperatures of HT ultrasonic sensors at these two locations should fit these requirements. The HT ultrasonic sensor adopting BIT film can operate at temperature up to more than 400°C, which is high enough for almost all polymer materials to be melted at the barrel. Fig. 3-26 shows seven BIT film HT ultrasonic sensors (UT1-7, using BIT films) fabricated directly on the barrel. This design provides the opportunity to diagnose the entire melting process in different zones of barrel. The diameter of the top electrode is 5mm, which is the active area size of the ultrasonic sensor. The length of the barrel is 265mm, the internal diameter is 14mm, and the external diameter at the areas of UT1-3, 5-7 and at that of UT4 are 40mm and 30mm, respectively. Fig. 3-27 (a) and (b) present the ultrasonic performance of the UTs. The center frequency, measured with the UT6, is 13MHz and 6dB bandwidth is 13MHz. The SNR of the L^1 echo is 31dB at 260°C. The performance of UT1-7 is almost the same.

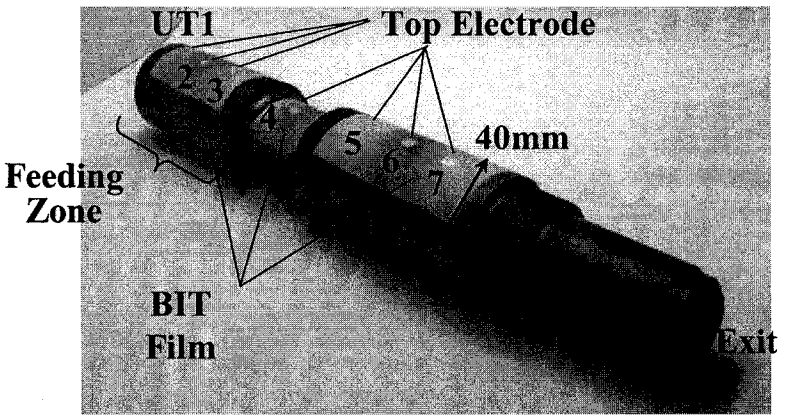

Fig. 3-26 Photograph of the barrel of MM machine with seven BIT film HT ultrasonic sensors (UT1-7).

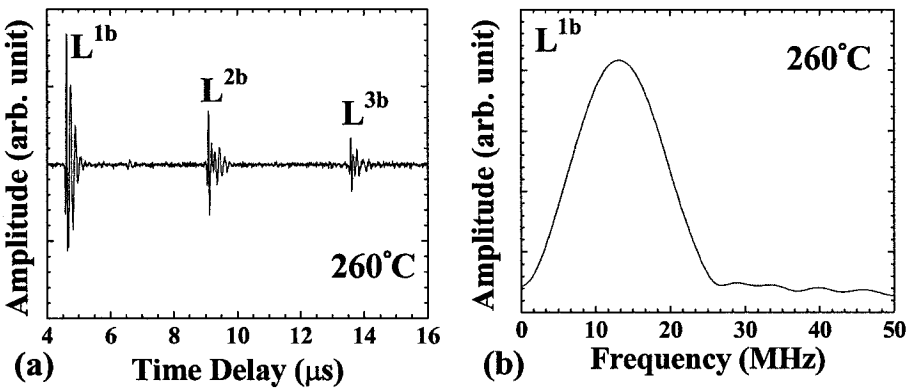

Fig. 3-27 (a) Longitudinal-wave ultrasonic signals reflected from the internal surface of the barrel; and (b) frequency spectrum of the L^{1b} echo at 260°C, measured with the UT6 in Figure 3-26.

The temperature requirement of ultrasonic sensor in the mold is less than that in the barrel. In this case, the HT ultrasonic sensors adopting PZT film, which can operate at temperature up to 250°C, are fabricated on the mold. Fig. 3-28 (a) and (b) present the photographs of the mold insert having a mold cavity for MM processes of polymer and nano-composite materials, respectively. The dimensions of the mold insert are 75mm in diameter and 7.5mm in thickness, respectively. In Fig. 3-28 (a) the dimensions of a rectangular cavity are 20mm-long, 2mm-wide

and 0.5mm-deep, and in Fig. 3-28 (b), those of a two-step cavity are 20mm-long, 4mm-wide and 590 and 320μm-deep. This mold insert with micro-cavity is a testing one. For practical applications, molders can design micro-cavities according to customers' requirements. A hole at the center is for the ejector pin. The polymer melt is injected into the mold cavity through a runner in Fig. 3-28 (a) and (b). During the experimental period, there was no cavity pressure sensor fitting the experimental specification available. In order to monitor the polymer melt flow and status inside the mold cavity, HT ultrasonic sensors need to be installed on the back side of mold insert above the micro-cavity. Due to the little space of cavity and mold, it is not practical to put many sensors for process diagnosis. Therefore, two PZT film HT ultrasonic sensors (UT1 and UT2) are fabricated on the opposite side of the cavity with an interval of 16mm. The diameter of the top electrode is 4mm, and the thickness of the film is 100μm, as shown in Fig. 3-28 (c). Their performances are similar; with center ultrasonic frequencies of 8-9MHz and 6dB bandwidth of 4-7MHz. Fig. 3-29 (a) and (b) present the performance of the ultrasonic sensor UT1 in Fig. 3-28 (c). It is noted that the HT ultrasonic sensors using PZT films at the mold have 10dB stronger ultrasonic signals than those using BIT films at the barrel. But they have lower operation temperature up to 250°C, which is high enough at the mold for MM process performed in this thesis.

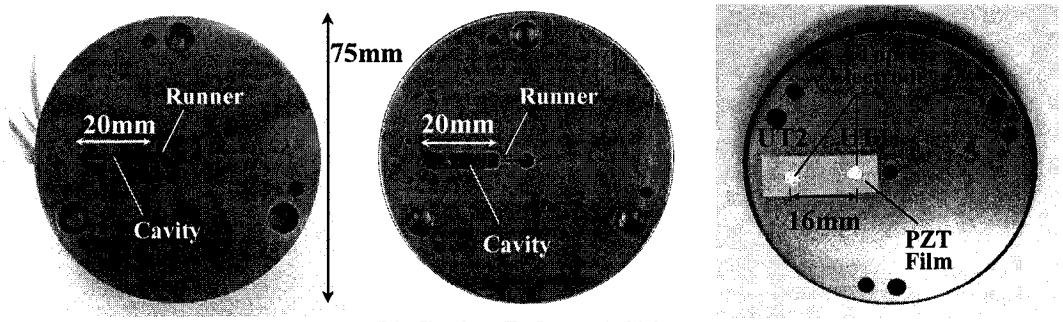

(a) Cavity (Polymer) Side of MM for polymer

(b) Cavity (Polymer) Side of nano-composite

(c) UT Side

Fig. 3-28 Photographs of mold inserts for (a) polymer and (b) nano-composite MM. (c) Two PZT film HT ultrasonic sensors fabricated on opposite side of the cavity.

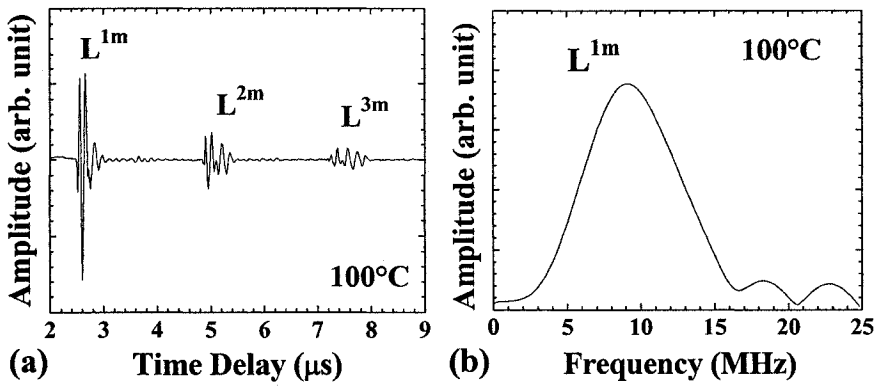

Fig. 3-29 (a) Longitudinal-wave ultrasonic signals reflected from the cavity surface of the mold insert; and (b) frequency spectrum of the L^{1m} echo at 100°C, measured with the UT1 in Figure 3-28 (c).

After fixing the electrical connection, the barrel and mold insert with integrated HT ultrasonic sensors are installed into MM machine. Fig. 3-30 (a) and (b) present the photograph of the barrel and mobile mold of MM machine. In Fig. 3-30 (a), the zone covered by heating band is melting zone, at which the polymer melts. In order to monitor the melting phenomena in the barrel, the data collected from HT ultrasonic sensor (UT6) in the melting zone is utilized. It is noted that the gap between the heating bands is only 6.5mm, and there is little space for installing sensors in the melting zone. However, the top electrode, which is the active area size of the ultrasonic sensor, is 5 mm-diameters, and this design can overpass the limitation caused by heating bands. In Fig. 3-30 (b), the mold insert with integrated HT ultrasonic sensors are installed into the mobile mold of the MM machine.

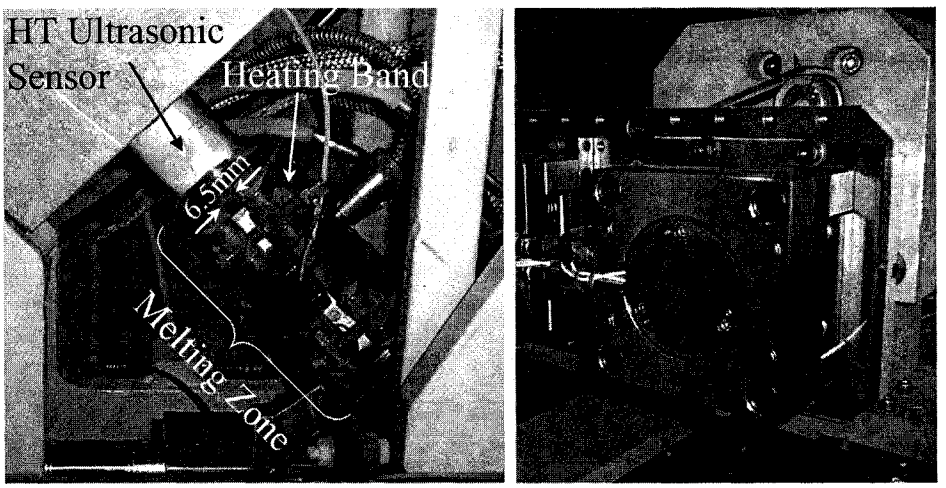

(a) Barrel (b) Mold

Fig. 3-30 Photographs of barrel and mobile mold with mold insert of MM machine.

The barrel and mold insert in Fig. 3-30 are installed into the MM machine (Microsystem50 from Battenfeld, Austria) in Fig. 3-31 for carrying out the experiments of MM for polymer and nano-composite. This machine has a plasticating unit with a screw of Ø14mm. The maximum injection speed is 760 mm/s, and the injection volume varies from 0.012 up to 1.1 cm^3.

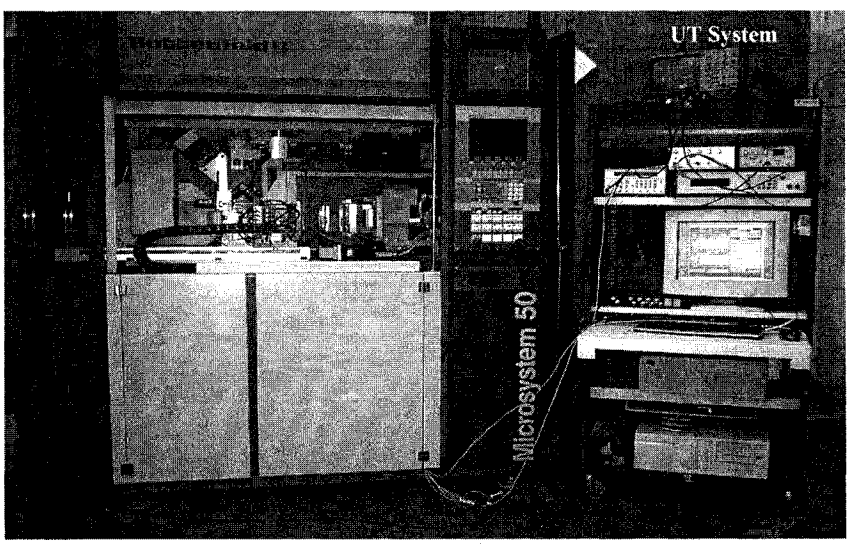

Fig. 3-31 Photograph of MM machine from Bettenfeld (Microsystem 50) and ultrasonic acquisition system.

3.4.5 MM for ceramic material

Due to different injected material and processing procedure, the mold design for MM of ceramic material is different from previous one. Fig. 3-32 (a) presents the photograph of the mold with a mold insert in the cavity side, for manufacturing a circular plaque of ceramic powder. The cavity has a diameter of 25mm and a depth of 1.5mm. The design of mold cavity is a testing one. For practical application, molder can mold micro-sized features on the mold and part surface. The insert is installed into the mobile mold of the MM machine. The melt feedstock will fill the circular cavity through the gate in the fixed mold. Therefore, the integrated HT ultrasonic sensors will be implanted in the back side of mold insert.

A PZT film is fabricated directly on the UT side of mold insert. Fig. 3-32 (b) shows a photograph of mold insert with five integrated HT ultrasonic sensors fabricated directly onto the mold insert. This design demonstrates the possibility of fabricating the sensor in any desired place and the application of sensor array. The performances of these HT ultrasonic sensors are similar; with center ultrasonic frequencies of 9-10MHz and 6dB bandwidth of 2-3MHz. Fig. 3-33 (a) and (b) present the ultrasonic performance of the UT1 in Fig. 3-32 (b) at 25°C. After the electrical connection of the ultrasonic sensors, the mold, mold insert with the integrated HT ultrasonic sensors are installed into the mobile plate of MM machine in Fig. 3-31 for carrying out the experiments of MM for ceramic materials. The experiments and results will be discussed in chapter 5.

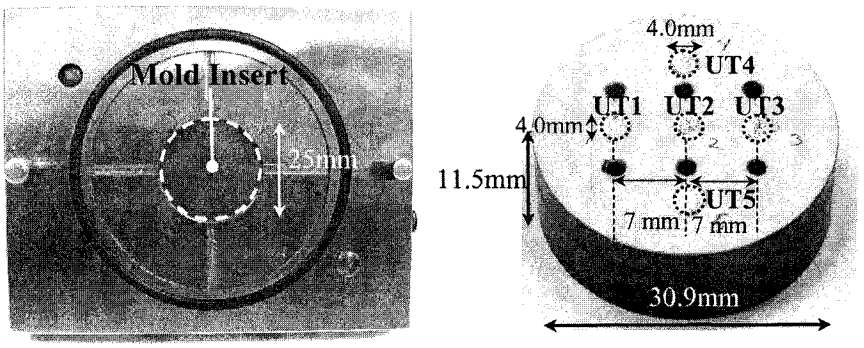

Mold (cavity side)
(a)

Mold Insert (UT side)
(b)

Fig. 3-32 Photographs of (a) mold with the mold insert (indicated by white dotted circle area) at cavity side and (b) mold insert with five PZT film HT ultrasonic sensors at UT side for MM of ceramic powder.

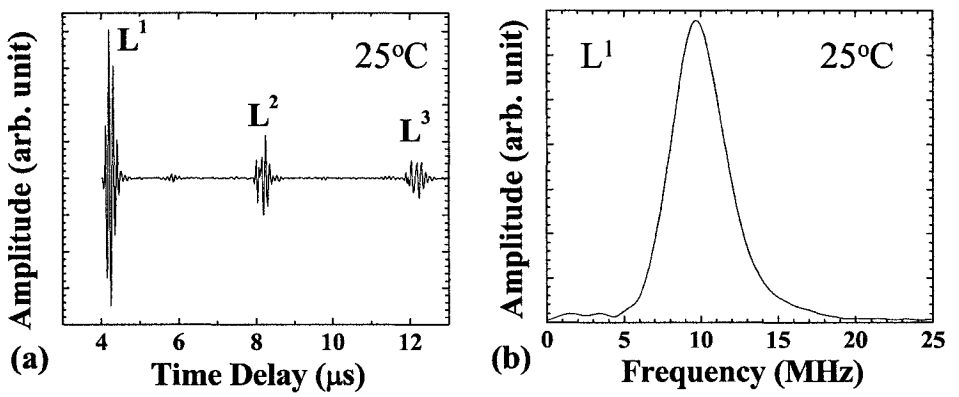

Fig. 3-33 (a) Longitudinal-wave ultrasonic signals reflected from the cavity surface of the mold insert; and (b) frequency spectrum of the L^1 echo at 25°C, measured with the UT1 in Figure 3-32 (b).

3.5 Summary

The integrated BIT or PZT film HT ultrasonic sensors have been successfully developed by using film HTUTs in this chapter, and shown that they can be customized for each IM machine and process. If the operation temperature is higher than 200°C, BIT film HTUT is used because of its high Curie

temperature. If the temperature of the sensing location is lower than 200°C, PZT film HTUT is used due to its high piezoelectric strength. Developed sensors can be fabricated either on flat mold inserts or curved barrel surfaces. When required, they can be miniaturized and made to fit each machine setup and process procedure. The electrical connection is carried out by fixing a coaxial cable. The sensors' central frequency range is 8~17MHz. Their signal-to-noise-ratios (SNRs) are above 30dB. Improvement of SNR is carried out by machining two spiral like V-grooves on the probe periphery to remove trailing echoes. To prevent damage of ultrasonic sensors from water leakage, sealing the sensor cavity of WAIM mold insert by a HT sealant is practiced. The integrated HT ultrasonic sensors reported here are fully developed, extensively tested, and are ready to be used in actual industrial processes.

In addition, ultrasonic measuring principles for obtaining ultrasonic signatures, such as ultrasonic velocity and attenuation, have been laid. A PC-based high-speed data acquisition system and its main components have been described for real-time process diagnosis application. Also, the ultrasonic PVT measurement system for off-line measuring ultrasonic signatures of the polymers is presented. The fabrication procedures of piezoelectric ceramic film HTUT by sol-gel spray technique have been presented.

Chapter 4

Large scale injection molding

4.1. Introduction

In terms of their scales, IM processes described in chapter 2 can be grouped into large and small categories. In this thesis, the large-scale IM processes include conventional IM, COIM, GAIM and WAIM processes, while the small-scale ones are IMMF and MM. Those in the latter category are studied here in conjunction with polymer, nano-composite and ceramic powder materials. The primary focus of this chapter will be on the large-scale IM processes diagnosis.

In COIM and GAIM/WAIM processes, fabrication of the molded parts, in particular formation of internal sandwiches and/or hollow structures, is complicated. As mentioned previously, research in this area has shown that the product quality is highly sensitive to variations of certain parameters. For instance, the viscosity ratio between skin and core materials, injection velocity, core temperature, and core content are important factors for COIM. For GAIM and WAIM, the critical parameters are melt temperature, melt injection rate and delay time between the end of melt injection and the start of fluid injection [156, 157]. However, methods to evaluate part quality, such as core dimension and thickness of layers and wall, are currently limited to visual appraisal and/or off-line inspection. These techniques are not suited for the real-time, time-critical, process control system, which is needed in this case, as they produce imprecise information and involve feedback loops with large time delays.

In order to circumvent these limitations, as part of the research for this thesis, integrated HT ultrasonic sensors which allow performing real-time, non-destructive and non-intrusive polymer processes diagnosis have been developed. The ability of the resulting diagnosis system to generate information on key process parameters, such as melt or liquid flow, flow speed, solidification, filling incompleteness, layer and wall thickness, will be demonstrated and its potential applications to process optimization and part quality evaluation will be explored.

4.2. Experiments

4.2.1 IM

For IM, the designed mold and developed integrated HT ultrasonic sensors in chapter 3 are installed into the IM machine. Fig. 4-1 presents a cross-sectional view of the mold (mobile and fixed), mold insert and molded part (polycarbonate) with four BIT film HT ultrasonic sensor inserts (UT1-4) for the IM process. Polymer melt is injected into the cavity of the mold through the gate at the center of the fixed mold. The depth of the cavity, which is the thickness of the part at sensor location, is 1mm. For comparison purpose with ultrasonic data, a temperature and cavity pressure sensor (6190A, Kistler Instrument AG, Winterthur, Switzerland) is attached to the fixed mold. Its sensing end has circular shape with a diameter of 4mm and is flushed with the internal surface of the fixed mold, Its probing end is facing to the UT1 as shown in Fig. 4-1. L^n (n=1, 2, 3...) represents n-th round trip echoes propagating in the HT ultrasonic sensor insert and reflected at the insert/polymer interface, and L_{2n} (n=1, 2, 3...) represents those in the polymer and reflected at the polymer/fixed mold interface.

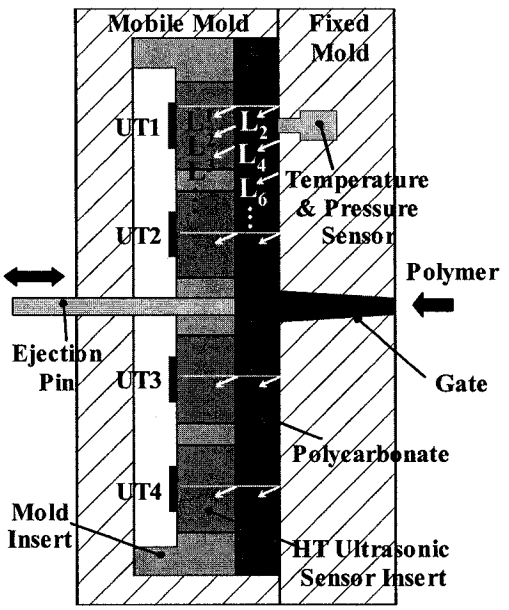

Fig. 4-1 Cross-sectional view of the mold (mobile and fixed), mold insert and molded part (polycarbonate) with four BIT film HT ultrasonic sensor inserts (UT1-4) for the conventional IM. L^n and L_{2n} (n=1, 2, 3...) represent n-th round trip echoes propagating in the HT ultrasonic sensor insert and those in the polymer, respectively.

The material employed in the experiment is an injection grade polycarbonate (PC: CALIBRE 200-14, Dow Chemical Co., Midland, MI). Fig. 4-2 is the photograph of a molded part. The molding conditions are listed in Table 4-1.

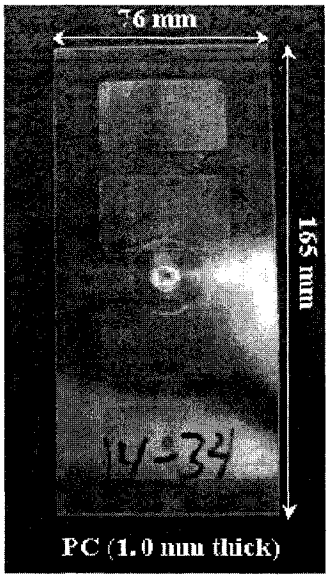

Fig. 4-2 Photograph of a molded PC part of 1mm thickness for IM.

Table 4-1 Typical molding conditions for IM.

Polymer	Melt temp.	Mold temp.	Melt speed	Screw speed	Holding pressure	Cycle time
PC	320°C	120°C	137.5ccm/s	110mm/sec	24MPa	30s

4.2.2 COIM

The procedure of the COIM process is more complex than IM process. The depth of the cavity, which is the part total thickness at the sensor location, is 3.54mm. Here, the ABS is chosen as skin and 2nd core material, and the PC as 1st core material. First, the ABS is injected to fill the mold cavity partially to form the skin. Then the PC is injected into the mold cavity becoming the 1st core. At the end of filling stage, around 20% of ABS, which is one-fifth volume percentage of the whole part, is injected again into the mold cavity to form the 2nd core and seal the gate. It is also our interest to monitor the formation of 2nd core. After the holding and cooling stages, the mold opens and the part is ejected.

Fig. 4-3 presents a cross-sectional view of the mold configuration for COIM. The skin and core materials are sequentially injected into the mold cavity through the gate at the centre of the fixed mold. A single nozzle equipped with a check valve directs the injected materials into the mold cavity.

Fig. 4-4 (a) and (b) show the paths of ultrasonic echoes observed at the UT location with COIM, where only 1st core arrives at the UT1 located near the end of the mold cavity in Fig. 4-4 (a), while both 1st and 2nd cores arrive at the UT2 near the gate in Fig. 4-4 (b). Besides L^n (n=1, 2...), L_2, L_2', L_2'', L_2''' and L_2'''' indicate the echoes propagating in the polymer. The L_2 and L_2'~ L_2'''' are those reflected from the polymer/fixed mold interface and the skin/core layer interfaces, respectively. The indication of each layer in Fig. 4-4 is the following. Skin layers 1 and 2 are composed of the skin material (ABS). Core layer in Fig. 4-4 (a) and core layer 1 and 3 in Fig. 4-4 (b) are composed of the 1st core material (PC). Core layer 2 in Fig. 4-4 (b) is composed of the 2nd core material (ABS), which is the same as the skin material. h and h_l (l =1~5) denote the thickness of the entire molded part and skin or core layer, respectively.

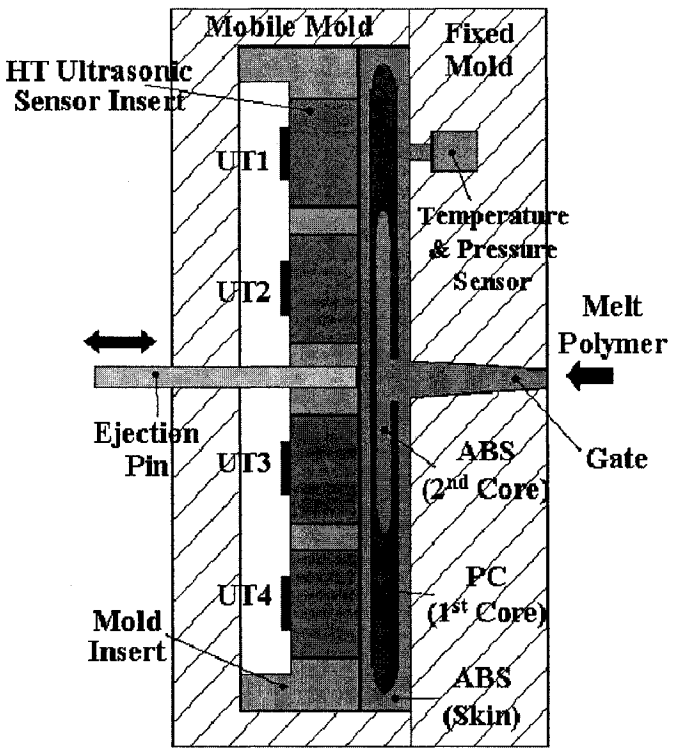

Fig. 4-3 Schematic cross-section of the mold with four BIT film HT ultrasonic sensor inserts (UT1-4) for COIM process.

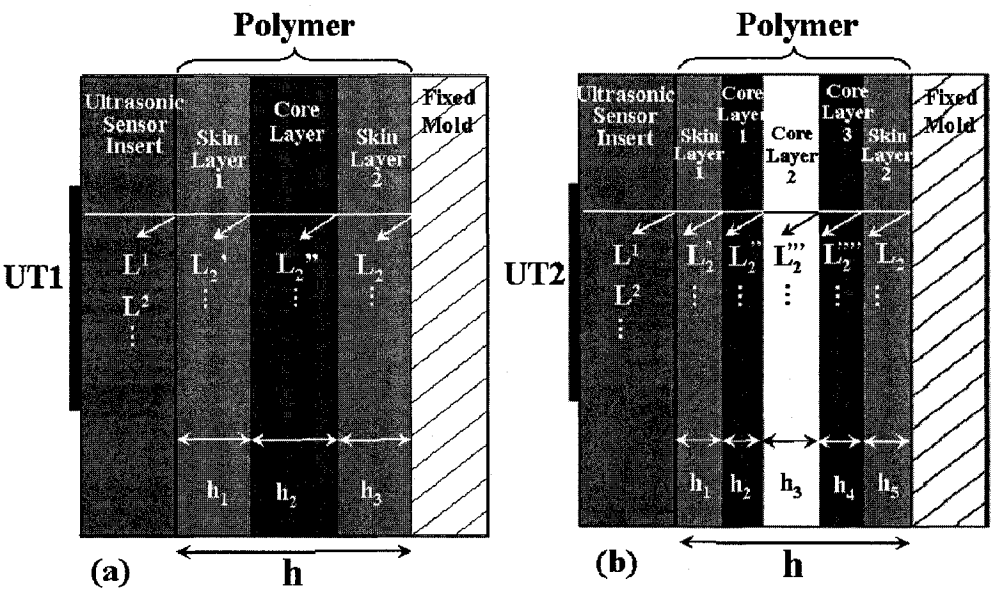

Fig. 4-4 Propagation paths of ultrasonic echoes in the mold and part at the (a) UT1 and (b) UT2 locations, where the 2nd core arrives at the UT2 near the gate but not at the UT1 near the cavity end during COIM process.

The materials employed in the experiment are an injection grade Acrylonitrile Butadiene Styrene (ABS) (Magnum 342EZ, Dow Chemical Co., Midland, MI) for the skin and 2nd core and polycarbonate (PC: CALIBRE 200-14, Dow Chemical Co., Midland, MI) for the 1st core. Shear viscosities of the ABS and PC are measured at the melt flow rates (MFRs) of 6g/10min and 14g/10min at 230°C and 300°C with a load of 3.8Kg and 1.2Kg, respectively. They are 2.6×10^2 Pa-s for the ABS and 1.8×10^3 Pa-s for the PC from the viscosity mastercurve at the shear rate of 10^3rad/s. The molding conditions for IM and COIM are listed in Table 4-2.

Table 4-2 Typical molding conditions for COIM.

Layer	Polymer	Melt temp.	Mold temp.	Injection speed	Screw speed	Holding pressure	Cycle time
1st Core	PC	270°C	60°C	50ccm/s	40mm/s	3MPa	30s
Skin/2nd core	ABS	250°C		50ccm/s	40mm/s		

In order to investigate the flow behavior of the core material during molding, the injected volume of the ABS and PC changes sequentially. The machine settings of the volume percentage for skin and core materials are listed in Table 4-3. In our experiment, the core volume percentage is calculated as the sum of a volume of the 1st and 2nd core materials. With each setting, molding process is repeated three times continuously to produce three parts. Fig. 4-5 (a) and (b) present the molded parts of COIM. In Fig. 4-5 (a), the molded part of COIM has the same external dimension as mold cavity. The skin and 2nd core (ABS) are semi-transparent, thus, one can see the dark color area in the part, which is the core (PC) colored with red for a visual inspection purpose. A purpose of coloring the PC (1st core) was to distinguish each layer for off-line thickness measurement by an optical microscope. The concentration of the color pigment used in the experiments was around 1% and it affected little our ultrasonic diagnostic results.

The setting core volume percentage for Fig. 4-5 (a) is 50%. White circles indicate the corresponding locations of the four HT ultrasonic sensors (UT1-4 in Fig. 4-3). The molded part is sectioned along the dashed line in Fig. 4-5 (a) to investigate the interface structure of the skin and core layers. The thickness of each layer at the UT location is measured using an optical microscope in order to compare with that measured by the ultrasonic technique presented in section 4.5.3. Fig. 4-5 (b) presents the cross-sectional view, along the straight line in Fig. 4-5 (a), of the five parts with different core volume percentages. Their settings of the core volume percentages are 58, 55, 50, 40 and 32% from #1 to #5, respectively. One can clearly see the difference of core dimensions among them.

Table 4-3 Volume percentage settings of the skin and core materials used in COIM.

No.	Skin % (ABS)	Core % (PC+ABS)
1	42	58
2	45	55
3	50	50
4	60	40
5	68	32

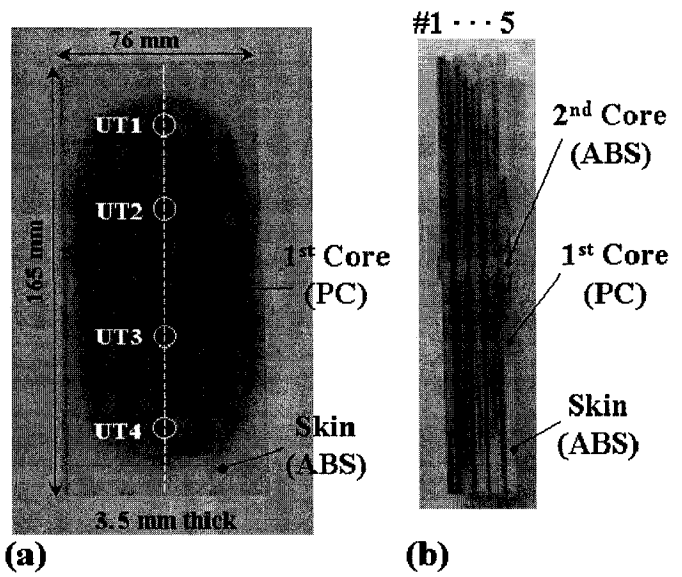

Fig. 4-5 Photographs of (a) a COIM molded part, where the white circles and the dotted line indicate the locations of four BIT film HT ultrasonic sensors and the cutting line, respectively, and (b) a cross-section of the co-injection molded parts with the core volume percentages of 58, 55, 50, 40 and 32% from #1 to #5, respectively.

4.2.3 GAIM

For GAIM, the designed mold and developed HT ultrasonic sensors presented in chapter 3 are installed into the IM machine. During the process, the "short shot" method is used to manufacture these parts, where the mold cavity is partially filled with polymer (the short shot) prior to the injection of gas [72, 73]. The gas bubble displaces the polymer melt to the end of the cavity in order to complete filling and the final part becomes hollow with a gas core. Prior to the mold opening the high-pressure gas is released from the mold to leave a hollow article. The distribution of the bubble and in particular the thickness of melt deposited against the cavity wall (residual wall thickness: RWT) is important to the product mechanical performance, cooling rate and aesthetics. Control of the gas pressure, melt temperature, melt injection rate

and delay time between the end of melt injection and the start of fluid injection are crucial factors in controlling the RWT.

Fig. 4-6 presents a schematic cross-section of the mold with the PZT film HT ultrasonic sensors for GAIM and WAIM, showing ultrasonic propagation paths and flows of polymer melt and fluid in the cavity during molding. Besides L^1 and L^2, L_S and L_G are the echoes reflected at the solid/liquid and at liquid/gas interfaces, respectively. In Fig. 4-6, ultrasound totally reflected back to liquid during GAIM, resulting in large ultrasonic energy of the L_G reflected at the liquid/gas interface. This will be further discussed with WAIM later. For comparison purposes with ultrasonic data, a temperature and cavity pressure sensor (Kistler type 6190A, ∅4.0mm), whose sensing end is flush with internal surface of the fixed mold and locating at the opposite side of UT-B, is attached as shown in Fig. 4-6.

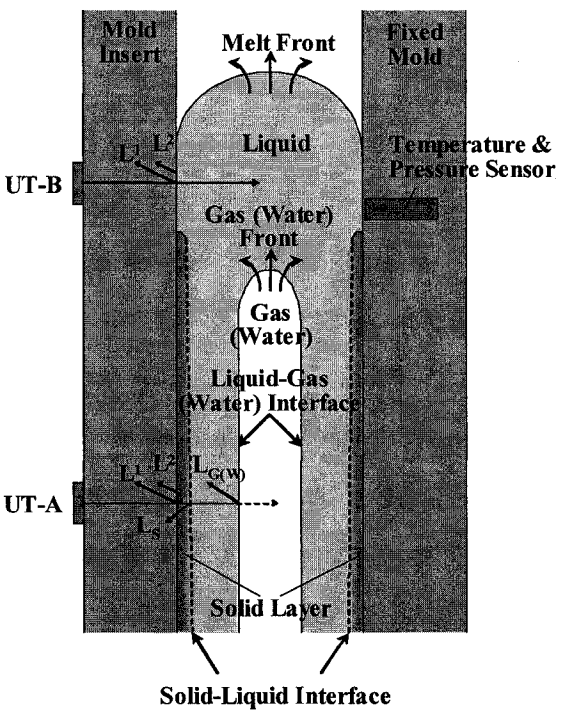

Fig. 4-6 Schematic cross-section of the mold with PZT film HT ultrasonic sensors, indicating ultrasonic propagation paths and flows of polymer melt and fluid (gas or water) in the cavity, with GAIM and WAIM.

The material employed in the experiments of GAIM is a high-density polyethylene (HDPE), from BP chemicals (BP Rigidex HD5050EA), which has good ultrasound propagation properties. Melt and mold temperatures are set at 250°C and 30°C, respectively, throughout and these are the mid point settings suggested by the material manufacturer. The melt injection rate is set to be 60ccm/s over the entire 135ccm melt delivery phase. However, since the peak available injection pressure is reached during the melt injection phase, the actual injection rate is measured to be around 40ccm/s. The gas injection pressures change in these experiments in order to change the RWT and therefore bubble front velocity [158-160]. The bubble propagation and RWT are expected to be monitored by ultrasound data during process. The gas injection pressure settings are 10, 12, 20MPa. The gas pressure is increased to the set value in a single step; holds for 6.0s and then the system valves are released for releasing gas pressure.

Fig. 4-7 presents a molded HDPE part of GAIM / WAIM with an inset of the cross-sections of the part at the UT-A, and RWT areas, where three continuous black dots indicate the corresponding areas of the ultrasonic sensors. The molded part is sectioned at the UT-A and B locations to investigate the dimensions of the hollow structure. The thicknesses and external diameters of the hollow structure at the UT and RWT locations are measured using a thickness gauge. The typical diameter is around 19.43mm and 9.83mm at UT-A and RWT locations, respectively. The measured thicknesses will be compared with those measured by the ultrasonic technique in section 4.6.2. The rough surface in the inside of the molded part at UT-A is caused by the gas / water bubbles during the injection process.

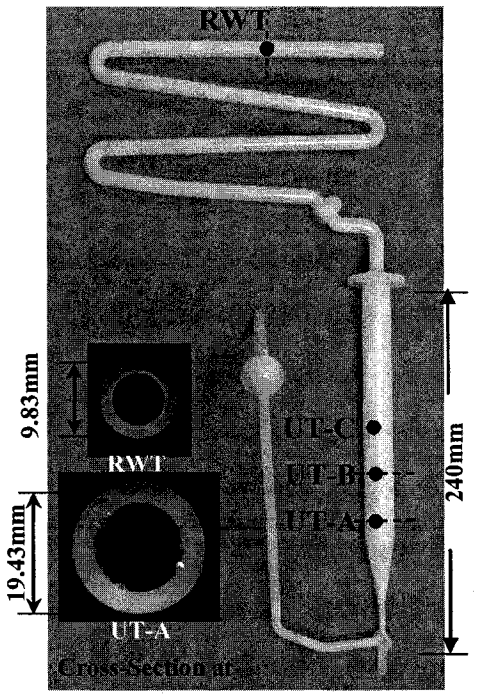

Fig. 4-7: Photograph of a molded HDPE part of GAIM/WAIM with an inset of the cross-sections of the part at the UT-A, and RWT areas, where three continuous black dots indicate the corresponding areas of the ultrasonic sensors.

4.2.4 WAIM

The WAIM experiments are practiced in the same IM machine as that in the GAIM experiment. However, the machine for WAIM is equipped with a water reservoir and the pressure controller. The water bubble functions like gas in GAIM, but its cooling efficiency is expected to be better than that of gas.

Ultrasonic propagation paths and flows of polymer melt and fluid in the cavity during molding for WAIM are indicated in Fig. 4-6. Besides L^1, L^2 and L_S, L_W is the echo reflected at the liquid/water interface. In Fig. 4-6, ultrasound partially transmits to water during WAIM, resulting in less ultrasonic energy of the L_W reflected at the liquid/fluid interface than that of the L_G in GAIM. This will be further discussed later. The material employed

in the experiments of WAIM and molding conditions are the same (HDPE) as in GAIM. The water injection pressure settings are 17.5, 20, 25MPa.

4.3. Results

4.3.1 IM

Fig. 4-8 shows a typical result of acquired signals with the UT1 during the IM process of a 1.0mm-thickness PC part. Although the signals are acquired during whole cycle (30s) in time delay range from 4μs to 24μs covering from the L^1 to L^5 echoes, only the signals at the beginning (from 4s to 9s) and the end (from 22s to 27s) of the process in the time delay range from 4μs to 9.6μs are shown in Fig. 4-8. One can see the L^1 and L^2 echoes reflected at the insert/polymer or air interface depending if the polymer existed at the UT location or not. S^1 represents the first round trip shear wave echo reflected at the insert/air or polymer interface. When the PC melt arrives at the UT1 location at the process time of 5.8s, the L_2 and L_4 echoes propagating in the PC starts to appear. At this moment, the L_6 and L_8 echoes are out of the time delay range shown in Fig. 4-8. At the process time of 25.5s, the L_2, L_4, L_6 and L_8 echoes vanish, which indicates that the molded part is detached from the UT sensor insert. The time delay of the L_2 echo gradually decreases from 6.4μs to 5.5μs with respect to the process time due to solidification and temperature reduction of the part, which will be discussed further in section 4.4.3. Since L_6 can be clearly seen under IM conditions given in Table 4-1, it is expected that the developed sensors can monitor a PC part of a 3mm-thickness.

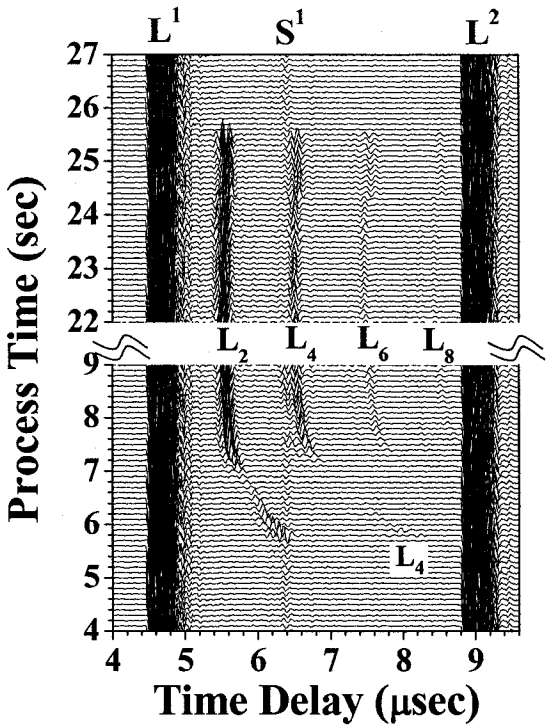

Fig. 4-8 Typical signals measured with the UT1 during IM process of a PC part.

In order to investigate further the correlation between ultrasonic signals observed and the process cycle, the amplitude values of the L^4 and L_2 echoes with respect to the process time are obtained using the signals measured with the UT1. Here the L^4 echo is chosen instead of the L^1 echo since, in principle, higher-order round trip echoes of L^n can lead to higher sensitivity to the ultrasonic sensor insert / polymer interface condition because of more reflections at this interface [161]. The results are presented in Fig. 4-9 (a). Temperature and pressure values measured by the Kistler sensor are also presented in Fig. 4-9 (b). It is noted that the ultrasonic data shown in Fig. 4-9 (a) are acquired with a different cycle from that for the data shown in Fig. 4-8. Hence the process time at which the L_2 echo appears or disappears in Fig. 4-9 (a) is different from that shown in Fig. 4-8. At the process time A, the polymer melt arrives at the UT1 and the Kistler sensor locations

simultaneously. The amplitude of the L^4 echo suddenly decreases and the L_2 echo starts to appear as seen in Fig. 4-9 (a) due to the fact that a proportion of the ultrasonic energy, which has previously been reflected back totally to the transducer when the cavity is empty, is transmitted into the polymer through the UT1 insert/polymer interface and then reflects back at the polymer/fixed mold interface in the mold.

At the same time A, the pressure and temperature rise up sharply from zero to 40MPa and from 116°C to137°C, respectively, as shown in Fig. 4-9 (b). It is noted that the pressure sensor has a threshold in its response, resulting in a slight time delay comparing with the ultrasonic data (~0.1sec with our experimental conditions). In addition, the measured temperature is smaller than the melt temperature of 320°C since it is not the melt temperature but "contact (or surface)" temperature of the part, which is significantly affected by the interface condition between the sensor and polymer surfaces.

Just after time A, the amplitude of the L_2 echo decreases and increases during a few seconds in the time range between 5s and 7s, which reflects the variation of ultrasonic attenuation in the polymer because of its solidification. This will be further discussed later. At process time B, the mold opens and the molded part is detached from the fixed mold. Consequently, the amplitude of the L_2 echo increases due to the almost total reflection at the polymer/air interface and the pressure drops to zero. At time C, the amplitude of the L^4 echo recovers to its initial value and the L_2 echo disappears, indicating that the part is detached from the UT1 insert due to the part ejection. Hence, the times of the flow front arrival, mold open and part detachment are clearly observed on the ultrasonic echoes as indicated by the arrows A, B and C, respectively, in Fig. 4-9 (a) and (b).

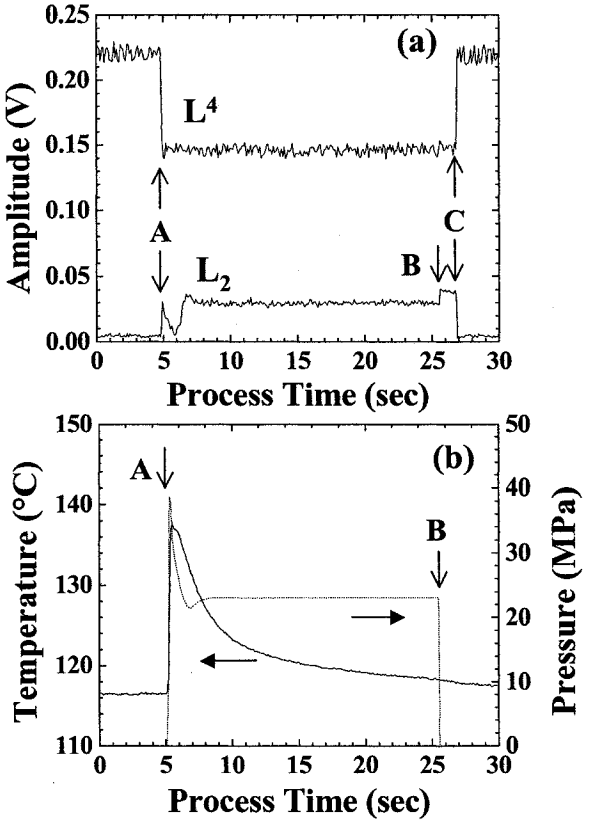

Fig. 4-9 (a) Amplitude variations of L^4 and L_2 echoes measured with UT1, and (b) temperature (solid line) and pressure (dotted line) variation measured with Kistler sensor during IM process. Arrows A, B and C indicate the time for flow front arrival at UT1 location, mold open and part ejection, respectively.

4.3.2 COIM

Fig. 4-10 (a) and (b) show the typical results of acquired signals with the UT1 and UT2, respectively, during one cycle of COIM when the core volume percentage is 58% (part #1 in Fig. 4-5 (b)). It is noted that, even there are four ultrasonic sensors in the mold, only the ultrasonic signals acquired by UT1 and UT2 are employed in this thesis. The total part thickness at the sensor location is 3.54mm. Besides L^1 and L^2 echoes, when the polymer melt arrives at the UT1 location, the L_2 echo is observed with the UT1 if the echo is stronger than

the noise level of the measurement system. The L_2 echo may not be observed if attenuation of ultrasound in the polymer is so high that the echo is attenuated away or becomes less than the noise level before returning back to the UT1. This is due to the high attenuation of the skin (ABS) and core (PC) materials in their liquid state [22, 142]. When the polymer temperature decreases and the part starts to solidify, the attenuation of the skin and core materials reduces and the L_2 echo may be observed. In the presented experiment, the L_2 appears at the process time of 15s in Fig. 4-10 (a). The time delay of the L_2 echo gradually decreases from 8.8μs to 8.2μs with respect to the process time due to solidification and temperature reduction of the part. The ultrasonic velocity increases as the polymer solidifies, which will be discussed further in section 4.4.3.

In addition to the L^1, L^2 and L_2 echoes, the echoes L_2' and L_2" propagating in the polymer and reflected at the skin layer1/core layer and core layer/skin layer2 interfaces, respectively, are also observed in Fig. 4-10 (a), indicating the arrival of the 1st core at the UT1 location. The echoes L_2' and L_2" appears at around 8.5s and 15s, respectively. This timing indicates the detection of the echo reflected at the skin layer1/core layer and core layer/skin layer2 interfaces due to the injection of the core material. The appearing time difference between L_2' and L_2" is because of the attenuation of core material, thickness of the core layer and shape of the core front. At the process time of 33.5s, the L_2, L_2' and L_2" echoes vanish, which indicates that the molded part is detached from the HT ultrasonic sensor insert due to the mold open. The time delay difference between the two adjacent echoes (Δt_l (l = 1, 2, 3) in Fig. 4-10 (a)) implied the thickness of the layer. The measurement of the layer thicknesses using these echoes will be discussed further in section 4.5.3.

In Fig. 4-10 (b), in addition to the L^1, L^2 and L_2 echoes, the echoes L_2', L_2", L_2"' and L_2"" reflected at the skin layer1/core layer1, core layer1/core

layer2, core layer2/core layer3 and core layer3/skin layer2 interfaces in Fig. 4-4 (b), respectively, are observed. Due to the picture resolution, the L_2'''' echo is not clear thus highlighted by dotted line. These multiple echoes indicate the arrival of the 1st (PC) and 2nd (ABS) core materials at the UT2 location. It is noted that only the 1st core (PC) but not the 2nd core (ABS) reaches the UT1 location in the presented experiment. The time delay difference between the two adjacent echoes implies the thickness of the layer as mentioned above. This also proves that the ultrasonic technology can measure the layer thickness of 5-layers part. The difference of the process times when the echo L_2' starts to be observed at the UT1 and UT2 locations shown in Fig. 4-10 (a) and (b), respectively, can be used to calculate the average speed of the core flow. This will be discussed further in section 4.5.1.

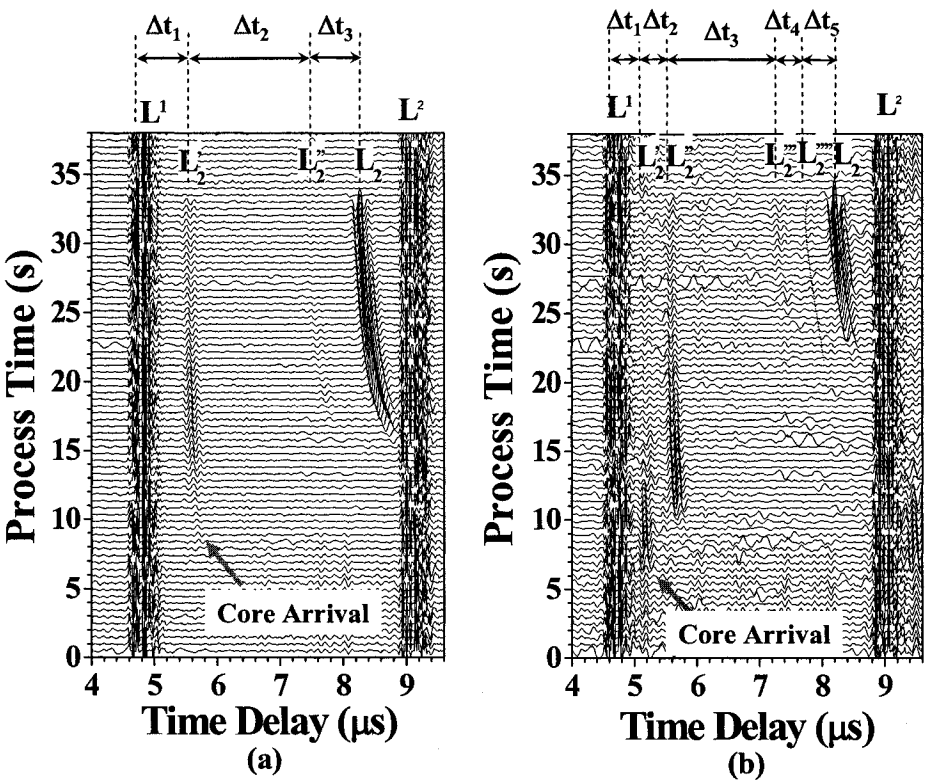

Fig. 4-10 Ultrasonic signals acquired during one cycle of COIM process at the (a) UT1 and (b) UT2 locations when the core volume percentage is 58%.

In order to investigate further the correlation between the ultrasonic signals observed with the UT1 and the molding cycle, the amplitude values of the L^1, L_2, L_2' and L_2" echoes in Fig. 4-10 (a) with respect to the process time are compared with the cavity pressure at the UT1 location. The results are presented in Fig. 4-11 (a) for the amplitude of the ultrasonic echoes and Fig. 4-11 (b) for the pressure. According to machine's recording, the skin, 1st and 2nd core materials are injected at the process time of 2.7s, 3.4s and 5.2s, respectively.

At the process time of 5.8s, the polymer melt arrives at the cavity area beneath the UT1, since the amplitude of the L^1 echo decreases. At this moment, the cavity pressure starts to increase as seen in Fig. 4-11 (b), and it reaches the peak value at 7.8s. At 8.5s, the L_2' echo starts to appear indicating the detection of the echo reflected at the skin layer1/core layer interface due to the injection of the core material. At 15s, the L_2" and L_2 echoes start to appear indicating that the detection of the ultrasound propagated in the polymer and reflected at the core layer/skin layer2 and skin layer2/fixed mold interfaces. The L_2" and L_2 echoes start to appear at 15s which is after 6.5s as the L_2' echo appearing, because the L_2" and L_2 echoes have longer propagation distance than L_2', resulting in higher attenuation for them than for the L_2'. At 33.5s, the amplitude of the L^1 echo recovers to the initial value and the L_2, L_2' and L_2" echoes disappear, because of total reflection at the probing end/air interface, indicating that the molded part is detached from the surface of the mold cavity due to the mold open. The cavity pressure also reduces to zero at this moment.

From Fig. 4-10 (a) and (b), one can see that the developed sensors can monitor a COIM part of a 3.54mm thickness by transmitted ultrasonic echoes under the IM conditions given in Table 4-2. However, according to Fig. 4-11 (a), the process of any thickness parts can be monitored by the reflected ultrasonic echo.

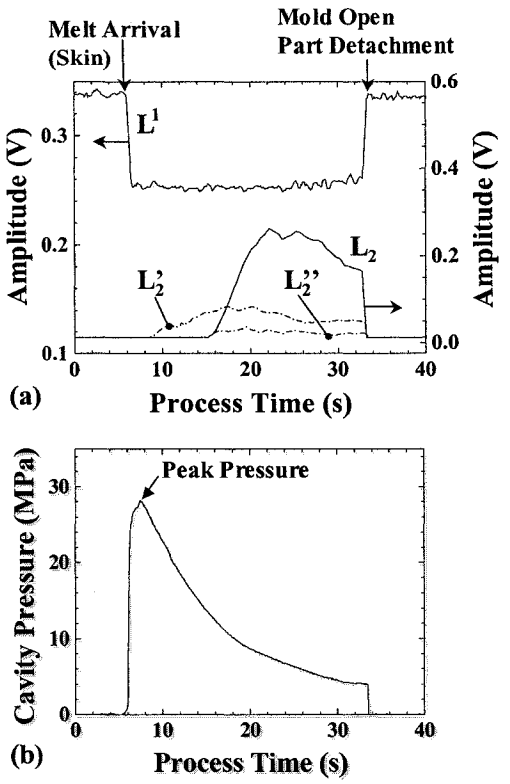

Fig. 4-11 Amplitude variations of (a) L^1, L_2, L_2' and L_2" echoes in Fig. 4-10 (a) measured by the UT1, and (b) cavity pressure measured by the pressure sensor facing to the UT1, with respect to the COIM process time.

4.3.3 GAIM

Fig. 4-12 shows a typical result of acquired ultrasonic signals with UT-A in Fig. 4-6 during one cycle of GAIM. The injected material is HDPE. In addition to the L^1 and L^2 echoes, the L_S and L_G echoes are observed. Around the process time of 9s after the gas is injected, the L_G starts to appear, indicating that the detecting gas front is observed at the UT-A location. Around 27s, the L_G and L_S echoes disappear, before the mold opens and the part ejects, due to the part detachment from the cavity surface at the UT areas because of the part shrinkage during cooling. At this moment, the time delay difference between the L_S and L_G echoes can be an evidence of that the HDPE melt is not completely solid. In the process time form 9s to 27s, the time delay

of the L_G echo varies from 14.5μs to 13μs indicating that the solidification, temperature reduction of the part and the wall thickness reduction due to the movement of gas bubble. However, in the same period, the variation of the L_S echoes only implies the solidification and temperature reduction of the part. The typical wall thickness of a GAIM part is 3.6mm. It is noted that the small echoes S^n (n=1, 2) always appearing at the time delay of 9μs and 12μs are the n^{th} round-trip shear-wave signals propagating in the mold insert.

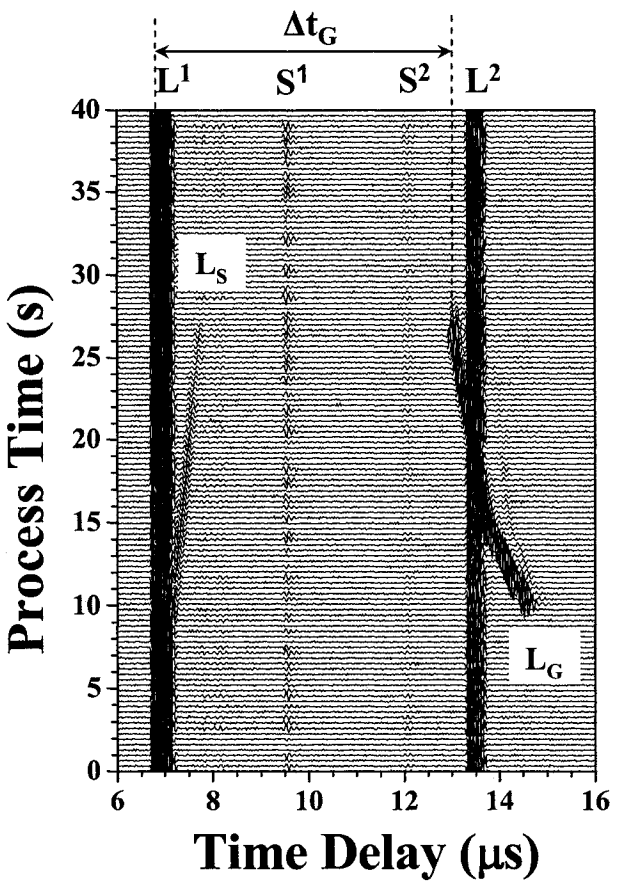

Fig. 4-12 Typical signals acquired during one cycle of GAIM process for a HDPE part of 3.6mm wall thickness.

In order to investigate further the correlation between the ultrasonic signals observed and the molding cycle, the amplitude values of the L^2 and L_G echoes, in Fig. 4-12, with respect to the process time are compared with the gas pressure, supplied by the gas controller, and cavity pressure, measured by

a pressure sensor in the UT-B location. The results are presented in Fig. 4-13 and 4-14. Here the L^2 echo is chosen instead of the L^1 echo, and the reason is explained above [161]. In Fig. 4-13, at process time of 6.3s, the polymer melt arrives at the cavity area beneath the UT-A, since the amplitude of the L^2 echo decreases. At process time of 6.5s, the cavity pressure starts to increase indicating that the polymer melt arrives at the cavity area beneath the UT-B as seen in Fig. 4-14. Thus average polymer melt speed, V_m, during molding can be measured using the time difference (Δt_m) of the drop of the L^2 echo at the UT-A and the appearance of the cavity pressure at the UT-B location. The V_m can also be measured by using the time difference (Δt_m) of the drop of the L^2 echo at the UT-A and UT-B locations. This phenomenon will be further discussed in section 4.4.1. The average polymer melt speed is around 175mm/s.

At 8.3s, gas is injected into the cavity, and gas pressure starts to increase, as seen in Fig. 4-14. In Fig. 4-13, the amplitude of the L_G echo starts to increase at 9.2s, indicating that the gas bubble is observed at UT-A location. From 13.8s to 21.7s, the amplitude of the L^2 and L_G echoes are blank out because of the overlap of the L^2 echo with L_G echo, as shown in Fig. 4-12. The overlapping signals deform and are different from the original ones. In Fig. 4-14, from 8.3s to 10.5s, the vibration of cavity pressure indicates the unsteady state of pressure due to the movement and filling of the gas bubble inside the polymer and the perturbation of gas pressure. The movement of gas bubble inside the mold would affect the measurement of cavity pressure. At 27.5s, the amplitude of the L^2 echo recovers to the initial value, and the L_G echo, gas pressure and cavity pressure disappear, indicating that the molded part is detached from the surface of the mold cavity due to part shrinkage during cooling. Ultrasonic contact duration is defined as the period from decreasing of the amplitude of the L^2 echo to recovering to its initial value, which is the process time from 6.3s to 27.5s in this experiment. The contact duration can

indicate the period during which the part and mold are in contact and help in evaluation of the cooling efficiency. This information will be discussed further in section 4.6.3.

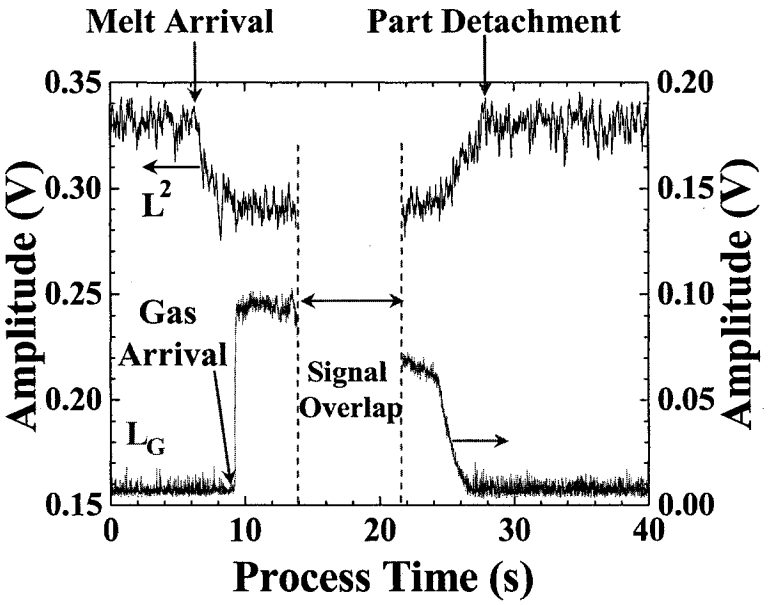

Fig. 4-13 Amplitude variations of L^2 and L_G echoes, measured by UTA with respect to the GAIM process time.

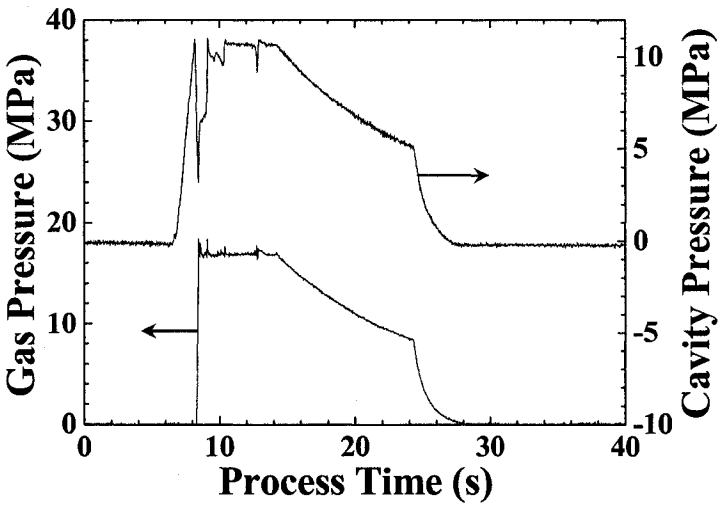

Fig. 4-14 Amplitude variations of gas pressure, supplied by the gas machine, and cavity pressure, measured by the pressure sensor facing to the UTB, with respect to the GAIM process time.

4.3.4 WAIM

Fig. 4-15 shows a typical result of acquired ultrasonic signals with UT-A during one cycle of WAIM. The injected material is HDPE. In addition to the L^1, L^2 and L_S echoes, the L_W appearing at the process time of 10s, at the time delay of 12.5μs, is an echo reflected from liquid (HDPE melt)/water interface. The reasons why the SNR of the L_W echo in Fig. 4-15 is poorer than that of the L_G echo in Fig. 4-12 is: ultrasound reflection coefficient at the liquid (polymer melt)/water interface is 0.2, thus 20% of ultrasound is reflected at this interface in WAIM, while that at the liquid/gas interface is 1 (totally reflect) in GAIM [154]; and the wall of the molded part made by the WAIM contains voids which scatters and/or attenuates ultrasonic signals propagating in the wall. The typical HDPE wall thickness of a WAIM part in the experiments is 3.6mm.

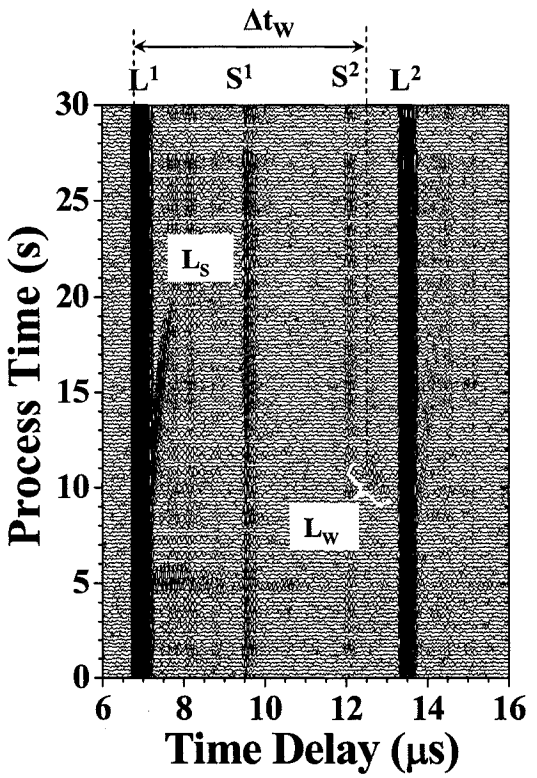

Fig. 4-15 Typical signals acquired during one cycle of WAIM process for a HDPE part of 3.6mm wall thickness.

4.4. Discussions in IM

4.4.1. Melt flow front and melt speed

During the filling stage, as shown in Fig. 2-1 (i), the flow front advancement and flow front velocity of melt PC are critical information. The flow front position can be used to control the plunger speed so as to allow smooth transition from the filling to the packing/holding stages, as shown in Fig. 2-1 (ii), to avoid part flashing and mold damage due to high impact. Fig. 4-16 shows the L^4 echoes measured with the UT3 and UT4, shown in Fig. 4-1. In this experiment, the signals are acquired every 3ms (333Hz) for higher time resolution. As mentioned previously, the amplitude of the L^4 echoes steeply decrease at the time A for UT3 and A' for UT4, indicating flow front arrival at each UT location. Therefore, the average flow front velocity, V_m, between the UT3 and UT4 is calculate to be 306mm/s by using

$$V_m = D / \Delta t_m \qquad \text{(Eq. 4-1)}$$

where D (=34.9mm) is the distance between UT3 and UT4, and Δt_m (=114ms) is the time difference between A and A'. This ultrasonic technology of measuring average flow speed can be applied to most of the IM processes.

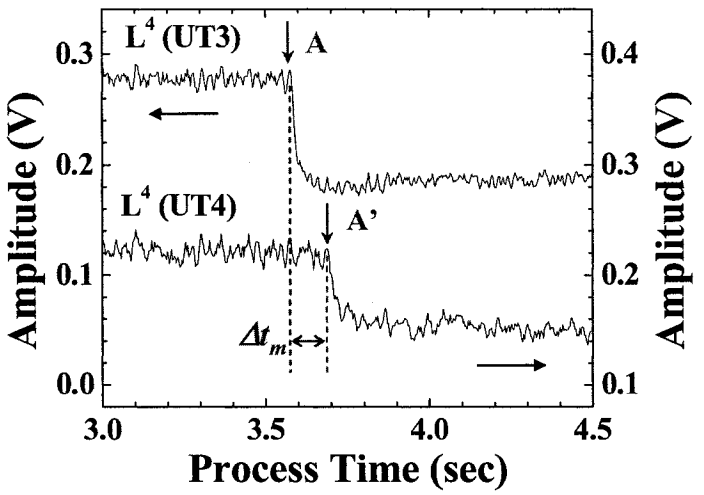

Fig. 4-16 Amplitude variation of L^4 echoes measured with UT3 and UT4 showing the time difference (A-A') of flow front arrival at each UT location during IM of a PC part.

4.4.2. Filling incompleteness

Filling completion of the mold with the materials is the most critical requirement for the molding process since the incomplete part must be rejected. Fig. 4-17 shows one incomplete (#1) and three complete (#2-4) PC parts molded successively under the same IM conditions. Accidentally the part #1 has defects on both bottom edges as indicated by arrows in Fig. 4-17. The volume filling rate for the part #1 is calculated to be 99%. Fig. 4-18 presents the amplitude of the L_2 echoes, obtained during the cycles for the parts #1-4 shown in Fig. 4-17, with the UT1-4, whose locations are indicated in Fig. 4-17. Even though the part is filled at UT3 and UT4 locations for the part #1, one can see that the L_2 echoes measured with the UT4 appears for a few seconds only at the beginning of the cycle. In addition, the amplitude of the L_2 echoes measured with the UT3 gradually decreases to noise level before the mold opens at time B. These are due to the fact that the part detachment at

the UT3 and UT4 locations occurs before the mold opens because of shrinkage of the part caused by the lack of enough filling pressure. The L_2 echoes measured with the UT2 for the part #1 appears in the entire time range between A and B, however the amplitude is a little smaller comparing with those for the part #2-4. It is concluded that the presented ultrasonic method has the ability to monitor the incomplete filling of the PC part during IM process even with filling rate of 99%.

It is noted that the part ejection time C is not observed on the L_2 echoes measured with UT2 and UT3 for the part #2-4, as shown in Fig. 4-18, since the part detachment at UT2 and UT3 locations has already occurred at time B, and no ultrasonic energy is transmitted and reflected from the part. This is due to that the center of the part along with gate area is weakly pulled towards the fixed mold when the mold opens at time B, as shown in Fig. 2-1 (iii), resulting in the slight bending of the center area of the part and detachment of this area from the UT2 and UT3 locations which are near the gate in the fixed mold. The gate area is cut from the molded parts after the ejection; hence it is not seen on the parts shown in Fig. 4-17.

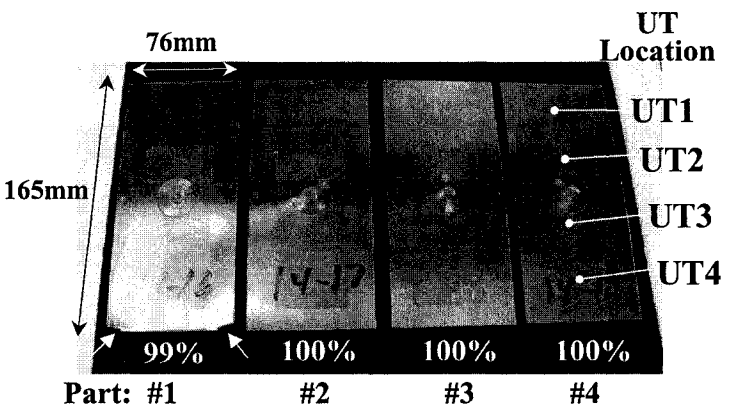

Fig. 4-17 One incomplete (#1) and three complete (#2-4) PC parts of 1mm-thickness molded successively under the same IM conditions. Filling rate of part #1 is 99%.

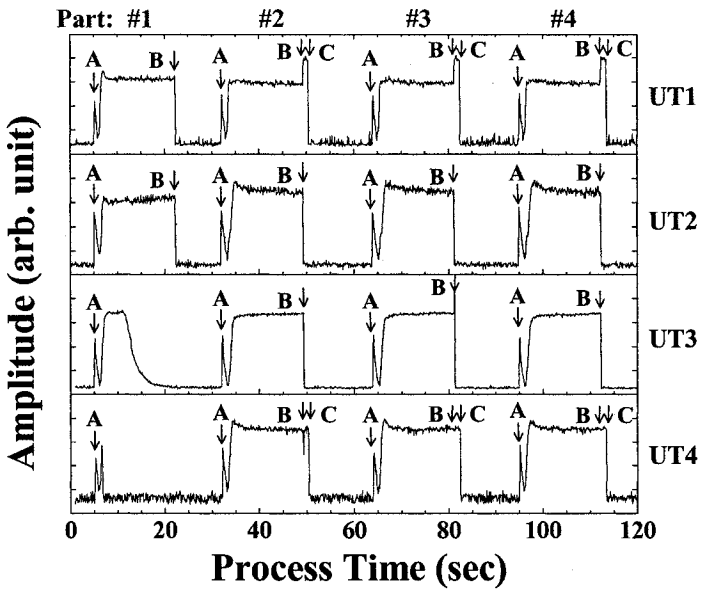

Fig. 4-18 Amplitude variation of L_2 echoes measured during injection cycles for the PC parts #1-4 shown in Fig. 4-17 during IM process.

4.4.3. Solidification

Ultrasonic velocity and attenuation inside the molded parts are strongly related to the physical properties of the molded part. Therefore, solidification of the molded part may be monitored with the velocity and attenuation during the process. They can be determined using the time delay and amplitude variations of the L_{2n} echoes propagating in the polymer, as shown in Fig. 4-8, provided that the echoes have sufficient SNR. The ultrasonic velocity in the polymer, V_P, is determined by (Eq. 3-14),

$$V_P = 2h / \Delta t_h \qquad \text{(Eq. 3-14)}$$

where h=1.0mm is the thickness of the mold cavity measured at the UT location by a micrometer, with an accuracy of $\pm 1\mu m$, and $\Delta t_h = t_2 - t_4$. t_2 and t_4 are the time delay of the L_2 and L_4 echoes, respectively.

During the molding process, the attenuation, α, of the amplitude of the L_{2n} echo, which is associated with the ultrasonic attenuation in the molded part, is calculated by:

$$\alpha = \frac{10}{h}\log_{10}\left(\frac{|L_2|}{|L_4|}\right) \qquad \text{(Eq. 3-16)}$$

where $|L_2|$ and $|L_4|$ are the amplitude of the L_2 and L_4 echoes, respectively [140-141]. The spline interpolation and moving average techniques are conducted on the acquired signals to obtain the time delay and amplitude of the echoes used for velocity and attenuation measurements, respectively.

Fig. 4-19 presents the ultrasonic velocity and the attenuation of the L_{2n} echo obtained at the UT2 location using (Eq. 3-14) and (Eq. 3-16), respectively. At the process time between 6.3s and 7.2s, indicated by the dotted lines in Fig. 4-19, the data are missed, since the ultrasonic attenuation in the polymer is so high due to the solidification [26] that the L_4 echo doesn't have sufficient SNR to determine its time delay and amplitude. The measured velocity inside the PC varies from 950m/s to 1600m/s and the attenuation from 6dB/mm to 3dB/mm due to the variation of the material properties of the part, such as elastic constants, viscosity and density, indicating a transformation of the polymer from the molten state to solid state [26]. The ultrasonic velocity increases as the polymer solidifies. Such a variation of ultrasonic velocity in the polymer can be used to monitor the solidification behavior of the polymers in the mold cavity during processing

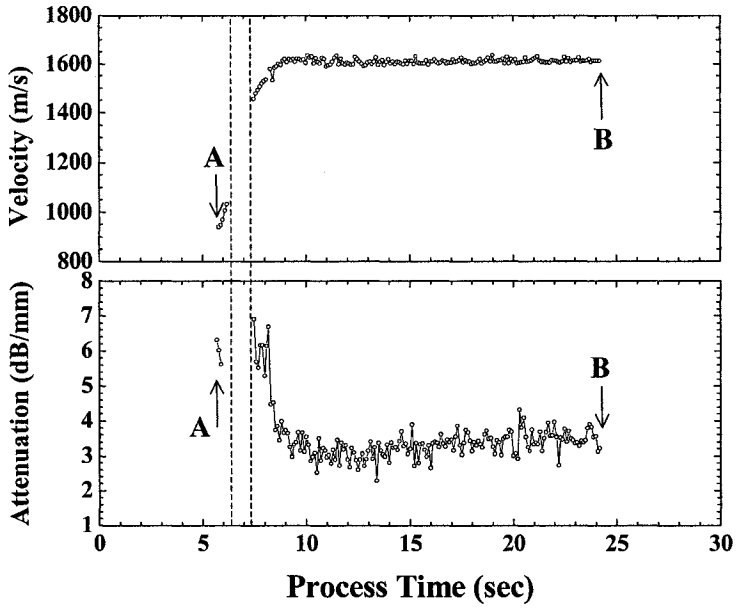

Fig. 4-19 Ultrasonic velocity in the molded PC part and attenuation of L_{2n} echo obtained using L_2 and L_4 echoes measured with UT2.

4.5. Discussions in COIM

4.5.1 Core flow speed

Tracking the flow speed of a melt core material during molding may present an opportunity to investigate the physical properties of the materials as well as process conditions. In order to measure the melt core flow speed inside the mold during the COIM process, the amplitude variation of the L_2' echo measured by the UT1 and UT2 with respect to the process time are obtained. The results are presented in Fig. 4-20. The L_2' echoes at the UT2 and UT1 locations start to appear at 6.5s and 8.5s, since the 1st PC core arrives at the areas beneath the UT2 and UT1, respectively. The ultrasonic energy transmitted into the melt is reflected partially at the skin layer1 (ABS)/core layer (PC) and skin layer1 (ABS)/core layer 1 (PC) interfaces as shown in Fig. 4-4 (a) and (b), respectively. Thus, the average core flow speed (Vc) between

the UT2 and UT1 is estimated using the time difference (Δt_{fc}) of the appearance of the L_2' echoes at the UT2 and UT1 locations by (Eq. 4-1), where L is the same value as in section 4.4.1. The slope of the amplitude variation of the L_2' with the process time measured by the UT2 is steeper than that by the UT1, suggesting that an instant flow speed at the UT2 location near the gate is faster than that at the UT1 location near the cavity edge. It is noticed that when the setting core volume percentage is less than 45%, the 1st core material (PC) does not reach to the UT1 location, thus the average core flow speed cannot be estimated using the UT2 and the UT1 by the presented method. However, the amplitude slope may be used to evaluate the instant melt flow speed at each UT location.

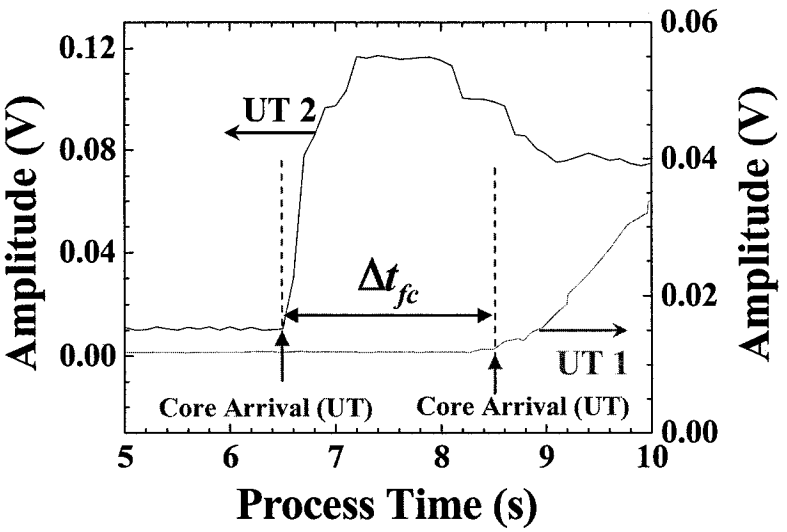

Fig. 4-20 Amplitude variations of L_2' echoes, measured by the UT2 and UT1, with respect to the process time during COIM process.

4.5.2 Cavity pressure

In order to investigate the material behavior during molding, the peak

cavity pressure and melt core flow speed are studied with respect to the core volume percentage. The measured average melt core flow speeds (Vc) and the peak cavity pressures, when the actual core volume percentages are larger than 45%, are presented in Fig. 4-21. Actual core volume of each part is measured by the movement of injection piston. It is noted that, even under the same machine volume setting, the actual core volume are different from the setting values and varies within 5% due to the inaccuracy of machine. In the range of the core volume percentage from 48 to 60%, the average core (melt PC) flow speed increases monotonically from 4.9 to 16.3mm/s, and the peak cavity pressure decreases from 36.8 to 26.5MPa. This is because when the skin material is less, the melt core flows more easily, resulting in higher melt core speed and less cavity pressure. This information can be used to adjust injection speed and core volume percentage to avoid break through. These data also provide valuable insights into the actual processing conditions that can be utilized to validate the results from mold filling simulations.

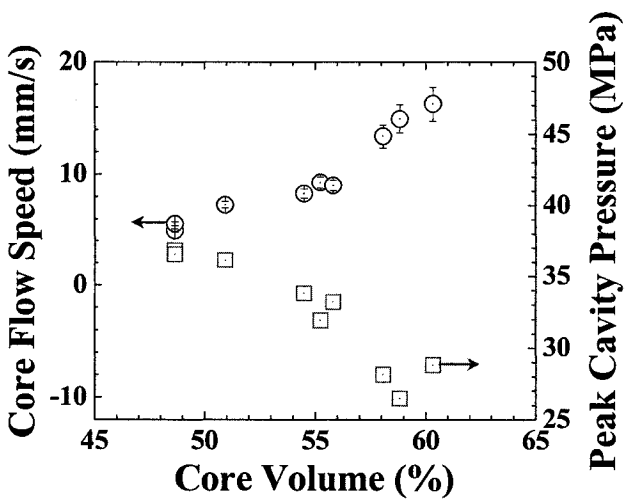

Fig. 4-21 Core (melt PC) flow speeds (circles) between the UT2 and UT1, measured by ultrasonic technique, and peak cavity pressures (squares), measured by the pressure sensor facing to the UT1, with respect to the actual core volume percentages measured.

4.5.3 Layer thickness

A control of thicknesses of a skin and core of the molded part as well as a core volume percentage is crucial for COIM. However, it would be difficult to measure such parameters noninvasive and nondestructively during molding when the skin material is not transparent, to which optical methods may not be applicable. Thus a real-time ultrasonic thickness measurement of the parts, involving the skin and core layer thicknesses, is conducted during COIM process.

The layer thicknesses of the h_1 (ABS), h_2 (PC) and h_3 (ABS) in the UT1 location in Fig. 4-4 (a) can be determined during molding using the time delay of the L^1, L_2, L_2' and L_2" echoes in Fig. 4-10 (a). If the ultrasonic velocities in the skin layer1 (V_1), skin layer2 (V_3) and core layer (V_2) are known, the thicknesses can be calculated by (Eq. 3-17):

$$h_l = (V_P \times \Delta t_l)/2 \text{ , (p, } l = 1, 2, 3) \qquad \text{(Eq. 3-17)}$$

where Δt_1, Δt_2 and Δt_3 are the time delay difference between L^1- L_2', L_2' - L_2" and L_2" - L_2, respectively, in Fig. 4-10 (a).

The total part thickness of h can be obtained by: $h = h_1 + h_2 + h_3$. In order to obtain the ultrasonic velocities of the ABS (V_1 and V_3, where $V_1 = V_3$) and PC (V_2), each material is completely injected into the mold cavity to produce the entire part. The velocity is determined using the time delay of the L_2 and L_4 echoes propagating in the polymer by (Eq. 3-14), where h (=3.54mm) is the depth of the mold cavity at the UT1 location measured by a micrometer with an accuracy of ± 1μm, and t_2 and t_4 are the time delay of the L_2 and L_4 echoes, respectively, for each material.

For each core volume percentage setting, we chose one of the three molded parts to measure the skin and core thicknesses at the UT1 location by the ultrasonic technique. Subsequently, the parts are sectioned and the layer thicknesses are measured using an optical microscope. The molded parts have the core volume percentage settings of 58, 55, and 50%. Fig. 4-22 shows a photograph of a cross-section of the molded part with the core volume percentage setting of 50% at the location of the UT1 in Fig. 4-4 (a), 4-5 (a). The measuring results of the skin and core thicknesses are presented in Fig. 4-23. The experimental results presented in Fig. 4-23 are related to the core volume percentage settings of 58, 55 and 50%.

In the ultrasonic method, the time delays of the echoes, in Fig. 4-10 (a), at the process time when the mold is about to open are used. The measured thicknesses of the h_1, h_2 and h_3 are presented by square, circle and triangle symbols (filled: optical microscope technique, open: ultrasonic technique), respectively. In the range of the actual core volume percentage from 48 to 60, the core layer thickness increases linearly while the skin layer thickness decreases linearly. The results measured by the ultrasonic method have the agreement with those by the optical microscope within accuracy of ±17%. The error bars in Fig.4-23 are the estimated measurement errors (less than 5%). The same method can be applied to measure the layer thickness in UT2 location. Therefore, ultrasonic technique can be used to measure the thicknesses of the core and skin layers in real-time within certain accuracy and without cutting the molded parts. This information can also be used to adjust the core volume percentage to achieve the desired part quality and optimize the process parameters.

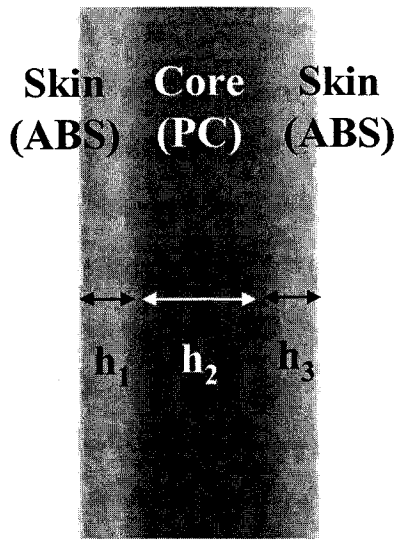

Fig. 4-22 Photograph of a cross-section of the molded COIM part at the location of the UT1, shown in Fig. 4-4 (a), 4-5 (a).

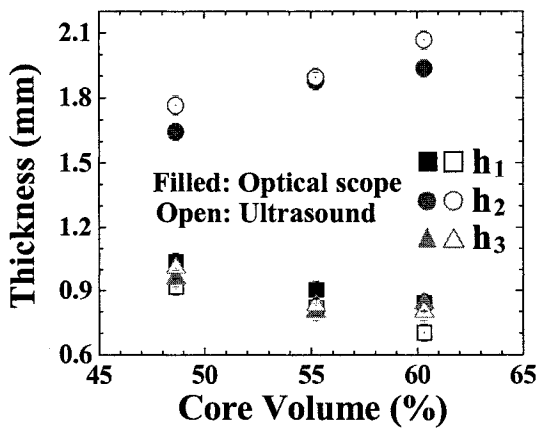

Fig. 4-23 Thicknesses of the skin layer1, skin layer2 (ABS) and core (PC) layer (marked as □, Δ, and ○, respectively) of the molded COIM parts measured by an optical microscope (filled symbols) and the ultrasonic technique (open symbols) at the UT1 location with respect to the actual core volume percentages

4.5.4 Core length

In COIM, the dimension of the core material in the molded part affects the performance and mechanical properties of molded parts. Real-time monitoring of core material movement is desirable. However, in general, core materials are covered by opaque skin materials, thus, an optical technique may be difficult to be applied unless the molded part is sectioned. Therefore, it is our intention to estimate the core dimension by an ultrasonic technique in real-time. Fig. 4-24 presents the core lengths (circle) and widths (square) with respect to the actual core volume percentages. The lengths and widths are measured by a caliper with an accuracy of ± 10μm. In the range of actual core volume percentages from 24 to 60%, the core length increases linearly from 68 to 164mm. While, the core width increases linearly up to 44% but is saturated to be around 72mm, which is 4mm shorter than the mold cavity width, after 48%.

It is noted that when the core volume percentages are larger than 45%, only the 1st core material can reach the UT1 location in the presented experimental conditions. Thus, in the following discussion, only the molded parts with the actual core volume percentages of more than 45% are investigated because the core may reach the edge of the cavity (break-through of the skin), which is undesired for the molded parts. Three parameters, such as the core thickness, core flow speed and peak cavity pressure are investigated in order to estimate the length of the core of the molded parts. A correlation between the core thickness at the UT1 location, measured by the ultrasonic technique presented in section 4.5.3, and the core length, measure by a caliper, is studied. The results are shown in Fig. 4.25. In the core length range from 138.95 to 164.13mm, the core thickness increases linearly from 1.76 to 2.06mm. The straight line is obtained by a least square fitting method. The standard deviation (SD) is 2.6mm. It is noted that the correlation between

core length and thickness is affected by mold geometry, core volume and process variables, such as injection speed, melt and mold temperature. Here, only the core volume is changed. If other parameters change, the correlation would vary relatively.

A correlation between the average core flow speeds, measured by the ultrasonic method presented in section 4.5.1, and the core length is shown in Fig. 4-26. In the range of the average core flow speed from 4.9 to 16.2mm/s, the core length increases linearly from 138.95 to 164.13mm. The SD is 4.1mm. A correlation between the peak cavity pressure, measured by the pressure sensor in Fig. 4-3, and the core length is shown in Fig. 4-27. In the range of the peak cavity pressure from 26.2 to 36.9MPa, the core length decreases linearly from 164.13 to 138.95mm. The SD is 4.5mm. Among the three parameters, the core length has better correlation with core thickness. Through estimating the core dimension, optimizing process parameters can be achieved.

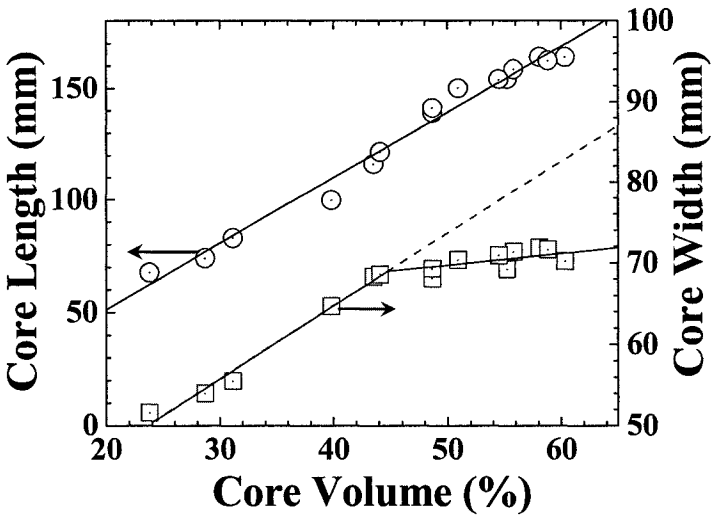

Fig. 4-24 Core length (o) and width (□), measured by a caliper, with respect to the actual core volume percentages measured.

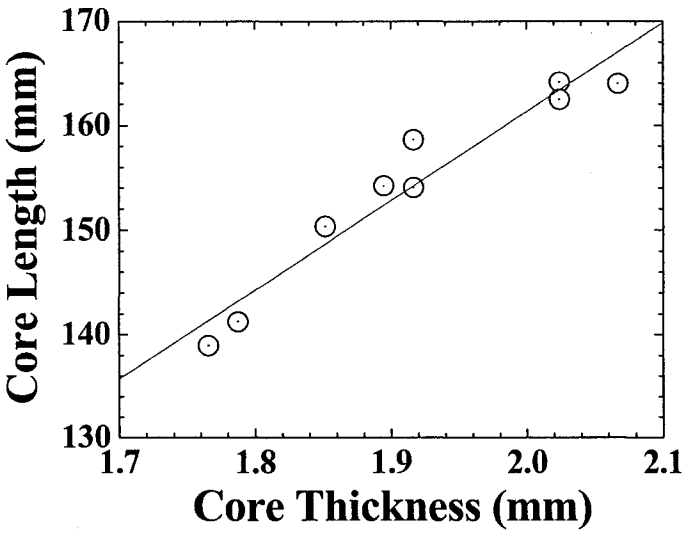

Fig. 4-25 Core lengths, measured by a caliper, with respect to core thicknesses, measured by the ultrasonic technique at the UT1 location, for the molded COIM parts in Fig. 4-21.

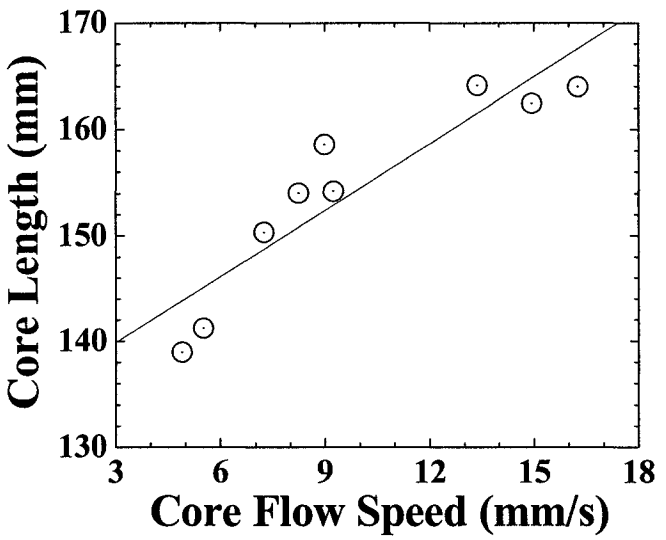

Fig. 4-26 Core lengths with respect to core flow speeds between the UT2 and UT1 measured by the ultrasonic technique, for the molded COIM parts in Fig. 4-21.

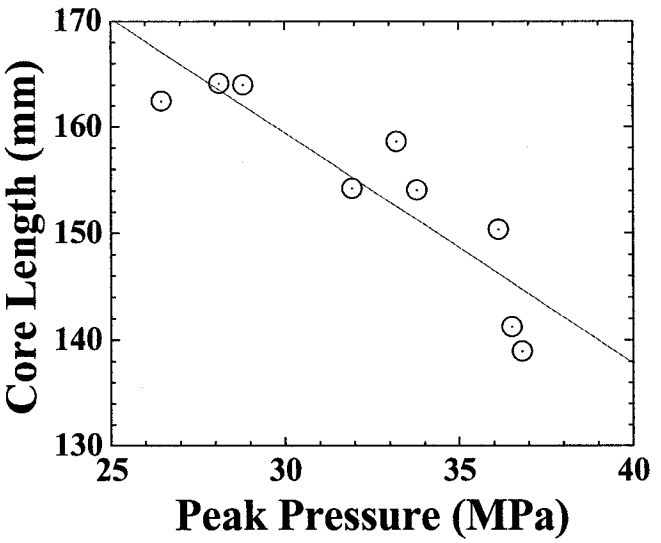

Fig. 4-27 Core lengths with respect to the peak cavity pressures, measured by the pressure sensor facing to the UT1, for the molded COIM parts in Fig. 4-21.

4.6 Discussions in GAIM and WAIM

4.6.1 Gas flow speed

Tracking the flow front speed of the gas bubble over molding cycles may present an opportunity to detect needle blockages or reductions in gas supply pressure to the mold. Fig. 4-28 presents the amplitude variations of the L_G echoes, measured by UT-A and UT-B, with respect to the process time. The injected material is HDPE. The L_G echoes begin to be observed at 9.2s and 9.7s with the UT-A and UT-B, respectively, when gas arrived at each UT location. Therefore, average gas flow speed (V_g) can be estimated using the time differences (Δt_{fg}) of appearances of the L_G echoes at the UT-A and UT-B locations by (Eq. 4-1), where D (=35mm) is the distance between the UT-A and UT-B. The results are presented in Fig. 4-29. Gas flow speed increases with gas pressure. The bubble speed is linked to the formation of the RWT, where higher speed (higher pressure) results in a thinner RWT. In addition,

these data provide valuable insights into the actual processing conditions that can be utilized to validate the results from mold filling simulations.

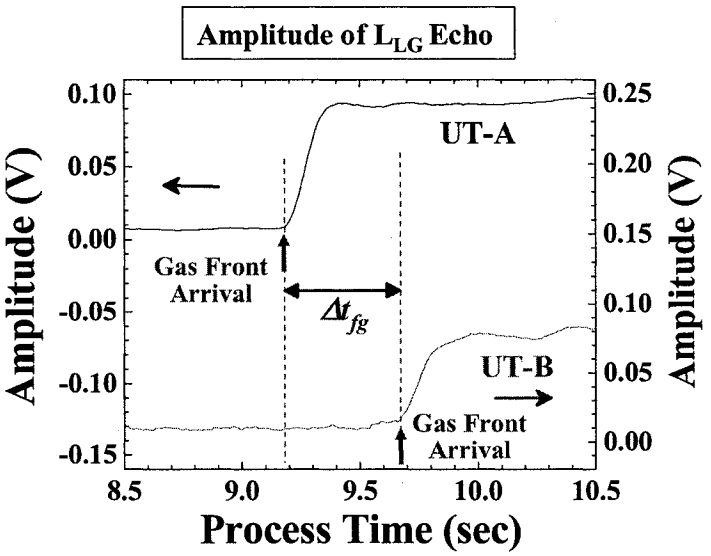

Fig. 4-28 Amplitude variations of L_G echoes, measured by UT-A and UT-B, with respect to the GAIM process time. Rapid increase of the amplitudes indicates the gas front arrival at each UT location.

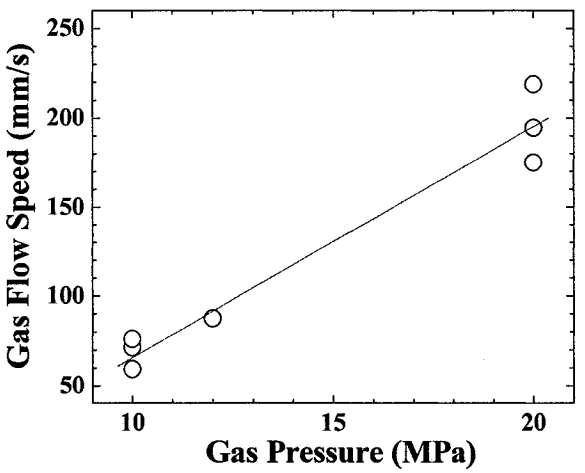

Fig. 4-29 Gas flow front speed between the UT-A and UT-B measured by ultrasonic technique with different gas pressures.

4.6.2 Wall thickness

Quality control to evaluate the wall thickness of the molded part is crucial for fluid assisted injection molding. But currently the measuring method is limited to off-line techniques, in which the parts are cut to measure the wall thickness. Thus, real-time ultrasonic thickness measurement of the parts is conducted during fluid assisted injection molding process. After molding, the molded parts are sectioned and a thickness gauge, with the accuracy of ±1μm, is used to measure wall thickness at the locations corresponding to the UT-A and UT-B positions in Fig. 4-6. The measuring results of HDPE part wall thickness for GAIM and WAIM are shown in Fig. 4-30 and 4-31, respectively. In these two figures, the closed squares (■) and circles (●) represent the measured wall thickness by a thickness gauge at the UT-A and UT-B areas, respectively. The wall thicknesses at the UT-B (●) are greater than those at the UT-A (■) close to the gas or water injection nozzle, except for part #9 in Fig. 4-30 and part #2 in Fig. 4-31. This anomaly is thought to be an end effect since the UT-A location is close to the tapered transition section where gas or water flow rate is expected to be unsteady, or the unsteady gas or water flow when the gas or water pressure is low.

The wall thicknesses are estimated by (Eq. 3-17) (l = G, W), where h_l is wall thickness estimation in mm, V_P is ultrasonic velocity in the HDPE, and Δt_G and Δt_W are the time delay difference between L^1- L_G and L^1 - L_W in Fig. 4-12 and 4-15, respectively. The time delay differences of Δt_G and Δt_W are chosen at the process time of 27.0s in Fig. 4-12 and 11.0s in Fig. 4-15, respectively. These timings are just before the L_G and L_W echoes disappear. In the estimation, the ultrasonic velocities of 1108m/s and 1297m/s in the HDPE just before the part detachment are used to calculate the wall thicknesses for GAIM and WAIM, respectively. These velocities are obtained using the time delay differences and the measured wall thicknesses at 20MPa. The

estimated thicknesses are given in Fig. 4-30 and 4-31 with open squares (□) and circles (○) using the data obtained with the UT-A and UT-B, respectively. It is noted that, in Fig. 4-31, parts #1, 4 and 5 cannot provide estimated wall thicknesses at UT-B, and part #5 cannot provide that at UT-A. In Fig. 4-30, the measured and estimated HDPE part wall thicknesses have good agreement within an accuracy of ±7% except for the parts #5 at the UT-B and #9 at the UT-A, indicated by the arrows. In Fig. 4-31, the agreement is within an accuracy of ±10% except for the parts #2 at the UT-B, indicated by the arrow. This suggests that bubble inclusions within the residual wall or part deformation may have occurred in these parts after the part detachment from the mold surface.

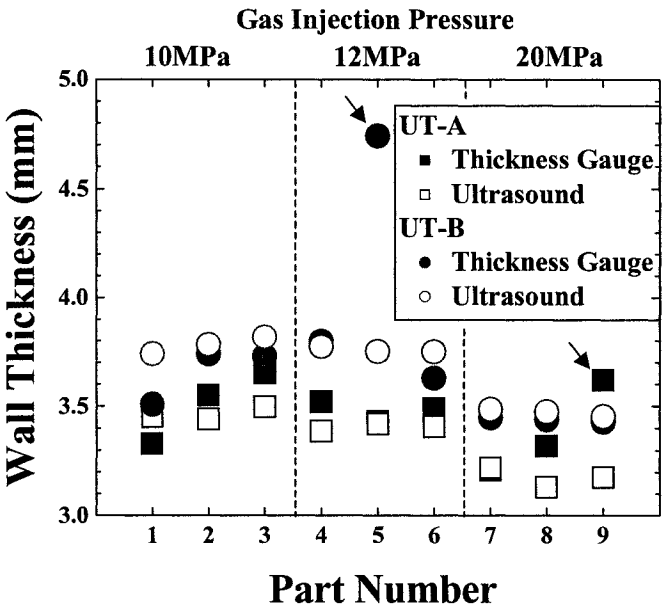

Fig. 4-30 Comparison of wall thicknesses measured by thickness gauge after sectioning the HDPE parts of GAIM process and those estimated by ultrasonic technique during molding with different gas pressures.

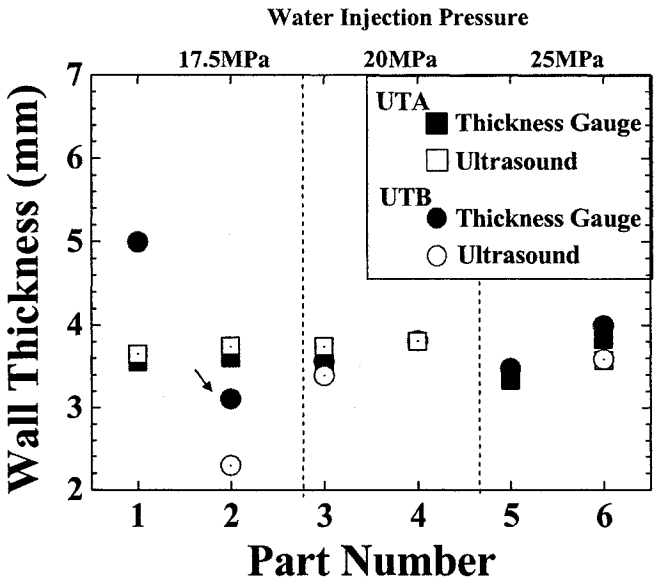

Fig. 4-31 Comparison of wall thicknesses measured by thickness gauge after sectioning the HDPE parts of WAIM process and those estimated by ultrasonic technique during molding with different water pressures.

4.6.3 Dispersion of diameter

Fluid assisted injection molding incorporates gas or water injection in the mold filling cycle to form the hollow components. Therefore, to keep the hollow structure from deformation is the basic requirement for part quality. In our experiments, the gas or water is injected into the mold during the filling process with the pressure of 10, 12, 20MPa, and 17.5, 20, 25MPa, respectively. In order to understand the correlation between the formed hollow structure and the injected gas or water pressure, two parts with gas pressure of 10 and 20MPa are sectioned in UT-A and UT-B locations. Fig. 4-32 presents the photograph of these two sets of the sectioned parts. It is clearly seen that the part with gas pressure of 10MPa has a serious deformation and more bubbles exist in the inner surface of the hollow structure. But the part with gas pressure of 20MPa presents a uniform shape and less bubbles. The deformation

situation of the part with gas pressure of 10MPa in UT-B is more serious than that in UT-A location close to the gas injection nozzle, implying a higher gas pressure or more uniform pressure.

Here, the external diameter distribution (EDD), a parameter representing the level of deformation for the molded hollow structure, is presented with gas or water injection pressure. The EDD can be calculated by:

$$EDD = (D_{max} - D_{min}) \times 100\% / D_{min} \qquad \text{(Eq. 4-3)}$$

where D_{max} and D_{min} are the external maximum and minimum diameters in each UT location.

A caliper, with accuracy of ±10μm, is used to measure the diameter. The measured EDD in UT-A, B and C location, represented by closed square (■), circle (●) and triangle (▲), respectively, with respect to the gas pressure are presented in Fig. 4-33. The EDD in three UT locations are less than 1% when the gas pressure is 20MPa. However, those are from 4.6% to 9.9%, with respect to UT-A to UT-C location, respectively, when the gas pressure is 12MPa.

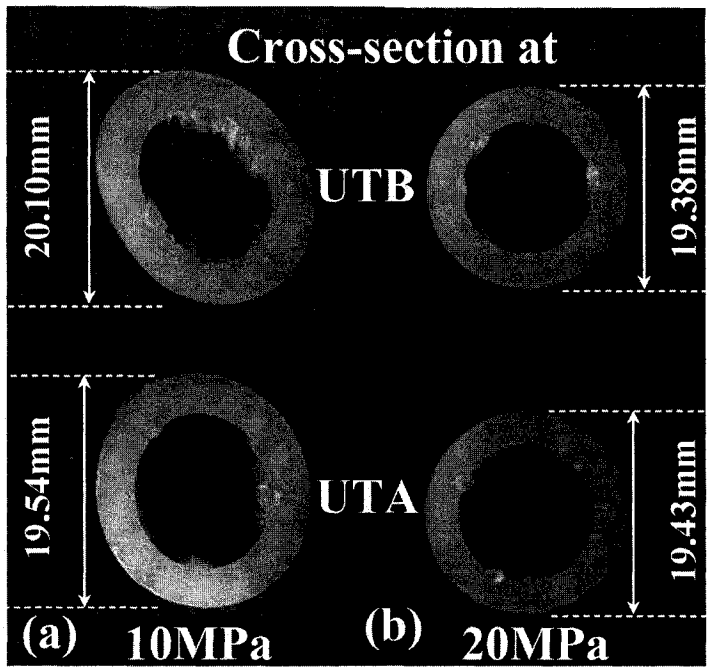

Fig. 4-32 Photograph of the sectioned HDPE parts at the UTA, and UTB locations with respect to gas pressure of (a) 10MPa and (b) 20MPa.

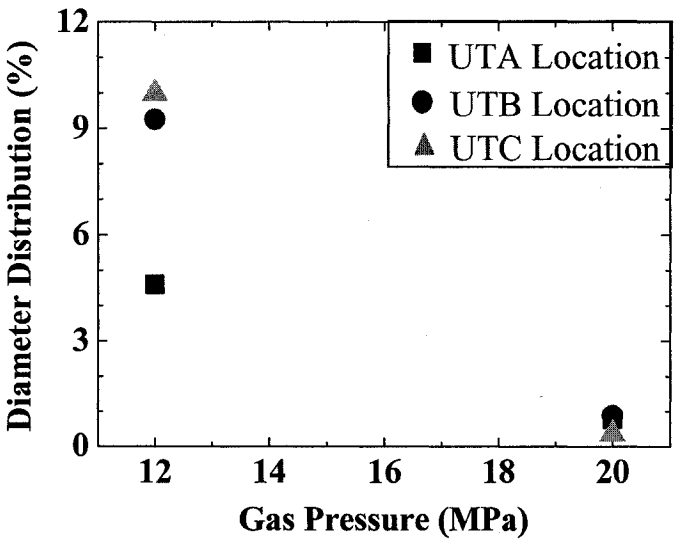

Fig. 4-33 External diameter distribution of the molded HDPE parts at UT-A, B, and C locations with respect to different gas pressures in GAIM process.

Ultrasonic contact duration may also present the relationship between the cooling efficiency and EDD. Fig. 4-34 and 4-35 present the ultrasonic contact duration with respect to different liquid (gas or water) pressure in GAIM and WAIM processes. Ultrasonic contact duration increases with liquid pressure (gas or water), except part A (10MPa) and part B (20MPa) indicated by arrows in Fig. 4-34. When the liquid (gas or water) pressure is less than 20MPa, the contact duration is not stable and shorter. The contact durations of WAIM are shorter than those of GAIM, indicating the cooling efficiency of water is faster than gas. These results show that insufficient gas or water pressure cause insufficient cooling period for molded part, and part deformation during cooling and/or part detachment. The deformed level of molded parts increases with the distance apart from gas or water nozzle. In addition, these data provide valuable insights into the actual processing conditions that can be utilized to validate the results from mold filling simulations.

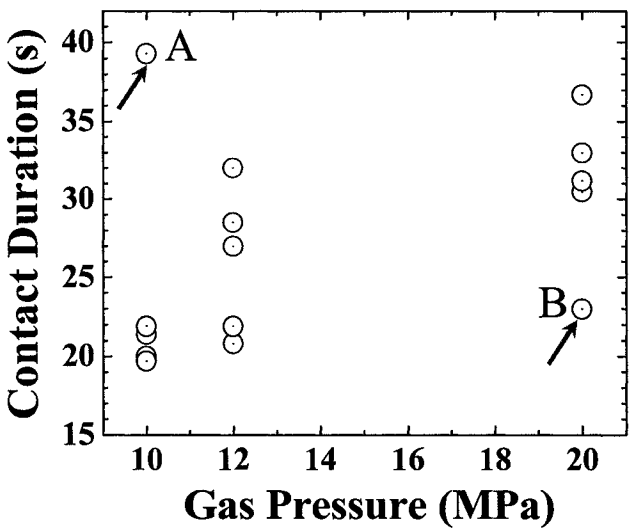

Fig. 4-34 Ultrasonic contact time measured by UT-B, during the GAIM process, with respect to different gas pressures.

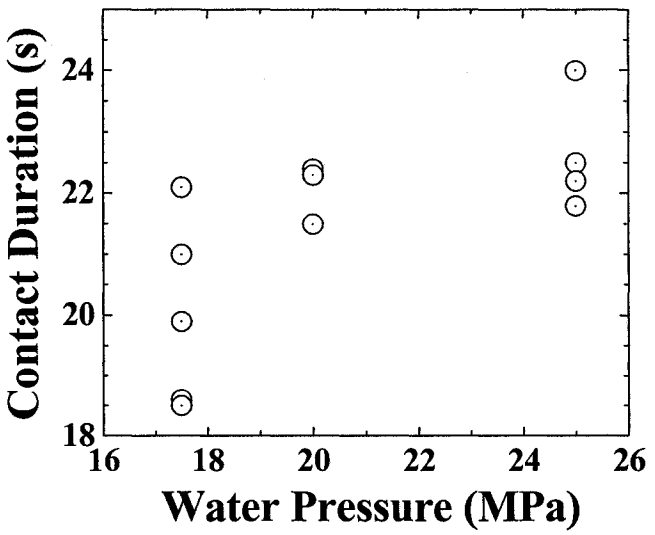

Fig. 4-35 Ultrasonic contact time measured by UT-B, during the WAIM process, with respect to different water pressures.

4.7 Summary

Integrated BIT and PZT film HT ultrasonic sensors have been successfully deployed to perform conventional IM, COIM, GAIM and WAIM processes diagnosis. The materials used are PC, PC and ABS, HDPE, and HDPE, respectively. From the experimental results, the integrated ultrasonic sensors mounted at different locations inside the mold cavity are proved to be able to provide information on strategic process parameters such as melt/core/gas/water flow front arrival, average flow speed and part detachment available.

During the IM process, solidification and filling incompleteness of 1.0mm-thickness PC parts can be monitored by ultrasonic velocity and transmitting echo. During solidification, ultrasonic velocity increases due to temperature cools down. The minor defects in the molded PC parts due to

incomplete mold filling, based on volume differences as small as 1%, can be detected by ultrasonic signatures.

For COIM, melt PC core flow movement, skin (ABS)/core (PC) layer thickness and core length can be estimated by ultrasonic signatures. The estimated skin/core layer thickness has an agreement with optical measurement within ±17%. The entire thickness of five-layer COIM part is around 3.5mm. The core length can also be estimated quantitatively using the measured core thickness by ultrasound.

For GAIM/ WAIM, the wall thickness and deformation of hollowed HDPE part can be monitored by ultrasonic signatures. The wall thicknesses of around 3.6mm can be measured within an accuracy of ±7% for GAIM and ±10% for WAIM. The deformation of the hollow tube with a diameter of 20mm increases along the injection direction when the gas/water pressure drops below 20MPa.

The results indicate that the proposed integrated HT ultrasonic sensors and techniques can diagnose the formation of the complex multi-layers or hollow structures and monitor melt flow arrival, melt speed, and part detachment of the IM COIM, GAIM and WAIM molded part of any thickness by reflected ultrasonic echo at the mold/polymer melt interface. Therefore, they have the potential of being used in real-time process control systems that can diagnose above IM processes and generate several desired information for their optimization.

Chapter 5

Small scale injection molding

5.1 Introduction

Applications of integrated HT ultrasonic sensors to large-scale IM processes were examined in chapter 4. The focus of this chapter is on the diagnosis of small-scale IM processes, including IMMF and MM. The MM processes are mainly used in conjunction with polymer, nano-composite and ceramic materials.

For micro-fabrication processes the parts, being small in size, require reduced mold size and shorter processing periods. Ideally, one still would like to improve the part quality and optimize the process by monitoring and controlling the entire process (that is, from the feed hopper to the part exit), in real-time. However, the miniaturized mold cavity and the products' highly detailed microstructures add to the difficulties of designing and installing diagnostic sensors and, thus, meeting product quality requirements. The injected materials also need to be selected in order to meet the requirements of narrow processing windows, including melt flow, solidification and microstructure development in micro size channels/structures.

In order to overcome these difficulties in some measure, the integrated HT ultrasonic sensors are employed to diagnose the processes that take place in the barrel and mold. Therefore, the roles of these sensors in improving productivity, efficiency and part quality are presented.

5.2 Experiments

5.2.1 IMMF

The designed mold, mold insert and PZT film HT ultrasonic sensors developed in chapter 3 are installed into the IM machine. Fig. 5-1 presents the schematic view of a cross-section of the mold (mobile and fixed mold), mold insert and molded part (polymethyl methacrylate, PMMA) with two ultrasonic sensors (UT1 and UT2). Ultrasonic waves are transmitted into the PMMA and received by the UT1 and UT2 in pulse-echo mode. In Fig. 5-1, L^n (n=1,2,...) represents n-th round trip longitudinal-wave echoes reflected at the probing end, and L_{2n}, L_{2n}' and L_{2n}" are those propagating in the polymer and reflected at the polymer/mold insert interface. Here, the L_{2n}' and L_{2n}" signals are the reflected echoes from the bottom of the microstructures.

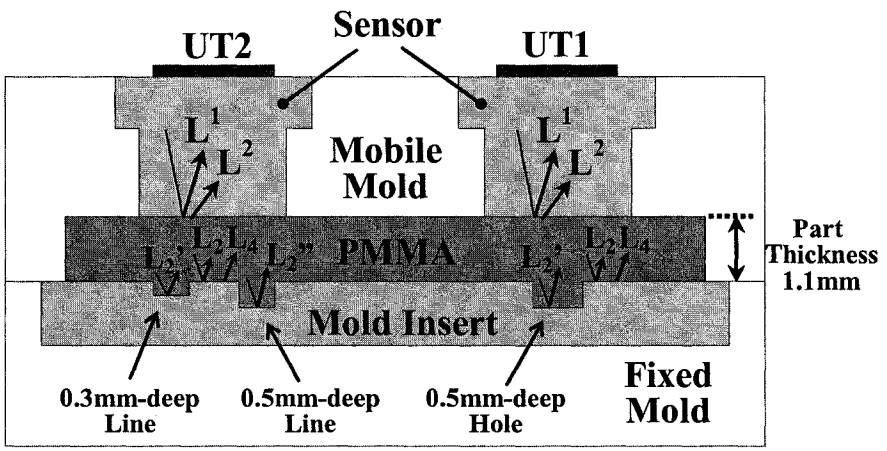

Fig. 5-1 Schematic view of a cross-section of the mold (mobile and fixed mold), mold insert and molded part (PMMA) with two sensors (UT1 and UT2) during IMMF process. L^n and L_{2n} (n=1,2,...) represent n-th round trip echoes propagating in the buffer rods and those in the polymer, respectively.

A typical molding condition employed in the experiments is: melt and mold temperatures are 230°C and 60°C, respectively; injection and holding pressures are 10MPa; and holding and cooling times are 3sec and 10sec, respectively. A photograph of a typical molded part is given in Fig. 5-2. The material employed is a polymethyl methacrylate (PMMA, Acrylite® M30, Cytec Industries, West Paterson, NJ) in injection molding grade. The patterns are printed on the surface

of the PMMA part as shown in Fig. 5-2. The white line circles in the figure indicate the areas corresponding to the probing end areas of the two probes (UT1 and UT2) on the opposite side of the patterns. The probing ends are located above the hole with depth of 0.5mm for the UT1, as shown in Fig. 5-1, and the two lines with depths of 0.3mm and 0.5mm for the UT2.

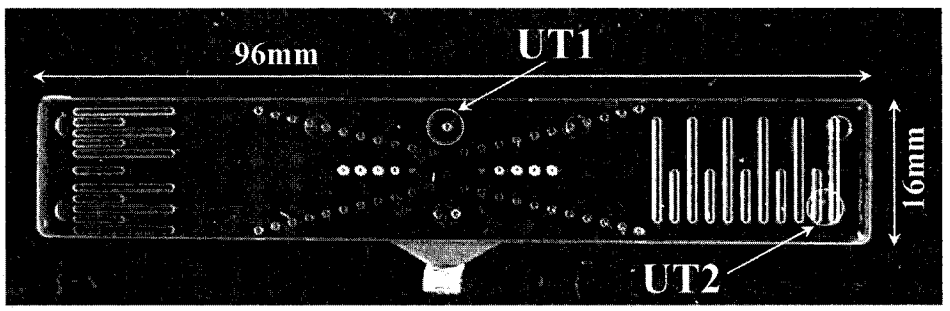

Fig. 5-2 A photograph of a molded PMMA part having test patterns with different shapes and dimensions of IMMF process. The white line circles in the figure indicate the areas corresponding to the probing end areas of the UT1 and UT2 on the opposite side of the patterns.

5.3.2 MM for polymer and nano-composite

As mentioned above, though the Boy machine can fabricate the parts with micro-channels, it will be more complicated and difficult in control to produce smaller parts for this machine. Therefore, the experiments of MM for polymer and nano-composite are practiced in a MM machine.

As mentioned in chapter 3, in order to monitor temperature and state of polymer inside the barrel and avoid material degradation due to over heating, seven HT ultrasonic sensors are fabricated directly on the curve surface of barrel. However, only the data collected from UT6 will be presented in this thesis. This barrel is installed into the MM machine for further experiments. A schematic view of a cross-section of the barrel with the UT and the extrusion screw is presented in Fig. 5-3, explaining the paths of ultrasound propagating in the barrel and

polyacetal copolymer (POM) melt. The width of the screw root was 5mm, which is comparable to the UT size (5mm) at the barrel. When electric pulses are applied on the piezoelectric film through the top and bottom electrodes, where the barrel itself served as the bottom electrode as shown in Fig. 5-3, ultrasonic waves are excited and transmitted into the barrel. In Fig. 5-3, the n-th round trip ultrasonic longitudinal-wave echoes reflected at the barrel/POM melt interface are indicated by L^{nb} (n=1,2…), and those from the flight or root of the screw through the melt are L_{2nf} or L_{2nr}, respectively. It is noted that the L_{2r} echo appears only when an area between the barrel and screw is filled with the materials (not with air). In order to evaluate ultrasonic performance of these ultrasonic sensors, such as center frequency, frequency bandwidth and SNR, the ultrasonic signals are measured when there is no polymer inside the barrel.

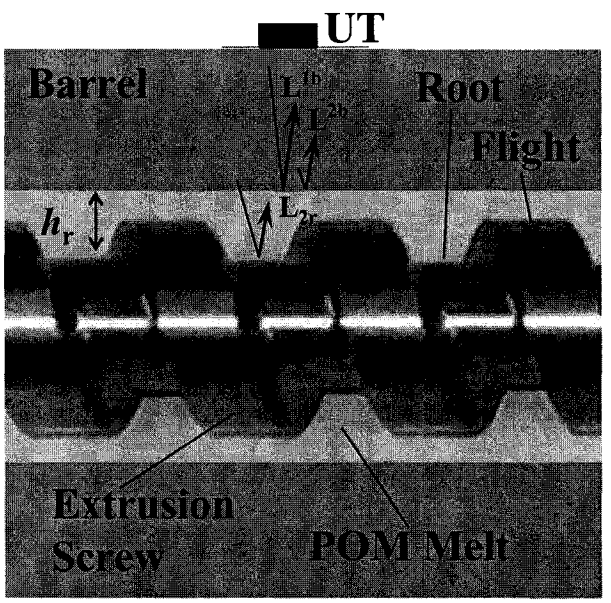

Fig. 5-3 Schematic view of cross-section of the barrel with the ultrasonic sensor and the extrusion screw, showing the paths of ultrasonic signals propagating in the barrel and POM melt.

Fig. 5-4 (a) and (b) present the schematic drawings of the cross-sections of the mold inserts and the fixed molds during MM for POM and nylon66 (PA66) with polyhedral ligomeric silsesquioxanes (POSS) materials. PZT film sensors are

fabricated onto the steel sensor insert shown in Fig. 3-28. It illustrates ultrasonic propagating paths in the mold insert and polymer melt. The round trip ultrasonic longitudinal-wave echo reflected at the mold insert/polymer melt interface is indicated by L^n (n=1, 2 ...) and that from the surface of the fixed mold half through the polymer melt is L_{2n} (n=1, 2, 3...). The mold designs for these MM processes are the testing ones. The depths of mold cavities are 0.5 and 0.32/0.59mm in Fig. 5-4 (a) and (b), respectively. It is noted that in these MM processes, the cavity pressure sensor is not available in the experimental period. However, the machine is equipped with Dynisco PCI-4011 and PCI-4006 piezo load transducers for injection and cavity pressure measurements, respectively, Temposonics R-series displacement transducer for displacement and velocity measurements of the injection pin, and J-type thermocouple for mold temperature measurement [162].

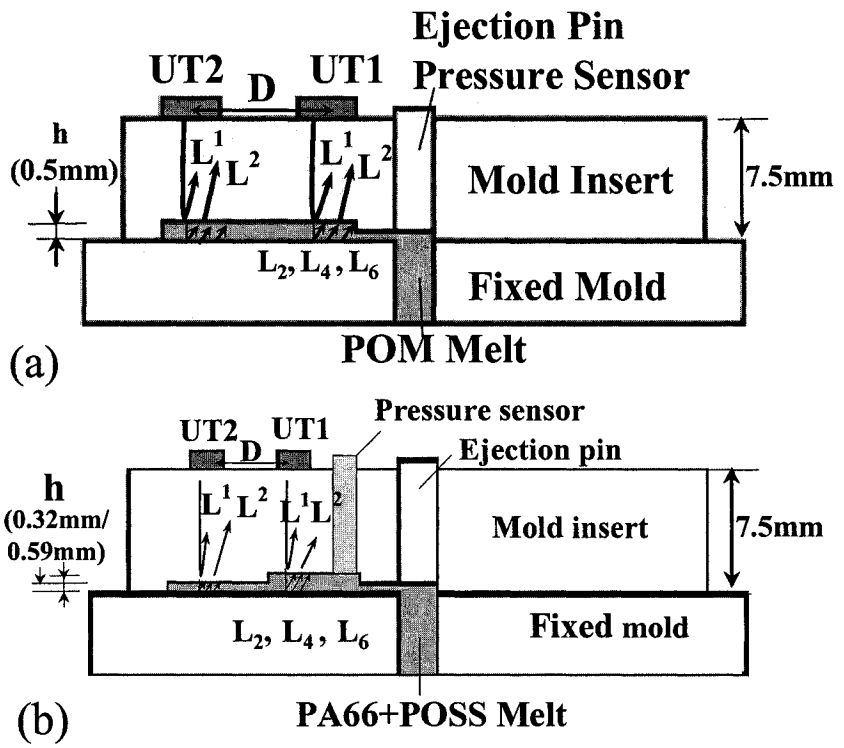

Fig. 5-4 Cross-sectional view of the mold insert with the ultrasonic sensors and the paths of ultrasonic signals propagating in the mold insert and polymer melt during MM processes for (a) POM and (b) PA66+POSS materials.

The materials employed are a POM (grade: POM109C from Chem Polymer, UK) and a PA66 with the POSS content of 0, 4 and 8wt% (from Brandford University) for MM processes of polymer and nano-composite, respectively. The typical molding conditions employed in the experiments are listed in Table 5-1.

Table 5-1 Typical molding conditions for MM of POM and PA66+POSS materials.

Molding conditions	Material	Melt temp.	Mold temp.	Screw speed	Packing time	Cooling time
Polymer MM	POM	200°C	75°C	500mm/s	0.3sec	5sec
Nano-composite MM	PA66+POSS	290°C	40°C	400mm/s	0.3sec	1.8sec

The photographs of the molded parts for MM of POM and PA66+POSS are given in Fig. 5-5 (a) and (b), respectively. The white/black dotted line circles indicate the corresponding areas of the ultrasonic sensors above the cavity, as shown in Fig. 5-4 (a) and (b). The runner area of the molded part in Fig. 5-5 (a) is removed and not shown in the photograph. The dimensions of the parts are listed in Table 5-2.

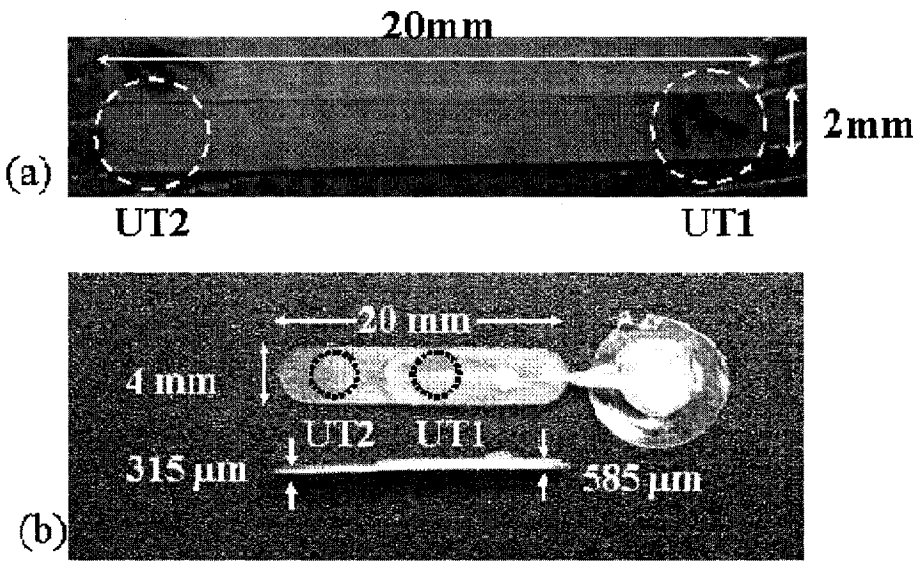

Fig. 5-5 Photographs of the molded parts for MM of (a) POM and (b) PA66+POSS. The white/black dotted line circles indicate the corresponding areas of the ultrasonic sensors above the cavity, as shown in Fig. 5-4 (a) and (b). The runner area of the part in (a) is removed and not shown in the photograph.

Table 5-2 Dimensions of parts for MM of POM and PA66+POSS.

Process	Length/Diameter	Width	Thickness
POM MM	20mm	2mm	0.5mm
PA66+POSS MM	20mm	4mm	315/585μm

5.2.3 MM for ceramic powder

The experiments of MM for ceramic powder are practiced in the same MM machine. However, the mold design and fabrication process are different. The mold, designed mold insert and HT ultrasonic sensors developed in chapter 3 are installed into the MM machine for process diagnosis. Fig. 5-6 presents the schematic drawings of the cross-sections of the ultrasonic sensors, mold inserts and the fixed molds during MM for ceramic powder. It illustrates ultrasonic propagating paths in the mold insert and polymer melt. The L^n (n=1, 2...) represents round trip ultrasonic longitudinal-wave echo reflected at the mold insert/feedstock interface and L_{2n} (n=1, 2....) represents those from the surface of the fixed mold half through the feedstock. The depth of mold cavity is 1.5mm. The machine during the experiment is also equipped with Dynisco piezo load transducers PCI-4011, PCI-4006, Temposonics R-series displacement transducer and J-type thermocouple [162].

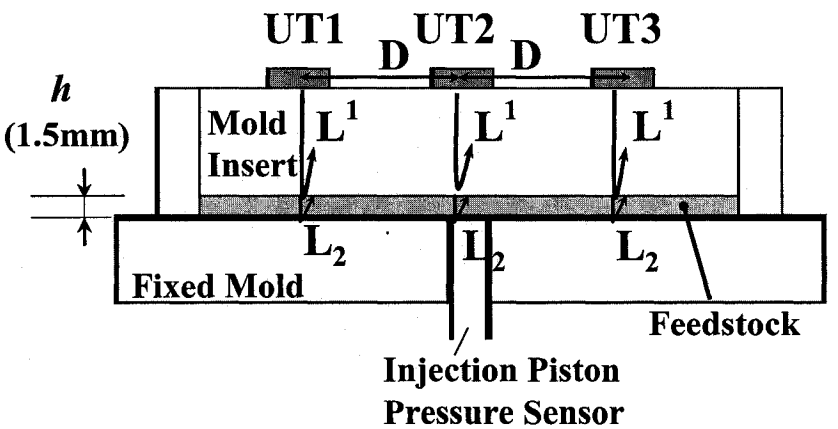

Fig. 5-6 Cross-sectional view of the mold insert with the ultrasonic sensors and the paths of ultrasonic signals propagating in the mold insert and feedstock melt during MM processes for ceramic powder.

The material employed is a ceramic powder (from INMATEC, Rheibach, comprising aluminum oxide plus processing additives and binders). The typical molding condition employed in the experiment is listed in Table 5-3.

Table 5-3 Typical molding conditions for MM of ceramic powder.

Molding conditions	Material	Melt temp.	Mold temp.	Screw speed	Packing time	Cooling time
Ceramic powder MM	Feedstock	165°C	40°C	200mm/s	0.2sec	7.8sec

The typical packing speed is 5mm/s, and the dosing amount (volume of material injected) is 820mm^3. There are two experimental settings for testing the effects of injection and packing speed, which are expected to have relationship with injection and packing pressure during the molding process. In the first set of experiments (described in sections 5.6.1~5.6.4), the fabrication of molded parts is carried out with a constant material dose set of 820mm^3 and at an injection speed of 200mm/s. During the packing stage, different packing speeds of 3, 5, 7, and 9mm/s are employed for injecting a piston displacement of 1mm, in order to investigate the changes in packing parameters. The range of packing speeds is selected to avoid incomplete filling or flashing. In the second set of experiments (described in section 5.6.5), the fabrication of molded parts is carried out with the same material dose set of 820mm^3 and at different injection speeds of 150, 200, 250, and 300mm/s, in order to investigate the changes in injecting parameters. During the packing stage, a packing speed of 5mm/s is selected.

After ejecting the part from the mold, the as-molded parts passes through the debinding and sintering processes to remove the binder and obtain the final shape. The debinding process contains two steps: water and thermal debinding. During the water debinding, the as-molded parts are put into a water pat with moving water for 24hours to remove the binder. After drying, the as-molded parts are put into the furnace for thermal debinding to remove the binder further, and sintering to melt the ceramic powder. This will remove porosity and become the sintered

parts with the final shapes. The temperature settings for debinding and sintering processes are listed in Table 5-4.

Table 5-4 Debinding and sintering conditions for MM of ceramic powder.

No.	Treating item	Intermits	Tempe. range	Process time
1	Water debinding	Water	Room temp.	24h
2	Thermal debinding	Air	25-300°C	19h
3	Thermal sintering	Air	25-1600°C	11h

The photographs of the as-molded and sintered part are presented in Fig. 5-7. The black dotted line circles indicate the corresponding areas of the ultrasonic sensors above the cavity, as shown in Fig. 5-6. The diameter and thickness of as-molded and sintered parts are 24.8, 1.47 and 21.2, 1.25mm, respectively. The average shrinkage ratio between the as-molded and sintered parts is 15%.

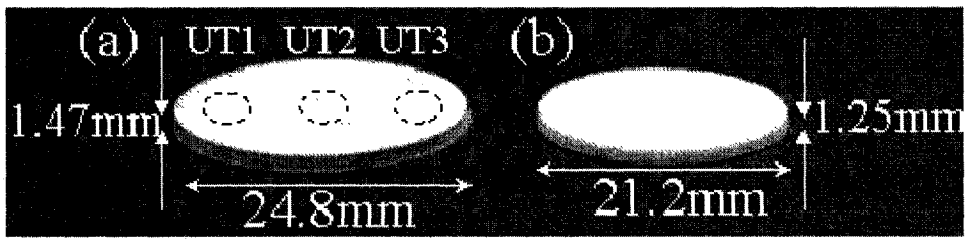

Fig. 5-7 Photographs of (a) the as-molded and (b) the sintered part of MM for ceramic powder. The black dotted line circles indicate the corresponding areas of the ultrasonic sensors above the cavity, as shown in Fig. 5-6.

In order to measure the Young's modulus of sintered parts, two conventional longitudinal and shear wave UTs (20MHz, Panametrics) are chosen to obtain ultrasonic velocities in the parts. For all sintered parts, the density is proved as the same within measurement error later; here, six sintered parts with low porosity are selected to measure ultrasonic longitudinal and shear velocities for estimation of Young's modulus.

5.3 Results

5.3.1 IMMF

Fig. 5-8 presents typical signals measured with the UT1 in Fig. 5-1 during one cycle of IMMF process. The thickness of the molded PMMA part at sensor location is about 1.1mm. The L_2 and L_4 are the echoes reflected from the top surface of the mold insert, while the L_2' is the echo reflected from the bottom surface of a 0.5mm-deep hole, as illustrated in Fig. 5-1. At the process time from 3 to 7sec, the time delays of the L_2, L_4 and L_2' echoes gradually decrease since the ultrasonic velocity in the polymer increases due to solidification, which has been discussed in section 4.4.3. At the process time of around 18sec, those echoes vanish, which indicates that the mold opens and the molded part is detached from the probing end. With the UT2, the L_2, L_2', L_2" and L_4 echoes propagating in the polymer, shown in Fig. 5-1, are observed as well. (The data is not shown here.) Through the time-delay differences between the L^1, L_2, L_2', L_2" echoes, the ultrasonic velocity in the polymer, the thicknesses of molded parts, as well as the height of the printed patterns, can be calculated according to section 4.5.3 and 4.6.2.

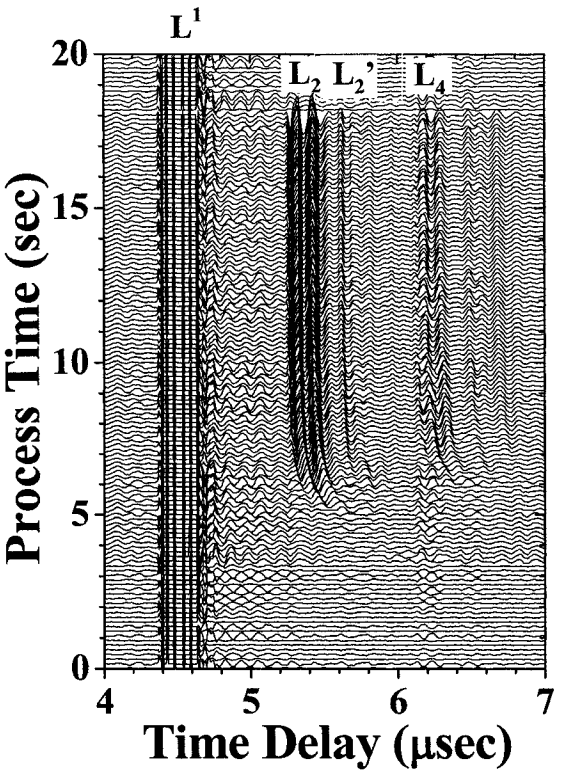

Fig. 5-8 Typical signals measured with the UT1 in Fig. 5-1 during one cycle of IMMF process of a PMMA part.

In order to investigate the correlation between ultrasonic signals observed and the molding cycle, the amplitude values of the L^1 and L_2 echoes with respect to the process time are obtained using the signals measured with the UT1 during one molding cycle, as shown in Fig. 5-9. When the PMMA melt arrives at the UT1 location and contacted its probing end at the process time of 3sec, the amplitude of the L^1 echo suddenly decreases, due to the fact that a part of the ultrasonic energy is transmitted into the polymer through the probing end/polymer interface. At this moment, the L_2 echo, reflected from the polymer melt/fixed mold interface, starts to appear. Between 3sec and 8sec, the amplitude of the L_2 echo decreases and increases, which reflects the variation of ultrasonic attenuation in the polymer because of its solidification, as discussed in section 4.4.3. At 18s, the amplitude of the L^1 echo recovers to the initial value and the L_2 echo disappears, because of total reflection at the polymer/air interface. This indicates

that the mold opens and the molded part is detached from the surface of the mold cavity. The ultrasonic contact duration is from process time 3s to 18s, which is defined in chapter 4. The contact duration can indicates the period during which the part and mold are in contact and helps in evaluation of the cooling efficiency and part quality. This information will be discussed further in sections 5.4.2 and 5.6.3. Through the appearing time difference and location distance between two UT sensors, the melt speed in the mold cavity can be calculated, as described in section 4.4.1. During experiments, filling incompleteness can also be diagnosed.

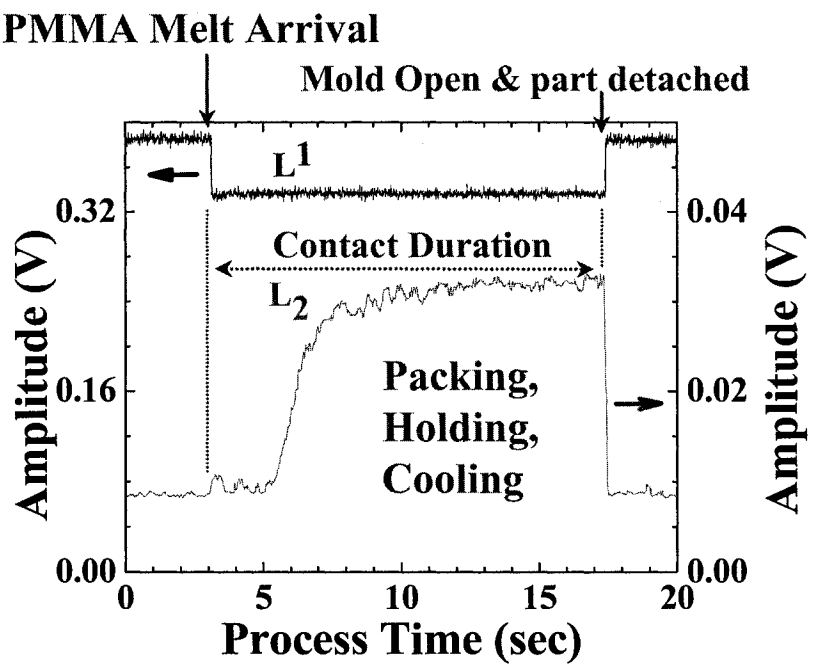

Fig. 5-9 Amplitude variations of the L^1 and L_2 echoes measured with the UT1 at the mold insert in Fig. 5-1 during one cycle of IMMF molding process of a PMMA part.

5.3.2 MM for polymer and nano-composite

Fig. 5-10 shows a typical waveform acquired with the BIT film UT6 at the barrel in Fig. 3-26 when the POM melt filled the inside of the barrel. One can see that the L_{2r} echo reflected at the POM melt/screw root interface, as illustrated in

Fig. 5-3. The width of the screw root is 5mm, which is comparable to the UT size (5mm) at the barrel. The gap distance between the internal surface of the barrel and the screw root is 3.275mm. The signals reflected from the root have the SNR of more than 10dB and enable the measurement of ultrasonic velocity and attenuation in the POM melt. The time delay and amplitude of the L_{2r} echo are associated with the ultrasonic velocity and attenuation of the polymer melt, respectively, as described later. A signal appearing at 7μs is an ultrasonic shear-wave propagating in the barrel and reflected at barrel/polymer interface.

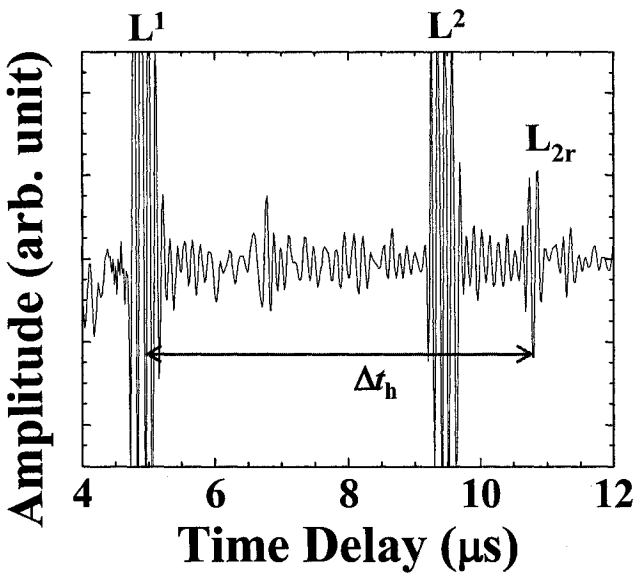

Fig. 5-10 Typical signals measured with the BIT film UT6 at the barrel in Fig. 3-26. L_{2r} is the echo reflected at the POM/screw root interface, as illustrated in Fig. 5-3.

Fig. 5-11 presents the trace of waveforms acquired with the PZT film UT1 at the mold insert in Fig. 5-4 (a) with respect to the process time during one cycle of MM process. The thickness of the molded POM part is 0.5mm. Only a portion of the acquired signals from 0.4s to 1.0s with a process time interval of 5ms are shown in the figure though the signals are acquired every 1ms for the entire one cycle (8s). One can see that the L^1 and L^2 echoes reflect from the mold cavity

surface of the mold insert. After the POM melt arrived at the UT location, the L_2, L_4 and L_6 echoes are observed while the POM contacts the cavity surface. The ultrasonic velocity, V_P, in polymer melt inside the mold cavity can be determined by (Eq. 3-14), where h is the depth of the cavity at the UT location in Fig. 5-4 (a), and Δt_h is the time delay difference between the L_2 and L_4 in Fig. 5-11. The ultrasonic velocities measured at the mold insert during molding will be presented in section 5.5.3. The ultrasonic waveforms of PA66+POSS MM are similar with Fig. 5-11, except the signal appearing for the whole process.

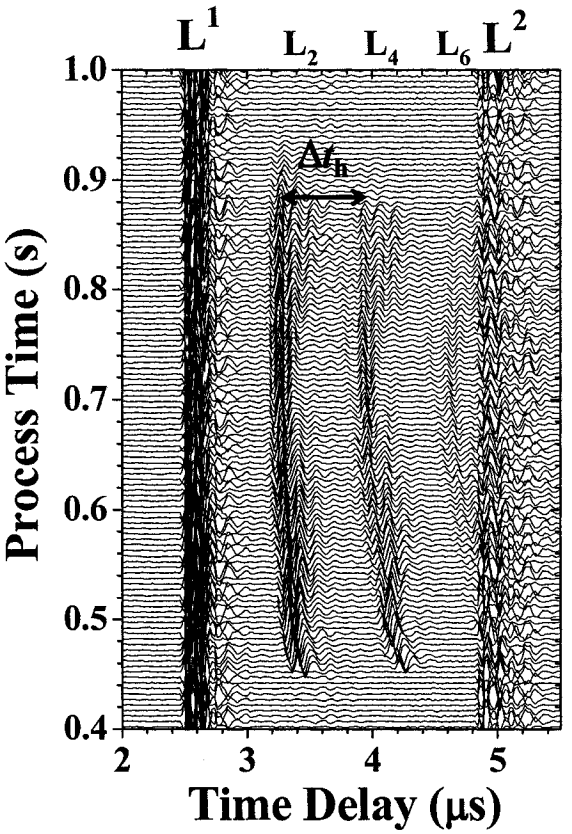

Fig. 5-11 Typical signals measured with the PZT film UT1 at the mold insert in Fig. 5-4 (a) during one cycle of MM process. L_{2n} (n=1,2...) is the echo reflected from the POM/fixed mold interface, as illustrated in Fig. 5-4 (a).

In order to investigate further the correlation between the ultrasonic signals observed and the molding cycle, the amplitude values of the L^1 and L_2 echoes

with respect to the process time are obtained using the signals measured with the UT1 at the mold insert. The results are presented in Fig. 5-12. At process time of 0.45s, the POM melt arrives at the cavity area beneath the UT1, since the amplitude of the L^1 echo decreases and the L_2 echo starts to appear. At 0.96s, the amplitude of the L^1 echo recovers to the almost initial value and the L_2 echo disappears, because of total reflection at the polymer/air interface, indicating that the molded part is detached from the surface of the mold cavity. This will be further discussed in section 5.5.3. At 6s, slight increase of the amplitude of the L^1 echo is observed when the mold opens.

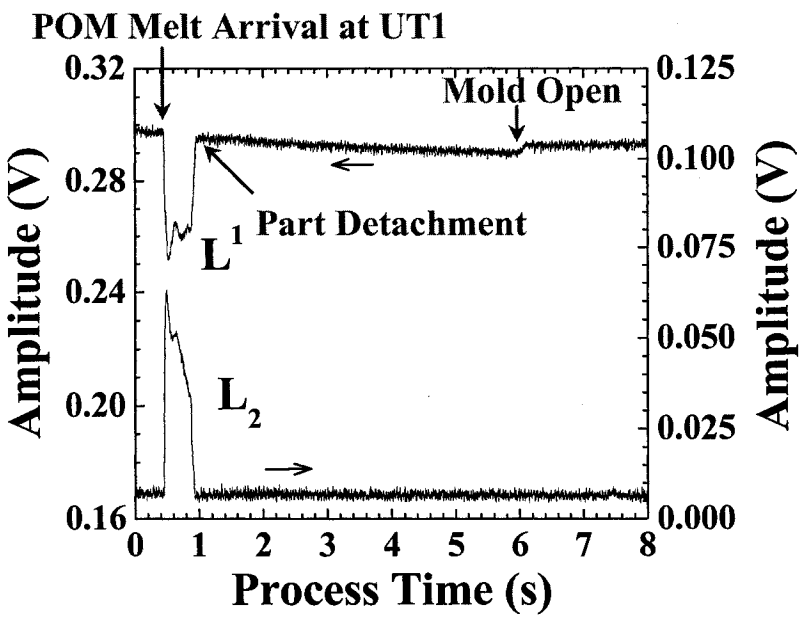

Fig. 5-12 Amplitude variations of the L^1 and L_2 echoes measured with the UT1 at the mold insert in Fig. 5-4 (a) during one cycle of MM of a POM part.

Fig. 5-13 (a) presents variations of a cavity pressure, measured by a pressure sensor attached at the end of an ejector pin (opposite to the polymer side), as shown in Fig. 5-4 (b). Fig. 5-13 (b) shows the amplitude of ultrasonic signals, obtained with the UT2, respectively, during one cycle of MM for PA66+POSS. At 2s, the polymer melt is injected into the cavity, showing the highest pressure of 64MPa in Fig. 5-13 (a). After this timing, the pressure reduces and is then kept at

20MPa during cooling to solidify the polymer from 2.5 to 4.2s, and becomes zero when the mold opens at 4.2s. In Fig. 5-13 (b), at 2s, the amplitude of the L^1 suddenly decreases and the L_2 starts to appear, indicating that the polymer melt arrives at the UT2 location in the cavity. At 4.2s, the amplitude of the L^1 recovers to the initial value and the L_2 disappears due to the mold open and part detachment from the mold.

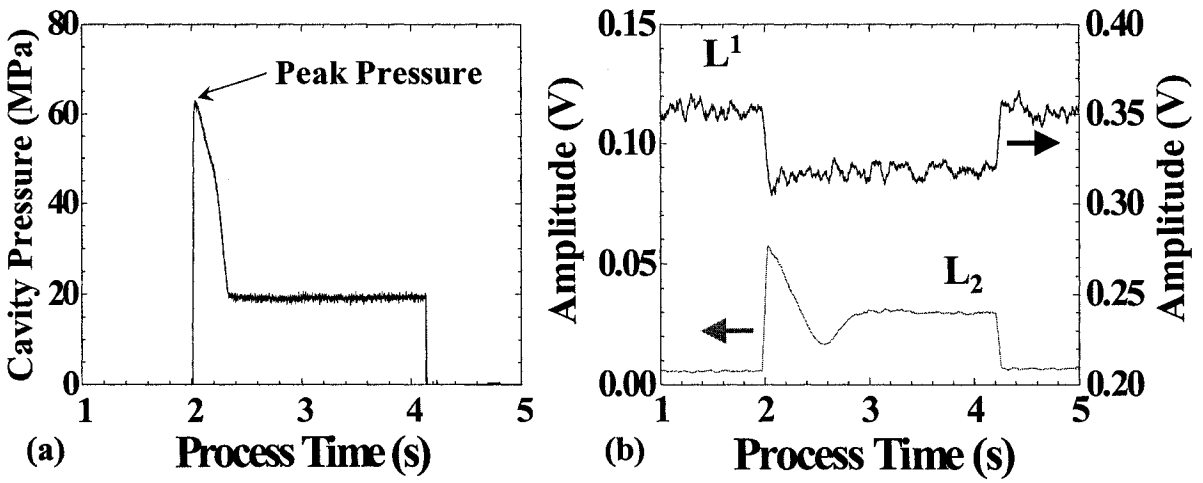

Fig. 5-13 Variations of (a) the cavity pressure and (b) the amplitude of ultrasonic echoes measured with the UT2 during one cycle of molding for MM of PA66+POSS.

5.3.3 MM for ceramic powder

Fig. 5-14 presents the trace of ultrasonic waveforms acquired with UT1 at the mold insert (signal path shown in Fig. 5-6) with respect to the process time during one cycle of MM of ceramic powder material. The thickness of as-molded ceramic part is 1.47mm. Ultrasonic signals are acquired every 2ms during the entire cycle, but for clarity a process time interval of 70ms has been selected and shown in Fig. 5-14 for a cycle time of 0s to 10s. The L^1 and S echoes, propagating in the mold insert and reflected at the mold cavity surface of the mold insert, are observed to be present throughout the cycle. The signal "S" appearing

at 5.9μs is ultrasonic shear-wave. The L_2 echo appears when the feedstock arrives at the UT1 location, and remains for the duration of contact between the feedstock and the mold-cavity interface. For the data shown in Fig. 5-14, the time delay of the L_2 echo varies from 6.41μs at a process time of 0.77s, to 5.62μs at a process time of 9.1s. This change in time delay is directly related to changes in ultrasonic velocity and indicates the solidification and cooling of the injected feedstock material inside the mold cavity. The ultrasonic velocity increases as the feedstock solidifies. The ultrasonic velocity, V_P, in the feedstock can be determined by (Eq. 3-14), where h is the depth of the cavity at the transducer location and Δt_h is the time delay difference between the L^1 and L_2 echoes as observed in Fig. 5-14.

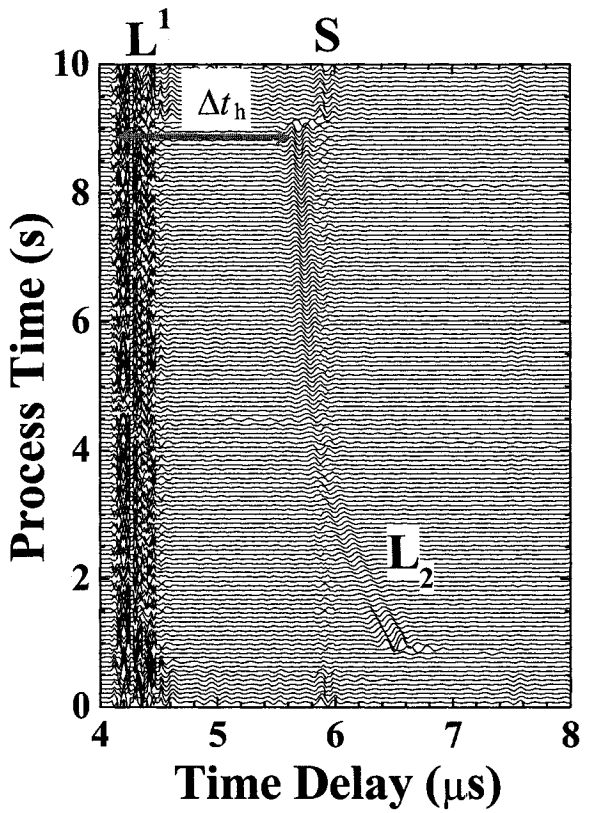

Fig. 5-14 Typical signal measured with the UT1 shown in Fig.5-6 during one cycle of MM for ceramic powder of 1.47mm as-molded part thickness.

Fig. 5-15 (a) and (b) present both the amplitude of the L^1 echo (measured using UT1 at the mold insert), and the injection pressure measured by a pressure sensor installed at the end of the injection piston for typical molding cases. In Fig. 5-15 (a), at a process time of 0.34s an increase in injection pressure is observed, indicating entry of the feedstock into the mold cavity. At a process time of 0.77s, the end of injection stage, the magnitude of injection pressure reaches the first of two peaks, and the feedstock arrived at the location of UT1, as evidenced by a sharp decrease in the amplitude of the L^1 echo. After a process time of 0.77s the amplitude of the L^1 echo gradually decreases further, due to densification during packing. At a process time of 1.7s, which correlates to the end of the packing stage, the injection pressure reaches a second peak value and the L^1 echo amplitude reaches a minimum value, which is maintained throughout the remainder of the cycle until part detachment.

At a process time of 9.1s, the amplitude of the L^1 echo recovers to the initial value due to total reflection at the mold insert/air interface, indicating that the mold has opened and the molded part is detached from the surface of the mold cavity. In some cases, as shown in Fig. 5-15 (b), it is possible for part shrinkage to cause detachment to occur before the mold opens, evidenced at a process time of 5s in Fig. 5-15 (b), thereby limiting the efficacy of the mold in cooling the part and implying the possibility of reducing cycle time. The amplitude of the L^1 echo can be used to aid this by indicating part detachment in-situ before mold opening.

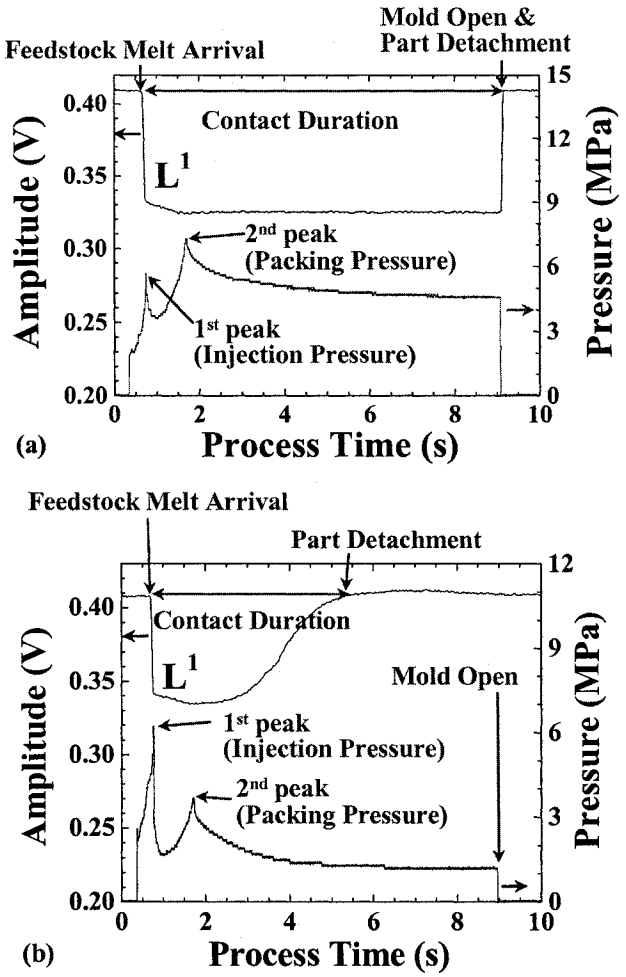

Fig. 5-15: Amplitude variations of the L^1 echo reflected at mold insert/feedstock interface measured using the UT1, and pressure, measured by a pressure sensor. (a) These signals are acquired for the parts keeping contact with mold surface until mold open. (b) These signals are acquired for the parts detached from the mold surface before mold open.

5.4 Discussions in IMMF

5.4.1. Cooling efficiency and holding pressure

Ultrasonic contact duration in Fig. 5-9 indicates the period during which the PMMA part and mold are in contact and helps in evaluation of the cooling efficiency. Fig. 5-16 gives variations of amplitude of the L^1 with the different

holding pressures during one IMMF molding cycle. When the PMMA arrives at the UT1 location and contacts its probing end at the process time of around 3sec, the amplitude of the L^1 echo suddenly decreases. At 18sec, the amplitude of the L^1 is recovered to the initial value in the cases of the holding pressures of 7.5, 10 and 15MPa since the mold opens and the molded part is detached from the probing end. At this moment the L^1 is totally reflected at the probing end/air interface. On the other hand, the amplitude of the L^1, with holding pressures of 2.5, 5 and 6MPa, is gradually recovered to the initial values at 5, 6.2 and 10.2sec, respectively, before the mold opens since the part is gradually detached from the probing end (i.e. the mold surface) because of shrinkage of the part, caused by the lack of sufficient holding pressure. The contact duration, indicated by the dashed arrows in Fig. 5-16, is shorter when the holding pressure is below 6MPa.

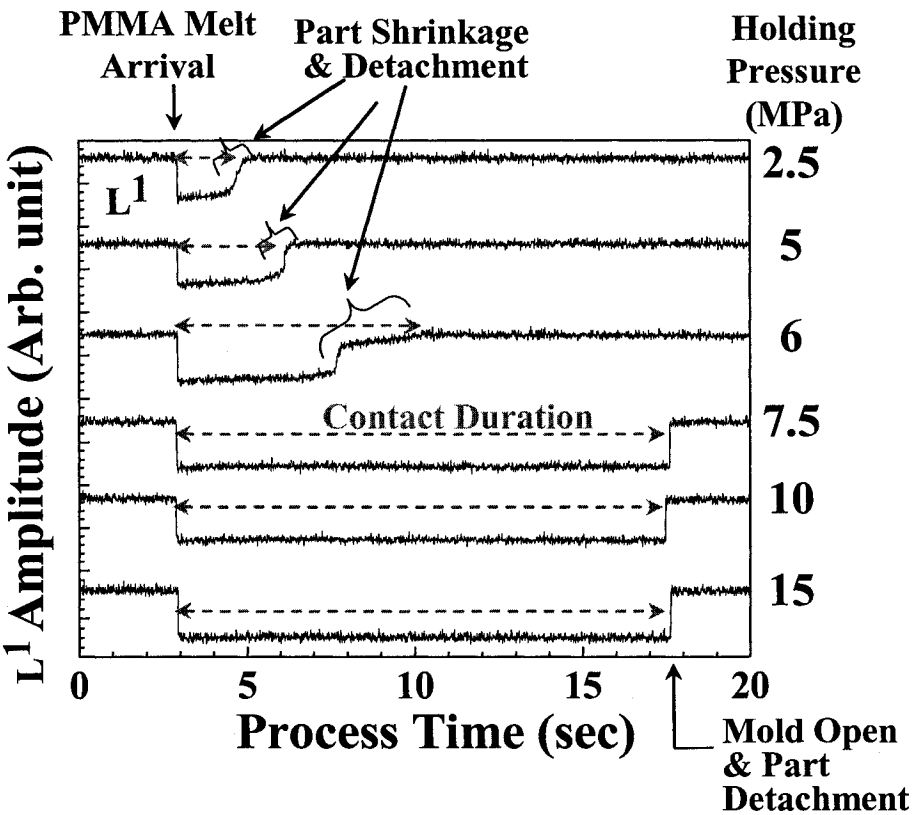

Fig. 5-16 Amplitude variations of L^1 echoes with respect to the process time during one IMMF molding cycle, obtained by UT1 with different holding pressures.

Fig. 5-17 shows the contact durations obtained by the UT1 (open circles) and UT2 (closed circles) with respect to the holding pressure. Three PMMA parts are continuously molded for each holding pressure. The contact duration is almost constant value of 15sec with the holding pressure higher than 7.5MPa. At 6MPa, the contact duration varies between 4sec and 15sec, which mean that this pressure value may be critical to have a stable molding condition. Below 6MPa, the contact durations obtained with the UT1 are slightly greater than those with the UT2. This suggests that the area at the UT1 near the gate have higher holding pressure or have more polymer injected than the area at UT2 near the edge of the cavity. Hence, through measuring the ultrasonic contact duration, the requirement of stable molding process can be shown. The lowest holding pressure for stable molding process under these experimental conditions can be used to reduce the process cost.

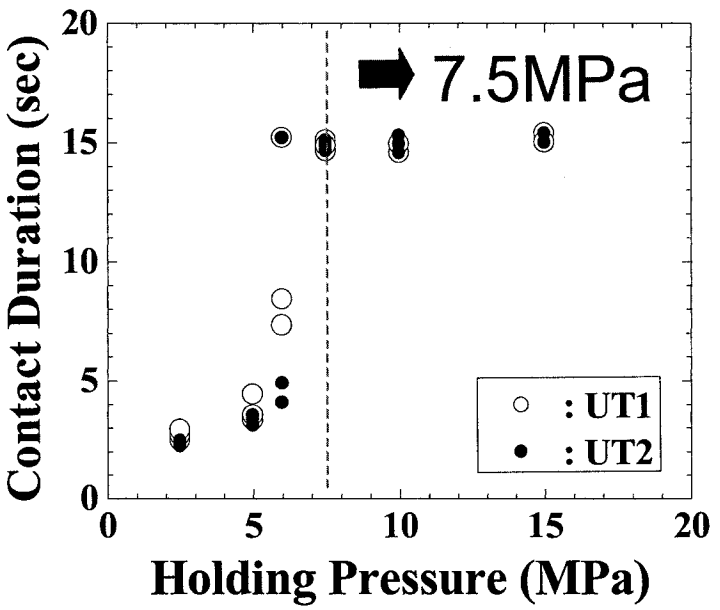

Fig. 5-17 Contact duration obtained from amplitude variation of the L^1 echoes shown in Fig. 5-16 with respect to the holding pressure during IMMF of a PMMA part.

5.4.2. Part surface profile

In order to study the effect of the holding pressure on quality of molded PMMA parts, we have measured surface profile along the line pattern at the right side edge of the part, shown in Fig. 5-2, using an optical interferometory technique [163]. The measurement results are given in Fig. 5-18 and the maximum variation of the surface profile is summarized in Table 5-5. When the holding pressure is higher than 7.5MPa, the surface is almost flat with a maximum variation of 5μm or less. However, the maximum variation becomes larger as the holding pressure is lower than 6MPa. The maximum variation is 24μm at 2.5MPa. This is due to the fact that the molded part detached from the mold surface before solidified probably because of the lack of sufficient holding pressure when it is lower than 6MPa. Therefore, it is concluded that the holding pressure is required to be higher than 7.5MPa for a stable molding condition and for good parts having flat surface on the line pattern under our experimental conditions with the presented IM machine, the mold including the mold insert, and material employed in this study.

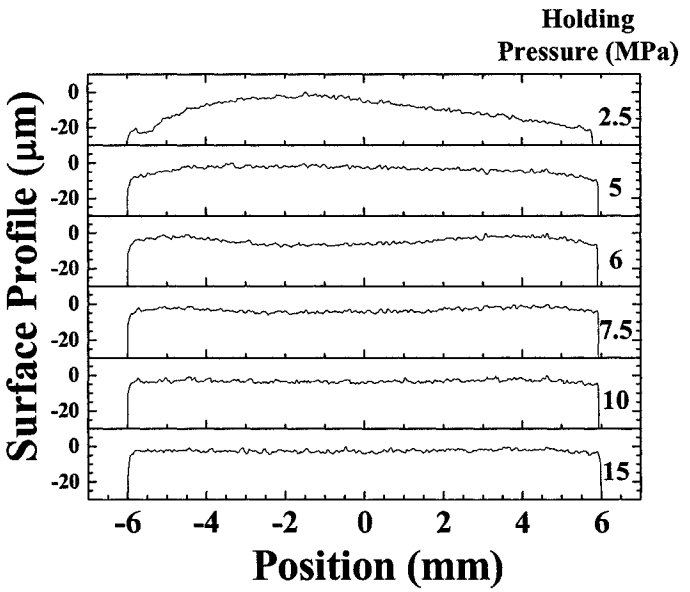

Fig. 5-18 Surface profile on the line pattern at the right edge of the PMMA part, shown in Fig. 5-2, measured by an optical interferometory technique.

Table 5-5 Maximum variation of surface profile on the line pattern of molded PMMA parts shown in Fig. 5-18, with different holding pressures.

Holding Pressure (MPa)	2.5	5	6	7.5	10	15
Maximum Variation (μm)	24	15	8	5	5	4

5.4.3. Ultrasonic velocity in PMMA

Ultrasonic velocities in the molded part are strongly related to its physical properties. Therefore, solidification behavior of the polymer in the cavity may be monitored using the ultrasonic velocity in the polymer during the molding process. The velocity can be determined using the L_{2n} echoes propagating in the polymer, as described in section 4.4.3. The ultrasonic velocity, V_P, is determined by (Eq. 3-14), where h is the depth of the mold cavity at the UT location, and Δt_h is the time delay difference between the L^1 and L_2 or the L_2 and L_4 shown in Fig. 5-8.

Fig. 5-19 presents the ultrasonic velocity with respect to the process time obtained with the UT1 at different holding pressures. At the process time between 3.6sec and 5sec, indicated by the dotted lines in Fig. 5-19, the data are missed since the echoes from the polymer (L_{2n}) are not observed. This is due to that the ultrasonic attenuation in the PMMA is so high during this period and we could not observe the L_{2n}. This will be further discussed later. The measured velocity in the polymer at 7.5, 10 and 15MPa varies from 1000m/s to 2400m/s, indicating the variation of the elastic properties of the part, such as elastic constants, viscosity and density due to a transformation of the polymer from the liquid state to solid state. At the process time of 10sec, the velocity becomes almost constant and the maximum value of 2400m/s. However, at 2.5, 6 and 5MPa, the velocities are obtained only before the part detaches from the probing end due to its shrinkage, as described previously.

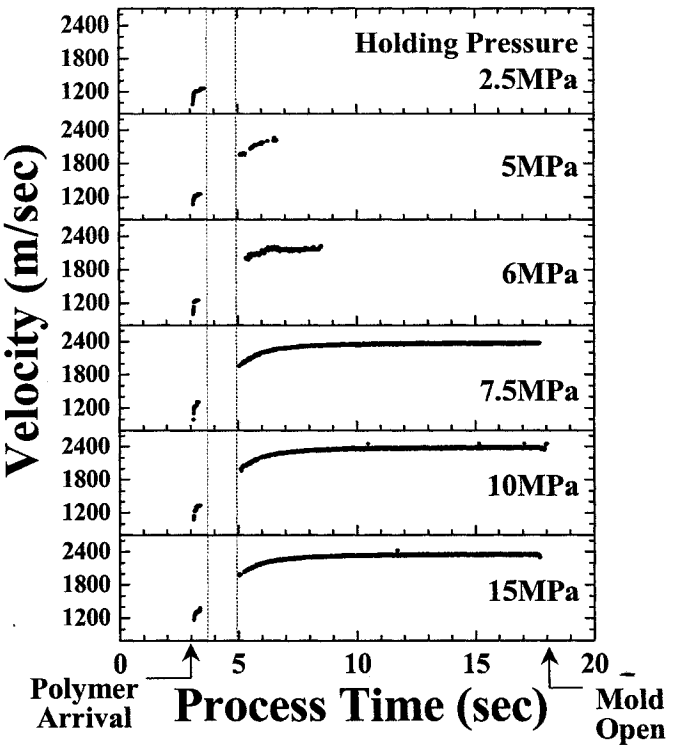

Fig. 5-19 Ultrasonic velocity variation with different holding pressure obtained by the UT1 during one cycle of IMMF process of a PMMA part.

In order to predict the state of the PMMA inside the cavity using the ultrasonic velocities obtained during molding, we have conducted off-line measurements of ultrasonic properties of the same PMMA using an ultrasonic PVT measurement system, described in chapter 3. Fig. 5-20 presents measurement results with the PMMA in the temperature range from 250°C to 50°C during cooling at a pressure of 10MPa. Ultrasonic frequency is 2.5MHz and cooling rate is –2°C/min. Fig. 5-20 (a) shows the specific volume. A knee is observed at 86°C, corresponding to the glass transition temperature, T_G. Above or below T_G, the PMMA is in (viscous or rubbery) liquid or (glassy) solid state, respectively, under the presented condition. Ultrasonic velocity and attenuation of the PMMA are given in Fig. 5-20 (b). The knee is also observed in the velocity curve at T_G, where the ultrasonic velocity is 2300m/s. In the attenuation curve, large peak (α peak) and small one (β peak) are observed at 160°C and 90°C, respectively, related to relaxation phenomena.

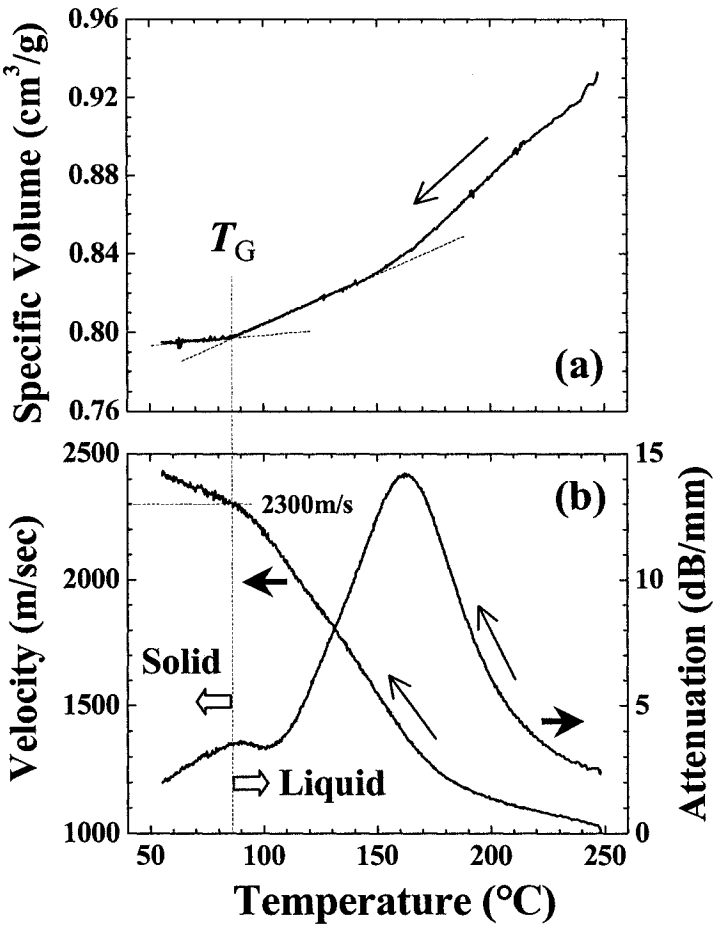

Fig. 5-20: Specific volume (a); and ultrasonic velocity and attenuation (b) of the PMMA with respect to the temperature during cooling, measured by an ultrasonic PVT measurement system. The pressure was kept at 10MPa during the measurement.

Here our attempt is to interpret the solidification behavior of the PMMA in the mold and the surface profile in Fig. 5-18, by correlating the off-line measurement results in Fig. 5-20 to the ultrasonic velocities in Fig. 5-19 obtained during molding. It is noted that temperature dependence of the material properties in Fig. 5-20 is sensitive to the thermal history of the material, pressure and ultrasonic frequency employed. Therefore, we can only explain the behavior of the PMMA in the mold cavity qualitatively since the cooling rate in the

molding is much larger than that in the off-line measurements. In the molding, the melt (230°C) is cooled down to mold temperature (60°C) within 15sec under the presented molding condition while in the off-line measurements the cooling rate is –2°C/min as mentioned previously.

When the molten polymer is injected into the mold cavity with the holding pressure of 7.5, 10 and 15MPa, and arrives to the UT location at 3sec, the velocity is about 1000m/s as seen in Fig. 5-19, corresponding to the velocity in the liquid state in Fig. 5-20 (b). The ultrasonic signals from the polymer (L_{2n}) are temporary lost in the time range from 3.6sec to 5sec in Fig. 5-19 due to the large attenuation peak during cooling caused by α relaxation as shown in Fig. 5-20 (b). Then the velocity increases gradually and, becomes almost constant and maximum value of 2400m/s after the process time of 10sec in Fig. 5-19, which is larger than that (2300m/s) at T_G, indicating that the part temperature is less than T_G and the part is already in the solid state. Thus, further cooling may not have been necessary after 10sec, and shorter cycle time may be achieved. From this information, we can control the cooling time and improve the process efficiency of part manufacturing.

While with the holding pressure of 2.5, 5 and 6MPa, the ultrasonic signals (L_{2n}) are totally lost before the velocity reaching to 2300m/s which is the velocity value at T_G since the molded part is detached from the probing end (mold surface). This means that the part is apart from the mold surface when it is still soft in viscous or rubbery state. The lower the holding pressure, the smaller the ultrasonic velocity finally reaches as shown in Fig. 5-19 at 2.5, 5 and 6MPa. This can explain why the roughness of the part surface increases with the lower holding pressures as shown in Fig. 5-18 and Table 5-5. Thus, the part surface quality of the molded parts and the holding pressure can be optimized by monitoring the ultrasonic velocity of the material to reach the desired value in real-time during molding using the presented ultrasonic miniature sensors and

technique.

5.5 Discussions in MM for polymer and nano-composite

5.5.1 Melt temperature evaluation in barrel

As mentioned previously, polymer melt temperature at the barrel needs to be precisely controlled in order to achieve desirable melt quality for injection and to prevent material degradation due to over heating. Ultrasonic propagation characteristics (velocity and attenuation) in the polymer are strongly related to the material properties (viscosity, density, composition, etc.) and process parameters (temperature and pressure). Thus, such characteristics can be used to monitor the polymer state during polymer processing. The ultrasonic velocity, V_P, in polymer melt inside the barrel can be determined by (Eq. 3-14), where h_r is the 3.275mm gap distance between the internal surface of the barrel and the screw root at the UT location in Fig. 5-3, and Δt_h is the time delay difference between the L^1 and L_{2r} in Fig. 5-10. In addition, the attenuation can be determined using the amplitude difference between the L_{2r} and L_{4r}, where the L_{4r} is the second round trip echo propagating in the polymer (the echo is not shown in Fig. 5-10).

Fig. 5-21 shows the variation of the ultrasonic velocity in POM measured with the UT6 at the barrel with different barrel temperatures of 180, 200 and 220°C, and screw rotation speeds of 15 (squares), 30 (circles) and 45RPM (triangles). The velocities linearly decrease with respect to the barrel temperature in this temperature range. From such information, we can determine the variation of the average temperature of the melt in the barrel using the ultrasonic velocity measured. The detailed explanation will be given in section 5.5.3. In order to achieve desirable melting quality of polymer, diagnosing the melting process inside the barrel of MM machine is important for high quality products. This will be further discussed in chapter 6.

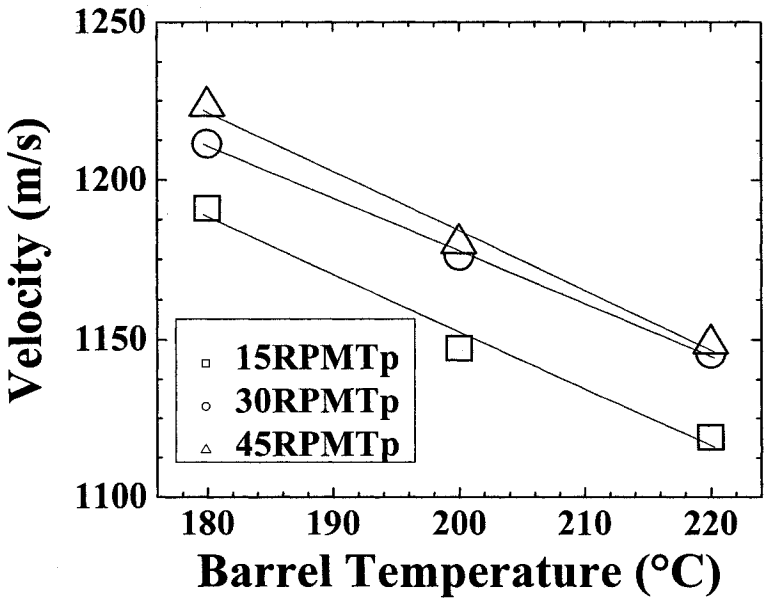

Fig. 5-21: Variations of ultrasonic velocity of the POM melt with different barrel temperatures and screw speeds, measured with the UT6 at the barrel.

5.5.2 Cavity pressure

Ultrasonic velocity is related to process parameters such as material temperature and cavity pressure. Fig. 5-22 shows the ultrasonic velocity in the PA66, measured using the UT1, with respect to the peak cavity (injection) pressure, as shown in Fig. 5-13 (a). The ultrasonic velocity is obtained at the time when the pressure was maxima. In the pressure range of 50-150MPa, the velocity linearly increases with the pressure with a changing ratio of 2.6(m/s)/MPa. Therefore, ultrasonic velocity can be utilized to evaluate the injection pressure during molding.

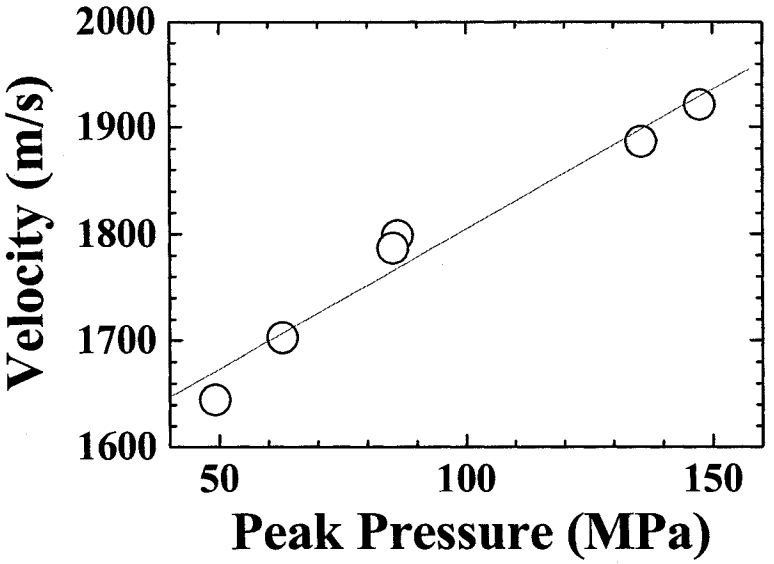

Fig. 5-22: Ultrasonic velocity of PA66 inside the mold cavity with respect to peak cavity pressure.

5.5.3 Solidification and shrinkage of the POM inside the mold cavity

Here, we use the ultrasonic velocity to investigate the POM state in the cavity during molding. Fig. 5-23 presents the ultrasonic velocities with respect to the process time obtained with the UT1, together with the amplitude variation of the L^1 echo in Fig. 5-11. At 0.45s, the POM melt arrives at the UT1 area as mentioned previously, and the ultrasonic velocity of the POM measured was 1240m/s. Then the velocity gradually increases up to 1500m/s, suggesting the solidification of the POM melt due to cooling by the lower mold temperature (75°C) than the melt.

The amplitude of the L^1 in Fig. 5-23 increases gradually after 0.86s, indicating the part is partially detached from the mold cavity surface due to the shrinkage of the part solidified. During the melt solidifying, the shrinkage of the polymer is compensated with the additional melt by the holding pressure, and the contact between the polymer and the cavity surface is kept steadily. However, once the melt is completely solidified, the polymer is no longer added into the

cavity because of the frozen of the gate.

During the part shrinkage from 0.86s to 0.96s, the decrease of the velocity is observed in Fig. 5-23. At this period, thin air gaps partially develop between the cavity and the polymer surfaces due to the part shrinkage, which may have affected on the measurement of the ultrasonic velocities in the polymer. Further investigation needs to be performed to verify such effect on the velocity measurements. At 0.96s, the part detaches from the mold cavity as described previously. Thus, further cooling may not be necessary after 0.96sec, and a reduction of the cooling time may be practiced. From this information, we can reduce the cycle time so as to improve the process efficiency of part manufacturing.

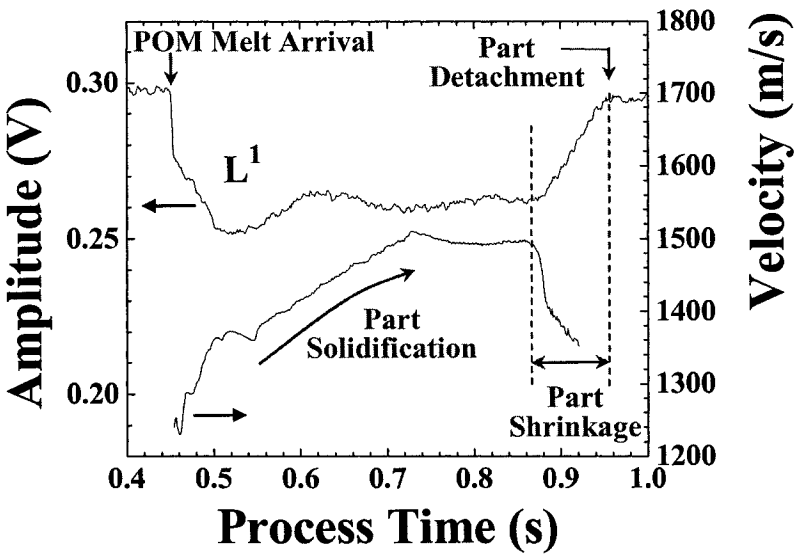

Fig. 5-23 Ultrasonic velocity in the POM inside the mold cavity measured with the UT1 at the mold insert in Fig. 5-4(a), and variations of the amplitude of the L^1 echo in Fig. 5-11.

In order to predict the state of the POM inside the cavity during molding using the ultrasonic velocities in Fig. 5-23, by correlating them with temperatures

of the polymer, we have conducted an off-line measurement of ultrasonic properties of the same POM using an ultrasonic PVT measurement system mentioned in chapter 3. Since it is difficult to realize the same experimental condition as actual molding conditions under which temperature, pressure and cooling rate in the mold dynamically change, the measurement is conducted in the temperature range from 210°C to 50°C during cooling with a constant pressure of 10MPa. Ultrasonic frequency of an UT employed is 2.5MHz and the cooling rate was –2°C/min.

The measured ultrasonic velocity and attenuation of the POM are given in Fig. 5-24 (a). During cooling, the ultrasonic velocity and attenuation start to increase steeply at 157°C, corresponding to crystallization temperature, T_C. At T_C, crystallization ultrasonic velocity, V_C, is 1253m/s. Such steep increase in velocity and attenuation continues until the temperature reaches to 150°C, which is solidus temperature T_S. From 157 to 150°C, sharp increase of the velocity and attenuation is caused by the crystallization of the POM, in which phase transformation of the POM occurred from liquid to solid state. At 150°C, the solidus ultrasonic velocity, V_S, is obtained to be 1447m/s. From 157 to 150°C, the specific volume of the POM, presented in Fig. 5-24 (b), also shows sharp reduction. Therefore, the polymer state inside the mold cavity during molding can be predicted using the velocities measured as follows: the polymer is in the liquid state when the velocity is lower than V_C (1253m/s); and in the solid state if higher than V_S (1447m/s), in the temperature range from 210°C to 50°C at 10MPa.

In the liquid state, the velocity changing ratio with the melt temperature is –1.78(m/s)/°C in the range between 180°C and 210°C in Fig. 5-24 (a), which is almost the same as that with the barrel temperature, –1.76±0.11(m/s)/°C, obtained from the three data with different rotation speeds in Fig. 5-21. Thus, the relative variation of the temperature of the melt in the barrel can be obtained using the ultrasonic velocities measured at the barrel during extrusion as mentioned previously. Ultrasonic velocities obtained at the barrel are the average values

through the thickness of the melt, which directly reflects whole state of the polymer where ultrasound is propagating. Therefore, the melt temperature obtained by the ultrasonic velocity can be used to control the electric heater to adjust the barrel temperature more precisely, appropriately and timely than that measured by temperature sensors at the barrel, which may have a time lug or offset from the true value of the melt temperature.

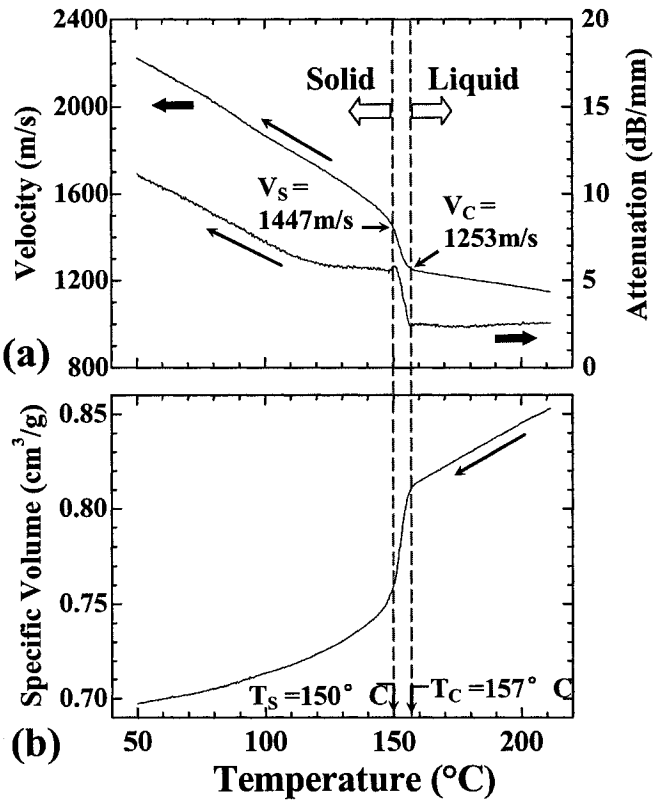

Fig. 5-24 (a) Ultrasonic velocity and attenuation; and (b) specific volume of the POM with respect to the temperature during cooling, measured by an ultrasonic PVT measurement system.

Here our intension is to interpret the solidification behavior of the POM in the mold insert by correlating the off-line measurement results in Fig. 5-24 to the ultrasonic velocities in Fig. 5-23 obtained during molding. It is noted that temperature dependence of the material properties in Fig. 5-24 is sensitive to the

thermal history of the material, pressure and ultrasonic frequency employed. Therefore, we can only explain the behavior of the POM in the mold cavity qualitatively since the cooling rate in the molding is much larger than that in the off-line measurements. In the molding, the POM melt (200°C) is cooled down to mold temperature (75°C) within 8s under the presented molding condition while in the off-line measurements the cooling rate was –2°C/min as mentioned previously. In addition, the cavity pressure during molding is not constant [75]. The cavity pressure depends on injection pressure controlled by the injection piston speed, and solidification behavior of the polymer melt in the cavity. If excessive injection pressure is used, the mold may be forced open and the polymer will escape (flash) [164]. If insufficient, the mold cavity may not be completely filled with the polymer (short shot). Ultrasonic technique can sensitively detect the filling incompleteness, which is presented elsewhere [96].

When the POM melt is injected into the mold cavity, the velocity is about 1240m/s at 0.45s, as shown in Fig. 5-23, which was just slightly smaller than V_C, indicating that the polymer was in the liquid state. Then the velocity increases gradually and reaches to constant and maximum value of 1500m/s at 0.72sec in Fig. 5-23, which is larger than V_S, indicating that polymer is in the solid state. Too low mold temperature solidifies the molten polymer quickly, often resulting in deterioration of the molded part quality, such as blisters, delamination, mold filling incompleteness, warpage, etc [164]. Too high mold temperature increases a cooling time for part solidification, reducing process efficiency, in addition to deterioration of the part quality. Therefore, proper mold temperature is crucial to produce high quality parts efficiently. The measured velocities can feedback to control system and adjust timely mold temperature and cooling time, in order to optimize the process conditions.

5.5.4 Filler concentration of POSS

Small amount of nano filler can dramatically change the characteristics of

the host material. But, if the concentration of nano filler is above certain level, such as 10 wt% of host material, the effect of nano filler reduces. Hence, to investigate the filler concentration during molding process may be necessary. Ultrasonic velocity in the polymer is strongly related to the material properties and process parameters. It may be a candidate to diagnose the filler concentration during molding process. Fig. 5-25 presents ultrasonic velocity variation with respect to the process time for the PA66 with different POSS concentrations during molding process. The velocities monotonically increase with the process time, indicating dynamic status of the polymer from liquid to solid state during cooling. At around 4s before mold open, the velocities become almost constant, which indicates the polymer is cooled enough and in the solid state. This can be evidenced by the PVT measurement data. The incorporation of the POSS with the PA66 decreases the ultrasonic velocity in this concentration range, as seen in Fig. 5-25, due to the change of physical and rheological properties of the materials. This suggests that nano filler concentrations and process variations can be evaluated using ultrasound during molding.

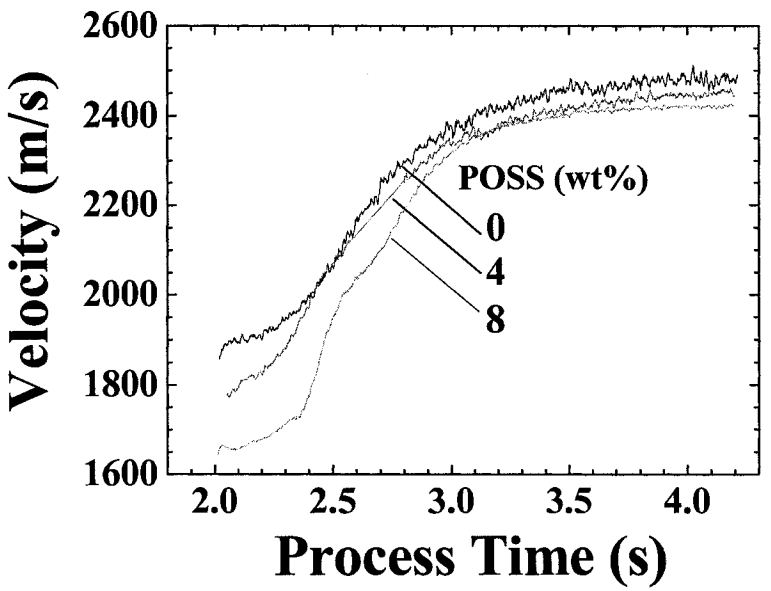

Fig. 5–25 Ultrasonic velocity variations of PA66 with different POSS concentrations during MM process.

5.6 Discussions in MM for ceramic powder

5.6.1 Evaluation of part thickness and weight

To evaluate the quality of the parts of MM for ceramic powder, the thickness of as-molded and sintered parts is measured using a micrometer with stated accuracy of ±1μm, and the weight by a balance with stated accuracy of ±2mg. The results are shown in Fig. 5-26. The open (e.g. ○) and filled (e.g. ●) symbols represent as-molded and sintered parts, respectively. The straight lines for these two sets of symbols are obtained by a least square fitting method. In the thickness range of 1.452mm to 1.484mm and 1.235mm to 1.292mm for the as-molded and sintered parts, respectively, the weight increases linearly from 1.951g to 2.024g for the as-molded parts. The densities of as-molded and sintered parts are 2.78±0.009 (±0.33%) and 3.88±0.021 (±0.53%) g/cm^3, respectively. The densities of parts are measured by Archimedes method. The values are within our measurement error and don't have clear correlation with packing speed.

In this figure, we can also compare the shrinkage of thickness for each part. Due to our un-optimal debinding-and-sintering process at present time, the diversion of thickness for sintered parts is larger than that of as-molded parts. In Fig. 5-26 the maximum thickness differences of all as-molded and sintered parts are 32μm and 57μm, respectively. This difference may exceed the desired specification of the micro PIM parts, e.g. the required accuracy of some special clock components is ±5μm. Furthermore the dimension inconsistency may be a serious problem when parts dimensions are small, e.g. the required diameter of a gearwheel is 257μm [165, 166]. Part thickness and weight show no correlation with packing speed, as shown in Fig. 5-26. Differences in part thickness and weight evident in Fig. 5-26 for as-molded parts are likely to have been caused by inconsistent dosing during each fabrication cycle even with the same machine setting of 820mm^3.

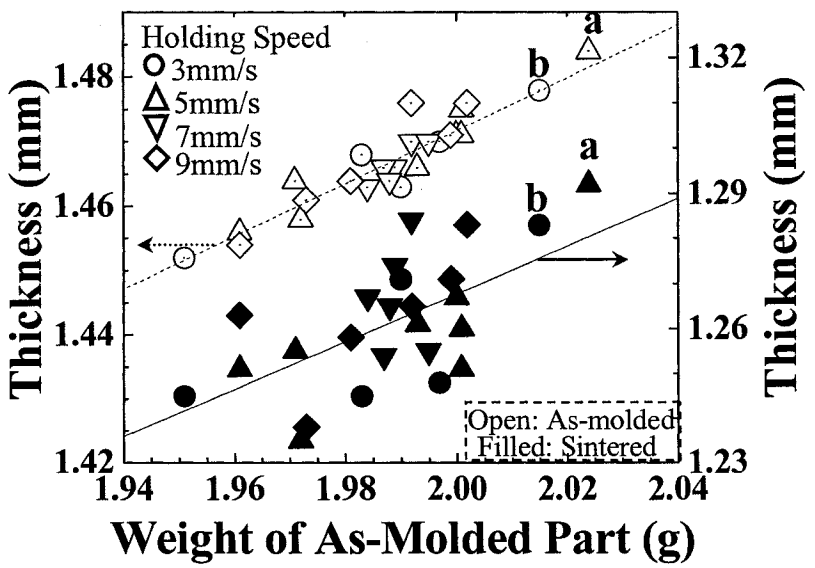

Fig. 5-26 Thickness of as-molded (open symbols) and sintered (filled symbols) ceramic parts of MM process, measured by a micrometer at UT1 location in Fig. 5-6, with respect to weight of as-molded part measured by a balance. Dosing amount setting was 820mm^3.

5.6.2 Correlation of ultrasonic velocity with part thickness

To verify our assumption that the inconsistencies in part thickness and weight are due to poor dosing repeatability, simple molding experiments using two different machine dosing settings of 820mm^3 and 850mm^3 are conducted. In these experiments no packing speed is applied. The ultrasonic velocity in the part is obtained at a processing time of 1s, where process time is defined to start when the injection piston movement begins. The measurement at the processing time 1s is chosen because the part detaches from mold surface after 1.5s for most cases and the temperature, which will affect the ultrasonic velocity in the part, is expected to have little variation with this timing. The relationships between measured ultrasonic velocity, part thickness and weight are shown in Fig. 5-27 where it is apparent that part thickness and weight increase with increasing dosing volume. Small differences in part thickness and weight might have been caused

by minor differences in dosing under the same machine setting. Ultrasonic velocity is sensitive to pressure. The cavity pressure would be higher when there is more material inside the cavity during molding process. Therefore, the data in Fig. 5-27 also provides an indication that ultrasonic velocity may be able to relate with the part thickness and weight. However, in these simple experiments no packing speed is applied.

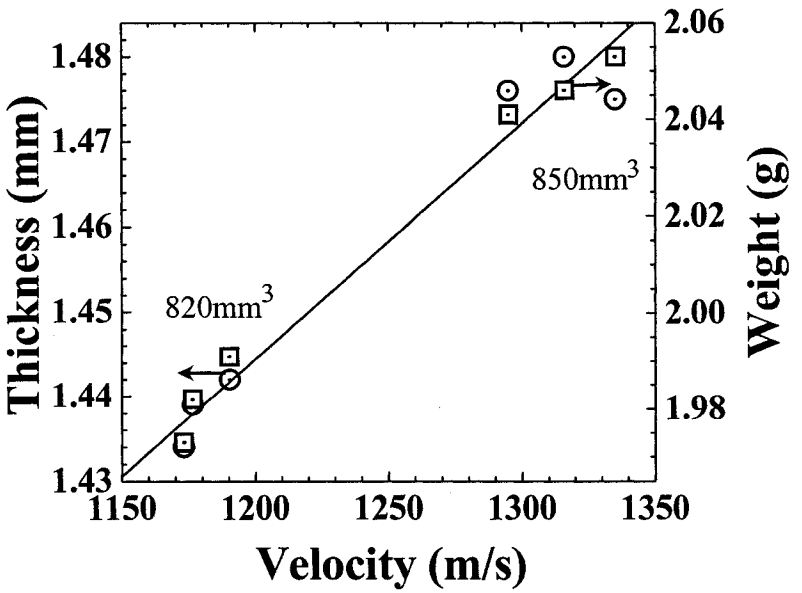

Fig. 5-27 Thickness and weight of as-molded ceramic parts at different dosing amount settings with respect to ultrasonic velocity in feedstock at the processing time of 1s in Fig. 5-15.

Typically during the MM process, a packing speed is applied to aid packing. Ultrasonic velocity has been determined for each of the parts shown in Fig. 5-26 at a processing time of 1s. The choice of 1s is because many parts detach from mold surface after 1.5s, and the fixed timing would cause less temperature variation. The relationships between the ultrasonic velocity and the measured part thickness and weight are shown in Fig. 5-28. There is a linear relationship existed between them. The standard deviations in thickness and weight of as-molded parts are ±2.3μm and ±4.6mg, respectively. This strongly suggests that ultrasonic

velocity may be a parameter related to the thickness and weight of the fabricated ceramic MM parts. Part thickness changes over time due to shrinkage. The thicknesses of all parts are less than the cavity depth of 1.5 mm.

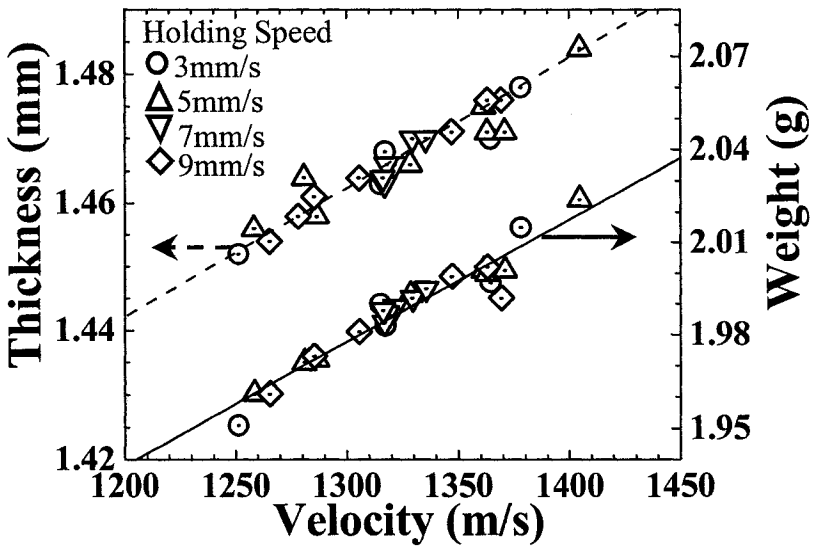

Fig. 5-28 Thickness and weight of as-molded ceramic parts with respect to ultrasonic velocity in feedstock at the processing time of 1s in Fig. 5-15. The parts are the same as those in Fig.5-26.

5.6.3 Correlation of cooling efficiency with part thickness

Ultrasonic contact duration in Fig. 5-15 indicates the period during which the ceramic part and mold are in contact and helps in evaluation of the cooling efficiency. A consistent contact duration implies a uniform cooling profile, and may help repeatability of final part properties as illustrated below. The contact duration is defined as occurring between melt arrival and mold opening or part detachment. The contact duration measured by the L^1 echo at the UT1 position is compared with the part thickness measured at the UT1 location and the results are shown in Fig. 5-29. The standard deviations in thickness of as-molded and sintered parts are ±4.6μm and ±12.1μm, respectively. It is noted that, due to our un-optimal debinding-and-sintering process at present time, the standard deviation

in thickness of sintered parts is larger than that of as-molded ones. In Fig. 5-29, all the parts are identical to those shown in Fig. 5-26. It implies that if one can maintain constant ultrasonic contact duration, the weight and thickness variations of the PIM parts may be reduced. For instance, the two parts of a and b, shown in Fig. 5-29 (and Fig. 5-26), their contact durations are 8.4s. Their thicknesses are 1.481±0.003mm and 1.287±0.005mm for the as-molded and sintered parts, respectively. Fig. 5-29 suggests that ultrasonic contact duration may be another parameter to assist the consistency of part thickness of as-molded and sintered parts during the MM process for ceramic powder. However the deviation in part thickness versus ultrasonic velocity in the part shown in Fig. 5-28 (±2.3μm) is better than that versus ultrasonic contact duration shown in Fig. 5-29 (±4.6μm).

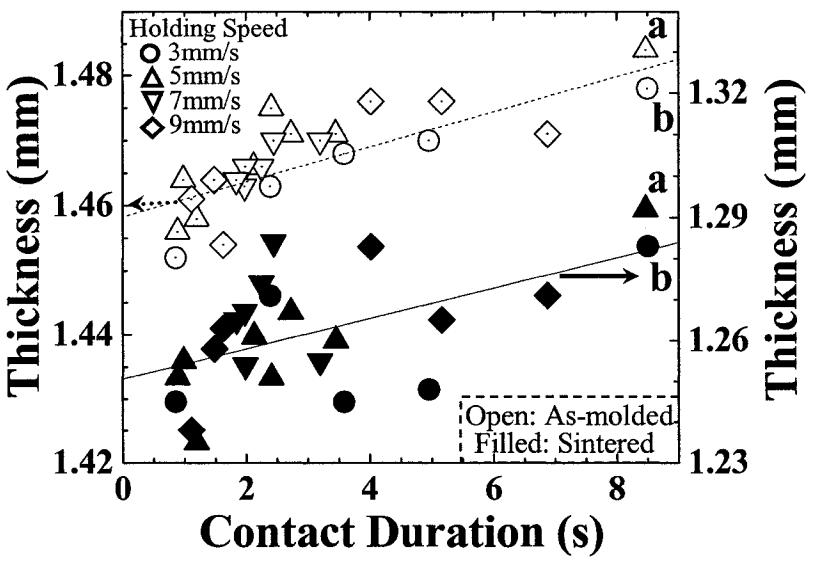

Fig. 5-29: Thickness of as-molded (open) and sintered (filled) ceramic parts with respect to ultrasonic contact duration of L^1 echo measured by the UT1 in Fig. 5-6. The parts are the same as those in Fig. 5-26.

5.6.4 Effects of pressure

It is our intention to adjust packing pressure at the end of packing stage by

change the packing speed and to evaluate the effects. All the parts in Fig. 5-26 are fabricated under the same dosing amount setting of 820mm^3 and the same injection speed of 200mm/s, but with different packing speeds (3, 5, 7, 9mm/s) for a further injection piston movement of 1mm. The experimental results show us there is no correlation between the packing speed and the packing pressure.

The relationship between the measured packing pressures versus the part thickness for all as-molded parts in Fig. 5-26 is presented in Fig. 5-30. The standard deviation in thickness of as-molded parts is ±4.8μm. The data suggests that a higher injection pressure, which is a function of injection speed and dosing volume, leads to an increase in part thickness. However the deviation in part thickness versus ultrasonic velocity in the ceramic part shown in Fig. 5-26 (±2.3μm) is better than that versus packing pressure shown in Fig. 5-30 (±4.8μm).

During these experiments there is no cavity pressure sensor installed. Since commercially available sensors need to be in direct contact with the part, holes must be machined in the mold inserts in order to accommodate them, and they may not withstand the conditions of friction and high pressures in the cavity. The integrated ultrasonic sensors presented here are non-invasive and provide an advantageous alternative to conventional intrusive piezoelectric-based or capacitance-based pressure sensors.

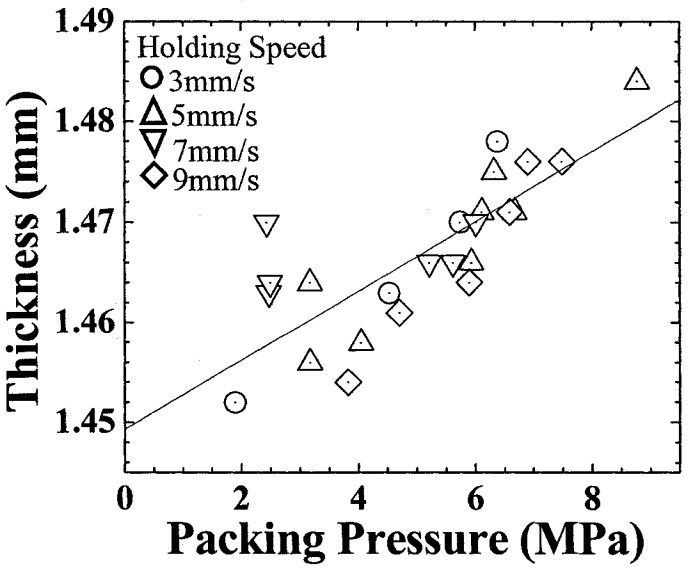

Fig. 5-30 Thickness of as-molded ceramic parts versus the packing pressure in Fig. 5-15. The parts are the same as those in Fig. 5-26.

5.6.5 Evaluation of injection speed

The effect of changing injection pressure by adjustment of the injection speed has been evaluated. Four injection speeds are selected, namely 150, 200, 250, 300m/s. Dosing volume is set to 820mm^3 and a constant packing speed of 5mm/s (for a further injection piston displacement of 1mm) is set. Fig. 5-31 presents the relationship between the injection speed and the injection pressure. Injection pressure increased with injection speed but there is considerable scatter. The thickness of as-molded parts is measured for comparison with injection speed. The experimental results show us there is no clear correlation between injection speed and part thickness of as-molded parts, which indicates that injection and packing speeds cannot be used to optimize part dimension.

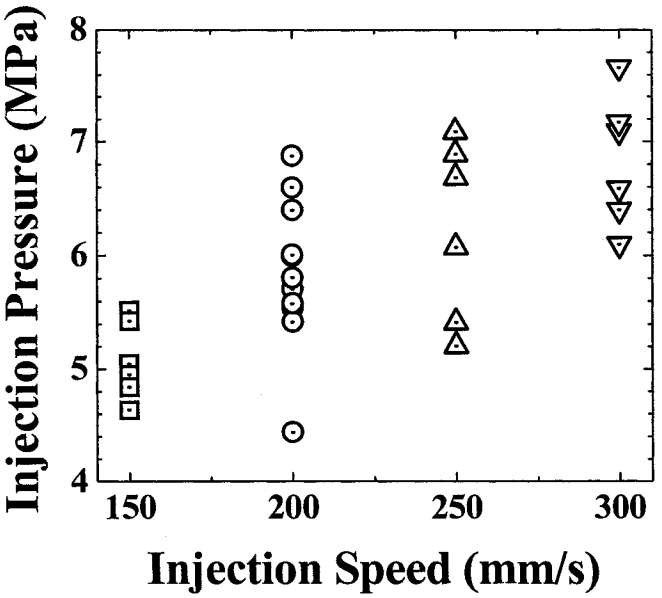

Fig. 5-31 Injection pressure in Fig. 5-15 versus different injection speeds.

5.6.6 Estimation of Young's modulus

Young's modulus and stiffness are two of the important factors for materials and fabricated products. Measurement of Young's modulus (Y) can provide the information related to the stiffness of the products made by the given material. Young's modulus is defined as the ratio, for small strains, of the rate of change of stress with strain. The estimating methods of Young's modulus by measuring ultrasonic longitudinal and shear wave velocity are presented in Appendix A. These estimated results of the Young's modulus of the chosen parts are presented in Fig. 5-32. In the density range from 3.87 to 3.90 g/cm^3, the Young's modulus seems to increase monotonically from 375.5 to 392.6GPa. These values (384.1±8.6GPa) are within the measurement error (±18.3GPa, ±4.7%). These results show that the proposed UTs can be used to estimate the Young's modulus of tested parts. For on-line application, one can fabricate HT ultrasonic longitudinal and shear wave sensors on the mold insert [167-168]. Assuming the density of the feedstock is the same during the measurement, the Young's

modulus of the as-molded part can be estimated by measuring the longitudinal and shear wave velocity of the part real-time.

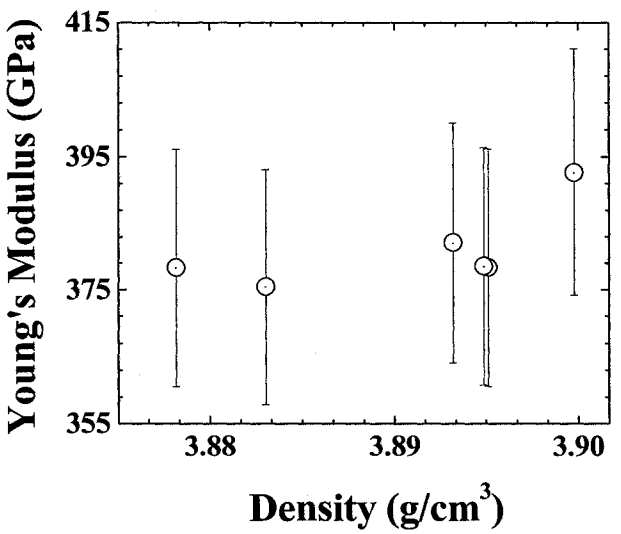

Fig. 5-32: Young's modulus with respect to density of the sintered parts.

5.7 Summary

Integrated, miniature HT ultrasonic sensors have been successfully utilized in real-time process monitoring of IMMF, MM processes. The materials used are PMMA, POM, PA66 with POSS filler, and alumina ceramic powder, respectively. Using these sensors, monitoring process phenomena, such as melt flow front arrival, average flow speed, solidification, part detachment, are shown to be possible.

For IMMF, the surface flatness of molded PMMA parts with 1.1mm thickness varies with holding pressure. Ultrasonic contact-duration and velocity are deployed to provide information on sufficient holding pressure (> 7.5MPa) for producing parts with flat surface (roughness < 5μm).

For MM processes involving POM and PA66+POSS materials, the

temperature variation of the melt in the barrel (180 ~ 220°C) can be obtained by processing the data collected on ultrasonic velocity. Ultrasonic signal is clearly collected after passing through the 3.275mm gap distance. This information can be employed in preventing material degradation. The cavity pressure inside mold can be detected by ultrasonic velocity. This result can be used to control the injection speed in order to avoid part flash. The part thicknesses are 0.495mm and 0.315/0.585mm for POM and PA66+POSS materials, respectively. The concentration of nano-filler in the part (0 ~ 8%) can also be evaluated by ultrasonic velocity during a molding process.

For MM of alumina ceramic powder material, precise part dimension is one of the critical requirements for part quality. According to the experimental results, the thickness variations of as-molded and sintered parts are 32μm and 57μm, respectively. This part thickness variation can be detected by ultrasonic velocity, contact duration, and packing pressure. Among them, the ultrasonic velocity has the best correlation with the part thickness. Young's modulus of part can also be estimated by ultrasonic signatures.

Thus, the integrated HT ultrasonic sensors are suitable for use in micro-fabrication machines, and can be used for real-time, nondestructive diagnosis of micro-fabrication processes. Their deployment increases on-line process efficiency, by reducing the cycle time, and allows part quality control, by optimally adjusting the holding pressure and injected dosing amount.

Chapter 6

Melting quality in internal mixer

6.1 Introduction

As described in chapter 5, the melting quality of polymer in the barrel of IM machine will affect the following product quality in the mold. Therefore, the diagnosis and control of the melting process in the barrel is important for providing polymer melt in good quality. In order to understand the entire melting process deeply in the barrel, experiments using the internal mixer are conducted in this chapter.

The internal mixer is one of the key instruments widely used in laboratories to study melting and extrusion processes of polymers. It is usually equipped with the torque meter and thermocouple. Due to the small dimensions of the mixing chamber (bowl) of internal mixer, torque data measured by the torque meter are reasonably representative of the actual torque exerted on the polymer melt. Based on the measured torque, four distinct rheological phases of the melting process simulating those in the extrusion are identified [15]. They are: (1) elastic solid pellets; (2) deformable solid pellets; (3) transition materials and, (4) viscoelastic fluid. When polymer pellets become fully viscoelastic fluid, the torque reaches a steady state. The complete melting time for polymers is seen as the torque reaching the steady state, and it depends on the material and processing conditions (temperature and rotor speed, etc.).

Ultrasonic technique is one of the candidates for monitoring the different melting stages during process. To demonstrate this, a research applying the ultrasonic delay line probe for process diagnosis in the internal mixer is initiated. The objective of this study is to investigate ultrasonic techniques for melting process diagnosis in order to improve productivity and efficiency.

6.2 Experimental setup and experiments

As mentioned in chapter 1, clad buffer rods (CBRs) have evolved over the last several years [169-171]. Fig. 6-1 presents the photograph of CBR with cooling section and a UT. These items compose the ultrasonic delay line probe employed in the chapter. The rod is fabricated by cladding stainless steel [172-174] with a steel core by the electric arc thermal spray technology [47]. This cladding layer has the ability of maintaining good ultrasonic guidance in the core even if the cladding is machined. This CBR gives superior performance for longitudinal and shear waves. It can be machined and made of metals with high melting temperature.

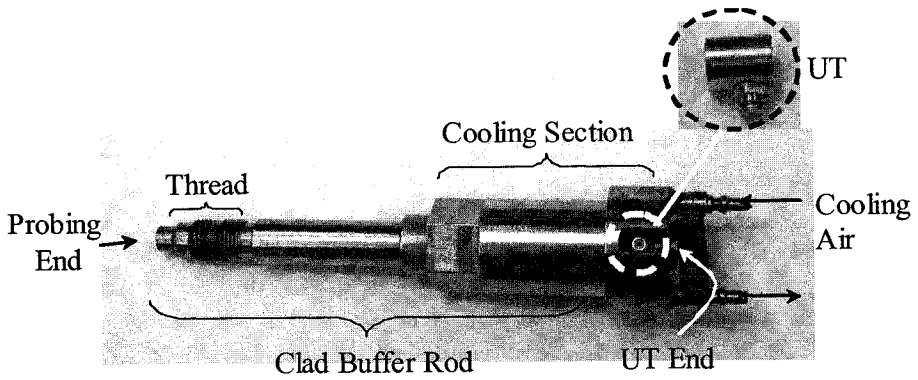

Fig. 6-1 Photograph of the CBR (ultrasonic delay line probe) with cooling section and a UT.

This ultrasonic delay line probe [175] is installed into the mixing chamber of the internal mixer (C. W. Brabender 2000) for real-time melting process diagnosis, as shown in Fig. 6-2. The central frequency of the employed UT is 10MHz. The ultrasonic probe has the geometry and interfaces that are compatible with conventional temperature and cavity pressure sensors (for example, TPT 467XL, Dynisco Instruments & Polymer Test, Franklin, MA). Therefore, it can be installed into the internal mixer machine without modification of the existing chamber. It also means that temperature, pressure and ultrasonic sensors are interchangeable. The Ultrasonic delay line probe can operate up to 700°C, which

is sufficiently high to encompass the full range of melt temperatures typically encountered in polymer processing. The UT end of the probe is cooled down by the compressed air to a temperature lower than 40°C.

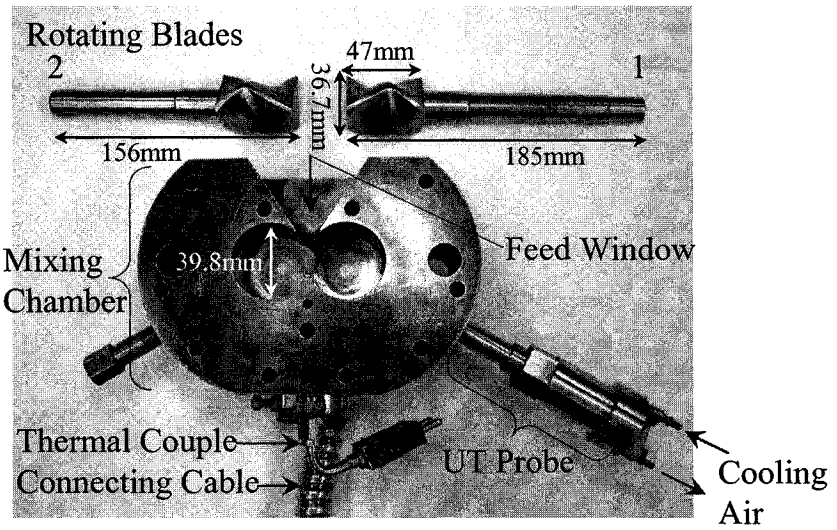

Fig. 6-2 Photograph of mixing chamber with rotation blades, thermocouple, Ultrasonic delay line probe.

The internal mixer is equipped with a mixing chamber and two rotating blades with roller shape, which replicates the shape of the screw in the extruder, as shown in Fig.6-2. The mixing chamber has two cylindrical cavities for melting and mixing process. The cavity has a diameter of 39.8mm and a depth 48.5mm. These two cavities have the capacity of 60ml, with the roller blades. There are heating coils surrounding the mixing chamber. The internal mixer can operate up to 300°C and rotate up to 108 rotation per minute (RPM). The testing material is fed into the mixing chamber from a feed window in the top. The dimensions of the head of the rotating blade are 36.7mm in diameter and 47mm in length. As shown in Fig. 6-2, the total lengths of rotating blade 1 and 2 are 185 and 156mm, respectively. The blade 1 is directly fitted on the rotor shaft, while blade 2 is geared to the shaft. The RPM of the blade 1 and 2 are the same. The mixing chamber, rotation blades, thermocouple and ultrasonic delay line probe are

installed into the internal mixer machine for diagnosis of melting process, as shown in Fig. 6-3.

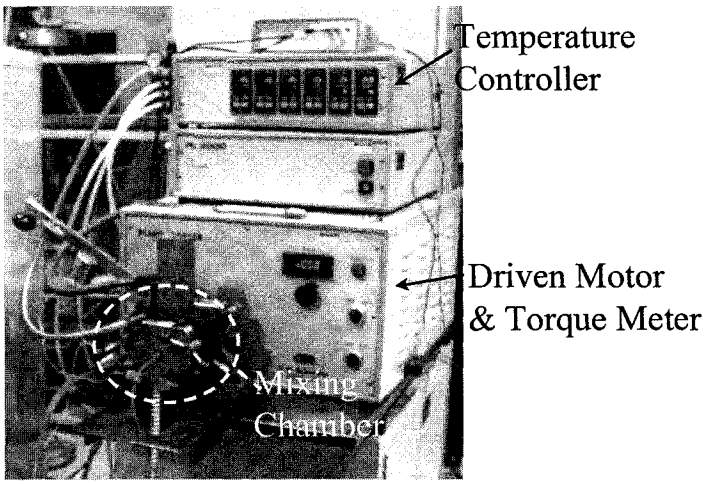

Fig. 6-3 Photograph of the internal mixer (C.W. Brabender 2000).

A schematic drawing of a cross-section of the mixing chamber with the ultrasonic delay line probe, rotating blades and thermocouple, is given in Fig. 6-4. It illustrates the paths of ultrasound propagating in the probe and the polymer melt. The probing end faces the rotating blade 1. The first round trip ultrasonic longitudinal-wave echo, indicated by L^1, is reflected at the probe end/air or polymer interface, depending on whether the polymer is attached to the inside surface of mixing chamber or not. The n-th round trip echo from the flight of the rotating blade half through the polymer melt is L_{2nf} (n=1, 2...).

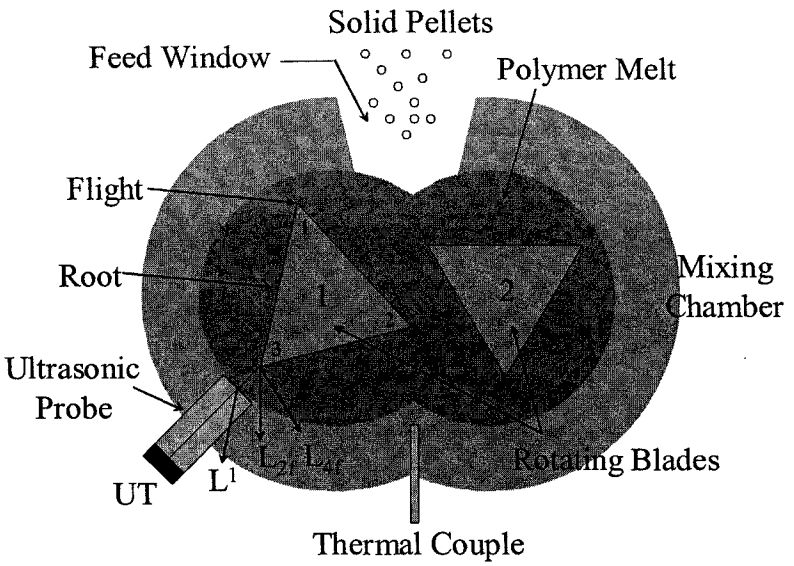

Fig. 6-4 Schematic drawing of a cross-section of the mixing chamber, including the ultrasonic delay line probe, rotating blades and thermocouple, presents the ultrasonic paths in the probe and polymer.

The internal mixer is also equipped with a torque meter, attached to the rotator of the driving motor, and a K-type thermal couple, located at 0.2mm-depth from the inside surface of mixing chamber bottom, as shown in Fig. 6-4. The torque and temperature data, acquired during the entire melting cycle, are used for comparison with ultrasonic data for all the experiments.

The polymer employed is a low-density polyethylene (LDPE) (from Nova Chem., Alberta, Canada). The density is 0.926 g/cm^3 from the company. The maximum capacity of the mixing chamber with the roller blades is 56g of LDPE in the experiments. The procedures of melting process are as follows: first, the empty mixing chamber is heated up to the setting temperature and the blades are rotating at the desired speed. Then the polymer pellets, 50g, are fed into the cavity for melt. The melting conditions employed in the experiments are as follows: the setting temperatures of the mixing chamber are 170, 200 and 230°C; the rotation speeds of blades are 14, 28 and 42 RPM.

6.3 Results

Fig. 6-5 shows the amplitude variations of the torque and temperature during the melting process of 50g LDPE under the temperature setting of 200°C and rotation speed of 28 RPM. In the process time of 30s, 50g of LDPE are fed into the mixing chamber. From process time of 30 to 50s, the torque value increased due to the friction and temperature decreased due to the heating transfer between polymer pellets, rotating blades and mixing chamber. At process time of 50 and 52s, the torque and temperature reach to their peak and bottom values, respectively. After that, the torque decreases due to the reduction of the viscosity of the polymer melt, and temperature increases due to the heat coming form the heating coils, friction and shear forces exceeds that absorbed by the polymer. At process time of 210s, the melting process stops since the torque reaches a steady state and the temperature almost recovers its original value.

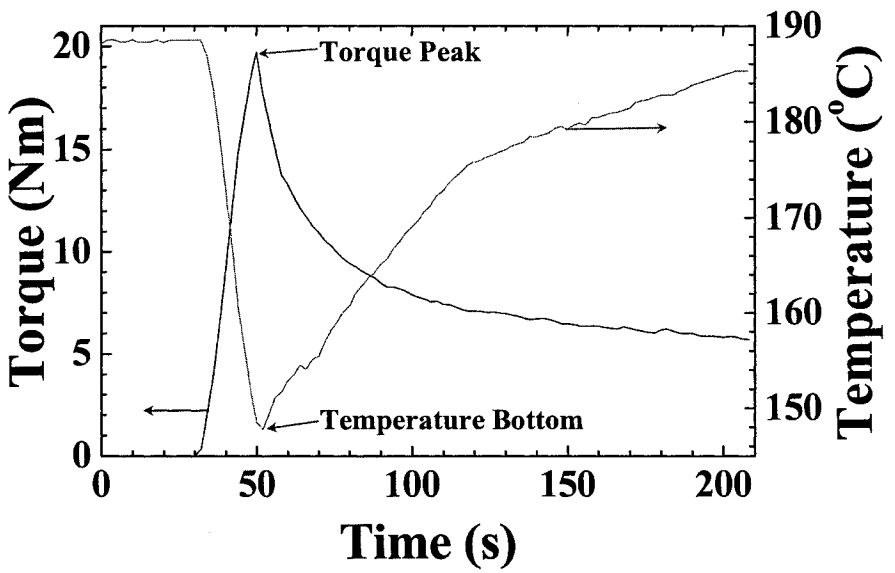

Fig. 6-5 Variation of torque and temperature during melting process of 50g LDPE. Temperature, 200°C and rotation speed, 28RPM.

Fig. 6-6 (a) ~ (f) are photographs of the melting process in Fig. 6-5 at the process time of 37, 50, 64, 79, 121, and 200s, respectively, taken from the feed window. In the beginning, the mixing chamber is empty. At process time of 30s, the polymer pellets are fed into the mixing chamber. In Fig. 6-6 (a), at the process time of 37s, which is 7s after polymer fed into chamber, some of the pellets are still in the feed window and not enter into the mixing chamber yet. In Fig. 6-6 (b), at process time of 50s, which is the time at which the torque reaches to its peak value, most of the pellets are in the elastic solid form and bound with rotating blade. Few pellets melt and attach to the surface of the mixing chamber. In Fig. 6-6 (c), at process time of 64s, which is 14s after the peak value of torque, most of the solid pellets have melt and been dispersed in the mixing chamber. But some of the partially melt pellets still exist within the melt, as indicated by the dashed circle.

In Figs. 6-6 (d) ~ (f), the process time from 79s to 210s, even though the torque and temperature still vary, there are no solid or partially melt pellets left and the polymer melt doesn't appear to change significantly. This may indicate that, after the process time of 79s, most of the pellets were already melt. In Figs. 6-6 (e) and (f), the bubble shape material shown in the left side of figure is the polymer melt brimming out of the chamber. This may be due to density reduction in higher temperature, and it is confirmed from the PVT measurement. It is our interest to diagnose the dynamic melting process after most pellets having been melted. In order to feed the additional material into the mixing chamber, the amount of LDPE should be reduced to 40g to avoid the polymer melt brimming out of the chamber. The melting phenomena in Fig. 6-6 are expected to happen early when the amount of material is 40g.

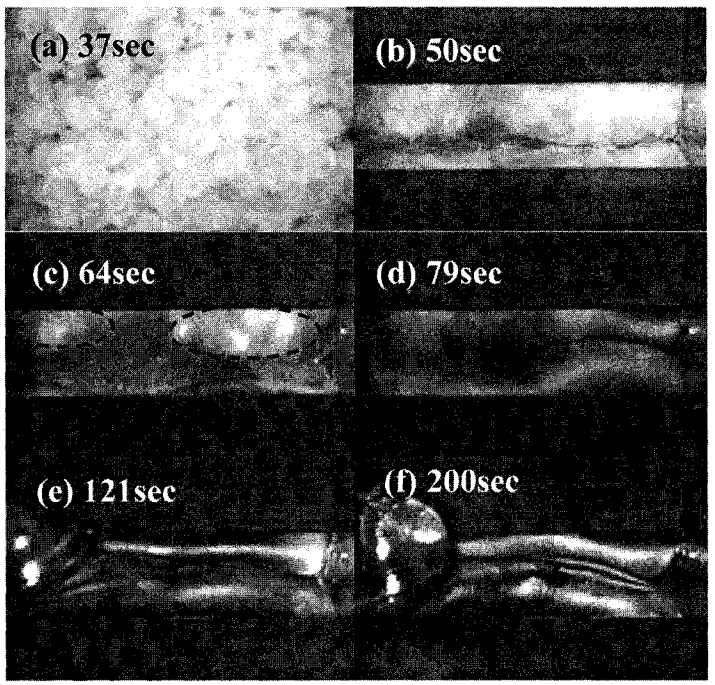

Fig. 6-6 Photographs from feed window of melting process in Fig. 6-5 at the process time of 37, 50, 64, 79, 121, and 200sec.

Fig. 6-7 shows the trace of ultrasonic waveforms acquired with the ultrasonic probe in Figs. 6-2 and 6-3 during the process time when polymer has melted. Ultrasonic signals are acquired every 8.3ms (i.e. 120Hz) during the entire cycle. However, a process time interval of 16.7ms (i.e. 60Hz) has been selected for clarity and shown in Fig. 6-7 for a period of 83.90s to 84.10s. The L^1, propagating in the delay line probe and reflected at the probing end/polymer melt interface, are observed throughout the period. When the flight of the rotating blade arrives below the probe location, the L_{2f} and L_{4f} echoes appear from the process time 83.94 to 84.04s, at time delay of 50.4 and 53μs, respectively. The L_{2f} and L_{4f} echoes exist while the top surface of the flight is facing the probe location. Echoes reflected from the other two flights have the similar waveforms which are observed when their top surfaces arrive below the probe location. For the data shown in Fig. 6-7, the time delay Δt between the L^1 and L_{2f} echoes, or L_{2f} and L_{4f} echoes, is directly related to ultrasonic velocity in the polymer and indicates the phase and melting condition of the polymer inside the mixing chamber [176, 177].

The ultrasonic velocity decreases, or the time delay increases, as the polymer melts.

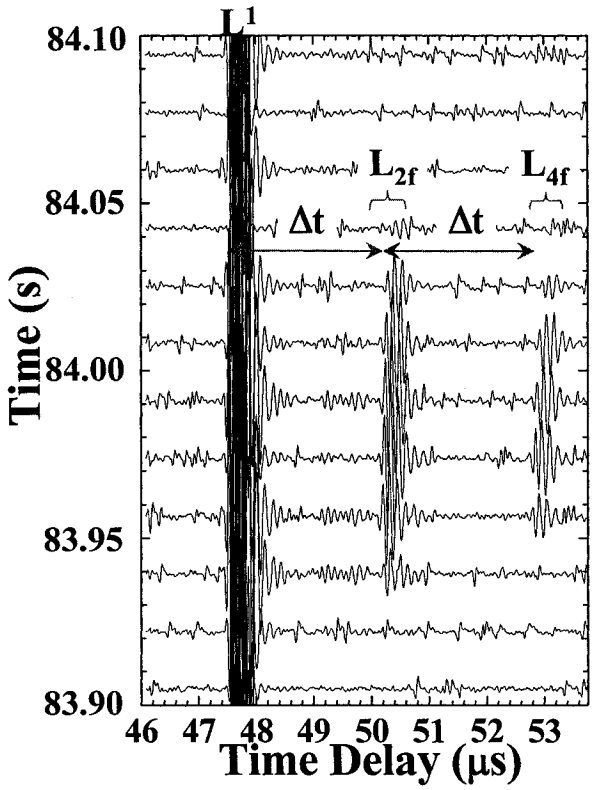

Fig. 6-7 Sample traces of an ultrasonic waveforms showing delay times between L^1 and L_{2f} and between L_{2f} and L_{4f} echoes.

Fig. 6-8 presents the amplitudes of the L_{2f} echoes from three flights of the rotating blade 1 with respect to the process time, when the polymer is melted. It is noted that the processing period here is different from that in Fig. 6-7. In Fig. 6-8, at process times around 75.6, 76.3 and 76.9s, peaks of the L_{2f} echoes are observed, indicating the arrival of each flight of the blade 1 beneath the probe location. The peak amplitudes of three L_{2f} echoes varies, due to different ultrasonic reflecting areas on the three flights of blade 1, as shown in Fig. 6-2. The duration of each pulse is around 0.1s. The amplitude of L_{2f} echo and the time

delay between the L^1 and the peak L_{2f} echoes are used as the indicator for the melting quality. This will be discussed further in section 6.4.1.

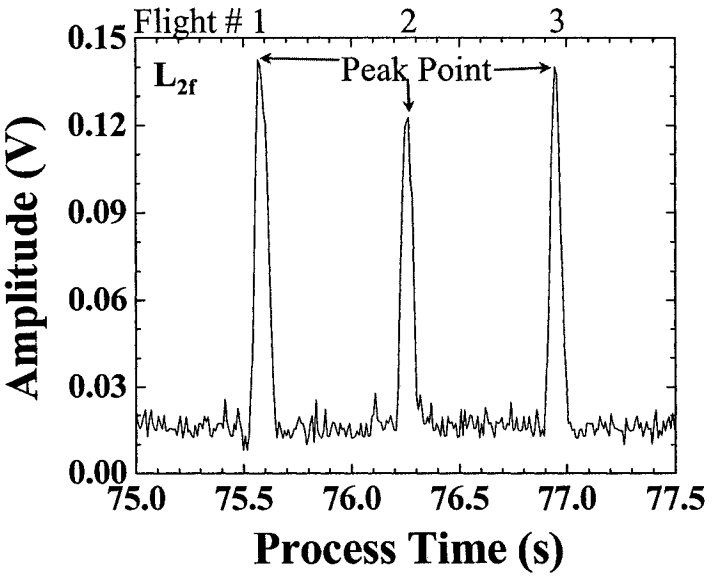

Fig. 6-8 Amplitude of L_{2f} echoes of flights 1, 2 and 3 of rotating blade 1 (see Fig. 6-3) in process time after polymer is melted.

6.4 Discussions

6.4.1 Melting completeness

Determination of the melting completeness using ultrasound would give an opportunity to end the melting process earlier than the conventional method, which requires the torque reaching a steady state and the temperature recovering its initial value. In this experiment, 40g of LDPE, as the host material, are first fed into mixing chamber for melt, and, after the previous polymer have been melted completely, additional 4g of same material are fed for diagnosing dynamic melting process. Fig. 6-9 (a) and (b) present the variation of amplitude for torque and temperature acquired by the torque meter and thermal couple. Fig. 6-9 (c), (d) and (e) show the variation of amplitude for L^1, peak value of L_{2f} and the time delay between L^1 and L_{2f}, respectively, during the melting process. The time delay between L^1 and L_{2f} and the peak value of L_{2f} are shown in Fig.6-7 and Fig. 6-8,

respectively. The amplitude of L^1 echo is normalized by its maximum value. It is noted that the presented peak amplitude of L_{2f} and the time delay between L^1 and L_{2f}, are from the same flight of the blade 1. The temperature setting of the mixing chamber and the rotation speed of the blade are 200°C and 28RPM, respectively.

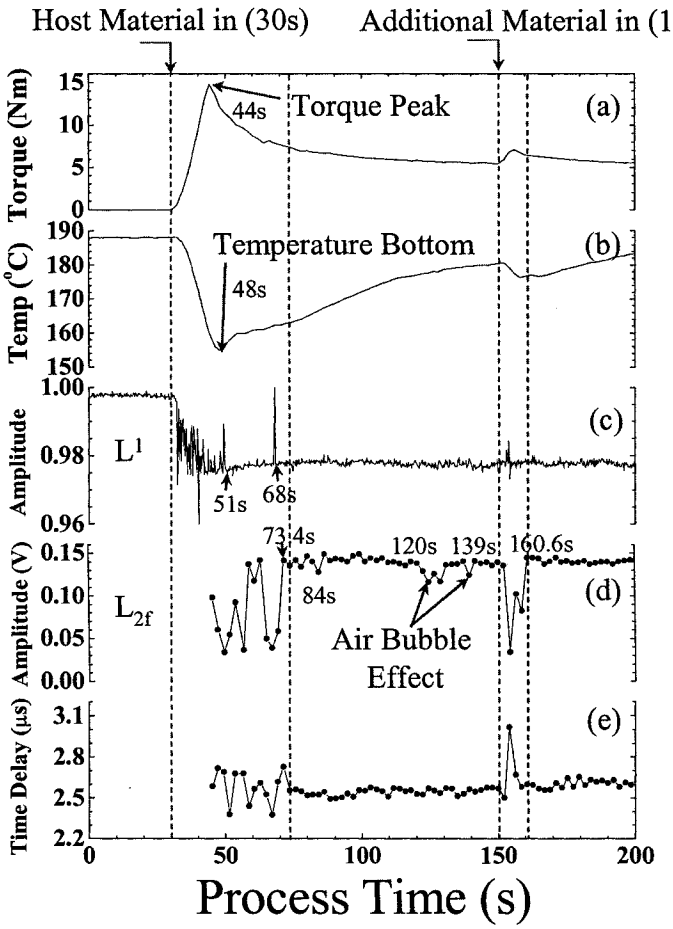

Fig. 6-9 Variation of (a) torque, (b) temperature, (c) amplitude of L^1, (d) peak value of L_{2f}, and (e) time delay between L^1 and L_{2f} during melting process. LDPE introduced: 40g at 30s; 4g at 150s.

Before the process time of 30s, the mixing chamber is heated up to 190°C and the blade rotates at the speed of 28RPM. It is noted that even under the temperature setting of 200°C, the actual chamber temperature is 190°C, due to the heating loss from the feeding window. At the process time of 30s, since the host

material (LDPE) of 40g is fed into the mixing chamber, the torque value rises up quickly. At the process times of 32 and 31.6s, the temperature and amplitude of L^1 echo start to decrease, respectively. It is noted that there is a time difference between torque, temperature and ultrasonic measurement. This is due to the fact that the torque value reflects an overall or an "integrated" material state, while the temperature and ultrasonic measurements detect local conditions. The torque and temperature values vary as described previously. The drop in the value of L^1 echo is due to the fact that, since some LDPE pellets are already melt and they get attached to the inner surface of mixing chamber, part of the ultrasonic energy is transmitted into the polymer melt through the probe end/polymer melt interface. The fluctuation of L^1 echo indicates the random contact of soft pellets and molten polymer to the probing end surface.

At the process time of 44 and 48s, the torque and temperature value reach to the peak and bottom value of 14.8Nm and 154.9°C, respectively. Around this time, the amplitude of L^1 echo also reaches to its lower level, but keeps fluctuating. According to Fig. 6-6 (b), during this period, most of the pellets are still solid with partially melting. At the process time of 45s, the ultrasonic echo L_{2f} reflecting from the polymer melt/flight of the blade 1 interface starts to appear. In the process time from 45 to 73.4s, the peak amplitude of L_{2f} echo and the time delay between L^1 and L_{2f} echoes fluctuate, indicating the non-uniformity of the melting condition. This is also evident from Fig. 6-6 (c). Except one peak occurring at the process time of 68s, fluctuations of the amplitude of L^1 stop at the process time of 51s. This peak may has been resulted from a partially melt pellet.

After the process time of 73.4s, the peak amplitude of L_{2f} echo reaches to its upper level, and the time delay between L^1 and L_{2f} echoes enter into a stable state, indicating that there is no solid or partially melt pellets and all of the LDPE pellets are melt. Fig. 6-6 also supports those diagnosed by ultrasonic technique. After this moment, the increase of time delay between L^1 and L_{2f} echoes from 73.4s to 150s in Fig. 6-9(e) is due to increase of melt temperature. Therefore, when the

amplitude of L_{2f} echo reaches to its upper stable level and the time delay between L^1 and L_{2f} echoes becomes stable, all of the material have completely melt and further heating or rotating may not be necessary. However, the torque and temperature values provide such information later. The information on melting completeness can be useful to optimize the process. At process times 84, 120 to 130 and 139s, the amplitude of L_{2f} drops slightly. This may be due to air bubbles introduced between the probe and blade surface resulting from insufficient material. This phenomenon will be further discussed in section 6.4.2. However, air bubbles don't alter the time delay between L^1 and L_{2f} echoes significantly.

In order to diagnose the dynamic melting process, at process time of 150s, a 4g LDPE is fed into the mixing chamber. The reactions of these five parameters are similar with those of host material. At process time of 160.6s, the peak amplitude of L_{2f} echo recovers its original value and the time delay between L^1 and L_{2f} echoes stops fluctuating, indicating complete melt of the additional material. These results present that ultrasonic signatures are able to diagnose the dynamic melting process. Since the dynamic melting phenomena of additional material are similar with the host material, the rest experiments will focus on the 40g host material only.

In order to capture the timing of melting completeness through the ultrasonic signals, moving standard deviations (MSDs) of the ultrasonic parameters are calculated. The MSD is a statistic calculating and analyzing method, through which the variation of system can be captured, when the system structure changes or noise or perturbation are added to the system. MSD has been used to predict the stock prices on the Stock Markets (see Appendix B). Fig. 6-10 (a), (b) and (c) show the MSD values for a window size of 3 points apply to the amplitude of L^1 echo, peak amplitude of L_{2f} echo and time delay between L^1 and L_{2f} echoes, respectively. In Fig. 6-10 (a), after the host material of 40g LDPE is fed into the mixing chamber, the MSD of L^1 echo rapidly increased to 0.062 at the process time of 31.6s, and then decreased gradually to noise level at the process

time of 50s, except one peak at the process time of 68.5s. In Fig. 6-10 (b) and (c), the MSDs of peak amplitude of L_{2f} echo, and time delay between L^1 and L_{2f} echoes start to appear and increase at the same process time of 49.3s, and decrease to noise level at process time of 75.6 and 77.3s, respectively. According to Fig. 6-6 (d), the timing when the MSDs of peak amplitude of L_{2f} echo and time delay between L^1 and L_{2f} echoes reach to the noise level can be used to indicate the complete melting point. The time period, when the host material is fed into the mixing chamber until it reaches its melting completeness, is defined as the melting period for mass material. In the MSD of time delay between L^1 and L_{2f} echoes, the first bottom of the "M" shape curve may indicate the phase change from solid pellets to melt. This is evident from Fig. 6-6 (b) and (c), and the "M" shape curve is seen in other experimental results.

At process time of 150s, the additional material of 4g LDPE is fed into the mixing chamber, causing the MSDs of three parameters to rise simultaneously. At process time of 155s, the MSD of amplitude of L^1 echo reaches to the noise level. At process time of 164.8 and 162.7s, the MSDs of peak value of L_{2f} echo and time delay between L^1 and L_{2f} echoes reach to the noise level, respectively, indicating that the impulse material is melted completely. Therefore, the presented ultrasonic technique produces a measurement of melting completeness, which can be used to optimize the process parameters.

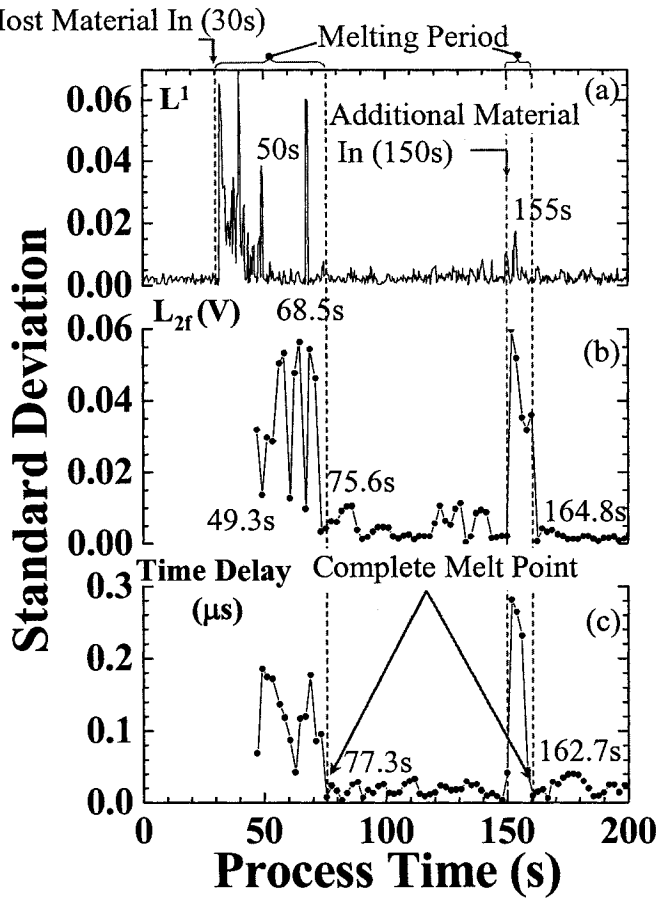

Fig. 6-10 Moving standard deviation (MSD) of (a) amplitude of L^1, (b) peak amplitude of L_{2f} and (c) time delay between L^1 and L_{2f}. Window size of MSD is 3 sample points.

6.4.2 Air bubble effect

To prove our assertion concerning the effect of the air bubbles on the peak amplitude of ultrasonic L_{2f} echo in the section 6.4.1, two simple experiments are carried out. The settings of the temperature of the mixing chamber and the rotation speed of the blades are 200°C and 28RPM, respectively. The amounts of material for these two experiments are 30g and 50g of LDPE, representing insufficient and full amount of material, respectively. Fig. 6-11 (a) and (b) show the results of the peak amplitude of L_{2f} echo for these two experiments during the melting process. In Fig. 6-11 (a), the peak amplitude of L_{2f} echo reaches to the

upper level at process time of 71.7s and keeps in the stable state until 80.3s. From the process time of 80.3 to 150s, air bubbles alter the peak amplitude of L_{2f} echo around 11 times. The drop of peak amplitude of L_{2f} echo in Fig. 6-11 (a) is deeper than those in Fig. 6-9 (d). This indicates that the air bubbles in the 30g experiment are larger and more than those in the 40g experiment. In Fig. 6-11 (b), the peak amplitude of L_{2f} echo reaches to the upper level at the process time of 78.6s and keeps in the stable state until 150s. Air bubbles do not alter the peak amplitude of L_{2f} echo in Fig. 6-11 (b) during the melting process, because the presence of full material in the mixing chamber minimizes the creation of the air bubbles.

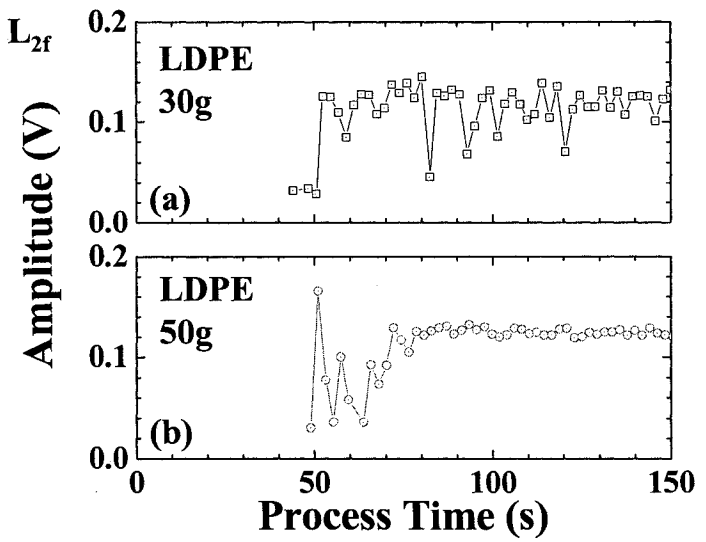

Fig. 6-11 Peak amplitude of L_{2f} echo. (a) 30g and (b) 50g LDPE.

Fig. 6-12 (a) and (b) show the results of time delay between L^1 and L_{2f} echoes, which also indicate the same phenomena in Fig. 6-11 (a) and (b). The time delay value in Fig. 6-12 (a) is lower than that in Fig. 6-12 (b), indicating the higher melt temperature in Fig. 6-12 (a), due to fewer polymer pellets involved. Because the time delay between L^1 and L_{2f} echoes is more stable than peak amplitude of L_{2f} echo, the MSD of time delay between L^1 and L_{2f} echoes will be used as an indicator for melting completeness in the following sections. These two

experiments also show that more material needs longer time to melt completely. Our other experiments also demonstrate that faster rotation speeds introduce more air bubbles.

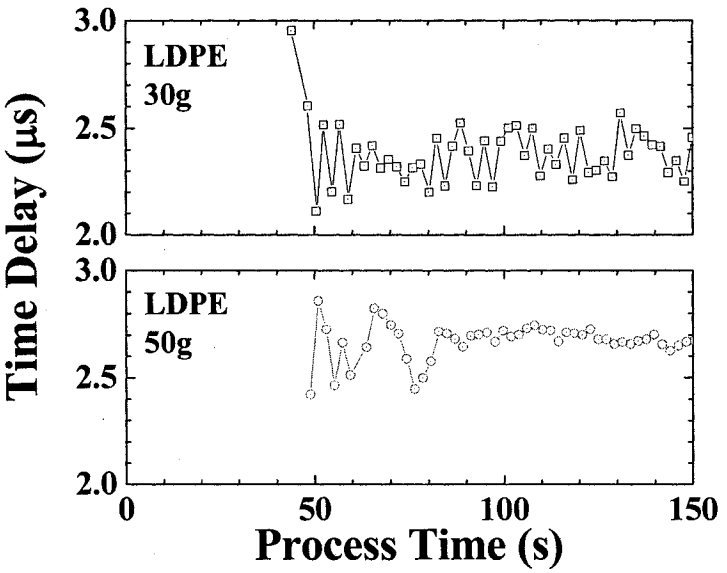

Fig. 6-12 Time delay between L^1 and L_{2f} echoes. (a) 30g and (b) 50g LDPE.

6.4.3 Temperature effect

The temperature of mixing chamber affects the melting process significantly. Higher temperature settings help polymer melt faster, but also cause faster material degradation. Therefore, choosing a proper temperature setting is critical for increasing melting efficiency and optimizing the process. In order to investigate the temperature effect on the melting process, the temperatures of the mixing chamber are set at 170, 200 and 230°C, separately, to melt 40g LDPE with fixed rotation speed of 28RPM. The experimental results of torque and MSD of time delay between L^1 and L_{2f} echoes with respect to process time are presented in Fig. 6-13 (a) to (d). In Fig. 6-13 (a), the melting process with lower temperature setting requires higher torque values and needs more time to reach to the steady state. In Fig. 6-13 (b) to (d), the MSD of time delay between L^1 and L_{2f} echoes

reaches to the noise level earlier, when the melting process is set at a higher temperature. The timings of melting completeness are at process times of 104.9, 93.9 and 67.5s for the temperature settings of mixing chamber at 170, 200 and 230°C, respectively.

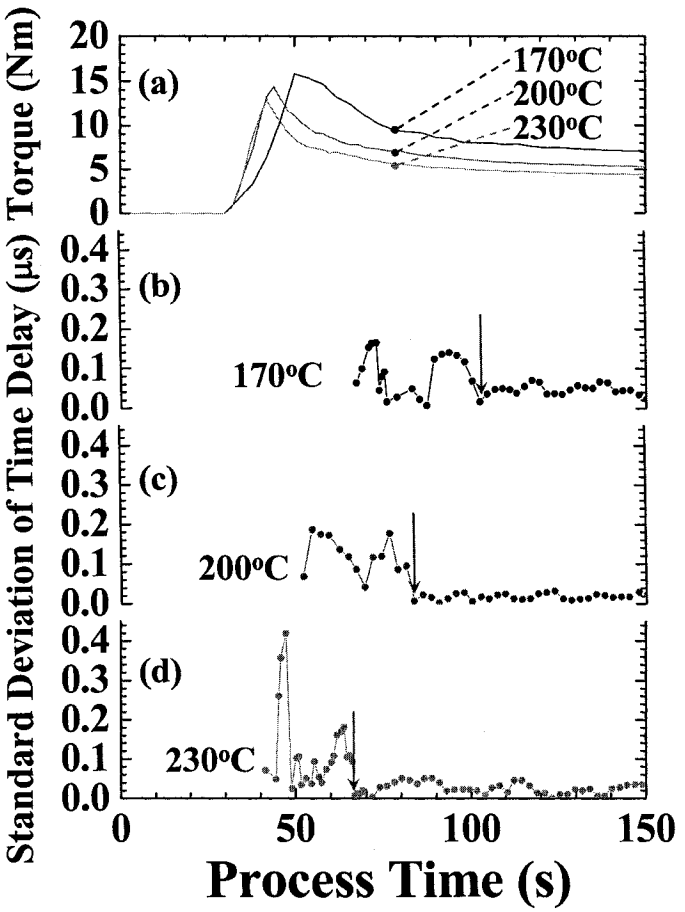

Fig. 6-13 Effect of temperature setting on melting process: (a) torque measurements, (b), (c) and (d) MSD of time delay between L^1 and L_{2f} echoes. Rotation speed: 28RPM; load: 40g LDPE.

In order to view clearly the temperature effect, the melting period and peak torque value are compared with the temperature settings of the mixing chamber. The results are shown in Fig. 6-14. In the temperature range from 170 to 230°C, the melting period decreases from 72.7 to 36.8s and the peak torque value

decreases from 15.8 to 12.96Nm. This indicates that the higher temperature setting of mixing chamber would cause lower torque response and reduce the melting period. The ultrasonic technique can clearly indicate the melting completeness at each temperature setting, while the torque and temperature techniques do not.

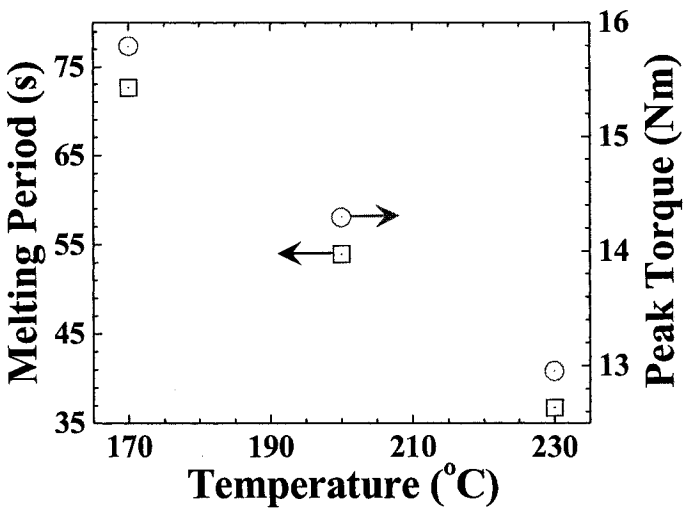

Fig. 6-14 Variation of melting period and peak torque with temperature setting of mixing chamber.

6.4.4 Rotation speed effect

It may appear that the rotation speed of the blade will affect the melting process as much as the temperature of the mixing chamber. In order to confirm this, the rotation speeds of the roller blade are set with 14, 28 and 42RPM, to melt 40g LDPE with the fixed temperature setting of mixing chamber of 200°C. The experimental results of the torque and MSD of time delay between L^1 and L_{2f} echoes with respect to the process time are presented in Fig. 6-15 (a) to (d). In Fig. 6-15 (a), the melting process with lower rotation speed setting indicates lower torque value and needs more time to reach to a steady state. In Fig. 6-15 (b) to (d), the MSD of time delay between L^1 and L_{2f} echoes reaches to the noise level

earlier, when the melting process is set at the higher rotation speed. The complete melting timings are at process time of 84.7, 84 and 74s for the rotation speed setting of 14, 28 and 42RPM, respectively.

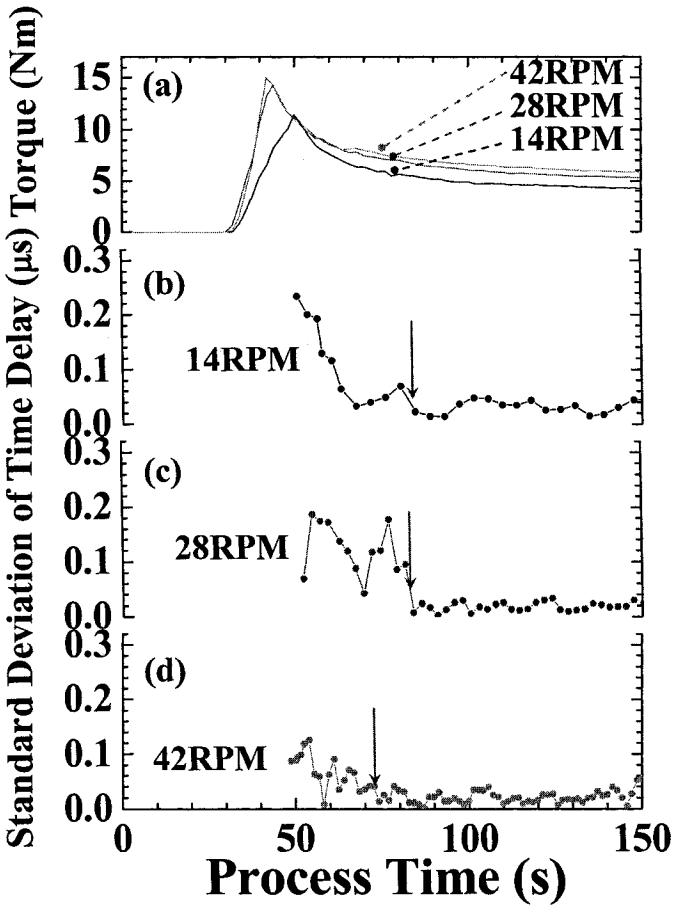

Fig. 6-15 Effect of rotation speed on melting process: (a) torque measurements, (b), (c) and (d) MSD of time delay between L^1 and L_{2f} echoes. Temperature setting: 200°C; load: 40g LDPE.

In order to view clearly the rotation speed effect, the melting period and peak torque value are examined for different rotation speed settings. The results are shown in Fig. 6-16. In rotation speed range of 14 to 42RPM, the melting period decreased from 54.7 to 44s and the peak torque value increased from 11.4 to 15Nm monotonically. The rotation speed of 28RPM seems to be approaching a

saturating level. This indicates that faster rotation speed would cause higher torque response, which calls for higher mechanical force, but reduces the melting period. Again, the ultrasonic technique can clearly indicate the melting completeness, while the torque and temperature techniques do not.

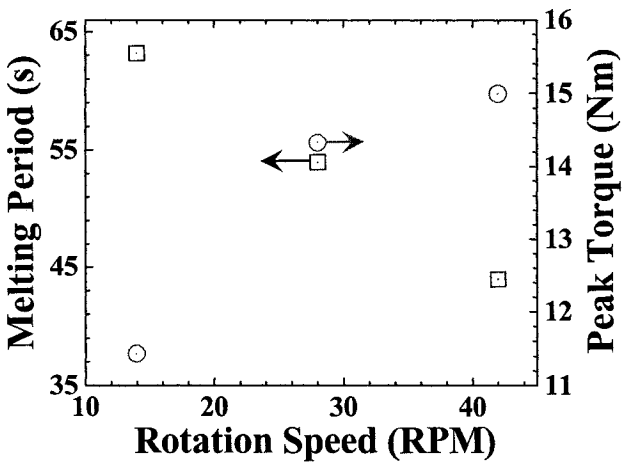

Fig. 6-16 Variation of melting period and peak torque with rotation speed.

6.4.5 Torque evaluation

Torque measurement is popular in internal mixer and extruder for the diagnosis of the viscosity and adjustment of the process parameter (temperature and rotation speed) to reach the optimal process conditions and product quality. Values from ultrasonic measurements present an opportunity to provide the torque producing information as well as melting and mixing quality for optimizing process. The Principle Component Analysis (PCA), a static calculating and analyzing method for a pattern recognition and data modeling technique on multivariate system, is used to evaluate torque through ultrasonic signals (see Appendix C). Here, the output is the measured torque value, and state variables for the process monitoring are the amplitude of ultrasonic echo L^1, peak amplitude of L_{2f} echo and time delay between L^1 and L_{2f} echoes. According to the availability and characteristics of ultrasonic signals measured in our experiments,

the evaluation procedure is separated into six segments, described in Table 6-1. In order to clarify the amplitude values of the L^1 echo shown in Fig. 6-9 (c) and match with the timing of torque measurement, signal processing is conducted as follows: 1) moving average of 15-20 points of the amplitude values obtained with respect to the process time, and 2) spline interpolation on the acquired signals to determine the amplitude value of the echo.

Table 6-1 Segments and periods for torque value by ultrasonic measurements

Segment No.	1	2	3	4	5	6
Time (s)	0 to 45	45 to 62	62 to 77	77 to 150	150 to 164	164 to 200

Segment 1 is the period from the start of experiment to appearance of ultrasonic L_{2f} echo. In this segment, the amplitude of ultrasonic echo L^1 solely determines the torque value. From segment 2 to 6, the amplitude of L^1 echo, peak amplitude of L_{2f} echo and time delay between L^1 and L_{2f} echoes are the factors to evaluate torque value. The principles for separating the timings from segment 2 to 6 are:

Segment 2 to 3: the first bottom in the "M" shape curve of the MSD of time delay between L^1 and L_{2f} echoes in Fig. 6-10 (c),
Segment 3 to 4: the complete melting point for the host material in Fig. 6-10 (c),
Segment 4 to 5: the fed of the additional material in Fig. 6-9,
Segment 5 to 6: the complete melting point for additional material in Fig. 6-10 (c).

The evaluation result is presented in Fig. 6-17, where the torque value and evaluated torque value by ultrasound are presented by straight line and straight line with dotted points, respectively. In segment 2, the evaluated torque values by ultrasound also present the practical situation inside the mixer; namely partially melt pellets. Except for this situation and the fast rising segment, the evaluated toque value has an agreement with the raw data within 5%. Therefore, the presented ultrasonic measurement contains the same information as torque

measurement, namely viscosity. However, ultrasonic measurement can provide the melting situations additionally, while torque measurement does not. This information and technique can be extended to the extruder and MM machine, in which the torque measurement is necessary but unattractive due to its high cost.

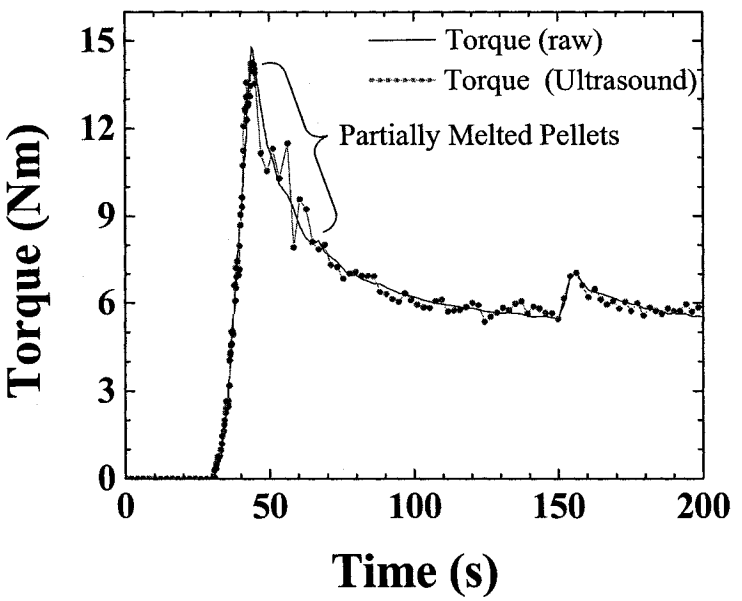

Fig. 6-17 Comparison of torque measurement (solid line) and estimation of torque (line with dotted points) predicted from ultrasonic measurements.

6.5 Summary

Real-time, non-intrusive and non-destructive monitoring of melting process in the internal mixer has been performed using ultrasonic delay line probe (CBR). The melting process from solid pellets to polymer melt is diagnosed by observation, torque, temperature, and ultrasonic signatures.

The timing of melt completeness can be clearly judged by the moving standard deviations of amplitude and time delay of ultrasonic echoes. The

partially melted pellets and air bubbles during melting process can also be detected.

The melting period is reduced when the temperature of mixing chamber or rotation speed of the blade increase. This can be diagnosed by ultrasound as well as torque. The ultrasonic signatures can be used to estimate torque values. The estimated torque can provide additional information, such as partially melted pellets.

Therefore, the presented ultrasonic techniques may be an excellent approach to diagnose melting processes nondestructively and noninvasive, in order to optimize the process parameters, reduce cost and evaluate melt quality.

Chapter 7

Conclusions

7.1 Thesis summary

7.1.1 Thesis accomplishment

In this thesis, through the practical development of integrated HT ultrasonic sensors, the piezoelectric films HTUTs have been successfully customized for each IM machine and process. The integrated HT ultrasonic sensors are "ready" for use and have been extensively evaluated for real-time diagnoses of large- and small- scale IM processes, such as IM, COIM, GAIM, WAIM, IMMF and MM. For micro-fabrication processes, the integrated and miniaturized HT ultrasonic sensors have overcome the barrel, mold and cavity space limitations, and been proved to be suitable for processes diagnoses of fabricating micro products. It is shown that the proposed HT ultrasonic sensors, systems, and techniques can provide real-time, non-destructive and non-intrusive measurements that are suitable for diagnosing material property, process control and optimization, as well as part quality assurance.

7.1.2 Chapter summary

Ultrasonic technique is one of the candidates for real-time diagnosis of polymer processes because of its ability to provide information on process dynamics, material characteristics, and product quality. Application of

ultrasonic diagnosing technology can provide feedback signals to the process control system for timely adjustments of process parameters. This will be a step towards reaching the goal of process optimization, part quality assurance, and low process cost, and would help a manufacturing company to improve its production efficiency. The evolution of ultrasonic monitoring technology has been described in chapter 1. The limitations of conventional ultrasonic transducers, in particular their inability to operate at HT environment and being installed on curved machine surfaces have been highlighted. These limitations provide the rationale for the objectives of this thesis, which are to develop HT, miniaturized, ultrasonic sensors using piezoelectric film HTUTs and process diagnostic techniques, and to demonstrate their suitability for real-time, nondestructive, diagnosis of IM processes.

Various polymer processes are introduced in chapter 2. COIM, GAIM and WAIM are the techniques for manufacturing multi-layer or hollow structure plastic products, using recycled, low-cost materials or injecting air or water during filling process. These techniques improve part performance, reduce cycle time and lower part production cost. IMMF, MM processes have the capability to manufacture micro parts with precise dimensions, tight tolerances, and high aspect ratio for diverse applications in biomedical, optical and telecommunication fields. General process diagnostic techniques, including pressure, temperature, torque, optical and fluorescent detecting techniques are introduced. However, they are limited by certain requirements, such as drilling a hole, having direct contact with the detected material, being insensitive to local variation, installing a transparent window or adding a foreign material. Therefore, it is highly desirable to develop a sensor that is

free of these limitations and can meet the needs of real-time, non-destructive, non-intrusive process diagnosis for various polymer IM processes.

The integrated HT ultrasonic sensors have been successfully developed in chapter 3 by using piezoelectric BIT and PZT film HTUTs to meet the above needs, and shown that they can be customized for each IM machine and process. BIT film HTUT can operate up to more than 400°C due to its high Curie temperature. Below 200°C PZT film HTUT is used due to its high piezoelectric strength. These sensors can be fabricated either on flat mold inserts or curved barrel surfaces. When required, they can be miniaturized and made to fit each machine setup and process procedure. Their electrical connections are via coaxial cables. The sensors' central frequency can range from 8 to 17MHz. Their SNRs are above 30dB. Improvement of SNR is accomplished by machining two spiral like V-grooves onto the miniature probe periphery to remove trailing echoes during IMMF process. To prevent damage of ultrasonic sensors from water leakage, sealing the sensor cavity of WAIM mold insert by a HT sealant is carried out. These developed integrated BIT and PZT film HT ultrasonic sensors are "ready" for applying to actual industrial processes. In addition, a framework for using ultrasonic measurements to obtain ultrasonic signatures, such as ultrasonic velocity and attenuation, has been presented. A PC-based high-speed data acquisition system with its key components has been described for real-time process diagnosis application. Also, details of an ultrasonic PVT measurement system, which allows ultrasonic signatures of polymers to be obtained offline from ultrasonic measurements, are provided. Furthermore, fabrication procedures of

piezoelectric ceramic film HTUT by sol-gel spray technique have been presented.

Process diagnosis of large-scale IM processes, such as IM, COIM, GAIM and WAIM, by the developed HT ultrasonic sensors has been demonstrated in chapter 4. Four BIT film HT ultrasonic sensors are integrated onto the surfaces of sensor inserts of a 150 tons Engle machine for molding flat PC parts of 1.0mm-thick. For an IM process, PC melt flow front and melt flow speed inside the mold cavity have been successfully monitored during fabrication of the PC plate. The filling incompleteness of 1% can be detected by ultrasonic transmitting signals. The solidification of PC inside the mold provides useful information to reduce the cycle time. For COIM process, melt PC core flow speed and cavity pressure inside the mold cavity have been diagnosed for the five-layer PC/ABS sandwich parts of 3.5mm-thick. Measurements of layer thicknesses by ultrasound are within ±17% of optical measurements, which is considered to be in good agreement. The PC core thickness can be used to estimate the core length qualitatively. Three PZT film HT ultrasonic sensors are integrated on the mold insert surface of a Battenfeld gas or water assisted IM machine for molding a cylindrical hollow HDPE part with a diameter of 20mm. For GAIM or WAIM process, detection of gas or water flow and gas flow speed has been monitored during molding process. The wall thickness of around 3.6mm estimated by ultrasound is in agreement with that measured by gauge, with accuracies of ±7% and ±10% for GAIM and WAIM, respectively. The HT ultrasonic sensors developed here can diagnose the formation of the complex multi-layers or hollow structures and monitor melt flow arrival, melt speed, and part detachment of the IM, COIM,

GAIM and WAIM molded part of any thickness by reflected ultrasonic echo at the mold/polymer melt interface, in order to provide information for optimizing process and improving part quality.

Diagnosis of IMMF and MM processes has been successfully carried out in chapter 5. The MM processes are mainly conjugated with polymer, nano-composite and powder materials. For IMMF, two miniature PZT film HT ultrasonic sensors have been installed into the mold of a 30 tons Boy machine for fabricating 1.1mm-thick PMMA parts with micro-structures on their surfaces. Ultrasonic contact duration can indicate the presence of sufficient holding pressure (>7.5MPa) for producing parts with flat surface (roughness <5μm). BIT and PZT film HT ultrasonic sensors have been fabricated on the barrel and mold surface of a Battenfeld MM machine, respectively, for fabricating POM and PA+POSS micro-parts. Increase of melt temperature (180 ~ 220°C) in the barrel, with a gap distance of 3.275mm, will decrease ultrasonic velocity in the POM linearly. The mold cavity pressure also has a linear relationship with the ultrasonic velocity in the PA66 during the fabrication process of two-step parts of 0.315/0.585mm-thick. The increase of POSS concentration will decrease ultrasonic velocity in the PA66+POSS. For MM of alumina ceramic powder material, five PZT film HT ultrasonic sensors have been mounted on the mold surface of a Battenfeld MM machine for manufacturing the circle ceramic part of 1.47mm-thick. Part thickness variations can be evaluated by ultrasonic velocity in the feedstock, ultrasonic contact duration and peak holding pressure. Among these, the ultrasonic velocity has higher correlation with the part thickness. The Young's modulus of sintered parts can be estimated by measuring ultrasonic longitudinal and

shear wave velocity of the parts. The presented HT ultrasonic sensors can be integrated onto the small mold or curved barrel space of micro-fabricate machine to diagnose the thickness and surface profile of microstructures, in order to optimize process and assure part quality.

The ultrasonic delay line probe has been installed into the mixing chamber of the internal mixer for the diagnosis of melting process of LDPE in chapter 6. During the melting process, different melting stages of LDPE can be indicated by the variations in ultrasonic velocity. For these stages, the timings obtained using ultrasonic signatures are earlier than those given by torque and temperature measurements. The presence of air bubbles inside the chamber can be detected by ultrasonic signatures. Higher temperature setting of mixing chamber will reduce the melting period, indicated by MSD of ultrasonic velocity. The rotation speed has similar effect. Ultrasonic signatures contain information on the polymer's viscosity and can be used to estimate torque values.

The estimating method of Young's modulus through ultrasonic signatures is presented in Appendix A. Two statistic analysis methods, namely, moving standard deviation (MSD) and principle component analysis (PCA), are utilized to determine the different segments of melting process and estimate the torque measurement, respectively, during the process. Their descriptions are presented in the Appendix B and C.

7.2 Claims of originality

The contributions of this thesis to the field of IM have been pointed out in different chapters. They are outlined below:

1. The HT ultrasonic sensors have been developed using BIT and PZT film HTUTs. They can be fabricated on flat mold or curved barrel surfaces of IM machines for process diagnosis. Significant improvements in SNR and protection of integrated sensors have been achieved. [178-180].
2. Filling completeness of molded PC part is diagnosed by ultrasonic transmitting signals, and even 1% of volume defect can be detected. [54, 181]
3. Melt PC core flow movement and core dimensions are diagnosed by HT ultrasonic sensors. Core thickness and length are related to product performance and usually measured offline, using destructive methods. The ultrasonic estimation method offers the capability of estimating core thickness and core length on-line. [182]
4. Gas or water flow movement and hollow HDPE structure dimension are diagnosed by HT ultrasonic sensors. For WAIM, the presented ultrasonic technique is a novel way to diagnose water flow and estimate wall thickness. For GAIM or WAIM, ultrasonic contact duration can detect optimal gas or water pressure for sufficient cooling and improved part quality. [183]
5. Optimal holding pressure for improved part quality and reduced cycle time are obtained using ultrasonic contact duration and velocity in the PMMA for IMMF. [178-179]
6. Process diagnosis, from the barrel to mold end, is carried out in

newly MM machine and process [56]. Evaluation of POSS concentration is also carried out in MM process [184].

7. Thickness variation of micro part is evaluated in MM process for alumina ceramic powder material. Ultrasonic velocity in the feedstock, ultrasonic contact duration and peak holding pressure are utilized to estimate ceramic part thickness. [185]
8. Utilizing the ultrasonic PVT measurements, the PMMA and POM status inside the mold can be estimated during molding process. This can reduce the cycle time and process cost.
9. LDPE melting completion indicated by ultrasonic signature is carried out in internal mixer. The information can be used to reduce cycle time and save process cost. The application of MSD to process diagnosis and control is a pioneering idea.
10. Estimation of torque value by the correlation existing between the ultrasonic signatures and the torque has been carried out during LDPE melting process. These results show that ultrasonic signatures contain viscosity information which can be extracted during melting process.

7.3 Future works:

1. Improvement of signal strength of ultrasonic sensors for thicker (or multi-layer) parts or high-attenuation materials.
2. Development of diagnosis technique using frequency spectrum analysis for fabrication of very thin or micro parts.
3. Extending the diagnostic technique developed in chapter 6 to process diagnosis of extruders and the micro-fabrication machines.

Appendix A: Modulus of material

There are some additional parameters which characterize polymer properties; such as, dynamic longitudinal (L) and shear (G) modulus, bulk modulus (K), and Young's modulus (Y). These parameters are of interest here as they can be estimated from ultrasonic velocity and attenuation measurements [26]. The basics relations for these parameters are outlined below.

A. Dynamic Longitudinal Modulus

The storage (L') and loss (L'') components of the dynamic longitudinal modulus ($L = L' + jL''$) can be expressed as [186]:

$$L' = \rho_P V_{PL}^2 \left[(1 - F^2) / (1 + F^2)^2 \right] \quad \text{(Eq. A-1)}$$

$$L'' = 2\rho_P V_{PL}^2 \left[F / (1 + F^2)^2 \right] \quad \text{(Eq. A-2)}$$

where,

$F = \alpha_{PL} V_{pL} / \omega$

ρ_P : Density of polymer

V_{PL} : Longitudinal ultrasonic velocity in the polymer

α_{PL} : Ultrasonic longitudinal attenuation in polymer.

ω : $2\pi f$, f is the ultrasonic frequency

When $F << 1$, then (Eq. A-1) and (Eq. A-2) are approximated to,

$$L' = \rho_P V_{PL}^2 \quad \text{(Eq. A-3)}$$

$$L'' = 2\rho_P \alpha_{PL} V_{PL}^3 / \omega \quad \text{(Eq. A-4)}$$

B. Dynamic Shear Modulus

The storage (G') and loss (G'') components of the dynamic shear modulus ($G = G' + j\ G''$) can be similarly expressed as:

$$G' = \rho_P\ V_{PS}^2 \left[(1 - H^2) / (1 + H^2)^2 \right] \qquad \text{(Eq. A-5)}$$

$$G'' = 2\rho_P\ V_{PS}^2 \left[H / (1 + H^2)^2 \right] \qquad \text{(Eq. A-6)}$$

where,

$H = \alpha_{PS} V_{pS} / \omega$,

V_{PS} : Shear ultrasonic velocity in the polymer

α_{PS} : Ultrasonic shear attenuation in polymer.

When $H << 1$, then (Eq. A-5) and (Eq. A-6) are approximated to,

$$G' = \rho_P\ V_{PS}^2 \qquad \text{(Eq. A-7)}$$

$$G'' = 2\rho_P\ \alpha_{PS}\ V_{PS}^3 / \omega \qquad \text{(Eq. A-8)}$$

C. Dynamic Bulk Modulus

The bulk modulus components, K' and K'' ($K = K' + j\ K''$) are defined in terms of the longitudinal and shear modulus parameters, according to,

$$K' = L' - 4G'/3 \qquad \text{(Eq. A-9)}$$

$$K'' = L'' - 4G''/3 \qquad \text{(Eq. A-10)}$$

D. Dynamic Young's modulus

The dynamic Young's modulus components, Y' and Y'' ($Y = Y' + j\ Y''$) are similarly defined in terms of the bulk and shear modulus parameters,

$$Y' = 9K'G'/(3K' + G') \qquad \text{(Eq. A-11)}$$

$$Y'' = 9K''G''/(3K'' + G'') \qquad \text{(Eq. A-12)}$$

Appendix B: Moving Standard Deviation (MSD)

General

In the field of probability and statistics, standard deviation (SD) indicates the spread of sample values for a population, relative to their expected values [187]. SD is the most common measure of statistical dispersion (or variance), quantifying how widely values of a data set are spread in their common range. A high SD means that many data points are far from the mean value and vise verse. In forecasting, SDs (obtained from the variance matrix) set bounds on deviations from the predicted values, which are calculated from the past information.

The Moving Standard Deviation (MSD) is an extension of the basic relation for calculating SD for a data set, which has applications in online systems. It has been used as a tool to capture and analyze changes occurring in stock prices on the Stock Markets. In this thesis, the concept of MSD has been deployed to identify transitions in the polymer state; specifically, the time of melting completion (Chapter 6). Such transitions are accompanied with changes in the parameters that characterize the polymer, making MSD the appropriate online tool to detect the onset and the completion of such changes. To the author's knowledge, MSD has been rarely used in process control systems and its use in the work reported in this thesis may qualify as "a first". [188].

MSD Calculation

For a process variable X, the MSD is defined based on a time window containing the N past samples of X, ending with the most recent sample. The N samples in this window are used to calculate the MSD of X according to,

$$MSD = \frac{1}{N}\sqrt{\sum_{i=1}^{N}(X_i - \bar{X}_{MEV})^2} \qquad \text{(Eq. B-1)}$$

where $\overline{X}_{MEV}$ is the Moving Expected Value (MEV) of X over the selected time window, given by,

$$\overline{X}_{MEV} = \frac{1}{N}\sum_{i=1}^{N} X_i \qquad \text{(Eq. B-2)}$$

On arrival of a new sample, the window is shifted forward in time by one sampling period and MEV and MSD are recalculated. The forward shift is accomplished by simply dropping the oldest sample and adding the most recent sample to the window. This procedure is continued in time, creating a time series for the MSD values.

MSD Application

Monitoring the MSD time series can provide information on transitions in the material state. This is due to the fact that such transitions are accompanied by movements in the process variables. These movements are often obscured by the measurement noises and cannot be often observed by monitoring the variable itself. However, since MSD is largely obvious to the presence of measurement noises, it can clearly indicate the onset and and completion of such transitions.

The choice of N (i.e. the length of the time window) and, therefore, the sampling rate, are critical to the quality of the information generated by MSD. These quantities have to be chosen carefully, making sure that they are suitable for the time constant associated with the phenomenon to be captured.

Appendix C: Principle Component Analysis (PCA)

The ideas behind the Principle Component Analysis (PCA) have been known since the times of Gauss. However, this technique has become popular in the last century when its outstanding ability in performing pattern recognition/factor analysis in the field of psychometrics was discovered. This technique has been also successfully used in the fields of econometrics and chemometrics in the past decades. In this thesis, in order to identify the correlation existing between torque measurements and ultrasonic signatures in chapter 6, the PCA technique [189-191] has been deployed. A high correlation between these two quantities is a strong indicator that they both contain the same information and it would be possible to build a dynamic model of the torque from ultrasonic measurements.

The PCA operates on a multivariate system based on decomposition of the system eigenvectors. Its procedure is presented in the following.

An mxn matrix **Y** can be decomposed into the sum of the product of n vector pairs. Each pair consists of two vectors $\mathbf{x}_i$ (nx1) and $\mathbf{a}_i$ (mx1), often referred to as the *loadings* and the *scores* vectors, respectively. In terms of $\mathbf{x}_i$ and $\mathbf{a}_i$, **Y** can be expressed as,

$$\boldsymbol{Y} = \boldsymbol{a}_1 \boldsymbol{x}_1^T + \boldsymbol{a}_2 \boldsymbol{x}_2^T + \ldots\ldots + \boldsymbol{a}_n \boldsymbol{x}_n^T \qquad \text{(Eq. C-1)}$$

Note that each $\boldsymbol{a}_i \boldsymbol{x}_i^T$ is an mxn matrix and the matrix of loadings vectors **X** forms a new orthogonal basis for the space spanned by **Y**. The individual $\mathbf{x}_i$ are the eigenvectors of the nxn scatter matrix of **Y**, defined as

$$\text{Scatter } (\boldsymbol{Y}) = (\boldsymbol{Y}^T \boldsymbol{Y})/(m-1) \qquad \text{(Eq. C-2)}$$

Thus

Scatter $(\boldsymbol{Y})\ \boldsymbol{x_i} = \lambda_i\ \boldsymbol{x_i}$ (Eq. C-3)

where λ_i is the eigenvalue associated with the eigenvector $\mathbf{x}_i$, which are often referred to as principal components. The scores vector $\mathbf{a}_i$ is simply the projection of $\mathbf{Y}$ onto the new basis vector $\mathbf{x}_i$; that is,

$\mathbf{a}_i = \boldsymbol{Y}\boldsymbol{x_i}$ (Eq. C-4)

The value of each λ_i is an indicator of the covariance in the data set that defines $\boldsymbol{Y}$, in the direction of $\mathbf{x}_i$. The fraction variance, ρ_i, in direction $\mathbf{x}_i$

$$\rho_i = \lambda_i / \sum_{j=1}^{n} \lambda_j \quad \text{(Eq. C-5)}$$

If the data set used in building $\boldsymbol{Y}$ has been normalized to have variables of zero mean and unity for standard deviations, then

$$\sum_{i=1}^{n} \lambda_i = \mathrm{n} \quad \text{(Eq. C-6)}$$

In this case, each scores vector $\mathbf{a}_i$ has a mean of zero and a standard deviation of λ_i. The data set can be further adjusted to produce unity variance through dividing $\mathbf{a}_i$ by its associated eigenvalue λ_i.

Once the eigenvectors of Scatter $(\boldsymbol{Y})$ have been determined, the score vectors can be calculated. These scores are often useful for showing the relationships between the samples in the data set. For instance, a projection of the samples onto two eigenvectors shows the relationship between the samples in two dimensions. This explains the effectiveness of PCA as a pattern recognition and sample classification technique. It is also found that, in many cases, only the first few eigenvectors are associated with systematic variations in the data, and that the remaining ones are related to noise. The noise here refers to uncontrolled experimental and instrumental variations arising from random processes.

The statistical tendency of the data can be estimated by projecting it into the PCA model, which is the plane formed by the first few eigenvectors associated with systematic variation in the data set. This PCA model often has significantly lower order than the original one. For a reduced matrix of loading vectors $\mathbf{X}_k$ (where only the first k of the n total eigenvectors are kept), the estimated data set $\hat{Y}$ can be obtained from:

$$\hat{Y} = \hat{a}_1 x_1^T + \hat{a}_2 x_2^T + ... + \hat{a}_k x_k^T \qquad \text{(Eq. C-7)}$$

where $\hat{\mathbf{a}}_i$ is the score vector of $\hat{Y}$ in the direction of loading vector $\mathbf{x}_i$. Then the fitting level between the original and estimated model can be monitored by calculating the data residual, defined as

$$\mathbf{r} = \mathbf{Y} - \hat{Y} \qquad \text{(Eq. C-8)}$$

The optimal estimate of the model is to minimize the magnitude of data residual **r**, which is the sum of square of the components of **r**. It is the solution of the linear-least-square problem. After getting the optimal estimated score vectors $\hat{\mathbf{a}}_i$, the estimated outputs can be generated according to Eq. C-7.

Reference

[1] Osswald, & Menges, "Materials science of polymers for engineers," Hanser publisher, Cincinnati, Ohio, chapter 1, pp. 1-17, 1995.

[2] R.T. Fenner, "Principles of polymer processing", Chemical Publisher, 1980.

[3] D.V. Rosato, "Concise encyclopedia of plastics", Kluwer, 2000.

[4] D.V. Rosato, "Extruding plastics: a practical processing handbook", Kluwer publisher, 1998.

[5] D.V. Rosato, "Plastics processing data handbook", 2nd Ed., Kluwer publisher, 1997.

[6] D.V. Rosato, et. al., "Injection molding handbook", 3rd Ed. Kluwer publisher, 2000.

[7] R.E. Farrell, "Artificial intelligence in injection molding", *SPE-IMD*, no. 35, 1994.

[8] P.A. Toensmeier, and L. Hilpold, "New co-injection designs add applications potential", *Modern Plastics*, vol.29, no. 7, pp. 77-78, July, 1999.

[9] R.G. Speight, A.J. Monro, and A. Khassapov, "Benefits of velocity phase profiles for injection molding", *Proc. SPE-ANTEC*, pp. 520-524, 1998.

[10] A.R. Agrawal, I.O. Pandelidis, and M. Pecht, "Injection-molding process control – a review", *Polym. Eng. Sci.*, vol. 27, no. 18, pp. 1345-1357, 1987.

[11] R.E. Farrel and L. Dzeskiewicz, "Expert system for injection molding", *Proc. SPE ANTEC*, pp. 692-695, 1994.

[12] R. Speight, P. Coates, and J. Hull, "The use of process measurements for real time injection moulding process control" , *Proc. SPE ANTEC*, vol. 40, pp. 696-700, 1994.

[13] P. Coates, A. Haynes, and R. Speight, "In-line characterization of polymer deformation in melt and solid phase processing", *Polymer*, vol. 35, no. 18, pp. 3831-3843, 1994.

[14] A.J. Bur, F.W. Wang, C.L. Thomas, and J.L. Rose, "In-line optical monitoring of polymer injection molding", *Polym. Eng. Sci.*, vol. 34, no. 8, pp. 671-679, 1994.

[15] C.K. Shih, D.G. Tynan and D.A. Denelsbeck, "Rheological properties of multicomponent polymer systems undergoing melting or softening during compounding," *Polym. Eng. Sci.*, vol. 31, pp. 1670-1673, 1991.

[16] M.D. Wetzel, D.A. Denelsbeck, S.L. Latimer, C.-K. Shih, "A perturbation method to characterize reactive extrusion", *Proc. SPE ANTEC*, pp. 3791-3796, 2003.

[17] A.S. Birks, R.E. Green, and P. Mclntire, "Nondestructive testing handbook", 2nd Ed., American society for nondestructive testing, 1991.

[18] I.A. Rawabdeh, "In-line monitoring of injection molding operations: a literature review", *J. Inj. Mold. Tech.*, vol. 3, no. 2, pp. 47-53, 1999.

[19] S.I. Rokhlin, D.K. Lewis, K.F. Graff, and L. Adler,"Real-time study of frequency dependence of attenuation and velocity of ultrasonic waves during the curing reaction of epoxy resin", *J. Acous. Soc. Am.* vol. 79, no. 6, pp. 1786-1793, 1986.

[20] O. Lee and J. Williams, Jr., "Ultrasonic wave characterization of polymers", *Material Evaluation*, pp. 351-355, 1991.

[21] A. Tanaka and K. Nitta, "Ultrasonic velocity and attenuation of polymeric solids under oscillatory deformation. II: high density and linear low density polyethylene and their blends", *Polym. Eng. Sci.*, vol. 31, pp. 571-576, 1991.

[22] J. Tatibouet, and L. Piché, "Ultrasonic investigation of semicrystalline polymers: study of poly (ethylene terephthalate)", *Polymer*, vol. 32, pp. 3147-3153, 1991.

[23] W. Huang and S.I. Rokhlin, "Low-frequency normal incidence ultrasonic method for thin layer characterization", *Materials Evaluation*, pp. 1279-1284. November 1993.

[24] J. Prassianakis, N. Kompoti, and J. Varakis, "Curing effects on the acoustical properties of epoxy polymers", *Experimental Mechanics*, vol. 33, pp. 77-80, 1993.

[25] L. Piche, D. Levesque, R. Gendron, and J. Taibouel, "Ultrasonic probe of polymer flows", *Proc. SPE ANTEC*, vol. 41, pp. 2715-2719, 1995.

[26] L. Piche, F. Massines, A. Hamel, and C. Neoron, "Ultrasonic characterization of polymers under simulated processing conditions", USA Patent: 4,754,645, July 5, 1988.

[27] N. Nishiwaki, S. Hori, and M. Tsutsumi, "Monitoring of molding process of plastics using ultrasonics", *JSPE*, vol. 52, no. 3, pp. 507-513, 1986.

[28] N. Nishiwaki, S. Hori, H. Orita, A. Cui, and M. Konno, M., "A new ultrasonic method for measurement the crystallinity of thermoplastics used in injection molding products", *Int. conf. manufacturing systems and environment,* Tokyo, Japan, pp. 217-222, 1990.

[29] M. Konno, A. Cui, N. Nishiwaki, and S. Hori, "Measurement of polymer melt temperature in injection molding machine by using ultrasonic techniques", *Proc. SPE ANTEC*, vol. 39, pp. 2798-2803, 1993.

[30] C.L. Thomas, "Sensor concepts for polymer injection molding", PhD thesis, Drexcel University, 1993.

[31] C.L. Thomas, A.O. Adebo, and A.J. Bur, "Ultrasonic measurement of polymer material properties during injection molding", *SPE ANTEC Tech Papers*, vol. 40, pp. 2236-2239, 1994.

[32] E.C. Brown, T.L.D. Collins, A.J. Dawason, P. Olley, and P.D. Coates, "Ultrasound: a virtual instrument approach for mornitoring of polymer melt variables", *J. Rein. Pla. Comp.*, vol. 18, no. 4, pp. 331-338, 1999.

[33] R. Gendron, L. Daigneault, J. Taibouet, and M. Dumoulin, "Residence time distribution in extruders determined by in-line ultrasonic measurements", *Adv. Polym. Tech.*, vol. 15, pp. 111-125, 1996.

[34] H. Wang, B. Cao, C.K. Jen, K.T. Nguyen, and M. Viens, "On-line ultrasonic monitoring of the injection molding process," *Polym. Eng. Sci.*, vol. 37, no. 2, pp. 363-376, 1997.

[35] S.S.L. Wen, C.K. Jen, and K.T. Nguyen, "Advances in on-line monitoring of the injection molding process using ultrasonic techniques", *Int. Polym. Proc.*, vol. XIV, no. 2, pp. 175-182, 1999.

[36] R. Kazys, A. Voleisis, R. Sliteris, B. Voleisiene, L. Mazeika, P. H. Kupschus, and H. A. Abderrahim, "Development of Ultrasonic Sensors for Operation in a Heavy Liquid Metal" *IEEE Sensor J.*, vol. 6, p. 1134, 2006.

[37] T.N. Nguyen, M. Lethiecq, B. Karlsson and F. Patat, "Development of a broad-band ultrasonic transducer for high temperature applications", *Acta Acustica*, vol. 3, pp. 331-338, 1995.

[38] B.W. Maxfield and C.M. Fortunko, "The design and use of electromagnetic acoustic wave transducers (EMATs)", *Material Evaluation*, vol. 41, no. 12, pp. 1399-1408, 1983.

[39] D.A. Stubbs and R.E. Dutton, "An Ultrasonic Sensor for High-Temperature Materials Processing", *JOM*, vol. 48, no. 9, pp. 29-31, 1996.

[40] K. Kawashima, K.T. Hyoguchi and T. Akagi, "On-line measurement of plastic strain ratio of steel sheet using resonance mode EMAT", *J. Nondestructive Evaluation*, vol.12, no.1, pp. 71-77, 1993.

[41] D.T. Quebeillalt and H.N.G. Wadley, "Temperature dependence of the elastic constants of solid and liquid $Cd_{0.96}Zn_{0.04}Te$ obtained by laser ultrasound", *J. Appl. Phys.*, vol. 83, no. 8, pp. 4124-4133, 1998.

[42] R.J. Dewhurst et al., "A Remote Laser System for Material Characterization at High Temperatures," *Review of Progress in Quantitative Nondestructive Evaluation,* vol. 7B, ed. D.O. Thompson and D. Chimenti, New York: Plenum Press, p. 1615, 1988.

[43] A. McNab, K.J. kirk and A. Cochran, "Ultrasonic transducers for high temperature applications", *IEEE Proc. Sci. Meas. Technol.*, vol. 145, pp. 229-236, 1998.

[44] R. Kazys, A. Voleisis, R. Sliteris, L. Mazeika, R.V. Nieuwenhove, P. Kupschus, and H.A. Abderrahim, "High temperature ultrasonic transducers for imaging and measurements in a liquid Pb/Bi eutectic alloy", *IEEE UFFC*, vol. 52, no. 4, 2005.

[45] C.-K. Jen, Z. Sun and M. Kobayashi, "Ultrasonic monitoring of barrel wear and screw status", *Proc. SPE ANTEC*, pp.402-406, 2004.

[46] D. Ramos França, C.K. Jen, K.T. Nguyen and R. Gendron, "On-line ultrasonic monitoring of polymer extrusion", *Polym. Eng. Sci.*, vol.40, no.1, pp.82-94, 2000.

[47] C.K. Jen, J.G. Legoux and L. Parent, "Experimental evaluation of clad metallic buffer rods for high temperature ultrasonic measurements", *NDT&E International*, vol. 33, pp. 145-153, 2000.

[48] C.K. Jen, and J.G. Legoux, "High performance clad metallic buffer rods", *Proc. IEEE Ultrasonics Symp.*, pp. 771-776, 1996.

[49] J.D. Greathouse, "Portable high temperature ultrasonic testing (UT) piezo probe with cooling apparatus", US Patent 5,936,163, Aug. 10, 1999.

[50] C.K. Jen, B. Cao, K.T. Nguyen, C.A. Loong, and J.G. Legoux, "On-line ultrasonic monitoring of a die-casting process using buffer rods", *Ultrasonics*, vol. 35, pp. 335-344, 1997.

[51] C.K. Jen, J.W. Liaw, T.F. Chen, A. Moreau, J.P. Monchalin, and C.C. Yang, "Ultrasonic evaluation of semi-solid metals during processing", *Meas. Sci. Technol.*, vol. 11, pp. 1-6, 2000.

[52] J. Cha, and J.L White, "Maleic anhydride modification of polyolefin in an internal mixer and a twin-screw extruder: experiment and kinetic model", *Poly. Eng. Sci.*, vol. 41, no. 7, pp. 1227-1237, 2001.

[53] M. Kobayashi and C.K. Jen, "Piezoelectric thick bismuth titanate/PZT composite film transducers for smart NDE of metals", *Smart Materials and Structures*, vol. 13, pp. 951-956, 2004.

[54] M. Kobayashi, Y. Ono, C.K. Jen, and C.C. Cheng, "High-temperature piezoelectric film ultrasonic transducers by a sol-gel spray technique and their application to process monitoring of polymer injection molding", *IEEE Sensors Journal*, vol. 6, pp. 55-62, 2006.

[55] P. Fuierer and B. Li, "Nonepitaxial orientation in sol-gel bismuth titanate films", *J. Am. Ceram. Soc.*, vol. 85, no. 2, pp. 299-304, 2002.

[56] Y. Ono, B.D. Whiteside, E.C. Brown, M. Kobayashi, C.C. Cheng, C.K. Jen, and P. Coates, "Real-time process monitoring of micromolding using

integrated ultrasonic sensors," accepted by *Transactions of the Institute of Measurement and Control*, Jan. 2006.

[57] D.V. Rosato, "Injection molding basics and overviews", *SPE-IMD Newsletter*, Issue. 48, 1998.

[58] R.G. Griskey, "Polymer process engineering", Chapman & Hall, 1995.

[59] D.V. Rosato, et. al., "Injection molding update", *SPE-IMD Newsletter*, no. 39, 1995.

[60] D. . Rosato, "Gas injection molding", *SPE-IMD Newsletter*, no. 40, 1995.

[61] D.V. Rosato, et. al., "Designing with plastics and composites: a handbook", Kluwer publisher, 1991.

[62] R. Selden, "Sandwich injection molding of thermoplastics – a literature survey," *J. Inj. Mold Technol.*, vol. 1, no. 4, pp. 189-203, 1997.

[63] R.C. Donovan, K.S. Rabe, W.K. Mammel, and H.A. Lord, "Recycling plastics by two-shot molding", *Polym. Eng. Sci.* vol. 15, no. 11, pp. 774-780, 1975.

[64] J.L. White, and H.B. Dee, "Flow visualization for injection molding of polyethylene and polystyrene melts", *Polym. Eng. Sci.*, vol. 14, no. 3, pp. 212-222, 1974.

[65] J.L. White, and B.L. Lee, "An experimental study of sandwich injection molding of two polymer melts using simultaneous injection", *Polym. Eng. Sci.*, vol. 15, no. 7, pp. 481-485, 1975.

[66] S.S. Young, J.L. White, E.S. Clark, and Y. Oyanagi, "A basic experimental study of sandwich injection molding with sequential injection", *Polym. Eng. Sci.*, vol. 20, no. 12, pp. 798-804, 1980.

[67] G. Akay, "Co-injection molding of reinforced polymers", *Polym. Comp.*, vol. 4, o. 4, pp. 256-264, 1983.

[68] S.C. Chen, K.F. Hsu, and J.S. Huang, "Observation of the polymer melt flow in injection molding process using co-injection molding technique", *Int. Comm. Heat. Mass Trans.*, vol. 21, no. 4, pp. 499-508, 1994.

[69] M. Kadota, M. Cakmak, and H. Hamada, "Structural hierarchy developed in co-injection molded polystyrene/polypropylene parts", *Polymer*, vol. 40, pp. 3119-3145, 1999.

[70] R. Selden, "Co-injection molding: effect of processing on material distribution and mechanical properties of a sandwich molded plate", *Polym. Eng. Sci.*, vol. 40, no. 5, pp. 1165-1176, 2000.

[71] C.T. Li, D.J. Lee, and A.I. Isayev, "Interface development and encapsulation in simultaneous coinjection molding of disk II. Two-dimensional simulation and experiment", *J. App. Poly. Sci.*, vol. 88, pp. 2310-2318, 2003.

[72] S.H. Chen, S.Y. Hu. W.R. Jong, and M.C. Jeng, "Structural analysis, process simulation, and warpage calculations for gas-assisted IM parts using a unified CAE model", *Proc. SPE ANTEC*, pp. 620-624, 1997.

[73] C.L. Clark, et al., "Overcoming process control challenges of gas-assist IM", *Proc. SPE ANTEC*, vol. 1, pp. 540-543, 1995.

[74] S. Shah, "Gas assisted injection molding: a technology overview", *J. Inj. Mold. Tech.*, vol. 1, no. 2, pp. 96-103, 1997.

[75] R.Y. Chang, S.C. Lin, K.C. Chen, C.H. Hsu and M.H. Tsai, "Computer-aided gas-assisted injection –molding of the front cover of motorcycle headlight," *Proc. SPE ANTEC*, pp.438-441, 1998.

[76] M. Knights, Plastics technology online article, http://www.ptonline.com/articles/200509fa1.html, Sep., 2005.

[77] J. Zhao, X. Lu, L. Fong, and H.H. Chiang, "Statistical experiment study of gas-assisted injection molding process", *SPE ANTEC*, pp. 454-459, 1998.

[78] S.Y. Yang and S.J. Liou, "Experimental study on gas-assisted injection molding", *Proc. SPE ANTEC*, pp. 404-407. 1994.

[79] C.H. Ahn, J.W. Choi, G. Beaucage, J.H. Nevin, J.B. Lee, A. Puntambekar, and J. Y. Lee, "Disposable Smart Lab on a chip for point-of-care clinical diagnositcs", *Proc. of the IEEE*, vol. 92, pp.154-173, 2004.

[80] J.D. Zahn, A.A. Deshmukh, A.P. Papavasiliou, A.P. Pisano, and D. Liepmann, "An Integrated microfluidic device for the continuous sampling

and analysis of biological fluids", *Proc. ASME-IMECE*, Nov.11-16, New York, N.Y., 2001.

[81] D. Sinton, L. Ren, X. Xuan, and D. Li, "Effects of liquid conductivity differences on multi-component sample injection, pumping and stacking in microfluidic chips", *Lab. Chip.*, vol. 3, pp. 173-179, 2003.

[82] J.W. Choi, S. Kim, R. Trichur, H.J. Cho, A. Puntambekar, R.L. Cole, J.R. Skimkins, S. Murugesan, K. Kim, J.B. Lee, G. Beaucage, J.H. Nevin, and C.H. Ahn, "A plastic micro injection molding technique using replaceable mold-disks for disposable microfluidic systems and biochips," *Micro Total Analysis Systems*, J. M. Ramsey et al., Eds. The Netherlands: Kluwer Academic, pp. 411-412, 2001.

[83] J.W. Choi, K.W. Oh, A. Han, N. Okulan, C.A. Wijayawardhana, C. Lannes, S. Bhansali, K.T. Schlueter, W.R. Heineman, H.B. Halsall, J.H. Nevin, A.J. Helmicki, H.T. Henderson, and C.H. Ahn, "Development and characterization of microfluidic devices and systems for magnetic bead-based biochemical detection", *Bio. Micro.*, vol. 3, no. 3, pp. 191-200, 2001.

[84] M.J. Madou, L. J. Lee, S. Daunert, S. Lai, and C.H. Shih, "Design and fabrication of CD-like microfluidic platforms for diagnostics: microfluidic functions", *Bio. Micro.*, vol. 3, no. 3, pp. 245-254, 2001.

[85] D. Sinton, L. Ren, and D. Li, "Visualization and numerical modelling of microfluidic on-chip injection process", *J. Col. Inter. Sci.*, vol. 260, pp. 431-439, 2003.

[86] B.D. Whiteside, M.T. Martyn, P.D. Coatees, "Micromoulding: Interrogating the Process", *Proc. of PPE*, 2003.

[87] A.M. Tom, and J.P. Coulter, "Advancements in micro-molding for small-scale product fabrication", *Proc. of ASME*, pp. 1-9, 2002.

[88] B.D. Whiteside, M.T. Martyn, P.D. Coates, G. Greenway, P. Allan, and P. Hornsby, "Micromoulding: process measurements, product morphology and properties", *Plastics, Rubber and Composites*, vol. 33, pp. 11-17, 2004.

[89] M. Heckele, and W.K. Schomburg, "Review on micro molding of thermoplastic polymers", *J. Micromech. Microeng.* vol. 14, pp. R1-R14, 2004.

[90] C.L. Weir, "Introduction to injection molding," Society of Plastics Engineers, Brookfield, CA, 1975.

[91] S.Y. Yang, S.C. Nian, and I.C. Sun, "Flow visualization of filling process during micro-injection molding", *Int. Poly. Proc.* vol. XVII, no. 4, 2002.

[92] A.W. Mcfarland, and J.S. Colton, "Production and analysis of injection molded micro-optic components", *Poly. Eng. Sci.*, vol. 44, no. 3, pp. 564-579, 2004.

[93] J. Zhao, R.H. Mayes, G. Chen, H. Xie, and P.S. Chan, "Effects of process parameters on the micro molding process", *Poly. Eng. Sci.*, vol. 43, no. 9, pp. 1542-1554, 2003.

[94] H. Schift, C. David, J. Gobrecht, A.D. Amore, D. Simoneta, W. Kaiser, and M. Gabriel, "Quantitative analysis of the molding of nanostructures", *J. Vac. Sci. Technol. B*, vol. 18, no. 6, pp. 3564-3568, 2000.

[95] M.S. Despa, K.W. Kelly, and J.R. Collier, "Injection molding using high aspect ratio microstructures mold inserts produced by LIGA technique", *Proc. SPIE*, vol. 3512, pp. 286-294, 1998.

[96] B.D. Whiteside, E.C. Brown, Y. Ono, C.K. Jen, and P.D. Coates,."Polymer degradation and filling incompletion monitoring for micromolding using ultrasound," *Proc. SPE ANTEC*, pp. 624-628, 2005.

[97] M. Alexandre, and P. Dubois, "Polymer-layered silicate nanocomposites: preparation, properties and uses of a new class of materials", *Mater. Sci. Eng.*, vol. 28, pp.1-63, 2000.

[98] L. Zheng, A.J. Waddon, R.J. Farris, and E.B. Coughlin, "X-ray characterizations of polyethylene Polyhedral Oligomeric Silsesquioxane copolymers", *Macromolecules*, vol. 35, pp. 2375-2379, 2002.

[99] R.M. German, "Powder Injection Molding: Design and Application", Innovative material solutions Inc. Publishers, State College, PA, pp. 1-8, 2003.

[100]T. Benzler, V. Piotter, T. hanemann, K. Mueller, P. Norajitra, R. Ruprecht, J. Hausselt, "Innovations in molding technologies for microfabrication", *Proc. SPIE*, vol. 3874, pp. 53-60, 1999.

[101]J.S. Kim, K. Jiang, and I. Chang, "A net shape process for metallic microcomponent fabrication using Al and Cu micro/nano powders", *J. Micromech. Microeng.*, vol. 16, pp. 48-52, 2006.

[102]Technical trends, "PIM sales forecast to treble by 2010", *Metal Powder Report*, pp. 22-25, Feb. 2001.

[103]V. Piotter, T. Benzler, T. Gietzelt, R. Ruprecht, and J. Haubelt, "Micro powder injection molding", *Adv. Engineer. Materials,* vol. 10, pp. 639-642, 2000.

[104]T. Gietzelt, V. Piotter, O. Jacobi, R. Riprecht, and J. Hausselt, "Fabrication of micromolds for gearwheels by micro powder injection molding", *Adv. Engineer. Materials*, vol. 5, pp. 139-145, 2003.

[105]V. Piotter, T. Gietzelt, and L. Merz, "Micro powder-injection moulding of metals and ceramic", *Sādhanā*, vol. 28, parts 1 & 2, pp. 299-306, 2003.

[106]D.D. Hongerholt, J.L. Rose, and R.M. German, "Using ultrasonic sensors for powder injection molding", *JOM*, vol. 24, pp. 24-28, 1996.

[107]D.D. Hongerholt, J.L. Rose, and R. M. German, "A self-tuning ultrasonic sensor based powder injection molding process", *NDT&E*, vol. 30, n0. 6, pp, 389-396, 1997.

[108]C. Rauwendaal, "Understanding extrusion", Hanser, Munich, 1998.

[109]N.P. Cheremisinoff, "Guidebook to extrusion technology", Prentice Hall, Englewood Cliffs, NJ, 1993.

[110]J.F. Chabot, "The development of plastics processing machinery and methods", John Wiley & Sons, New York, 1992.

[111]F. Hensen, "Plastics extrusion technology", Hanser, Munich, 1997.

[112]C.I. Chung, "Extrusion of polymers: theory and practice", Hanser, Munich, 2000.

[113]J. Cha, J.L. White, "Styrene grafting onto a polyolefin in an internal mixer and a twin-screw extruder: experiment and kinetic model", *Poly. Eng. Sci.*, vol. 41, no. 7, pp. 1238-1250, 2001.

[114]T. Jongen, "Characterization of batch mixers using numerical flow simulations," *AIChE Journal*, vol. 46, pp. 2140-2150, 2000.

[115]M.H.R. Ghoreishy and V. Nassehi, "Modeling the transient flow of rubber compounds in the dispersive section of an internal mixer with slip-stick boundary conditions," *Adv. Poly. Tech.* vol. 16, pp. 45-68, 1997.

[116]J. M. Zalc, .S. Szalai and F. J. Muzzio, "Characterization of flow and mixing in an SMX static mixer," *AIChE Journal*, vol. 48, pp. 427-436, 2002.

[117]J.E. Goodrich and R.S. Porter, ''A Rheological Interpretation of Torque-Rheometer Data,'' *Polym. Eng. Sci.*, vol. 7, pp. 45–51, 1967.

[118]G. Serpe, J. Jarrin, and F. Dawans, ''Morphology-Processing Relationships in Polyethylene-Polyamide Blends,'' *Polym. Eng. Sci.*, vol. 30, pp. 553–565, 1990.

[119]M. Bousmina, A. Ait-Kadi, and J. B. Faisant, "Determination of shear rate and viscosity from batch mixer data," *J. Rheol.* vol. 43, no. 2, pp. 415-433, 1999.

[120]O. Amano and S. Utsuhi, "Temperature measurements of polymer melts in the heating barrel during injection molding. Part I. temperature distribution along the screw axis in the reservoir", *Polym. Eng. Sci.*, vol. 28, no. 23, pp. 1565-1571, 1988.

[121]J. Chi and J. Sunderland, "Determination of ejection temperature and cooling time in injection molding", *Polym. Eng. Sci.*, vol. 32, no. 3, pp. 191-197, 1992.

[122]M.R. Kamal, W.I. Patterson, and V.G. Gomes, "An injection molding study. Part 1: melt and barrel temperature dynamics", *Polym. Eng. Sci.*, vol. 26 no. 12, pp. 854-866, 1986.

[123]M.R. Kamal, W.I. Patterson, N. Conley, D. Abu Fara, and G. Lohfink, "Dynamics and control of pressure in the injection molding of thermoplastics", *Polym. Eng. Sci.*, vol. 27 no. 18, pp. 1403-1410, 1987.

[124]J. Agassant, P. Avanas, J. Sergent, and J. Garreau, "Polymer processing: principles and modeling", Hanser-Gardner Publication, 1991.

[125]Y. Iwata, Y. Yamamoto, K. Yonekura, and Y. Kagami, "Computer simulation of molten metal flow in thin plate die castings", *Trans. NADCA 16th Int. Die Casting Congress and Exposition*, pp. 311-320, 1991.

[126]B. Cao, "On-line ultrasonic monitoring of injection molding and die casting processes", Master thesis, Department of Electrical Engineering, McGill University, Montreal, QC, 1996.

[127]M. Redwood, *Mechanical waveguides*, New York: Pergamon Press, p. 190, 1960.

[128]Kistler pressure sensor on-line data sheet: http://www.kistler.com/medias/ldNmha1czgCxP85D8YwBEd-30.pdf

[129]Dynisco pressure sensor on-line data sheet: http://www.rolfmuri.ch/pdf/RM-Spritzgiess_D.pdf

[130]F. Boca Raton, et al., "Measurement, instrumentation, and sensors handbook", CRC Press LLC publisher, 1999.

[131]Y.D. Cheong, J.W. Kin, S.H. Oh, and C.W. Lee, "Analysis and development of the angular twist type torque-meter", *Mechatronics*, vol. 3, pp. 82-85, 2000.

[132]J. Kristensen, T. Schaefer, and P. Kleinebudde, "Direct pelletization in a rotary processor controller by torque measurements I: influence of process variables", *Pharm Dev Technol.* vol. 5, pp. 247-256, 2000.

[133]J. Kristensen, T. Schaefer, and P. Kleinebudde, "Direct pelletization in a rotary processor controller by torque measurements II: effects of changes in the content of microcrystalline cellulose", *AAPS PharmSci.* vol. 2, no. 3, E 24, 2000.

[134]M.D. Wetzel, D.A. Denelsbeck, S.L. Latimer, and C.-K. Shih, "Quantification of melting progression during twin screw extrusion using pulse perturbation technique part II: physics of melting", *Proc. SPE ANTEC*, pp. 354-360, 2005.

[135]C. Belanger, P. Cielom and B. Favis, "Analysis of polymer blend morphology by transmission and reflection light scattering techniques", *Polym. Eng. Sci.*, vol. 30, pp. 1090-1097, 1990.

[136]A.J. Bur, and C.L. Thomas, "A multi-functional optical sensor for mornitoring polymer injection molding", *Proc. SPE ANTEC*, pp. 2798-2804, 1995.

[137]K.B. Migler, and A.J. Bur, "Measurement of temperature profiles during polymer processing", *Proc. SPE ANTEC*, pp. 278-2282, 1997.

[138]A. Bur, J. Shibata, T. Trout, F. Wang, and C. Thomas, *Polym. Eng. Sci.*, vol. 31, 1991.

[139]J. D. N. Cheeke, "Fundamentals and applications of ultrasonic waves", CRC Press LLC, 2002.

[140]G. Adebayo and M. Cakmak, "Design of a static temperature scanning ultrasonic measurement system and application to multi-phase polymer systems," *Intern. Polymer Processing,* vol. XVIII, no. 3, pp. 252-259, 2003.

[141]R. Gendron, J. Tatibouet, J. Guevremont, M. M. Dumoulin, and L. Piche, *Polym. Eng. Sci.*, vol. **35**, p. 79, 1995.

[142]B. Cao, "On-line ultrasonic monitoring of injection molding and die casting processes", Master thesis, Department of electrical engineering, McGill University, Montreal, Quebec, 1996.

[143]H. Adachi, Y. Kuroda, T. Imahashi, and K. Yanagisawa, "Preparation of piezoelectric thick films using a jet printing system," *Jpn. J. Appl. Phys.*, vol. 36, part 1, no.3A, pp. 1159-1163, March 1997.

[144]X. Zhao, J. R. G. Evans, and M. J. Edirisinghe, "Direct ink-jet printing of vertical walls," *J. Am. Ceram. Soc.*, vol. 85, no.8, pp. 2113-2115, 2002.

[145]K. L. Gentry, J. M. Zara, S.-D. Bu, C.-B. Eom, and S. W. Smith, "Thick film sol gel PZT transducer using dip coating," *Proc. IEEE Ultrasonics Symp.*, vol. 2, pp. 977-980, 2000.

[146]C. Galassi, E. Roncari, C. Capiani, and P. Pinasco "PZT-based suspensions for tape casting," *J. Eur. Ceram. Soc.*, vol.17, pp. 367-71, 1997.

[147]D.A. Barrow, T.E. Petroff, R.P. Tandon, and M. Sayer, "Characterization of thick lead zirconate titanate films fabricated using a new sol gel based process," *J. Appl. Phys.* vol.81, no.2, pp. 876-881, Jan. 1997.

[148]L. Zou, M. Sayer, and C.-K. Jen, "Sol-gel fabricated thick pieozoelectric ultrasonic transducers for potential applications in industrial material processes," *Proc. IEEE Ultrasonics Symp.*, pp. 1007-1011, 1997.

[149]Y. Chen, M. Sayer, L. Zou, and C.-K Jen, "Lithium tantalate/lead zirconate titanate composite ultrasonic transducers," *Appl. Phy. Lett.*, vol.74, no.17, pp. 2552-2554, April 1999.

[150]M. Kobayashi, T.R. Olding, M. Sayer, and C.-K. Jen, "Piezoelectric thick film ultrasonic transducers fabricated by a sol-gel spray technique," *Ultrasonics*, vol.39, pp. 675-680, 2002.

[151]J.S. Chang, P.A. Lawless, and T. Yamamoto, "Corona discharge processes," *IEEE Trans. Plasma Science*, vol. 19, no.6, pp. 1152-1166, Dec. 1991.

[152]D. Waller, T. Iqbal, and A. Safari, "Poling of lead zirconate titanate ceramics and flexible piezoelectric composites by the corona discharge technique," *J. Am. Ceram. Soc.*, vol.72, no.2, pp. 322-324, 1989.

[153]C.K. Jen and M. Kobayashi, "Integrated and flexible high temperature piezoelectric ultrasonic transducers", Chapter 2 in Ultrasonic and Advanced Methods for Nondestructive Testing and Material Characterization, Ed. by C.H. Chen, World Scientific Publishing, New Jersey, pp.33-55, 2007.

[154]A.R. Selfridge, IEEE transc. *Sonics and Ultrasonics*, vol. SU-32, no. 3, pp. 381-394, 1985.

[155]C.K. Jen, L. Piche, and J. F. Bussiere, "Long isotropic buffer rods," *J. Acoust. Soc. Am.*, vol. 88, p. 23, 1990.

[156]S.C. Chen, K.S. Hsu, and J.S. Huang, "Experimental study on gas penetration characteristics in a spiral tube during gas-assisted injection molding", *Ind. Eng. Chem. Res.* Vol. 34, pp. 416-420, 1995.

[157]A. J. Poslinski, and V. K. Stokes, "Gas-assisted displacement of a viscous liquid in a tube", *Proc. SPE ANTEC*, pp. 68-70, 1993.

[158]Cox, B. G., *J. Fluid Mechanics*, vol. 14, pp. 81-96, 1962.

[159]F. Belblidia, J.F.T. Pittman, A. Polynkin, J. Sienz, "Gas displacing viscous shear thinning liquids from tubes: Effects of cooling before gas injection", *Chemical Engineering Science*, vol. 60, pp. 4953 – 4956, 2005.

[160]P. Olley, L. Mulvaney-Johnson, P.D. Coates, "Non-isothermal experimental and simulation study of residual wall thickness in gas assisted injection moulding", *Plastics, Rubber and Composites*, vol. 35, no. 2, pp. 47-58, 2006.

[161]L. Piché, A. Hamel, R. Gendron, M. Dumoulin, and J. Tatibouët, "Ultrasonic characterization of polymer melts under processing conditions," US Patent 5,433,112, July 18 1995.

[162]B.R. Whiteside, M.T. Martyn, P.D. Coates, P.S. Allan, P.R. Hornsby, and G. Greenway, "Micromoulding: process characteristics and product properties", *Plastics, Rubber and Composites*, vol. 32, pp. 231-239, 2003.

[163]M.L. Dufour and B. Gauthier, *Proc. of SPIE*, vol. 5260, p. 173, 2003.

[164]D.M. Bryce, "Thermoplastics troubleshooting for injection molders", Society of Plastics Engineers, Brookfield, CA, 1991.

[165]K. Yoshikawa, and H.Ohmori, "Outstanding features of powder injection molding for micro parts manufacturing", *RIKEN* 34, pp. 13-18, 2001.

[166]V. Piotter, W. Bauer, T. Benzler, A. Emde, "Injection molding of components for Microsystems", *Microsystem Technologies*, vol. 7, pp. 99-102, 2001.

[167]C.K. Jen, Y. Ono and M. Kobayashi, "high temperature integrated ultrasonic shear wave probes", *Applied Phys. Lett.*, vol.89, pp.183506_1 to 3, Oct. 2006.

[168]Y. Ono, C.K. Jen and M. Kobayashi, "High temperature integrated ultrasonic shear and longitudinal wave probes", *Review of Scientific Instruments*, vol.78, pp.024903-1 to5, Feb. 2007.

[169]C.K. Jen, C. Neron, A. Miri, H. Soda, A. Ohno and A. McLean, "Fabrication and characterization of continuously cast clad metallic buffer rods", *J. Acoust. Soc. Am.*, vol.91, pp.3565-3570, June 1992.

[170]H. Soda, C.K. Jen, G. Motoyasu, S. Okumura, A. Ohno and A. McLean, "Fabrication and characterization of an aluminum clad, Al-Cu alloy cored rod", *Material Science and Tech.*, vol. 11, pp.1174-1179, Nov. 1995.

[171]C.K. Jen, D. Ramos-França, Z. Sun and I. Ihara, "Clad polymer buffer rods for polymer process monitoring", *Ultrasonics*, vol.39, pp.81-89, March 2001.

[172]C.K. Jen, C. Neron, E.L. Adler, G.W. Farnell, J. Kushibiki, and K., Abe, "Long acoustic imaging probes", *Proc. IEEE Ultrasonics Symp.*, pp. 875-880, 1990.

[173]C.K. Jen, C. Neron, A. Miri, H. Soda, A. Ohno, and A. McLean, "Fabrication and characterization of continuously cast clad metallic buffer rods", *J. Acoust. Soc. Am.*, vol. **91**, pp. 3565-3570, 1992.

[174]H. Soda, C.K. Jen, G. Motoyasu, S. Okumura, A. Ohno, and A. McLean, "Fabrication and characterization of an aluminum clad, Al-Cu alloy cored rod", *Material Science and Tech.*, vol. **11**, pp. 1174-1179, 1995.

[175]C.K. Jen, J.G. Legoux and 1. Parent, "Experimental evaluation of clad metallic buffer rods for high temperature ultrasonic measurements," *NDT&E international*, vol. 33, pp. 145-153, 2000.

[176]Z. Sun, C.K. Jen, H. L. Liang, and D.C.Y. Su, "A prototype ultrasonic system for monitoring polymer mixing process on an internal mixer," *Proc. CIDC*, 2004.

[177]Z. Sun, J. Tatibouët, C.K. Jen, H.L. Liang, and C.Y. Su, "Application of ultrasound in the determination of fundamental extrusion performance: monitoring of filler dispersion during twin-screw extrusion," *Proc. PPS*, 2004.

[178]Y. Ono, C.C. Cheng, C.K. Jen, J. Tatibouët, and J.F. Hétu, "Ultrasonic technique and probes for monitoring surface imperfection of microfluidic plastic devices during injection molding," *Proc. SPE ANTEC*, pp. 818-822, 2005.

[179]Y. Ono, C.C. Cheng, M. Kobayashi, C.K. Jen and N. Nardini, "Real-time monitoring for fabrication process of microfluidic plastic devices using

miniature ultrasonic sensor", *Proc. IEEE Ultrason. Symp.*, pp. 545-548, 2004.

[180]Y. Ono, C.C. Cheng, M. Kobayashi, and C.K. Jen, "Real-time monitoring of injection molding for microfluidic devices using ultrasound," *Polym. Eng. Sci.*, Vol. 45, pp. 606-612, 2005.

[181]Y. Ono, M. Kobayashi, C.K. Jen, C.C. Cheng, Abdessalem Derdouri, and Yves Simard ," Real-time, Non-intrusive and Non-destructive Ultrasonic Monitoring of Injection and Co-injection Molding Processes ", *Proc. SPE ANTEC*, pp.556-560, 2004.

[182]C.C. Cheng, Y. Ono, and C.K. Jen, "Real time diagnosis of co-injection molding using ultrasound," accepted by *Polym. Eng. Sci.*, Jun. 2007.

[183]L. Mulvaney-Johnson, C.C. Cheng, Y. Ono, E.C. Brown, C.K. Jen, P. D. Coates, "Real-time Diagnostics of Gas/Water Assisted Injection Moulding using Integrated Ultrasonic Sensors," *Plastics, Rubber and Composites: Macromolecular Engineering*, vol. 36, no. 3, pp. 111-121, 2007.

[184]Y. Ono, B.D. Whiteside, C.C. Cheng, M. Kobayashi, C.K. Jen, and P.D. Coates, "Real-time Diagnosis for Micromolding of Polymer Nanocomposites (PA66/POSS) using Ultrasound," *Proc. PPS*, Aug 14-17, 2005.

[185]C.C. Cheng, Y. Ono, B.D. Whiteside, E.C. Brown, C.K. Jen, and P. Coates, "Real-time diagnosis of micro powder injection molding using intergrated ultrasonic sensors," *International Polymer Processing*, Vol. XXII, pp. 140-145, 2007.

[186]H.J. McSkimin, "Ultrasonic methods for measuring the mechanical properties of liquids and solids", *Physical Acoustics*, ed. By W.P. Mason, Academic Press, vol. I-A, Chap. 4, pp. 271-334, New York, 1964.

[187]H.T. Hayslett, "Statistics made simple", Doubleday, 1968.

[188]S. Qin and T. Badgewell, "An overview of industrial model predictive control technology," *Chemical Process Control*, vol. 93, no. 316, pp. 232-256, 1997.

[189]B.M. Wise, N.B. Gallagher, S.W. Butler, D. White and G.G. Barna, "A Comparison of Principal Components Analysis, Multi-way Principal Components Analysis, Tri-linear Decomposition and Parallel Factor Analysis for Fault Detection in a Semiconductor Etch Process," *J. Chemometrics*, Vol. 13, pp 379-396, 1999.

[190]B.M. Wise, N. L. Ricker, D.F. Veltkamp and B.R. Kowalski, "A theoretical basis for the use of principal component models for monitoring multivariate processes," *Process Control and Quality*, Vol. 1, pp. 41-51, 1990.

[191]B.M. Wise, "Adapting Multivariate Analysis for Monitoring and Modeling of Dynamic Systems," Ph.D. Dissertation, University of Washington, Seattle, 1991.